Dissipation-assisted processes and quantum correlations

Nicolò Piccione

THÈSE DE DOCTORAT

Spécialité physique

École doctorale n° 553 Carnot - Pasteur

Dissipation-assisted processes and quantum correlations

Processus assistés par dissipation et corrélations quantiques

Thèse de doctorat de l'établissement Université Bourgogne Franche-Comté, préparée à l'Université de Franche-Comté par

Nicolò Piccione

Thèse présentée et soutenue à Besançon, le 18 décembre 2020

Directeur de thèse :	**Pierre Joubert** .....(Professeur, UBFC)
Co-encadrant de thèse :	**Bruno Bellomo** ..... (Maître de conférences, UBFC)

Jury

Présidente :	**Pérola Milman** ..... (Directrice de recherche, CNRS)
Rapporteur :	**Alexia Auffeves** ..... (Directrice de recherche, CNRS)
Rapporteur :	**Daniel Braun** ..... (Professeur, Université de Tübingen)
Examinateur :	**Benjamin Huard** ..... (Professeur, ENS de Lyon)
Directeur de thèse :	**Pierre Joubert** ..... (Professeur, UBFC)
Co-encadrant de thèse :	**Bruno Bellomo** ..... (Maître de conférences, UBFC)

Institut Utinam, équipe PhAs

UMR CNRS 6213, Besançon, France

Abstract

Dissipative dynamics of open quantum systems and quantum correlations are topics of great actual interest. The former because of its necessity when describing realistic systems and the latter because quantum correlations enable, in general, genuine quantum protocols.

This thesis aims to study physical processes relying on dissipation, also focusing on quantum correlations and their role in these processes, and on how to use dissipation to generate quantum correlations. We first introduce the reader to the various topics treated within the thesis which are connected to various research fields such as open quantum systems, quantum thermodynamics, quantum optics, and quantum information. Then, each chapter deals with a different subject.

The first part of the thesis consists of two studies in the context of quantum thermodynamics. The first study concerns a protocol of work extraction exploiting a single thermal bath. The work, defined within thermodynamic resource theory, is extracted from a resource and stored into a bipartite system by turning on and off its internal interaction. Then, we apply this protocol to two relevant physical systems: two interacting qubits and the Rabi model. In both cases, we obtain a work extraction comparable with the bare energies of the systems. In the second study, we investigate quantum thermal machines based on two-stroke thermodynamic cycles using two baths at different temperatures. The working fluid is composed of systems with evenly spaced energy levels, and all the considered interactions are of the exchange type. We maximize the power of two different cycles, also focusing on the role of the machines waiting time.

In the second part of this thesis, strongly connected to open quantum systems, we first study the Markovian and non-Markovian dynamics of a driven quantum harmonic oscillator within the collision model. While this is still a "work in progress" research project, we already have promising results such as the appearance of a non-adiabatic time-dependent term in the continuous limit of the Markovian dynamics. Then, we study the two-photon Dicke model in the bad-cavity limit, considering a quite general setup comprising finite temperature baths and coherent and incoherent drivings. We manage to derive an effective master equation for the qubits dynamics and compare it to the one-photon case. In the two-photon model, we point out an enhancement of the qubits spontaneous-like emission rate and an increment of the effective temperature perceived by the qubits. These differences lead to a faster generation of steady states with coherence and a richer dependence of the collective effects on temperature.

In the last part of the thesis, we explore the connection between energy and entanglement in an arbitrary finite non-interacting bipartite system, also finding the minimum energy entangled states (MEESs), i.e., the states having the minimum energy amount for a given degree of entanglement. We also study how these states can be generated both through unitary and dissipative processes, finding for the latter that the MEESs are practically the cheapest ones to produce. Moreover, the MEESs can be connected among them through local operations and classical communication and seem to have remarkable connections to quantum thermodynamics and many-body physics. Finally, we analyze how to use our results to lower the energetic cost of different quantum information protocols.

Abstract (version française)

La dynamique dissipative des systèmes quantiques ouverts et les corrélations quantiques sont des sujets de grand intérêt actuel. Le premier en raison de sa nécessité pour décrire des systèmes réalistes et le second parce que les corrélations quantiques permettent de réaliser, en général, des protocoles véritablement quantiques.

Cette thèse vise à étudier des processus physiques reposant sur la dissipation, en se concentrant également sur les corrélations quantiques et leur rôle dans ces processus, et sur la façon d'utiliser la dissipation pour générer des corrélations quantiques. Tout d'abord, nous présentons au lecteur les différents sujets abordés dans la thèse qui sont liés à divers domaines de recherche tels que les systèmes quantiques ouverts, la thermodynamique quantique, l'optique quantique et l'information quantique. Ensuite, chaque chapitre traite d'un sujet différent.

Une première partie de la thèse inclut deux études dans le domaine de la thermodynamique quantique. Une première étude concerne un protocole d'extraction de travail exploitant un seul bain thermique. Le travail, défini dans la théorie des ressources thermodynamiques, est extrait d'une ressource et stocké dans un système bipartite en activant et en désactivant son interaction interne. Ensuite, nous appliquons ce protocole à deux systèmes physiques pertinents : deux qubits en interaction et le modèle de Rabi. Dans les deux cas, nous obtenons une extraction de travail comparable aux énergies nues des systèmes. Dans une seconde étude, nous analysons des machines thermiques quantiques basées sur des cycles thermodynamiques à deux temps utilisant deux bains à des températures différentes. Le fluide de travail est composé de systèmes avec des niveaux d'énergie régulièrement espacés et toutes les interactions considérées sont de type d'échange. Nous maximisons la puissance de deux cycles différents, en nous concentrant également sur le rôle du temps d'attente des machines.

Dans une seconde partie de cette thèse, fortement liée aux systèmes quantiques ouverts, nous étudions d'abord la dynamique Markovienne et non-Markovienne d'un oscillateur harmonique quantique guidé au sein du modèle collisionnel. Même si ce projet de recherche est "en cours", nous avons déjà des résultats prometteurs tels que l'apparition d'un terme non adiabatique dans la limite continue de la dynamique Markovienne. Ensuite, nous étudions le modèle de Dicke à deux photons dans la limite de mauvaise cavité, en considérant un modèle assez général comprenant des bains de température finis et des pilotages cohérents et incohérents. Nous parvenons à dériver une équation maîtresse efficace pour la dynamique des qubits et à la comparer au cas à un photon. Dans le

modèle à deux photons, nous observons une augmentation du taux d'émission de type spontané des qubits et une augmentation de la température effective perçue par les qubits. Ces différences conduisent à une génération plus rapide d'états stationnaires avec cohérence et à une dépendance plus riche des effets collectifs sur la température.

Dans la dernière partie de la thèse, nous explorons la connexion entre l'énergie et l'intrication quantique dans un système bipartite fini arbitraire sans interaction, trouvant également les états intriqués d'énergie minimale (MEESs), c'est-à-dire les états ayant la quantité d'énergie minimale pour un degré donné d'intrication quantique. Nous étudions également comment ces états peuvent être générés à la fois par des processus unitaires et dissipatifs, trouvant, pour ces derniers, que les MEESs sont pratiquement les plus économiques à produire. De plus, les MEESs peuvent être connectés entre eux au moyen d'opérations locales et de communication classique et semblent avoir des connexions remarquables avec la thermodynamique quantique et la physique à plusieurs corps. Enfin, nous analysons comment utiliser nos résultats pour réduire le coût énergétique de différents protocoles d'information quantique.

Acknowledgements

I want to thank all the people I had the pleasure to meet during these three years. Indeed, I first thank my research supervisor Pierre Joubert for having let me conduct my thesis work and my co-supervisor Bruno Bellomo for its guidance throughout my Ph.D. I also thank the people I had the pleasure to work with: Benedetto Militello, Anna Napoli, Simone Felicetti, Gabriele De Chiara, and Heather Leitch. Many thanks also go to the jury members and all the scientists I had the pleasure to talk with of science during conferences and research visits.

I also wish to thank all my friends and nice people I interacted with during these years, be they in France, Italy, or anywhere else in the world. Special thanks go to Andrea Mattioni and Juliana Teti Meyer for the many discussions we had on topics related to life in science. Moreover, I thank Manon Glauser, Stefano Ariotta, and Laura Garcia-Alvarez for having helped me do little things associated with completing this thesis.

Finally, I thank my family for the support and help I received during these years and all the people that kept in contact with me during the COVID-19 induced isolation.

Contents

List of Figures

List of publications

This Thesis is mainly based on the following articles.

Published articles

1. N. Piccione, B. Militello, A. Napoli, and B. Bellomo.
   "Extraction of work via a thermalization protocol",
   Proceedings (extended abstract) for the conference IQIS 2018, special issue of Proceedings (MDPI). Proceedings **12**, 22 (2019).

2. N. Piccione, B. Militello, A. Napoli, and B. Bellomo.
   "Simple scheme for extracting work with a single bath",
   Phys. Rev. E **100**, 032143 (2019).

3. N. Piccione, B. Militello, A. Napoli, and B. Bellomo.
   "Energy bounds for entangled states",
   Phys. Rev. Res. **2**, 022057(R) (2020).

4. N. Piccione, G. De Chiara, and B. Bellomo.
   "Power maximization of two-stroke quantum thermal machines",
   Phys. Rev. A **103**, 032211 (2021).

Submitted articles

5. N. Piccione, S. Felicetti, and B. Bellomo.
   "Two-photon interaction effects in the bad-cavity limit",
   arXiv preprint arXiv:2007.07844 (2020).

6. N. Piccione, B. Militello, A. Napoli, and B. Bellomo.
   "Generation of minimum energy entangled states",
   arXiv preprint arXiv:2010.13644 (2020).

Chapter 1

General introduction

Quantum correlations have been intriguing physicists soon after the full development of quantum mechanics [1]. Nevertheless, their potential for designing protocols not feasible with classical systems has been investigated only much later [2]. The list of protocols employing quantum correlations includes quantum teleportation [3–5], quantum cryptography [6–8], quantum communication [9], quantum computation [10], and quantum energy teleportation [11]. The standard theoretical description of these protocols assumes that no dissipation and decoherence are present in the evolution of quantum systems. In particular, the absence of decoherence is crucial because its presence tends to deteriorate correlations between the systems [12, 13] and coherences internal to a single system.

Dissipation and decoherence affect a certain system due to the interaction of that same system with its surroundings [12]. In classical and quantum mechanics, an isolated system evolves deterministically and is not subject to dissipation or decoherence. However, while quantum mechanics theory initially concentrated on the description of isolated systems, the necessity of keeping into account the unavoidable interaction with the environment soon became evident [14] since perfectly isolating a system from its surrounding is impossible in the quantum realm as it is in the classical one[1]. Non-isolated quantum systems are called open quantum systems [12], and, over time, different approaches to describe them were used, but the interest in developing a formal approach encompassing all kinds of different open systems was initially purely academic. This academic research culminated in 1976 with the publication of the Gorini-Kossakowski-Sudarshan-Lindblad (GKSL) equation [14–16], which is the most general equation describing an open quantum system subject to a Markovian dynamics [12].

With the propulsion given by the quest for better isolating a quantum system, the study of open quantum systems surged in the last decades. Indeed, an improved comprehension of such systems properties can lead to improvements in devising quantum systems resistant to dissipation and decoherence. Moreover, the quantum features of the proposed protocols and their first experimental realizations (see, e.g., Refs. [17] and [4]) lead to huge investments from private industries and public actors. Thanks to the joined efforts of the public and private scientific community, we are now able to build and

[1] Even zero-point quantum fluctuations can be sources of dissipation and decoherence.

use the so-called NISQ (Noisy Intermediate-Scale Quantum) devices [18], i.e., devices in which the amount of decoherence and dissipation is low enough that their quantum features can actually give them an edge over their classical counterparts. Notably, the advancements in this regard have been so important that Google, very recently, claimed that its quantum computer reached the so-called quantum supremacy [19].

Although most efforts aim to reduce the dissipation and decoherence effects on quantum systems, there are situations in which the interaction with the environment enables the protocol instead of working against it. Thermal cycles are the archetypal example of such protocols [20]; the dissipation induced by the heat baths enables the functioning of a given cycle. Another example is given by the collective behavior of quantum systems interacting with a common bath, such as in the Dicke model [21], where a collection of qubits interacts collectively with a single mode of the electromagnetic field, usually mediated by a cavity [22]. More in general, dissipative processes have been used to generate quantum correlations and, in particular, entanglement between quantum systems [23–31].

1.1 In this thesis

This thesis aims to study physical processes relying on dissipation, also focusing on the role of quantum correlations in these processes and on how to use dissipation to generate quantum correlations (notably, entanglement). Therefore, this thesis subject situates in the vast field of open quantum systems, borrowing techniques and topics also from different physics fields such as quantum thermodynamics, quantum information, and quantum optics. Since this thesis faces different topics, we will introduce each of them in a dedicated section of chapter 2, focusing on the aspects more connected to our work. Let us now briefly describe the content of each chapter of the thesis.

In chapter 2, we will give the reader all the essential tools needed to understand the rest of the manuscript. Firstly, we will give an introduction to quantum correlations, paying special attention to entanglement. Secondly, we will quickly review the theory of open quantum systems, focusing on the topics of interest for the rest of the thesis. Thirdly we will introduce some concepts about thermodynamic resource theory and quantum thermal cycles. Finally, we will briefly present other concepts and theoretical tools that we used during our research.

Chapters 3 and 4 are devoted to the analysis of two different thermodynamic protocols. In particular, the protocol of chapter 3 consists of the "transfer of work"[2] from an external source to a quantum system of interest. Remarkably, just one thermal bath is sufficient to enable this process. This protocol will then be applied to two cases consisting of two interacting qubits and the Rabi model, respectively, thus letting us verify its validity with typical models studied in the literature. The protocol of chapter 4 consists of a thermal cycle between two thermal baths at different temperatures. There, we will study the properties of a cycle based on collisions between non-resonant systems with evenly spaced

[2]The concept of "transfer of work" will be better detailed in the same chapter 3.

energy levels, focusing on the case of qubit-qubit and oscillator-oscillator interactions. Moreover, we will pay great attention to the role of waiting times and their effects on the maximum power output of such cycles. Then, we will see how the addition of a mediator system could, in some situations, improve the performance of this cycle. Lastly, we will compare this cycle (without the mediator) to the quantum Otto cycle with shortcuts to adiabaticity, a model widely studied in the literature.

Chapter 5 contains the study of the dynamics of a driven quantum harmonic oscillator within a collision model. In particular, we will study these dynamics both in the Markovian and non-Markovian case, treating the latter with the Markovian embedding formalism. In both cases, we can recover some properties of this system usual description, while other properties are different. The main source of differences comes from the highly structured reservoir in the collision model. In particular, all the reservoir components are harmonic oscillators with the same frequency. On the contrary, in the standard case, the reservoir comprises many harmonic oscillators with different frequencies. Notice that this chapter refers to an investigation which is still in progress.

In Chapter 6, we will revisit the Dicke model by studying it in the case of two-photon interaction between qubits and a harmonic oscillator. The model will be studied in a quite general scenario since we will include a coherent pumping on the oscillator, an incoherent pumping on the qubits, and an arbitrary temperature bath for both the oscillator and the qubits[3]. In particular, we will study this model in the so-called bad cavity limit, in which the leakage of the cavity is assumed to be so strong that the fast dynamics of the cavity can be eliminated in order to obtain an effective master equation for the qubits. Using a novel adiabatic elimination technique [32, 33], we will manage to obtain this effective equation for both the one- and two-photon couplings. Then, we will compare them. In the two-photon model, we will see an enhancement of the qubits spontaneous-like emission rate and an increment of the effective temperature perceived by the qubits. These differences lead to a faster generation of steady-state coherence and a richer dependence of the collective effects on temperature.

Chapter 7 deals with minimum energy entangled states. Assuming no interaction between two subsystems, these are the states characterized by the minimum amount of energy for a given degree of entanglement. First, we will find the general form of these states and numerically show that, in most settings, they are extremely rare states. Nevertheless, they have connections with other physics fields and can be used to enhance different quantum information protocols from the energetic efficiency point of view. Since they are extremely rare, it should not be possible, in general, to obtain similar energetic performance by chance. Then, we will analyze some protocols whose aim is to generate such states. In particular, we will find three different families of unitary operators generating these states and five different kinds of interaction Hamiltonians such that these states constitute the ground state of the system and can, then, be obtained as the result of zero-temperature thermalization procedures.

[3]The oscillator and each qubits see their own, non-interacting, thermal bath. Each considered bath is at the same temperature.

Finally, we will conclude the thesis with Chapter 8, where we will do the sums of our work and make considerations on its possible future developments.

Chapter 2

Preliminary background

This introductory chapter aims to give the reader all the instruments necessary to understand the work done in the rest of the thesis and how it situates in the current literature. Since this thesis faces different topics, we will introduce each of them in the respective section, focusing on the aspects more connected to our work.

2.1 Entanglement and quantum correlations

In quantum mechanics, not every pure state can be written as the tensor product of states of its subsystems. Pure states of this kind are called entangled states [34] and their structure implies that the entropy of the subsystems states is not zero. Therefore, while we have maximal information about the system as a whole, we are "objectively" somewhat ignorant about its subsystems. This is in net contrast to the classical case, where having maximal information about a system is equivalent to having maximal information about all of its components. We can then conclude that the correlations in entangled pure states are of quantum nature.

Even if in this thesis we will particularly focus on the entanglement, it is worth to notice that entanglement is not the only type of quantum correlation. To see this, let us denote by ρ the state of a bipartite system S with subsystems A and B. Indeed, when $\rho = \rho_A \otimes \rho_B$ with $\rho_A \in \mathcal{H}_A$ and $\rho_B \in \mathcal{H}_B$[1], there are no correlations between the subsystems, while, when $\rho \neq \rho_A \otimes \rho_B$ we say that they are correlated. The standard way to measure how much two systems are correlated is to calculate the quantity called mutual information [10]:

$$S(A:B) \equiv S(\rho_A) + S(\rho_B) - S(\rho), \tag{2.1.1}$$

where $S(\rho)$ is the von Neumann entropy of the state ρ[2]. Indeed, the mutual information is equal to zero only when $\rho = \rho_A \otimes \rho_B$. Classical and quantum correlations can be discriminated through the use of quantum discord, for which we address the reader to

[1] $\mathcal{H}_A$ and $\mathcal{H}_B$ are, respectively, the Hilbert space of systems A and B.
[2] See Appendix 2.A.1 for the definition of von Neumann entropy.

Refs. [35, 36]. One important point here is that there can be quantum correlations even if the state ρ is separable[3]. This implies that entanglement is not entirely responsible for quantum correlations. However, entanglement remains the most peculiar of quantum correlations and, after a general introduction to its features and areas of application, we will see how it can be quantified in the theoretical framework of Local Operations and Classical Communications (LOCC).

The phenomenon of entanglement is one of the most, if not the most, exotic feature of quantum mechanics. Its counter-intuitive consequences have been highlighted, for example, in the famous paper [1] by Einstein, Podolsky and Rosen, whose content is now known as the EPR paradox. Later, John Bell returned on this question [37], by providing the famous Bell's inequality, which paved the way to experimentally test the so-called non-local features of entanglement. However, the most used inequality in actual non-locality experiments is the so-called CHSH inequality [38]. Up to now, the Bell and CHSH inequalities, which hold for classical systems, have always been unmet in quantum mechanics experiments on non-locality [39–41]. In addition to non-locality, entanglement can also be a crucial component used to model part of the measurement process [42, 43].

Apart from playing a crucial conceptual role in quantum mechanics, entanglement is widely considered a resource for quantum technologies since it enables various genuinely quantum protocols. For example, in the standard quantum teleportation protocol [3–5], the two parties implementing it share an entangled state at the start of the protocol. Let us call the two parties Alice and Bob, as it is customary in the quantum information field. Then, for example, the protocol enables[4] Bob and Alice to make a system in Alice possession go from an arbitrary state to the state of a local system of equal dimension in Bob possession. Indeed, by doing this, Bob's local system state changes since quantum states cannot be cloned [10].

Even quantum computation cannot be realized without entanglement, in the sense that it would not bring advantage over classical computation [10]. Let us assume of working with an idealized quantum computer with N qubits, in which the collective state of the qubits is a pure state. If we do not allow entanglement then the state must be separable and that means that the state can be characterized by two real numbers per qubit[5]. On the other hand, the Hilbert space of N qubits has dimension $\dim \mathcal{H} = 2^N$. Therefore, simulating the evolution of N non-entangled and non-entangling qubits would require much less classical resources than simulating N qubits which can become entangled.

Other examples of protocols exploiting entanglement consist of quantum cryptography [6–8], quantum communication [9], quantum energy teleportation [11], and protocols with repeated measurements [44–48].

[3]The state ρ is separable if it can be written as $\rho = \sum_i p_i \, (\rho_{i,A} \otimes \rho_{i,B})$, where p_i are probabilities ($\sum_i p_i = 1$) and $\rho_{i,A}$ and $\rho_{i,A}$ are possibly different local states of systems A and B, respectively. A separable state is not entangled by definition.

[4]By only using LOCC operations.

[5]We are neglecting "global" phase differences among the qubits. In other words, we are associating just a Bloch sphere to each qubit.

Although the majority of quantum information protocols rely on two-level systems [10], d-level systems (qudits) may be more powerful for information processing [49–53]. Indeed, the higher-dimensionality allows for information-coding with increased density, leading to a simplification of the design of circuits [54], since the number of logic gates is reduced. The realization of high-dimensional systems and their control has thus attracted much attention [55, 56]. Logical operations for qudits have already been implemented in systems like molecular magnet transistors [57], superconducting systems [58], and integrated optics [59–61]. In particular, single-qudit gates connected to the generalized CNOT gate [62], also called controlled-SUM [58], have already been experimentally implemented [63, 64][6]. Moreover, universal quantum computation based on trapped ions qudits has been suggested to be feasible [65].

Since entanglement has so many applications, the study of suitable protocols to generate entangled states in a great variety of physical setups has attracted much attention in the last decades [23, 24, 27–31, 66–75]. These protocols typically exploit unitary processes [71, 72, 74] and, possibly, measurements [71, 73, 75]. On the other hand, dissipative processes have been also identified as possible sources of entangled states, e.g, when the steady states of the dissipative dynamics are entangled [24, 27–31]. In particular, entangled states can be obtained through zero-temperature thermalization protocols requiring the implementation of suitable interaction terms such that the ground state of the total Hamiltonian is the desired entangled state.

However, generating quantum states with a certain amount of entanglement usually requires converting other resources into it, such as coherence [76, 77], non-equilibrium thermal resources [77], and energy [78, 79]. Among these resources, energy is one of the most important with regard to the evaluation of the generation cost so that, recently, some studies dealt with the energy cost of quantum operations [80], including the generation of correlations [78] and entanglement [81–83].

In this context, efficient ways to generate entangled states of arbitrary dimensions are desirable and understanding how energy and entanglement are connected can be crucial in order to design quantum technologies in a more efficient manner [84]. Other works investigated the energy cost of generating or extracting entanglement [81, 82]. In particular, some entanglement extraction protocols can be optimized by finding a minimum energy pure state with an assigned entanglement [82]. However, this has been done for interacting systems and the explicit solution has been found only for a specific toy model. Our contribution to this topic is given in chapter 7 of this Thesis, where we introduce what we call minimum energy entangled states (MEESs), i.e., states of a bipartite non-interacting system which have the minimum possible average energy for a given amount of entanglement.

Let us now introduce the LOCC framework and how entanglement can be quantified within it.

[6]The generalized CNOT gate will be used as a crucial ingredient of some of the protocols proposed in chapter 7.

2.1.1 The LOCC framework

Let us suppose that two experimenters have each one access to just one part of a bipartite system, respectively. Then, physically, they can only do local operations on their subsystems. Again, as it is customary in quantum information, we will call the experimenter with access to system A, Alice, and the one with access to system B, Bob. Assuming that they can avoid dissipation from the environment, their action on the systems will be described by local unitary operators and local measurements. Additionally, they can communicate between themselves by classical means. Local unitary operators have the form $U_A \otimes \mathbb{I}_B$ and $\mathbb{I}_A \otimes U_B$ and the measurements that they can do will be described by generalised measurements, which can be obtained as combinations of projective measurements and unitary operations [10]. A generalised measurement is described by a set of operators M_a with the property

$$\sum_a M_a^\dagger M_a = \mathbb{I}. \tag{2.1.2}$$

After, the measurement the state of the system is given by [10]

$$\rho_a = \frac{M_a \rho M_a^\dagger}{\mathrm{Tr}\left\{M_a \rho M_a^\dagger\right\}}, \quad \text{with probability} \quad p_a = \mathrm{Tr}\left\{M_a \rho M_a^\dagger\right\}. \tag{2.1.3}$$

In general, every operation on a quantum system can be described by a map called quantum operation, or quantum channel in quantum information [10]. A quantum operation $\Phi(\cdot)$ maps a state ρ into the state $\Phi(\rho)$, which does not need to be in the same Hilbert space of ρ. An LOCC quantum channel is a quantum operation obtainable by composing unitary operations, measurements, and communications allowed in LOCC.

A procedure in LOCC can be divided into rounds. During each round, both parts can perform any number of local operations but only one of them can send, once, classical information to the other part. If we take Alice to stay "on the left" and Bob "on the right", then if Alice send the information the single round is called **one-way right** and **one-way left** otherwise.

LOCC is an example of quantum resource theory. In general, a resource theory is a theory in which the possible operations that can be done on a system are restricted by some constraints and it is supposed that to perform a given protocol some special states belonging to other systems are unlimitedly available for free (see Ref. [85] for a general review of quantum resource theories). These external systems in these particular states are called "free resources" [85, 86]. In the case of LOCC the free resources are local systems not correlated with the systems of the other parties while the allowed operations are the LOCC-operations. We will introduce another quantum resource theory in section 2.3.1.

Regarding pure states, one natural question arises: whether Alice and Bob can obtain the state $|\phi\rangle$ from the state $|\psi\rangle$ using only operations allowed in the LOCC framework. We say that a pure state $|\psi\rangle$ is LOCC-equivalent to state $|\psi'\rangle$, written as $|\psi\rangle \sim |\psi'\rangle$, if one can be obtained from the other just by applying local unitary operators. This is

possible if and only if their Schmidt coefficients are equal[7]. Adding measurements and classical communications to the mix, the set of obtainable states starting from $|\psi\rangle$ is determined by Nielsen's theorem [10, 87].

2.1.2 Nielsen's theorem

Nielsen's theorem is based on the concept of majorization. Suppose $x \equiv (x_1, \ldots, x_d)$ and $y \equiv (y_1, \ldots, y_d)$ are real d-dimensional vectors. Then, x is majorized by y ($x \prec y$) if for each k in the range $1, \ldots, d$ one has

$$\sum_{j=1}^{k} x_j^{\downarrow} \leq \sum_{j=1}^{k} y_j^{\downarrow}, \tag{2.1.4}$$

with equality holding when $k = d$, and where the $\downarrow$ indicates that elements are to be taken in descending order, so, for example, $x_1^{\downarrow}$ is the largest element in $x_1, \ldots, x_d$. The majorization relation is a partial order on real vectors, with $x \prec y$ and $y \prec x$ if and only if $x = y$.

Suppose that Alice and Bob share a quantum state $|\psi\rangle$ and they want to transform it in the state $|\phi\rangle$ through LOCC. Being two pure states, they both have a Schmidt decomposition[7]

$$|\psi\rangle = \sum_i \sqrt{\lambda_i}\, |a_i b_i\rangle\,, \quad |\phi\rangle = \sum_i \sqrt{\gamma_i}\, |A_i B_i\rangle\,. \tag{2.1.5}$$

Define $\overline{\lambda}$ and $\overline{\gamma}$ as the vectors of the squared Schmidt coefficients of the two states, respectively.[8] Nielsen's theorem states that the transformation is possible if and only if $\overline{\lambda} \prec \overline{\gamma}$. The proof of Nielsen's theorem can be found in Refs. [10] or [87] (the original one). It is worth notice that there exists a generalization of Nielsen's theorem due to Vidal [88, 89], which applies for non-deterministic LOCC operations, also called stochastic LOCC or SLOCC.

Turning back to deterministic LOCC, a first consequence of Nielsen's theorem is that the maximum entangled state (suppose $N_A \leq N_B$)

$$|\psi\rangle = \frac{1}{\sqrt{N_A}} \sum_i |a_i b_i\rangle \tag{2.1.6}$$

is majorized by every other pure state. Therefore, any other pure state can be obtained from it through LOCC. A second consequence is that the Schmidt number of a state cannot be increased by LOCC operations. Let us suppose that $|\psi\rangle$ has Schmidt number r and $|\phi\rangle$ has Schmidt number $r+1$, then

$$\sum_{i=1}^{r} \lambda_i = 1 > \sum_{i=1}^{r} \gamma_i = 1 - \gamma_{r+1}, \tag{2.1.7}$$

[7] See Appendix 2.A.2 for a brief description of the Schmidt decomposition.

[8] If one of the vectors has more components than the other one, we just add null components to the vector with less components.

so $\overline{\lambda}$ is not majorized by $\overline{\gamma}$.

Finally, let us connect the Nielsen's theorem to the so-called entropy of entanglement. The entropy of entanglement $\mathcal{E}(|\psi\rangle)$ is the von Neumann entropy of one of the two reduced states of a bipartite system in a pure state[9]. The opposite of the entropy of entanglement, i.e., $-\mathcal{E}(\cdot)$ is an isotone function, that is a function $f : \mathbb{R}^d \to \mathbb{R}$ such that $y \succ x \implies f(y) \geq f(x)$. Isotone functions for LOCC transformations are also called entanglement monotones. Another important family of entanglement monotones is given by $\mathrm{Tr}\left(\rho_\psi^k\right)$, $\forall k \geq 1$, where ρ_ψ is one of the two reduced density matrices obtainable by tracing on a subsystem the pure state $|\psi\rangle$. Therefore, we have

$$|\psi\rangle \to |\phi\rangle \implies \mathcal{E}(|\phi\rangle) \leq \mathcal{E}(|\psi\rangle) \quad \text{and} \quad \mathrm{Tr}\left(\rho_\psi^k\right) \leq \mathrm{Tr}\left(\rho_\phi^k\right) \quad \forall\, k \geq 1. \tag{2.1.8}$$

If the Schmidt number is 2 the decreasing of the entropy of entanglement is also a sufficient condition for the existence of the LOCC transformation [87]. Moreover, notice that the second disequality of Eq. (2.1.8) concerns the purity for $k = 2$. Therefore, even purity of the subsystems is an entanglement monotone.

In chapter 7 we will find that MEESs[10] form a family of states in which, for every value of the entropy of entanglement, all MEESs with less entropy of entanglement can be obtained through LOCC so that the decreasing of the entropy of entanglement is a sufficient condition for the existence of the LOCC transformation even if the dimensionality of the systems is higher than 2×2[11]. In this sense, we will say that MEESs are LOCC-connected.

2.1.3 Entanglement quantifiers

In the limit of many copies, the majorization requirement for LOCC-transitions can be relaxed. Let us suppose that Alice and Bob have access to n copies of the state $|\psi\rangle$. Then, in the limit of many copies, it can be shown [90] that Alice and Bob can create m copies of the state $|\phi\rangle$ if and only if $n\mathcal{E}(|\psi\rangle) \geq m\mathcal{E}(|\phi\rangle)$[12]. This is the reason why the entropy of entanglement is the standard quantifier for entanglement in bipartite systems pure states [34, 91, 92].

Regarding mixed states, there is a plethora of entanglement quantifiers (or entanglement measures). We address the reader to Refs. [92] for more information. What interests us is that, following Ref. [92], they have to satisfy the following requirements:

1. An entanglement measure $\mathcal{E}_m(\rho)$ is a mapping from density matrices into real positive numbers.

2. $\mathcal{E}_m(\rho) = 0$ is the state ρ is separable.

[9] Alternatively, it can be seen as half of the mutual information [cf. Eqs. (2.1.1) and (2.A.4)].
[10] Minimum energy entangled states, see chapter 7.
[11] For a bipartite system with dimensions $N_A \times N_B$ the Schmidt number of a MEES is $\min\{N_A, N_B\}$.
[12] This proof is made simpler by Nielsen's theorem [87].

3. The entanglement measure does not increase under LOCC, i.e., $\mathcal{E}_m(\rho) \geq \mathcal{E}_m(\Phi(\rho))$ where $\Phi(\cdot)$ is the quantum channel referring to some LOCC transformation.

4. When applied to pure states, the entanglement measure reduces to the entropy of entanglement, i.e., $\mathcal{E}_m(|\psi\rangle\langle\psi|) = \mathcal{E}(|\psi\rangle)$.

Finally, it is also usually required that the entanglement measure is convex, i.e.

$$\mathcal{E}_m\left(\sum_i p_i \rho_i\right) \leq \sum_i p_i \mathcal{E}_m(\rho_i), \tag{2.1.9}$$

where $0 \leq p_i \leq 1$ and $\sum_i p_i = 1$. The convexity property will be the crucial element to extend our results on pure states to mixed states in chapter 7[13].

2.2 Open quantum systems

Quantum systems whose evolution are affected by the interaction with the environment are called *open quantum systems*, as opposed to closed ones. Indeed, every system, quantum or classical, can never be perfectly isolated from its environment, therefore the study of open quantum systems is ubiquitous and of great importance for the development of quantum technologies [18].

From a purely theoretical point of view, the evolution of the open system together with the reservoir could be analytically treated since it is the evolution of a closed system. In formulas:

$$\rho_T(t) = U_T(t, t_0)\rho_T(t_0)U_T^\dagger(t, t_0), \tag{2.2.1}$$

where $\rho_T(t)$ is the density matrix of the whole quantum system[14] and $U_T(t, t_0)$ its temporal evolution operator. Since one is usually interested in the dynamics of the open system alone, one should compute

$$\rho_S(t) = V(t, t_0)\rho_S(t_0) \equiv \mathrm{Tr}_R\left\{U_T(t, t_0)\rho_T(t_0)U_T^\dagger(t, t_0)\right\}, \tag{2.2.2}$$

where $\rho_S(t)$ is the system state and $V(t, t_0)$ is the quantum operation above defined. However, computing $\rho_S(t)$ in this way is usually impossible because the global system has too many degree of freedom with complex interactions. Therefore, methods to approximate the dynamics of $\rho_S(t)$ have been devised and we refer the reader to Ref. [12] for a comprehensive survey.

Whatever the kind of interaction with the environment, a quantum operation has necessarily the following properties [10, 12]:

1. It is linear, i.e., $\Phi(\rho + \sigma) = \Phi\rho + \Phi\sigma$.

2. It is positive, i.e., $\langle\psi|\Phi\rho|\psi\rangle \geq 0$ for each vector $|\psi\rangle$ and ρ such that $\langle\psi|\rho|\psi\rangle \geq 0$.

[13] See section 7.2

[14] Including the environmental degrees of freedom.

3. It is trace preserving: $\mathrm{Tr}\{\rho\} = \mathrm{Tr}\{\Phi\rho\}$.

4. It is completely positive, i.e., the map $\mathbb{I}_n \otimes \Phi$ is positive for any n[15].

Such kind of maps are also called completely-positive trace-preserving (CPTP) maps and, indeed, all of the above properties can be shown to hold good for the quantum operation of Eq. (2.2.2) [12].

The physical meaning of complete positivity is related to quantum correlations. Let us consider two systems A and B, described by the states ρ_A and ρ_B and suppose that we know only what is happening to system A. We assume that they evolve separately so that we can describe the action of a generic quantum operation as $\Phi_A \otimes \Phi_B$, where Φ_A and Φ_B are positive trace-preserving maps on A and B, respectively. If the initial state is a product state, then the dynamics is surely physical. However, the two systems could be correlated, so that $\rho \neq \rho_A \otimes \rho_B$. In this case we must require complete positivity. In fact, the operation can be rewritten as the composition of two operations

$$\Phi_A \otimes \Phi_B = (\Phi_A \otimes \mathbb{I}_B)\,(\mathbb{I}_A \otimes \Phi_B)\,, \tag{2.2.3}$$

where $\mathbb{I}_A$ and $\mathbb{I}_B$ are the identity maps in the respective spaces. Whatever the dimension of both systems, the map $\Phi_A \otimes \Phi_B$ will surely be positive if both Φ_A and Φ_B are completely positive. It follows that the map describing the evolution of the system under our control, i.e., system A, has to be completely positive since we could not know if A is correlated to another system that is not in our description.

One of the most-common description of an open system dynamics is given in terms of Markovian master equations, which we will now introduce.

2.2.1 Markovian dynamics

Assuming that at the start of the dynamics $\rho_T(t_0) = \rho_S(t_0) \otimes \rho_B(t_0)$, a common situation is that in which the open quantum systems dynamics does not affect the dynamics of the reservoir, i.e., the reservoir has its own dynamics such that, on the time-scale on which $\rho_S(t)$ evolves, we can always consider $\rho_B(t) = \rho_B(t_0)$ and treat the two systems as uncorrelated. This is called the *Born approximation* or *weak coupling approximation* [12]. Moreover, if we also assume that the dynamical effects due to the interaction with the environment are slow[16], the *Markov approximation* leads us to a Markovian dynamics for $\rho_S(t)$ [12]. A Markovian dynamics is a dynamics for which the evolution of a system only depends on its actual state and not on its past states. This is the reason for which, on the other hand, a non-Markovian dynamics is connected with the memory of the reservoir about the past state of the open quantum system.

From the mathematical point of view, if the total system Hamiltonian is time-independent, the operation $V(t, t_0)$ becomes dependent only on the time difference $t - t_0$

[15] We denote by $\mathbb{I}_n$ the identity operator in an n-dimensional Hilbert space.

[16] More precisely, one must assume that $\rho_S^I(t)$ is slowly-varying, where $\rho_S^I(t)$ is the density matrix in the interaction picture. See Ref. [12] for more details.

and the process is called homogeneous. Hereafter, we set $t_0 = 0$ so that we can just write $V(t)$. If the dynamics is Markovian, $V(t)$ also assumes the semigroup property [12]

$$V(t_1)V(t_2) = V(t_1 + t_2), \quad t_1, t_2 \geq 0. \tag{2.2.4}$$

Focusing on the case of homogeneous Markovian dynamics, under certain mathematical conditions [12], the operation $V(t)$ can be cast in the exponential form $V(t) = \exp(\mathcal{L}t)$, where $\mathcal{L}$ is the generator of the semigroup, it is called Lindbladian, and may be regarded as a generalization of the Liouville super-operator [12]. This immediately leads to the first-order differential equation for the state ρ_S of system S,

$$\frac{\mathrm{d}}{\mathrm{d}t}\rho_S(t) = \mathcal{L}\rho_S(t). \tag{2.2.5}$$

The above equation is called Markovian master equation.

For bounded operators, Lindblad proved in Ref. [16] that the most general form of the generator $\mathcal{L}$ is[17]

$$\mathcal{L}(\rho_S) = -\frac{i}{\hbar}[H, \rho_S] + \sum_{k=1}^{N_S^2-1} \gamma_k \left(A_k \rho_S A_k^\dagger - \frac{1}{2}\left\{ A_k^\dagger A_k, \rho_S \right\} \right), \tag{2.2.6}$$

where H is an Hermitian operator (usually strictly connected with the Hamiltonian H_S of system S), the A_k are arbitrary operators, $N_S = \dim \mathcal{H}_S$[18], and the γ_k are non-negative quantities. The second term of Eq. (2.2.6) is also called dissipator and denoted by $\mathcal{D}(\rho_S)$ so that the master equation can be written as

$$\frac{\mathrm{d}}{\mathrm{d}t}\rho_S = -\frac{i}{\hbar}[H, \rho_S] + \mathcal{D}(\rho_S). \tag{2.2.7}$$

With the same time-independent generator $\mathcal{L}$, we can also write the Heisenberg dynamics of a time-independent operator O in the Schrödinger picture. Its correspondent Heisenberg picture operator $O_H(t)$ evolves according to[19]

$$\frac{\mathrm{d}}{\mathrm{d}t}O_H = \mathcal{L}^\dagger(O_H) = \frac{i}{\hbar}[H, O_H] + \sum_{k=1}^{N_S^2-1} \gamma_k \left(A_k^\dagger O_H A_k - \frac{1}{2}\left\{ A_k^\dagger A_k, O_H \right\} \right). \tag{2.2.8}$$

The above equation is called adjoint master equation.

Although Markovian master equations have proven invaluable for the description of numerous situations, the interest in non-Markovian dynamics has recently surged due to the fact that numerous quantum systems exhibit pronounced memory effects [93]. Numerous techniques have been developed to deal with non-Markovian open quantum systems and to quantify how much a given dynamics is non-Markovian (see, for example,

[17] We drop the explicit temporal dependence of $\rho_S(t)$ to lighten the notation.
[18] $\mathcal{H}_S$ is the Hilbert space of system S
[19] We drop the explicit temporal dependence of $O_H(t)$ to lighten the notation.

[94]). Regarding the dynamics, a recent line of research consists in describing the non-Markovian dynamics of the open system by finding the Markovian dynamics of an enlarged virtual system [95–97]. This technique is sometimes called "Markovian embedding" [95]. This is particularly true in the case of open systems described through collision models [98, 99]. Finally, regarding the problem of measuring non-Markovianity, many efforts have been done in the specific case of gaussian dynamics [100, 101]. In particular, the use of Gaussian dynamics in collision models is an actual active research topic [102, 103] to which chapter 5 of this thesis belongs. We will briefly introduce collision models in this section and Gaussian states and dynamics later in this chapter.

2.2.2 Microscopic derivation and phenomenological approach.

To obtain a master equation describing the dynamics of a given open quantum system, the standard approach is to perform a so-called microscopic derivation [12]. To arrive at the final result, different approximations such as the Born-Markov approximation and the secular one [12] can be made based on the physical system at hand. We refer to Ref. [12] for different possible situations therein described. In particular, the most common elements[20] of most physical setups have been studied within this approach so that their master equation is available in literature. Master equations derived within this standard procedure are usually denoted as microscopic master equations. In most situations, the microscopic master equations are Markovian and have the form given in Eq. (2.2.6).

When the system at hand is composed of various interacting subsystems, another, easier, approach called "phenomenological approach" has been pursued in literature. In this case, one simply uses the Hamiltonian of the system to write the unitary part of the Lindbladian and adds the dissipators correspondent to each element of the setup independently. Usually, when the interaction among the subsystems is weak, the master equation based on this approach gives more or less the same results that the proper microscopic master equation would have given. An example of the possible differences between the two approaches is given in Refs. [104, 105]. We denote by phenomenological master equation the master equations written by making these approximations. The starting point of chapter 6 is obtained within this approach.

An important property of microscopic master equations is that, in general[21], they lead a multi-partite interacting system to a thermal state at temperature T when the reservoir is in the thermal state at temperature T and the system-environment coupling is weak [12]. On the contrary, the phenomenological master equations do not usually lead to the correct thermal state. For example, in Ref. [104] it leads the system to the tensor product of the thermal state of its components. It is worth to notice that the difference between the proper thermal state and the product state of subsystems thermal states is not significant when the interaction between the subsystems is weak compared to the energies of the bare subsystems.

[20] As examples of these common elements we cite the damped harmonic oscillator and the damped qubit.

[21] See Ref. [12] for more details on the conditions needed for the thermalization.

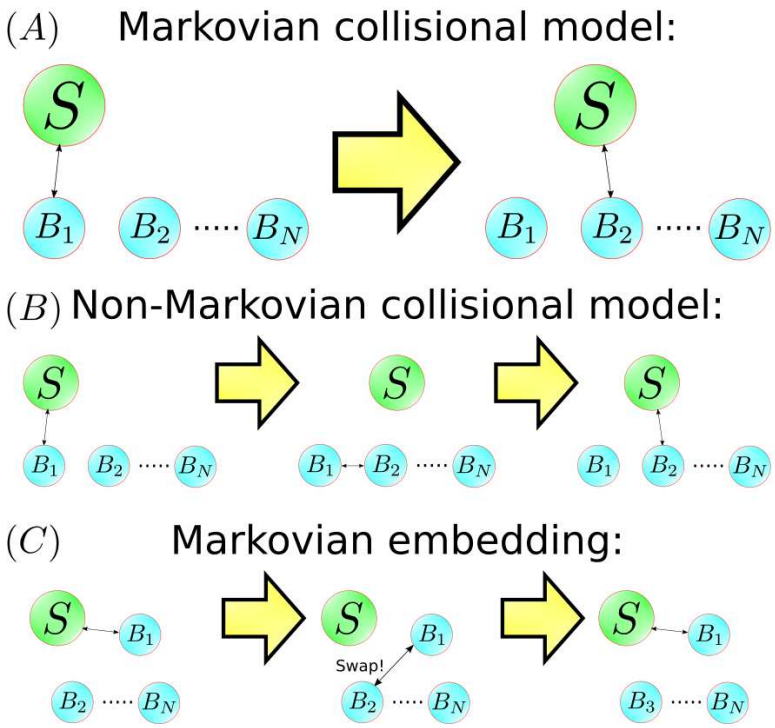

Figure 2.1: This figure illustrates schematically two collision models: a Markovian one (A) and a non-Markovian one (B). In the non-Markovian one, the intra-bath interactions are responsible for the memory effects. Panel (C) shows a pictorial representation of the so-called Markovian embedding.

2.2.3 Collisional models and Markovian embedding.

Another useful framework for describing the dynamics of open quantum systems is the so-called collision model (CM). In this model, the environment is composed of simple identical units (also called ancillas) which interact sequentially with the system of interest and also among themselves. Since both the open quantum system and the units are simple, the dynamics of their collisions can typically be treated analytically or, at least, the numerical simulation is feasible. Many different CMs can be constructed. Here, we will introduce one of the CMs used in Ref. [99] since it is also the one employed in chapter 5. This model we are going to introduce can be made both Markovian [Fig. 2.1 (A)] and non-Markovian [Fig. 2.1 (B)]. Since the Markovian case can be seen as sub-case of the non-Markovian one, we will directly introduce the non-Markovian one.

Let us consider a system S and a possibly infinite number of ancillary systems B_1, B_2 and so on. The initial state of the whole system is given by

$$\rho_T(0) = \rho_S(0) \otimes \rho_{B_1} \otimes \rho_{B_2} \otimes \dots, \tag{2.2.9}$$

where the initial state of the ancillas are all equal, i.e., $\rho_{B_n} = \rho_{B_m}$ for $n \neq m$. Let us

define the following unitary operators:

$$U_{S,n} = e^{-(i/\hbar)H_{SB,n}\tau}, \qquad V_{E,n} = e^{-(i/\hbar)H_{BB,n}\tau}, \tag{2.2.10}$$

where τ is the duration of each collision[22], $H_{SB,n}$ is the total Hamiltonian during the interaction S-B_n, and $H_{BB,n}$ is the total Hamiltonian during the interaction B_{n-1}-B_n. One also assumes that the states of systems B do not change when they are not involved in a collision[23] and that the time between two subsequent collisions is zero. Now we can define the first step of this CM and the following ones:

$$\Phi_1[\rho_T(0)] = \rho_T(1) = U_{S,1}\rho_T U_{S,1}^\dagger, \qquad \Phi_n[\rho_T(n-1)] = \rho_T(n) = U_{S,n}V_{E,n}\rho_T V_{E,n}^\dagger U_{S,n}^\dagger. \tag{2.2.11}$$

By denoting with $\mathrm{Tr}_{\overline{S}}$ the trace over all systems but S and $\Phi(n) = \Phi_n \circ \cdots \circ \Phi_1$, we get the state of system S after n steps as

$$\rho_S(n) = \Lambda(n)\rho_S(0) \equiv \mathrm{Tr}_{\overline{S}}\left\{\Phi(n)\rho_T(0)\right\}. \tag{2.2.12}$$

If we neglect the intra-bath interactions, i.e., we write $V_{E,n} = \mathbb{I}$, it is easy to see that the dynamics given by $\Lambda(n)$ is Markovian in the sense that the state $\rho_S(n)$ depends only on $\rho_S(n-1)$. Otherwise, the dynamics can be non-Markovian. Nevertheless, we can make use of the Markovian embedding procedure to describe the Markovian dynamics of an enlarged system and, knowing this, also obtain the non-Markovian dynamics of system S. In fact [see Fig. 2.1 (C)], it is possible to show that [99]

$$\Lambda(n)\rho_S(0) = \mathrm{Tr}_A\left\{\tilde{\Lambda}(n)\rho_{SA}(0)\right\}, \quad \tilde{\Lambda}(n) = \tilde{\Lambda}_n \circ \cdots \circ \tilde{\Lambda}_1, \quad \rho_{SA}(0) = \rho_S(0) \otimes \rho_{B_1}, \tag{2.2.13}$$

where

$$\tilde{\Lambda}_1 = \Phi_1, \quad \tilde{\Lambda}(n)\rho_{SA}(n-1) = \mathrm{Tr}_{B_{n-1}}\left\{U_{S,n}S_{1,n}\tilde{V}_{E,n}\rho_T\tilde{V}_{E,n}^\dagger S_{1,n}U_{S,n}^\dagger\right\}, \tag{2.2.14}$$

and $S_{n,m}$ is the standard Hermitian swap operator implying $S_{n,m}(\rho_n \otimes \rho_m)S_{n,m} = \rho_m \otimes \rho_n$ [99] and $\tilde{V}_{E,n}$ is equal to $V_{E,n}$ a part from being applied to systems B_1 and B_n instead of B_{n-1} and B_n[24].

To sum up, the advantage of using collision models is given by their simplicity and the physical insight they can provide. Nevertheless, while they can be used to describe highly ingegnerized baths really composed of units interacting sequentially with the open system, their connection to realistic bath typically treated within the microscopic approach is still nebulous.

[22] The duration of each collision is assumed to be the same for the sake of simplicity.

[23] This is not the case, for example, if we take ρ_{B_i} to be a non-equilibrium state subject to the evolution of its bare Hamiltonian.

[24] See Eq. (2.2.10).

2.2.4 Adiabatic elimination in open quantum systems

A common situation encountered in open quantum systems is the case of a bipartite system in which one subsystem dynamics is fast compared to that of the other one. In quantum optics, an example of this situation is given by the so-called bad-cavity limit, in which an optical cavity containing one or more atoms is very leaky. If one is interested only in the dynamics of the atoms within the cavity, it can perform the so-called adiabatic elimination on it and find an effective dynamics for the atoms [106, 107]. In Sec. 2.4.2 we will give more details about this specific physical setup and we will perform the adiabatic elimination in chapter 6 to compare the cases of one- and two-photon coupling between the atoms and the cavity. In particular, we will use a very recent technique to perform the adiabatic elimination [32, 33], which we briefly resume in this section.

To apply this technique we have to treat separately the two subsystems. We call "system A" the subsystem with fast dynamics and "system B" the one with the slow dynamics. Moreover, we must assume that the two subsystems interact weakly. As final requirement, system A has to converge to a unique steady state, which we call ρ_A^{st}, when it is influenced uniquely by its own Lindbladian. For a far more detailed discussion see Ref. [33].

Following the prescription of Ref. [33], the Lindbladian describing the evolution of the density matrix of the global system, ρ_G, is given by:

$$\dot{\rho}_G = \mathcal{L}_A(\rho_G) + \epsilon\mathcal{L}_B(\rho_G) - \frac{i}{\hbar}\epsilon[H_{\mathrm{int}}, \rho_G], \tag{2.2.15}$$

where ϵ is the quantity which will play the role of perturbative parameter in the expansion of system B dynamics and each Lindbladian is of the form

$$\mathcal{L}_r(\bullet) = -\frac{i}{\hbar}[H_r, \bullet] + \sum_n \mathcal{D}_{X_r^{(n)}}(\bullet), \tag{2.2.16}$$

where $r = A$, B, and

$$\mathcal{D}_{X_r^{(n)}}(\bullet) = X_r^{(n)} \bullet X_r^{\dagger(n)} - \frac{1}{2}\Big\{X_r^{\dagger(n)} X_r^{(n)}, \bullet\Big\}. \tag{2.2.17}$$

The interaction Hamiltonian can be written in the general form

$$H_{\mathrm{int}} = \hbar c \sum_{k=1}^{M} A_k \otimes B_k^{\dagger}, \tag{2.2.18}$$

where A_k and B_k are not necessarily hermitian and c is a constant with the dimensions of a frequency.

The goal of the adiabatic elimination procedure is to find the super-operator describing the dynamics of the reduced density matrix of system B, $\rho_B = \mathrm{Tr}_A\{\rho_G\}$, as

$$\dot{\rho}_B = \mathcal{L}_S(\rho_B) = \sum_{m\geq 0} \epsilon^m \mathcal{L}_{S,m}(\rho_B), \tag{2.2.19}$$

and to be able to return back to the global dynamics through

$$\rho_G = \mathcal{K}(\rho_B) = \sum_{m\geq 0} \epsilon^m \mathcal{K}_m(\rho_B), \tag{2.2.20}$$

where, at any order in ϵ, $\mathcal{L}_S$ is a Lindbladian and $\mathcal{K}$ is a Kraus map[25]. In the case analyzed in chapter 6, we want to obtain a second order equation for the dynamics of system B since, at first order, the adiabatic elimination will not give rise to dissipative terms.

Due to the peculiarities of the method employed, the zero-order terms can be chosen with a certain arbitrariness. Following Ref. [33], the simplest choice is $\mathcal{L}_{S,0}(\rho_B) = 0$ and $\mathcal{K}_0(\rho_B) = \rho_A^{\rm st} \otimes \rho_B$. Then, the first order reduced dynamics is given by [33]

$$\dot{\rho}_B = \epsilon \mathcal{L}_{S,1}(\rho_B), \tag{2.2.21}$$

where

$$\mathcal{L}_{S,1}(\rho_B) = -ic \sum_{k=1}^{M} \left[\mathrm{Tr}_A \left\{ A_k \rho_A^{\rm st} \right\} B_k^\dagger, \rho_B \right] + \mathcal{L}_B(\rho_B). \tag{2.2.22}$$

The super-operator $\mathcal{K}_1$ can be obtained as follows [33]:

$$\mathcal{K}_1(\rho_B) = -ic \sum_{k=1}^{M} F_k \left(\rho_A^{\rm st} \right) \otimes \left(B_k^\dagger \rho_B \right) + \text{h.c.}\,, \tag{2.2.23}$$

where $F_k\left(\rho_A^{\rm st}\right) = \tau \left[\mathcal{J}_A(A_k \rho_A^{\rm st}) - \mathrm{Tr}\{A_k \rho_A^{\rm st}\} \rho_A^{\rm st} \right]$, h.c. indicates the hermitian conjugate, and $\mathcal{J}_A$ and τ are defined in the following. In general, the $\mathcal{J}_A$ super-operator has the form

$$\mathcal{J}_A(Z) = \frac{1}{\tau} \int_0^\infty e^{t\mathcal{L}_A} \left(Z - R(Z) \right) \mathrm{d}t + R(Z), \tag{2.2.24}$$

where $\tau > 0$ such that $-\mathcal{L}_A\left(\tau \mathcal{J}_A(Z)\right) = Z - R(Z)$ and $R(Z) = \lim_{s\to+\infty} e^{s\mathcal{L}_A}(Z) = \mathrm{Tr}_A\{Z\}\rho_A^{\rm st}$. Notice that even if it could seem that the results of the procedure depend on the choice of the parameter τ, for the case we are going to examine in chapter 6 the value of this parameter will be irrelevant.

In order to find the second order dynamics of system B, it is useful to define two matrices whose elements are given by

$$X_{k,j} = c^2 \left[\mathrm{Tr} \left\{ F_j \left(\rho_A^{\rm st} \right) A_k^\dagger \right\} + \text{h.c.} \right], \quad Y_{k,j} = \frac{c^2}{2i} \left[\mathrm{Tr} \left\{ F_j \left(\rho_A^{\rm st} \right) A_k^\dagger \right\} - \text{h.c.} \right]. \tag{2.2.25}$$

The matrix X is Hermitian and positive semi-definite. Then, there exists a non-unique $M \times M$ matrix Λ such that $X = \Lambda\Lambda^\dagger$.

The second order dynamics is given by [33]

$$\dot{\rho}_B = \epsilon \mathcal{L}_{S,1}(\rho_B) + \epsilon^2 \mathcal{L}_{S,2}(\rho_B), \tag{2.2.26}$$

[25] A Kraus map $\mathcal{K}$ is a map that can be decomposed as $\mathcal{K}(\rho) = \sum_i K_i \rho K_i^\dagger$ where K_i are operators such that $\sum_i K_i^\dagger K = \mathbb{I}$ [33].

where

$$\mathcal{L}_{S,1}(\rho_B) = -i\sum_{k=1}^{M}\left[\mathrm{Tr}_A\left\{A_k\rho_A^{\mathrm{st}}\right\}B_k^\dagger,\rho_B\right] + \mathcal{L}_B(\rho_B),$$
$$\mathcal{L}_{S,2}(\rho_B) = -i\left[\sum_{k,j=1}^{M} Y_{k,j}B_kB_j^\dagger,\rho_B\right] + \sum_{p=1}^{M}\mathcal{D}_{L_p}(\rho_B), \quad L_p = \sum_{j=1}^{M}\Lambda_{j,p}^* B_j^\dagger. \tag{2.2.27}$$

2.3 Quantum thermodynamics

Quantum thermodynamics is a vast research field encompassing different areas of physics. It goes from conceptual topics like typicality [108–110] to more practical ones like improving the performance of thermal machines [20]. On the one hand, tipicality is a promising way to explain the emergence of themodynamics from quantum mechanics without invoking additional axioms. On the other hand, the interest on practical aspects of quantum thermodynamics has been recently growing due to the experimental advances and the possible applications in nanoscale devices [111]. For example, an experimental realization of a quantum thermal machine in which the working fluid consists of a single atom has been done very recently [112]. Many other platforms for quantum thermodynamic experiments are described in Ref. [20]. We refer the reader to Refs. [20, 110, 111] for more detailed discussions on both theoretical and experimental aspects of quantum thermodynamics. Here, we will deal with the more practical-oriented, but still theoretical, facets concerning thermal machines.

As already anticipated, one of the most intriguing problems concerns the realization of thermodynamic processes at a quantum level [113–119]. Many results have been recently obtained inside the theoretical framework of the thermodynamic resource theory (TRT), which, as the LOCC framework of section 2.1.1, is a quantum resource theory. Among all the possible quantum processes studied in TRT, work-extraction protocols play a relevant role [120, 121]. However, most of them are not easy to realize experimentally. For this reason, various efforts have been done to understand how to design realizable TRT protocols [122, 123] although most proposals require fine control of the system for an experimental realization. For example, in a process composed of many steps, it could be required to turn on and off a specific interaction for an amount of time specific to each step. We will propose and study a protocol not requiring fine tuning in chapter 3.

Another topic of actual interest is the study of quantum thermodynamic cycles focusing on the tradeoff between power and efficiency [20, 111, 124, 125], with power usually increased at the expense of efficiency. A very important result of the nineteenth century physics consists in the determination of the Carnot efficiency: the efficiency of a thermal engine operating between two thermal baths at different temperatures is limited by the Carnot value $\eta_C = 1 - T_c/T_h$ where T_h is the temperature of the hot bath and T_c of the cold one ($T_h > T_c$). However, the Carnot limit is a very general bound usually attained for ideal machines with vanishing power [20]. For an engine operating at maximum power, the efficiency is not bounded by a universal value, and its maximum value is usually model dependent. Often, the efficiency at maximum power

is limited by the so-called Curzon-Ahlborn efficiency[26] $\eta_{CA} = 1 - \sqrt{T_c/T_h}$ [126–132]. However, this limit is not always valid [20, 127–129, 131, 132] and can be surpassed [133, 134]. We will propose and study two thermodynamic cycles in chapter 4, focusing on the interplay of power and efficiency, and their relation with the waiting times of the machines implementing the cycles.

Let us now briefly introduce TRT.

2.3.1 Thermodynamic resource theory

In Sec. 2.1.1 we examined the LOCC framework, which allowed us to quantify the amount of entanglement of a given bipartite system state. The LOCC framework is an example of quantum resource theory [85]. In general, a resource theory is a theory in which the possible operations that can be done on a system are restricted by some constraints and it is supposed that to perform a given protocol some special states belonging to other systems are unlimitedly available for free (see Ref. [85] for a general review of quantum resource theories). These external systems in these particular states are called "free resources" [85, 86]. In the case of LOCC the free resources are local systems not correlated with the systems of the other parties while the allowed operations are the LOCC-operations. Here, we introduce the Thermodynamic Resource Theory (TRT), and refer the reader to Refs. [20, 86] for focused reviews.

An operation $\mathcal{T}(\rho)$ permitted by TRT and addressed as a Thermal Operation (TO) has the following structure:

$$\mathcal{T}(\rho) = \mathrm{Tr}_{\mathrm{bath}}\left\{U(\rho \otimes \rho_{\mathrm{bath}})U^{\dagger}\right\}, \quad [H + H_{\mathrm{bath}}, U] = 0\,, \tag{2.3.1}$$

where H is the Hamiltonian of the system described by the density operator ρ, H_{bath} is the Hamiltonian of the free resource (usually called bath) and U is a generic unitary operator that connects initial and final states of the total system (free resource included). The free resource (bath) is a system with an arbitrary Hamiltonian, assumed to be in a thermal state (ρ_{bath}) at a given temperature. In a thermal operation the bath is used only for the duration of the protocol so that the interaction between system and bath at the end and at the start of the protocol is identically zero. Then, the commutator $[H + H_{\mathrm{bath}}, U] = 0$ assures us that the global system has kept its energy unchanged (not only the mean value but also the entire distribution). This is needed because the aim of TRT is to keep track of all the energy terms involved in a possible thermal process and to find what bounds the constraints of TRT generate.

TRT requirements can be viewed as an axiomatization of thermodynamics. Therefore, it is possible to recover the thermodynamic laws from the definition of the allowed operations. This can indeed be done and even generalizations of these laws can be found [135, 136]. Moreover, regarding the resource interconversion, there exist the

[26] Most papers in literature denote this efficiency as the Curzon-Ahlborn efficiency. Others name it the Chambadal-Novikov efficiency or Chambadal-Novikov-Curzon-Ahlborn efficiency. In this thesis, we will use the more common name.

analogue of Nielsen's theorem in TRT, which instead of being based on the concept of majorization is based on that of thermo-majorization [120].

To define the thermo-majorization, we must first introduce the β-ordering. Consider a system in the state ρ. We denote by T the temperature of the bath that will be used to implement the TO and assume that the system Hamiltonian $H = \sum_i E_i \, |E_i\rangle\langle E_i|$ has no degeneracies[27]. We denote by $\overline{p}$ the population vector of ρ, with components $p_i = \langle E_i|\rho|E_i\rangle$. By putting in decreasing order the quantities $p_i e^{\beta E_i}$, where $\beta = 1/(k_B T)$, k_B being the Boltzmann constant, we obtain the vector we denote by $\overline{p}^{\downarrow\beta}$, which had the same components of $\overline{p}$ but permutated as explained and is called the β-ordered version of $\overline{p}$ [86].

Given the vector of thermal populations $\overline{g}$, with components $g_i = \langle E_i|\rho^{\rm th}|E_i\rangle$, where $\rho^{\rm th}$ is the thermal state, we can construct its β-ordered version $\overline{g}^{\downarrow\beta}$ by checking again the decreasing order of the quantities $p_i e^{\beta E_i}$. Then, we can define the so-called thermo-majorization curve $\mathbf{L}(\rho, H, T)$, obtained by plotting the set of points whose abscissa and ordinate are $(x_i, y_i) = (g_i^{\downarrow\beta}, p_i^{\downarrow\beta})$ for i going from 1 to N and adding the point $(0, 0)$. Let us now consider a target state ρ' with the property $[\rho', H] = 0$ and consider its thermo-majorization curve. The transition through TO from ρ to ρ' is possible if $\mathbf{L}(\rho, H, T)$ is always above $\mathbf{L}(\rho', H, T)$. We then say that ρ thermomajorizes ρ'. In symbols: $\rho \succ_g \rho'$. The condition

$$\rho \succ_g \rho' \implies \exists \, TO : \rho \to \rho', \tag{2.3.2}$$

becomes an "if and only if" when also ρ has the property $[\rho, H] = 0$ [120].

When the transition $\rho \to \rho'$ cannot be realized there could be situation in which, instead, the transition $\rho \otimes \sigma \to \rho' \otimes \sigma$, where σ is the state of an ancillary system, is feasible. In this case, we say that the ancillary system acts as a catalyst.

The class of permitted operations is sometimes extended. For example, in Ref. [137] authors make use of the so-called Gibbs-preserving operation. Considering a system state and the same system Hamiltonian as an object $p = (\rho, H)$, a transition $p \to \mathcal{G}(p) = (\mathcal{G}_H(\rho), \tilde{\mathcal{G}}(H))$ is *Gibbs-preserving* if there exist a quantum channel $\mathcal{G}_H$ and the map $\tilde{\mathcal{G}}$ mapping Hamiltonians onto Hamiltonians such that

$$\mathcal{G}_H\left(\frac{e^{-\beta H}}{\mathrm{Tr}\{e^{-\beta H}\}}\right) = \frac{e^{-\beta \tilde{\mathcal{G}}(H)}}{\mathrm{Tr}\left\{e^{-\beta \tilde{\mathcal{G}}(H)}\right\}}. \tag{2.3.3}$$

Since $\tilde{\mathcal{G}}(H)$ can be different from H, Gibbs-preserving operations can be used to analyze systems where the Hamiltonian changes. In addition, catalytic Gibbs-preserving transitions can be defined. A transition $p \to r$ is a catalytic Gibbs-preserving transition if there exists an object q such that $p \otimes q \to r \otimes q$ is a Gibbs-preserving transition. Further extension such as marginal-catalytic transitions or correlated-catalytic transitions can be found in Ref. [138]. What interests us here is that when considering the most general transitions allowed, there is a single condition for their existence, i.e., that the amount of

[27] This is just a simplifying assumption to not make the discussion uselessly long. See Ref. [120] for the case of degenerate Hamiltonians.

athermality decreases, which for an object p is defined as [138]

$$\Delta F_\beta(\rho, H) := \frac{1}{\beta} S(\rho||\rho^{\text{th}}) = F_\beta(\rho, H) - F_\beta(\rho^{\text{th}}, H), \tag{2.3.4}$$

where $F_\beta(\rho, H) = \text{Tr}\{\rho H\} - k_B T S(\rho)$ is the free energy of the state ρ. Given a certain temperature at which the systems at hand operate, athermality can then be considered as a quantifiable resource. Its variation will be used to define a work quantifier that we will use in chapter 3.

Work quantifiers

Defining work in quantum thermodynamics poses a challenge due to the multistep nature of work measurements. Indeed, one of the most diffused ways to measure work is the so called *Two Energy Measurement Approach* (TEMA) [139, 140], where the experimenter performs an energy measurement on the system before the protocol starts and another one when the protocol ends. This approach works fine when the system is in a block-diagonal state[28] at the start of the protocol but does not give intuitive results when the initial state possess coherences in the Hamiltonian basis [140]. For intuitive results we mean, for example, that we expect the average work to be given by $\text{Tr}\{H'\rho'\} - \text{Tr}\{H\rho\}$, where ρ, ρ', H, and H' are, respectively, the system states and Hamiltonians at the start and at the end of the protocol. The problems of these approaches come from the destructive nature of measurements in quantum mechanics, where a measure has great influence on the evolution of the system, therefore if two or more measurements are performed only the first one is not influenced by the other measurements. TRT circumvents the problem of defining work not by defining it on the basis of what happens to the system doing work, but by measuring it on another system called battery, the storage of work. In particular, in chapter 3 we will call R the system doing work and S the storage system.

In Ref. [137], various work quantifiers are analyzed by considering the set of possible processes described by TRT for a fixed environmental temperature and, moreover, assuming that they have to respect some axioms built in such a way that the second law of thermodynamics is automatically satisfied. Among those, in chapter 3, we will choose the one given as the difference in athermality between the start and the end of the protocol [cf. Eq. (2.3.4)]. Our specific choice of the work quantifier is motivated by the fact that, differently from other quantifiers, it can be used even if the resource R (which can be classical or quantum) and the storage S are correlated at the end of the process [137, 138]. Therefore, the work will be there defined as:

$$W = \Delta F_\beta\left(\rho'_S, H'_S\right) - \Delta F(\rho_S, H_S), \tag{2.3.5}$$

The quantities marked with an apex are related to the end of the process, while those not marked are related to the start of the process. We remark that this work definition quantifies how much the athermality amount of a system, given by $\Delta F_\beta(\rho, H)$, changes

[28] Block-diagonal means that $[\rho, H] = 0$, where ρ is the state of the system and H its Hamiltonian.

after a permitted operation. If $H'_S = H_S$, Eq. (2.3.5) simplifies to:

$$W = F_\beta\left(\rho'_S, H_S\right) - F_\beta\left(\rho_S, H_S\right). \tag{2.3.6}$$

Then, at zero temperature and for a not-changing Hamiltonian, the chosen definition of work coincides with the average energy difference of system S between the start and the end of the protocol, i.e., with the intuitive definition of work done on a system.

2.3.2 Quantum thermal cycles

Quantum mechanics is becoming more and more necessary in order to describe the functioning of thermal machines based on nanoscale devices. Thus, many efforts have been done on characterizing thermodynamic protocols in the quantum domain [20].

We can distinguish the thermodynamic machines functioning between multiple thermal baths in two main categories: continuous and reciprocating [20]. Continuous machines are not characterized by cycles. They work in a continuous manner. For example, a three-level maser can be treated as a continuous thermal machine whose output is in the form of light [20, 141].

Reciprocating machines are made of a series of strokes constituting a cycle. For example, the Carnot engine and the Otto engine are reciprocating thermal machines in which each cycle is constituted of four strokes. Both these cycles have their quantum counterpart [20, 113]. The quantum Otto cycle is one of the most studied cycles in literature, also because the Hamiltonian changes happen when the system does not interact with the bath, thus simplifying its analytical treatment. In particular, in this thesis we will deal with two-stroke reciprocating machines in Chapter 4.

Let us now describe the quantum Otto cycle as an example of reciprocating machine to which we will compare one of our owns in chapter 4. We consider a quantum system S as the so-called working fluid and denote its Hamiltonian at the start of the cycle by H_h. The four strokes of the cycle are described below.

1. The hot *isochore*: heat is transferred from the hot bath to the working fluid.

2. The expansion *adiabat* or the expansion stroke: the Hamiltonian of the working fluid is changed from H_h to H_c while it is decoupled from the baths.

3. The cold isochore: heat is transferred from the working fluid to the cold bath.

4. The compression *adiabat* or compression stroke: the Hamiltonian of the working fluid is changed from H_c to H_h while it is decoupled from the baths.

In practice, the change of Hamiltonian is usually reduced to the change of one of its parameters, such as the frequency for harmonic oscillators. In this specific case, when performed adiabatically, the efficiency of the cycle is given by

$$\eta_{\text{Otto}} = 1 - \frac{\omega_c}{\omega_h}, \tag{2.3.7}$$

being ω_c and ω_h the frequencies of the harmonic oscillator in the different phases of the protocol [113]. Notice that, in the adiabatic case, it is not necessary that $H_h = (\omega_h/\omega_c)H_c$ to obtain this efficiency. The only condition is that the populations of the thermal states adiabatically follow the instantaneous eigenstates during the $H_c \leftrightarrow H_h$ changes. In the case of qubits, the same efficiency can be obtained in the adiabatic case.

The adiabatic Otto cycle, as the ideal Carnot cycle, has vanishing power, because of the long-time condition for adiabaticity. To obtain a finite power, the cycle must be performed in finite time, usually at the expense of the efficiency. To improve the performance of the Otto cycle, the so-called "Shortcuts-to-adiabaticity" (STA) have been theoretically studied [142–144] for the Otto engine case. In general, STA aims to obtain, in finite time, the same final state of an adiabatic dynamics starting from the same initial state. More precisely, consider a time-dependent Hamiltonian $H(t)$; at the start of the dynamics, with $t_0 = 0$, the state is $\rho(0)$ and the Hamiltonian is $H(0)$. If the Hamiltonian varies slowly enough the adiabatic theorem can be applied to obtain the dynamics of $\rho(t)$. In general, however, this is not true. By adding the so-called counter-adiabatic terms to the Hamiltonian, one can implement a STA technique to try obtaining the same final state predicted by the adiabatic theorem [145]. Notice that STA techniques have already been experimentally implemented [146, 147].

Regarding the performances of the Otto cycle with STA, their computation depends on how one chooses to keep into account the cost of implementing the STA. For example, in Refs. [143] and [144] the cost is calculated differently. In both cases, however, the overall performance of the cycle improves with the addition of the STA compared to the same cycle with the non-adiabatic implementation without STA.

The cycles we will deal with in chapter 4 are a generalization of the two-stroke cycle introduced in Ref. [134]. There, two qubits are in contact, respectively, with a cold and a hot bath. The first stroke of the cycle consists in their interaction while the second stroke consists of their thermalization. Their interaction with the baths is not considered during the interaction stroke. In Ref. [134], they assume that the thermalization stroke takes so much time compared to the other one that the optimal interaction is the one maximizing the work per cycle. They then arrive at the conclusion that this optimal interaction is a swap between the two qubits. Interestingly, given the frequency of the two qubits (ω_c for the one in contact with the cold bath and ω_h for the other), the efficiency of the protocol is exactly given by Eq. (2.3.7). Moreover, this cycle can surpass the Curzon-Ahlborn efficiency. Both these results can be found also for our cycles of chapter 4[29].

2.4 Other topics

Up to now, we have made a brief introduction to quantum correlations, open quantum systems and quantum thermodynamics. However, the topics treated in this thesis are connected also to other areas of physics. Therefore, there are some arguments playing a

[29] More precisely, the surpass of the Curzon-Ahlborn efficiency when operating at maximum power will be checked only for the qubits case while we will show that the surpass cannot be obtained with harmonic oscillators.

substantial role in this thesis but that we have not yet wrote about. Since we do not deem proper to dedicate a section to each one of them, we introduce them all in this section.

2.4.1 Gaussian states formalism

In chapter 5 we will study a collision model in which all systems are treated as harmonic oscillators within the Gaussian formalism. In general, many common quantum systems employed in experiments can be described as harmonic oscillators and there is a set of states called Gaussian states which are easy to generate and manipulate [148]. Moreover, once the state of multiple harmonic oscillators is Gaussian, it remains Gaussian under a vast class of external drivings and internal interaction Hamiltonians. Finally, Gaussian states can be used to implement various quantum protocols [148] and can be part of the so-called Continuous Variable (CV) quantum circuits for computation even if Gaussian states alone are not sufficient to make quantum computation more powerful than the classical one [149]. For all these reasons there have been many theoretical efforts for the characterization of this kind of states [148, 150], giving rise to the Gaussian formalism. Notable examples of Gaussian states are the coherent states, squeezed states, and thermal states [148, 150].

Following Ref. [148], any Gaussian state can be written as

$$\rho_G = \frac{e^{-\gamma H}}{\mathrm{Tr}\{e^{-\gamma H}\}}, \tag{2.4.1}$$

where $\gamma \geq 0$ and H is an Hamiltonian that can be written as

$$H = \frac{1}{2}\boldsymbol{R}^\intercal \boldsymbol{H} \boldsymbol{R} + \boldsymbol{R}^\intercal \boldsymbol{R}. \tag{2.4.2}$$

Here, $\boldsymbol{R} = (x_1, p_1, \ldots, x_n, p_n)^\intercal$ is a $2N$-dimensional real vector whose components are the canonical operator x_i (position) and p_i (momentum) for the i-th harmonic oscillator of the system while $\boldsymbol{H}$ is a $2N \times 2N$ symmetric and positive definite matrix called "Hamiltonian matrix". Pure Gaussian states are included in the description by performing the limit $\gamma \to \infty$. When dealing with Gaussian states, however, it is more common to describe it in terms of the first moments vector $\overline{\boldsymbol{R}}$ and the covariance matrix $\boldsymbol{\sigma}$:

$$\overline{\boldsymbol{R}} = \langle \boldsymbol{R} \rangle , \quad \boldsymbol{\sigma} = \left\langle \left\{ (\boldsymbol{R} - \overline{\boldsymbol{R}}), (\boldsymbol{R} - \overline{\boldsymbol{R}})^\intercal \right\} \right\rangle , \tag{2.4.3}$$

where we used the outer product notation $(\boldsymbol{a}\boldsymbol{b}^\intercal)_{ij} = a_i b_j$[30] and, following Ref. [148], we defined

$$\{\boldsymbol{a}, \boldsymbol{a}^\intercal\} = \boldsymbol{a}\boldsymbol{a}^\intercal + (\boldsymbol{a}\boldsymbol{a}^\intercal)^\intercal , \quad [\boldsymbol{a}, \boldsymbol{a}^\intercal] = \boldsymbol{a}\boldsymbol{a}^\intercal - (\boldsymbol{a}\boldsymbol{a}^\intercal)^\intercal . \tag{2.4.4}$$

In terms of single matrix or vector elements, we can write the above equations as

$$\overline{R}_i = \langle R_i \rangle , \quad \sigma_{ij} = \langle R_i R_j \rangle + \langle R_j R_i \rangle - 2 \langle R_i \rangle \langle R_j \rangle . \tag{2.4.5}$$

[30] Notice that $\boldsymbol{a}\boldsymbol{a}^\intercal \neq (\boldsymbol{a}\boldsymbol{a}^\intercal)^\intercal$.

A Gaussian state is completely characterized by $\overline{\boldsymbol{R}}$ and $\boldsymbol{\sigma}$. Using this vector notation, the canonical commutation relation (CCR) $[x_i, p_i] = i\hbar$ can be written as [148] $[\boldsymbol{R}_R, \boldsymbol{R}_R^\intercal] = i\hbar\boldsymbol{\Omega}$, where $\boldsymbol{\Omega}$ is the what we call the standard symplectic matrix in $2N$ dimensions:

$$\boldsymbol{\Omega} = \bigoplus_1^N \Omega_2, \quad \text{where} \quad \Omega_2 = i\sigma_y = \begin{pmatrix} 0 & 1 \\ -1 & 0 \end{pmatrix}, \tag{2.4.6}$$

where σ_y is the standard Pauli matrix. In general, a matrix $\boldsymbol{S}$ is called symplectic if $\boldsymbol{S\Omega S}^\intercal = \boldsymbol{\Omega}$.

For a single harmonic oscillator, when we write the vector $\boldsymbol{R}$ in terms of the quadrature operators $X = (\sqrt{m\omega/\hbar})x$ and $P = (\sqrt{1/m\omega\hbar})p$, where m is the mass and ω the frequency of the harmonic oscillator, the description made through the covariance matrix simplifies. In particular, thermal states are given by [150]

$$\overline{\boldsymbol{R}} = 0, \quad \boldsymbol{\sigma} = \coth\left(\frac{\hbar\omega}{2k_BT}\right)\mathbb{I}_2 = (2\overline{n}+1)\,\mathbb{I}_2, \quad \overline{n} = \frac{1}{e^{\hbar\omega/(k_BT)} - 1}, \tag{2.4.7}$$

while coherent states $|\alpha\rangle$ are given by $\overline{\boldsymbol{R}} = \sqrt{2}(\mathrm{Re}\{\alpha\}, \mathrm{Im}\{\alpha\})^\intercal$ and $\boldsymbol{\sigma} = \mathbb{I}_2$. Moreover, the average number of excitations for of a single harmonic oscillator in a generic Gaussian state is $\overline{n} = (\mathrm{Tr}\{\boldsymbol{\sigma}\} - 2)/4$.

In general, using quadrature operators to write the vector $\boldsymbol{R}$, a complete characterization of a deterministic Gaussian CP-map can be given by

$$\overline{\boldsymbol{R}} \to \mathcal{X}\overline{\boldsymbol{R}}, \quad \boldsymbol{\sigma} \to \mathcal{X}\boldsymbol{\sigma}\mathcal{X}^\intercal + \mathcal{Y}, \quad \mathcal{Y} + i\boldsymbol{\Omega} \geq i\mathcal{X}\boldsymbol{\Omega}\mathcal{X}^\intercal, \tag{2.4.8}$$

where $\mathcal{X}$ and $\mathcal{Y}$ are real matrices of the appropriate dimensions, $\mathcal{Y}$ is symmetric, and the last condition is needed for the final state to satisfy the uncertainty condition $\boldsymbol{\sigma} + i\boldsymbol{\Omega} \geq 0$[31]. In the case of isolated systems, the equivalent of the Schrödinger equation is given by:

$$\frac{\mathrm{d}}{\mathrm{d}t}\overline{\boldsymbol{R}} = \boldsymbol{D}\overline{\boldsymbol{R}}, \quad \frac{\mathrm{d}}{\mathrm{d}t}\boldsymbol{\sigma} = \boldsymbol{D\sigma} + \boldsymbol{\sigma D}^\intercal, \tag{2.4.9}$$

where $\boldsymbol{D} = \boldsymbol{\Omega H}$ is the so-called drift matrix [151].

Gaussian formalism provides a great simplification regarding tracing out systems. On the one hand, when describing uncorrelated systems with covariance matrices, one simply has to make the direct sum of the covariance matrices instead of the tensor product [148, 150]. On the other hand, when tracing out a system possibly correlated to others it is sufficient to discard all elements of the covariance matrix pertaining to that system [148, 150]. Suppose we have systems A and B described by the total covariance matrix σ_S. We can divide it as follows:

$$\sigma_S = \begin{pmatrix} \sigma_A & \sigma_{AB} \\ \sigma_{AB}^\intercal & \sigma_B \end{pmatrix}, \tag{2.4.10}$$

where σ_A is the covariance matrix of system A, σ_B of system B and σ_{AB} keeps count of their correlations. Tracing out system B means that we just keep σ_A.

[31] This is the Gaussian formalism expression of the uncertainty principle in the Robertson-Schrödinger form [150].

2.4.2 The Rabi Hamiltonian and the Dicke model

The Rabi Hamiltonian

A qubit interacting with a harmonic oscillator is one of the more common physical situations studied in literature. One Hamiltonian describing this situation is the so-called Rabi Hamiltonian [152, 153]:

$$H_{\mathrm{Rb}} = \frac{\hbar\omega_q}{2}\sigma_z + \hbar\omega_h\hat{n} + \hbar g\sigma_x\left(a^\dagger + a\right), \tag{2.4.11}$$

where $\hbar\omega_q$ is the energy gap between the ground state $|g\rangle$ and the excited state $|e\rangle$ of the qubit, ω_h is the frequency of the harmonic oscillator[32], $\hat{n}$ is the number operator[33], $a^\dagger$ and a are the creation and annihilation operators, and σ_z and σ_x are the Pauli matrices. We will apply the thermodynamic protocol proposed in chapter 3 also to this model.

The Rabi model is very effective for example in cavity QED [22] and in circuit QED [154]. In the past decades this model has been mainly treated under suitable approximations such as the rotating wave approximation [12, 22] and the Bloch-Siegert approximation [155], which hold when the interaction is weak. Recently, a lot of attention has been devoted, both theoretically and experimentally [152–154, 156–161], to the study of the Rabi Hamiltonian beyond the weak coupling regime, also in view of the recent remarkable experimental realizations of physical situations characterized by high values of the interaction strength [154, 158, 159], and an analytical complete solution has been found [152, 161][34].

Although the first formal solutions of the Rabi model have been found in Ref. [152], the alternative derivation given later in [161] is, in our opinion, clearer and is the one we used to calculate the ground state of the Rabi model in Appendix 3.D. In most cases, however, when the coupling is weak $g \ll \omega_q, \omega_h$, one can safely apply the so-called rotating wave approximation and obtain the simpler Jaynes-Cummings Hamiltonian [22]

$$H_{\mathrm{JC}} = \frac{\hbar\omega_q}{2}\sigma_z + \hbar\omega_h\hat{n} + \hbar g\left(\sigma_- a^\dagger + \sigma_+ a\right), \tag{2.4.12}$$

where σ_- and σ_+ are the lowering and raising operators on the qubit, respectively. The Jaynes-Cummings Hamiltonian has been used, for example, to describe the confinement of a single qubit in an optical cavity. This may induce modifications of the atom absorption and emission rates such as the well-known Purcell effect [22].

Alternatively to the rotating-wave approximation, one can rely on the so-called Bloch-Siegert approximation, valid when g is small compared to $\Omega = \omega_q + \omega_h$, even when the Jaynes-Cummings Hamiltonian is not a good approximation anymore [162]. By defining the unitary operator

$$U_{\mathrm{BS}} = \exp\Big\{\Lambda(a\sigma_- - a^\dagger\sigma_+) + \xi(a^2 - a^{\dagger 2})\sigma_z\Big\}, \tag{2.4.13}$$

[32] Typically, $\omega_q \sim \omega_h$.

[33] With the number basis given by $\hat{n}\,|n\rangle = n\,|n\rangle$.

[34] See also [153] for a review.

where $\Lambda = g/\Omega$ and $\xi = g\Lambda/(2\omega_h)$, one gets the Bloch-Siegert Hamiltonian by calculating $U_{\rm BS}^\dagger H_{\rm Rb} U_{\rm BS}$ up to second order in Λ. The result is [162]

$$H_{\rm BS} = \frac{\hbar\tilde{\omega}}{2}\sigma_z + \hbar(\omega_h + \mu\sigma_z)a^\dagger a + \hbar g(a\sigma_+ + a^\dagger\sigma_-), \tag{2.4.14}$$

where $\mu = g^2/\Omega$ and $\tilde{\omega}_q = \omega_q + \mu$. The eigenstates of $H_{\rm BS}$ are found to be [162]

$$|n,+\rangle = -\sin(\theta_n)\,|e,n-1\rangle + \cos(\theta_n)\,|g,n\rangle\,, \quad |n,-\rangle = \cos(\theta_n)\,|e,n-1\rangle + \sin(\theta_n)\,|g,n\rangle\,, \tag{2.4.15}$$

where

$$\theta_n = \arctan\left[\frac{\Delta_n^{\rm BS} - \sqrt{(\Delta_n^{\rm BS})^2 + 4g^2 n}}{2g\sqrt{n}}\right], \quad \Delta_n^{\rm BS} = \omega_h - \omega_q + 2\mu n. \tag{2.4.16}$$

Turning back to the Rabi Hamiltonian, to second order in Λ, the excited eigenstates are found as

$$|n,\pm\rangle_{\rm Rb} = U_{\rm BS}\,|n,\pm\rangle\,, \tag{2.4.17}$$

while the ground state is given by[35]

$$|\psi_g\rangle_{\rm Rb} = U_{\rm BS}\,|g,0\rangle \simeq \left(1 - \frac{\Lambda^2}{2}\right)|g,0\rangle - \Lambda\,|e,1\rangle + \xi\sqrt{2}\,|g,2\rangle\,. \tag{2.4.18}$$

The Dicke model

Another common studied situation is the one consisting of many qubits interacting with the same harmonic oscillator. The collective nature of such interactions gives rise to a rich quantum phenomenology characterized, for example, by the emergence of quantum phase transitions [21] and by the qualitative modifications of optical properties [163]. Assuming the same frequency for all the qubits and that the distance between the atoms is much lower than the wavelength of the electromagnetic mode, we can describe this system with the well known Dicke model [21, 22]:

$$H_{\rm Rb} = \frac{\hbar\omega_q}{2}J_z + \hbar\omega_h\hat{n} + \hbar g J_x\left(a^\dagger + a\right), \tag{2.4.19}$$

where $J_z = \sum_i \sigma_z^{(i)}$, $J_x = \sum_i \sigma_x^{(i)}$, and $\sigma_z^{(i)}$ and $\sigma_x^{(i)}$ are Pauli operators on the i-th qubit. Even in this case, for low couplings, one can eliminate the so-called counter-rotating terms $J_+a^\dagger$ and J_-a. Within this model, a sub and a superradiant regime have been identified, respectively characterized by the dampening or the amplification of atomic absorption and emission rates with respect to the independent-emitter case [164]. These regimes have been extensively studied also in the presence of coherent or incoherent optical drivings [165–172].

[35] Both H_{JC} and $H_{\rm BS}$ have the same ground state, i.e., $|g,0\rangle$.

Besides the fundamental interest, collective quantum phenomena induced by light-matter interactions can be exploited in a variety of applications. In particular, the sub and superradiant regimes may be associated to the generation of collective states of the emitters, which are of great interest for quantum sensing [173, 174], generation of non-classical states [175], photon storage [176], and excitation transfer [177]. This phenomenology is of high experimental relevance, as collective light-matter interactions can be controllably implemented in a broad range of atomic and solid-state quantum systems, such as cold atoms [178], trapped-ions [179], metamaterials [180], plasmonic cavities [181], colour centres in diamonds [182], quantum dots [183], and superconducting circuits [184].

Among the many cases in which the Dicke model has been explored, much attention has been devoted to the so-called "bad-cavity limit" in which the confined mode is strongly dampened with respect to the interaction with the atoms [165–168, 170, 171]. In this context, the effective dynamics of the atoms can be obtained by adiabatically eliminating the confined mode [32, 33, 106, 107]. Intuitively, the bad-cavity limit consists in assuming that the cavity which contains the atoms is so leaky that it immediately emits all the photons it receives from the atoms. In the original treatment of this system [106, 107], the cavity is considered in contact with an environment at zero temperature so that its steady state is the ground one. Starting from the atoms state in which all the atoms are excited, the phenomenon of superradiance is well described within this approach.

Collective emission phenomena have so far been analyzed only for dipolar interactions, where light and matter are linearly coupled. However, it has been recently predicted that using atomic or solid-state systems it is possible to implement nondipolar light-matter couplings, where the linear interaction is inhibited and where quantum emitters and localized bosonic modes interact via the exchange of two excitation quanta. In particular, such two-photon couplings can be observed by engineering superconducting atom-resonator systems [185, 186] or by applying analog quantum simulation schemes in trapped-ions [187–189] or ultracold atoms [190, 191]. Notice that non-dipolar transitions have already been observed using superconducting artificial atoms [192], and that quantum-simulation techniques have already been experimentally applied to observe the physics of fundamental dipolar light-matter interaction models in extreme regimes of parameters [191, 193]. On the dissipative side, two-photon relaxation [194, 195] and pumping [194] have also been theoretically analyzed and experimentally implemented [196]. The fast-growing interest in two-photon couplings is motivated by a rich phenomenology, characterized by novel spectral features [197–202], high-order quantum optical nonlinearities [185, 186, 203], and quantum phase transitions [204–208]. In turn, this phenomenology can be exploited in different quantum-information applications [209–211].

The resonant Dicke model with two-photon coupling in the rotating-wave approximation is described by the Hamiltonian

$$H_2 = \hbar\omega a^\dagger a + \hbar\omega J_z + \hbar g \left(a^2 J_+ + a^{\dagger 2} J_-\right). \tag{2.4.20}$$

We will use it as a starting point for the study conducted in in chapter 6. There, we will analyze a quite complex setup comprising different external drivings and finite

temperature baths in the bad-cavity limit.

2.A Resume of some useful tools in quantum mechanics

This appendix gives a very short resume of some well-known theoretical tools used in this Thesis.

2.A.1 The von Neumann entropy

To quantify how much information is lacking in a mixed state we can use the von Neumann entropy [10, 110] defined as follows

$$S(\rho) \equiv -\operatorname{Tr}\{\rho \ln \rho\}, \tag{2.A.1}$$

where ln is taken in the natural basis. Since the trace is basis-independent we can search for the basis in which the density matrix is diagonal. In this basis[36],

$$\rho = \sum_{i=1}^{N} \lambda_i \, |\psi_i\rangle\langle\psi_i| \implies S(\rho) = -\sum_i \lambda_i \ln \lambda_i. \tag{2.A.2}$$

We can immediately see that the entropy of a pure state is zero[37]. The maximum entropy allowed for a system in an Hilbert space of dimension d is obtained for the so-called fully mixed state: $S(\mathbb{I}_d/d) = \ln d$, where $\mathbb{I}_d$ is the identity matrix of dimension d.

We also define the quantum relative entropy between two states ρ and σ:

$$S(\rho||\sigma) \equiv \operatorname{Tr}\{\rho \ln \rho\} - \operatorname{Tr}\{\rho \ln \sigma\}. \tag{2.A.3}$$

This quantity is always non-negative and can be infinite. It is zero if and only if $\rho = \sigma$. In practice, this quantity is sometime seen as a measure of the distance between two states, even if it does not respect all the requirement a proper distance measure necessitates [12].

2.A.2 The Schmidt decomposition

It can be shown [10], that every pure state $|\psi\rangle$ of a bipartite system can be written as

$$|\psi\rangle = \sum_i \sqrt{\lambda_i} \, |i_A\rangle \otimes |i_B\rangle \,, \tag{2.A.4}$$

where the $\lambda_i > 0$, $\sum_i \lambda_i = 1$, and the kets $|i_A\rangle$ and $|i_B\rangle$ belong to orthonormal bases in their respective Hilbert spaces. The numbers $\sqrt{\lambda_i}$ are called Schmidt coefficients while the number of Schmidt coefficients is called Schmidt number. A consequence of the Schmidt decomposition is that the reduced density matrices of both subsystems have the same eigenvalues and, therefore, the same entropy [see Eq. (2.A.2)].

[36] The basis is given by the kets $|\psi_i\rangle \in \mathcal{H}$ with $d = \dim \mathcal{H}$.

[37] In the limit $\lambda_i \to 0$, we have that $\lambda_i \ln \lambda_i \to 0$.

2.A.3 The thermal state

One assumption of thermodynamics is that a system in contact with an environment at temperature T will reach its thermal state at the same temperature. Here, we recall how thermal states are characterized in quantum mechanics.

The thermal state of a system with Hamiltonian H and temperature T is described by the state [12]

$$\rho^{\text{th}} = \frac{e^{-\beta H}}{Z}, \quad Z = \text{Tr}\Big\{e^{-\beta H}\Big\}, \tag{2.A.5}$$

where $\beta = 1/(k_B T)$ is the inverse temperature and k_B is the Boltzmann constant. The term Z, whose inverse acts as a normalization constant in the above equations, is actually an important quantity called "partition function". Through it, to calculate the average energy of the state, its variance, and all the thermodynamic potentials is possible. Here we cite:

$$\begin{aligned} \langle E \rangle = \text{Tr}\Big\{H\rho^{\text{th}}\Big\} = -\partial_\beta(\ln Z), \quad \Big\langle (E - \langle E \rangle)^2 \Big\rangle = \frac{\partial^2 \ln Z}{\partial \beta^2}, \\ F(\rho^{\text{th}}) = \langle E \rangle - k_B T S(\rho^{\text{th}}) = -k_B T \ln Z, \end{aligned} \tag{2.A.6}$$

where $F(\rho^{\text{th}})$ is the von Neumann free energy of the thermal state.

Chapter 3

Thermodynamic protocols: work extraction

3.1 Introduction

As detailed in section 2.3, one argument of actual interest in the wide context of quantum thermodynamics consists of work extraction protocols describable within the thermodynamic resource theory (TRT) framework. In this chapter, we conceive a work-extraction protocol exploiting a single bath and making use of simple operations which should be easily implementable without need for fine operations. Indeed, we propose to extract work from a resource system R to a bipartite quantum system S exploiting simple operations such as a thermalization process and turning on and off the interaction between the two subsystems of S. We show that this thermalization protocol gives rise to a quite efficient single-shot work extraction. To quantify the work extracted, we use the work quantifier of Eq. (2.3.5). In order to make the procedure cyclic, we show in one of the considered models how to exploit the result of the thermalization protocol to charge an external device playing the role of a quantum battery through a quite simple transfer protocol. We stress that the various parts of the global protocol do not need for a fine control. For example, the interaction between the two subsystems of S does not need to last for a precise amount of time but only enough to let system S thermalize, while the procedures of switching on and off have to be just rapid enough to leave unaltered the state of the system.

To better appreciate the potentialities of our protocol we apply it to two different physical scenarios (a two-qubit system and a spin-boson system) described by different models. The first model can describe the interaction of two spins in an Ising chain [212–214], while the second is described by the ubiquitous Rabi Hamiltonian (see section 2.4.2).

The chapter is organized as follows. In section 3.2, we describe the thermalization protocol for an arbitrary bipartite system. In section 3.3, we describe a possible realization of our protocol in a system consisting of two qubits, while in section 3.4 we consider a spin-boson system whose interaction is described by the Rabi model. In section 3.4, we also briefly discuss the possibility to transfer the extracted work to another physical

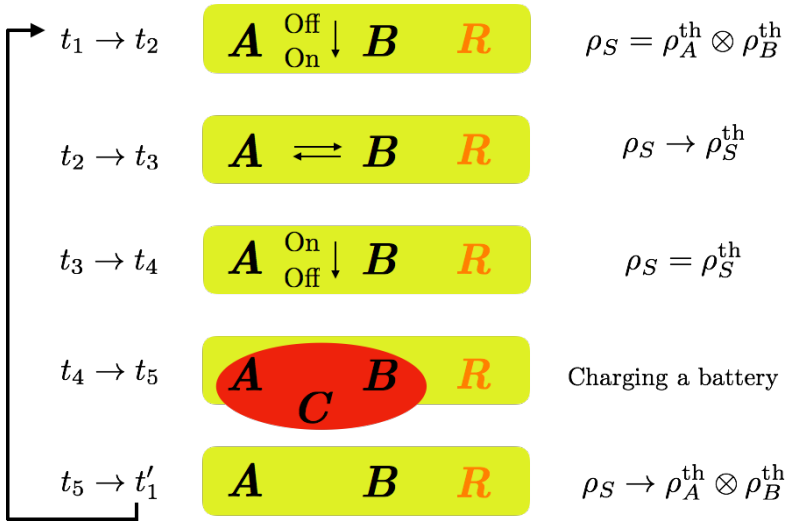

Figure 3.1: This figure illustrates schematically the phases of the thermalization protocol in the presence of a thermal bath (yellow box). At start (t_1) the subsystems do not interact. Then, the interaction is turned on and they thermalize together (from t_2 to t_3). Once they have thermalized their interaction can be turned off and the process of work extraction is completed (t_4). If one wants to transfer the extracted work to iterate the process he does so in the time interval $\delta_T t$ and, after having finished the process (t_5), the experimental setup could have to be reinitialized, from t_5 to t_1', where t_1' plays the role of the initial time of the new cycle.

system, effectively charging a battery. However, we will give more details about this charging process in Appendix 3.E. Finally, in section 3.5 we provide some conclusive remarks on our results. Some other details of our analysis can be found in the Appendices.

3.2 Work-extraction protocol

3.2.1 The thermalization protocol

Here, we describe the thermalization protocol in the case S is an arbitrary bipartite system composed of two subsystems A and B. In order to analyze the protocol we use as a work quantifier the one described in Eq. (2.3.5). Some comments on the possible links between this work quantifier and other thermodynamic quantities can be found in Appendix 3.A.

The protocol can be divided into different phases (see Fig. 3.1). For each phase, we compute the free energy of system S with the notation $F_i = F(\rho_S(t_i), H(t_i))$, where $\rho_S(t_i)$ is the state of S at time t_i and $H(t_i)$ its Hamiltonian[1]. The free energy is calculated

[1]Since in this chapter we deal with just one bath at a given temperature, we drop the subscript β from the free energies [cfr. section 2.3.1] to lighten the notation.

at temperature T, the fixed temperature of the single bath exploited in the protocol. Notice that, the presence of the environment is necessary during the thermalization from t_2 to t_3. During the other phases it would be enough to assume that the environment is at disposal if needed. However, in the following analysis we always refer to a realistic situation where the environment and system S are always interacting. In this case, we must assume that the interaction is so weak that, overall, whenever we have to take into account the evolution given by the interaction of $S+R$ with the bath, the total energy $H_S + H_R + H_{\text{bath}}$[2], where H_R and H_{bath} are, respectively, the Hamiltonians of the resource R and of the bath, is a conserved quantity and results from TRT can be applied.

At the start of the protocol ($t = t_1$) A and B are non-interacting, non correlated and spatially separated[3]. They are both in contact with the same thermal bath at temperature T so that:

$$\begin{aligned} H(t_1) = H_A + H_B = H_0, \quad \rho_S(t_1) = \rho_A^{\text{th}} \otimes \rho_B^{\text{th}}, \\ F_1 = F\left(\rho_A^{\text{th}}, H_A\right) + F\left(\rho_B^{\text{th}}, H_B\right), \end{aligned} \tag{3.2.1}$$

where $H_{A(B)}$ is the free Hamiltonian of $A(B)$, $\rho_{A(B)}^{\text{th}} = e^{-\beta H_{A(B)}} / \operatorname{Tr}\left\{\mathrm{e}^{-\beta H_{A(B)}}\right\}$ are the local thermal states and $\beta = 1/(k_B T)$[4]. Then, the interaction between A and B is turned on exploiting R during a time interval $\delta_1 t$ from t_1 to $t_2 = t_1 + \delta_1 t$, for example, by bringing the two subsystems closer. We suppose that the state of system S does not change during this time. This can be achieved if the turning on of the interaction is doable in a time interval much smaller than the typical evolution time of system S, during the switching on procedure, being it coupled to the bath. Defining $\langle H \rangle_{t_n} = \operatorname{Tr}\{\rho_S(t_n) H\}$, we have:

$$H(t_2) = H_0 + H_I, \quad \rho_S(t_2) = \rho_S(t_1), \quad F_2 = F_1 + \langle H_I \rangle_{t_2}, \tag{3.2.2}$$

H_I being the interaction Hamiltonian between A and B.

From time t_2 to time t_3[5], A and B thermalize as a whole so that at t_3:

$$H(t_3) = H(t_2), \quad \rho_S(t_3) = \rho_S^{\text{th}}, \quad F_3 = F\left(\rho_S^{\text{th}}, H_0\right) + \langle H_I \rangle_{t_3}, \tag{3.2.3}$$

where $\rho_S^{\text{th}} = e^{-\beta(H_0+H_I)} / \operatorname{Tr}\left\{e^{-\beta(H_0+H_I)}\right\}$ is the global thermal state when the interaction is on. Finally, from time t_3 to time $t_4 = t_3 + \delta_2 t$ we use again system R to turn off the interaction term between subsystems A and B, for example by spatially separating them,

[2] In order to apply TRT results one needs that $[U, H_S + H_R + H_{\text{bath}}] = 0$ where U is the unitary operator describing the whole process (see section 2.3.1 for more details).

[3] The spatial separation is not strictly required, but we think it facilitates the experimental implementation because it is, usually, easy to turn on and off the interaction between two systems by just joining and separating them spatially.

[4] Notice that we are assuming that systems A and B have thermalized independently. This is a reasonable assumption in many different scenarios, for example in the case when the systems are spatially separated before turning on the interaction.

[5] $t_3 - t_2 \gg \tau_r$, where τ_r is the typical evolution time of system S in this phase.

and supposing that the state of S remains unaltered. The situation at time t_4 is thus given by

$$H(t_4) = H_0, \quad \rho_S(t_4) = \rho_S(t_3), \quad \rho_{A(B)}(t_4) = \mathrm{Tr}_{B(A)}\{\rho_S^{\mathrm{th}}\} = \rho_{A(B)}^{\mathrm{rth}}, \quad F_4 = F(\rho_S^{\mathrm{th}}, H_0). \tag{3.2.4}$$

We remark that at $t = t_4$ the reduced states of A and B (we name them reduced thermal states) are different from the initial ones, which were the local thermal states.

The turning on and off of the interaction requires work from system R while, in general, R is not involved during the thermalization from t_2 to t_3[6]. In particular, using the work definition of Eq. (2.3.5), turning on the interaction costs a quantity $W_R(t_1 \to t_2)$, satisfying (more details in Appendix 3.B):

$$W_R(t_1 \to t_2) \geq F_2 - F_3 = \langle H_I \rangle_{t_2} + F_1 - F_3. \tag{3.2.5}$$

On the other hand, turning it off costs:

$$W_R(t_3 \to t_4) \geq F_4 - F_1 = -\langle H_I \rangle_{t_3} + F_3 - F_1. \tag{3.2.6}$$

Then, the minimum amount of work required to system R to make one cycle is $\langle H_I \rangle_{t_2} - \langle H_I \rangle_{t_3} = -\Delta \langle H_I \rangle$. We stress that, during the switchings, system R could lose a certain quantity of free energy due to dissipative effects, in addition to the required variations of athermality[7]. In the following, we identify the amount of athermality lost by R with the variation of its free energy because we assume that system R never changes Hamiltonian[8].

From the point of view of single-shot work extraction, the protocol ends at time t_4. In the next section, we quantify the amount of work extracted and the efficiency of this process. In order to iterate the process using the same systems A and B, one has to transfer the extracted work at time $t = t_4$ to an external storage system C. We provide an example of how to do this at the end of section 3.4 for a specific model. After the transfer ($t = t_5 = t_4 + \delta_T$), A and B are still in contact with the bath and, after a while, they will be again in their thermal state. Then, the protocol can be done again from the start. Notice that resource R is not reinitialized after each iteration of the entire protocol. We will however use the term cycle to describe the case where we iterate the process by referring to the cyclic behavior of system S.

3.2.2 Work and efficiency

Using the work definition of Eq. (2.3.5), the extracted work W is equal to $F_4 - F_1$:

$$W = \langle H_0 \rangle_{t_4} - \langle H_0 \rangle_{t_1} - k_B T \left[S(\rho_S^{\mathrm{th}}) - S\left(\rho_A^{\mathrm{th}} \otimes \rho_B^{\mathrm{th}}\right) \right]. \tag{3.2.7}$$

[6] Notice that resource R is not explicitly described here. For example, its Hamiltonian is not given. We assume that R is something that, in some way, turns on and off the interaction between the subsystems of S. As cited in the text, this could be obtained by changing the distance between A and B.

[7] See section 2.3.1 for the definition of athermality.

[8] See Eq. (2.3.6)

W is thus composed by two parts: one purely energetic and one of entropic nature. The entropic term appearing in Eq. (3.2.7) comes directly from the adopted definition of work. Its presence assures the validity of the second law of thermodynamics. Especially for finite systems, the entropic part can become much more important than the energetic one for non-vanishing temperatures. An example of this behavior is shown in section 3.3. At $T = 0$, instead, W is a simple difference of average energies. We stress that the work done on a system quantifies the change of athermality of the system, $\Delta F(\rho, H)$. Then, being $\Delta F(\rho, H)$ a function of the state and of the Hamiltonian of the system, it does not depend on the actual evolution that took place. Notice that resource R is not reinitialized after each iteration of the entire protocol. However, we will use the term "cycle" to describe the case where we iterate the process by referring to the cyclic behavior of system S.

The extracted work can be rewritten as

$$W = \Delta F\left(\rho_A^{\text{rth}}, H_A\right) + \Delta F\left(\rho_B^{\text{rth}}, H_B\right) + k_B T S(A:B), \tag{3.2.8}$$

where $S(A:B) = S\left(\rho_A^{\text{rth}}\right) + S\left(\rho_B^{\text{rth}}\right) - S\left(\rho_S^{\text{th}}\right)$ is the mutual information[9] between A and B for the state ρ_S^{th}, a real non-negative quantity [12]. In particular, the mutual information term quantifies the amount of correlations between the two subsystems and its behavior is strongly model-dependent. In Eq. (3.2.8), the only non-local entropic term is the mutual information as opposed to the local terms $S\left(\rho_A^{\text{rth}}\right)$ and $S\left(\rho_B^{\text{rth}}\right)$. Then, we can also define the local work

$$W_l = \Delta F\left(\rho_A^{\text{rth}}, H_A\right) + \Delta F\left(\rho_B^{\text{rth}}, H_B\right), \tag{3.2.9}$$

which in some cases could be the only accessible work after the protocol. It holds $W_l \leq W$, that is an already known result of information thermodynamics [215], meaning that the amount of extracted work benefits of the presence of correlations in the final thermal state. As can be seen in sections 3.3 and 3.4, the difference between local and global work can be significant.

The quantity $\Delta F\left(\rho_{A(B)}^{\text{rth}}, H_{A(B)}\right)$ can be written as [86]:

$$\Delta F\left(\rho_{A(B)}^{\text{rth}}, H_{A(B)}\right) = k_B T S\left(\rho_{A(B)}^{\text{rth}} || \rho_{A(B)}^{\text{th}}\right), \tag{3.2.10}$$

where $S(\rho||\sigma) = \text{Tr}\{\rho \ln \rho\} - \text{Tr}\{\rho \ln \sigma\}$ is the relative entropy and, even if it does not have all the properties of a distance measure, it is often used to quantify how much two density operators are different [12]. Therefore, the more the reduced thermal states are different from the local ones, the more should be the local work extracted. One then expects that W_l should typically increase as the strength of the interaction between the subsystems of S increases.

Another useful way to express the extracted work is through the partition functions of the systems. Calling $Z_{A(B)}$ the partition function of system $A(B)$ with Hamiltonian

[9] See section 2.1 for more details on the mutual information.

$H_{A(B)}$ and Z_S the partition function of the total system with interaction on, we can write:

$$W = k_B T \ln\left(\frac{Z_A Z_B}{Z_S}\right) - \langle H_I \rangle_{t_3} . \tag{3.2.11}$$

Through simple algebraic manipulations, we can also write

$$W = F_3 - F_2 - \Delta \langle H_I \rangle , \tag{3.2.12}$$

where we recall that $\Delta \langle H_I \rangle = \langle H_I \rangle_{t_3} - \langle H_I \rangle_{t_2}$. Then,

$$0 \leq W_l \leq W \leq -\Delta \langle H_I \rangle , \tag{3.2.13}$$

because F_3 has to be always lower or equal to F_2.

Using Eq. (3.2.11), it is easy to show that if both subsystems are finite, the high temperature limit of the extracted work is zero (see Appendix 3.C). This also implies, using Eq. (3.2.13), that the correlations between two finite subsystems in a thermal state always go to zero faster than $1/T$ in the high temperature limit since $W \to 0$.

Following the theorems of TRT, it is in principle always possible to transfer, without losses, a certain quantity of free energy from one system to another one through thermal operations. Achieving the maximum efficiency for this transfer may require, for example, the use of catalysts [86, 120, 137] (see also section 2.3.1). Thus, we define the ideal efficiency of the process as the work stored in system S divided by the minimum free energy lost by system R, i.e.

$$\eta = \frac{W}{-\Delta \langle H_I \rangle} = \frac{F_3 - F_2 - \Delta \langle H_I \rangle}{-\Delta \langle H_I \rangle} \leq 1. \tag{3.2.14}$$

In other words, we compare the work that system S gains with the work that system R would lose in the best-case scenario. This comparison makes sense because TRT assures us that it exists a thermal operation such that all the work lost by R is gained by S. Of course, considering the local work W_l, with the annexed efficiency η_l, instead of W, we get $\eta_l \leq \eta$.

In Appendix 3.A, we make some comments on the possible links between the work quantifier of Eq. (2.3.5) and other thermodynamic quantities, focusing on the thermalization protocol presented in this section. As can be seen from Eq. (3.A.5), the ideal efficiency of this process can be thought of depending explicitly on the entropy production of the thermalization, from time t_2 to t_3. With respect to the ideal switching case [Eq. (3.2.14)], system R could spend more work during the process because of dissipative effects.

It is worth noting that the extraction of work from R to S may imply the conversion of different forms of energy. Indeed, R could exploit any kind of possible form of energy to switch on and off the interaction between A and B, while the form of energy stored in S would depend on the specific choice of subsystems A and B. As an example of protocol implementation, we could think of a flying atom entering and exiting from a cavity. In this case, the internal levels of the flying atom are system A, the cavity is system B

and the wave function spatial part of the flying atom is the resource R. When the atom enters or exits, the A-B interaction switches on or off and energy can come from or go to R. The amount of work paid by system R may also depend on entropy variations and overall must be positive[10]. In this specific example, mechanic energy is transformed into electromagnetic one.

In order to make our analysis more quantitative and better exemplify the level of efficiency of our work-extraction protocol, we consider two possible realizations associated to two different models which can be realized in specific physical scenarios of experimental interest. In the next two sections we consider a two-qubit system and a spin-boson system described by the Rabi model.

3.3 Two interacting qubits

Here, we consider the case when S consists of two qubits governed by the Hamiltonian[11]

$$H = H_A + H_B + H_I, \tag{3.3.1}$$

where

$$H_A = \frac{\hbar\omega}{2}\sigma_z^{(A)},\ H_B = \frac{\hbar\omega}{2}\sigma_z^{(B)},\ H_I = \hbar g\sigma_x^{(A)}\sigma_x^{(B)}, \tag{3.3.2}$$

ω is the frequency of each qubit, $\sigma_z^{A(B)}$ and $\sigma_x^{A(B)}$ are Pauli matrices and g is the coupling frequency.

The extracted work and the efficiency for this model can be computed by using Eqs. (3.2.11) and (3.2.14) where the partition functions and the average interaction energy at time t_3[12] are given by

$$Z_A = Z_B = 2\cosh(\beta\hbar\omega/2), \quad Z_S = 2\left[\cosh\left(\beta\hbar\sqrt{\omega^2+g^2}\right) + \cosh\left(\beta\hbar g\right)\right], \tag{3.3.3}$$

and

$$\langle H_I\rangle_{t_3} = \frac{2\hbar g}{Z_S}\left[\frac{e^{-\beta\hbar\tilde{\omega}}}{g\mathcal{N}_+}\left(\tilde{\omega}-\omega\right) - \frac{e^{\beta\hbar\tilde{\omega}}}{g\mathcal{N}_-}\left(\tilde{\omega}+\omega\right) - \sinh(\beta\hbar g)\right], \tag{3.3.4}$$

where $\tilde{\omega} = \sqrt{\omega^2+g^2}$ and $\mathcal{N}_\pm = \left(2\tilde{\omega}/g^2\right)\left(\tilde{\omega}\mp\omega\right)$, while $\langle H_I\rangle_{t_2} = 0$.

At zero temperature, the extracted work and the efficiency assume the simple form:

$$W(T=0) = \hbar\omega\frac{g^2}{\omega^2+\omega\tilde{\omega}+g^2}, \quad \eta(T=0) = \frac{\omega}{\omega+\tilde{\omega}}. \tag{3.3.5}$$

Another analytical limit worth mentioning is the $g\to\infty$ limit. In this case we obtain:

$$W \to k_BT\ln\left\{1+\cosh\left[\hbar\omega/(k_BT)\right]\right\}, \quad \eta\to 0. \tag{3.3.6}$$

[10] See Eqs. (3.2.5) and (3.2.6)

[11] This Hamiltonian can be found, e.g., in Ref. [213].

[12] Obtained through lengthy but straightforward calculations.

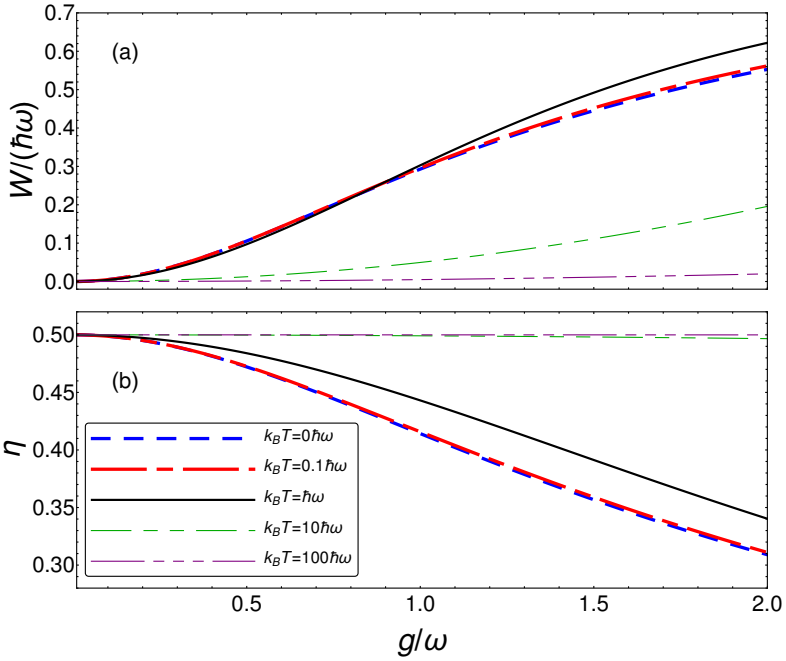

Figure 3.2: Two-qubit model: extracted work W (a) and efficiency η (b) of the thermalization protocol as a function of the coupling constant, g/ω, for different values of the temperature of the bath, $k_BT/(\hbar\omega)$.

The behaviors of W and η as a function of the dimensionless coupling constant g/ω are plotted in Fig. 3.2, for different temperatures of the bath. We notice that, for every temperature, increasing g/ω monotonically increases the extracted work. This behavior agrees with what was predicted in section 3.2.2 for the $T = 0$ case. In this limit, it holds $W = W_l$. Notice that an extraction of work comparable with the typical energies of the subsystems can be obtained. However, the efficiency also decreases monotonically. Then, for a given T, a sweet spot for the coupling constant does not seem to exist. On the contrary, a sweet spot for the temperature does exist. Indeed, as shown in Fig. 3.3, the most interesting feature of this model is that, given a value of g/ω, the maximal extraction of work is obtained for a value of temperature such that $k_BT \sim \hbar\omega$ with a greater efficiency with respect to the zero-temperature case.

The above result is especially clear for high values of g such as $g = 2\ \omega$. For this reason, we plot in Fig. 3.4 various quantities of the protocol as a function of the temperature, for $g = 2\ \omega$. The maximal extraction of total work W is obtained for $k_BT \simeq 1.51\ \hbar\omega$, marked with a grey vertical line in the figure. Around that temperature, there is a big difference between the total work W and the local one W_l. Their difference is exactly the mutual information multiplied by k_BT. So, a great part of the work is stored in the correlations between A and B, quantified by the non-local entropic term $k_BTS(A : B)$. Regarding the total extraction, we can notice also how much the global

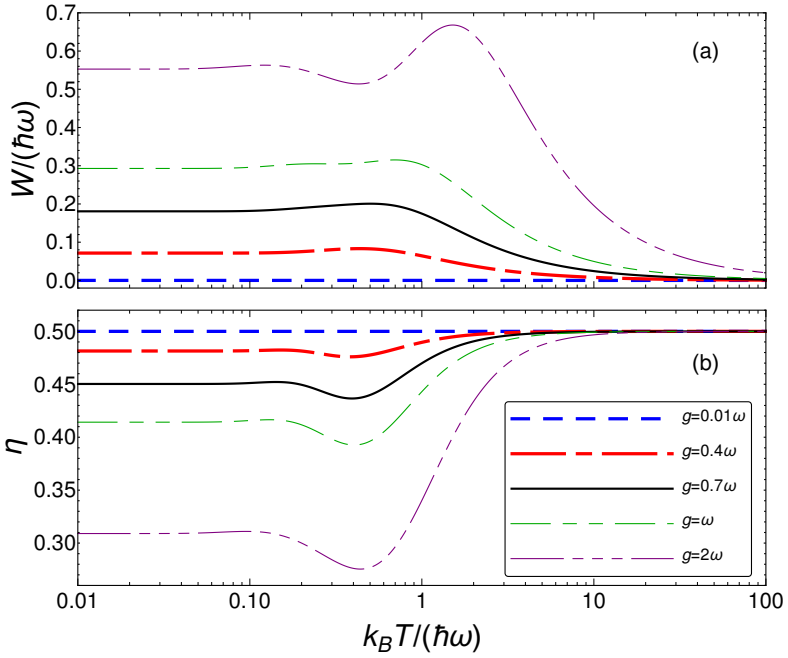

Figure 3.3: Two-qubit model: extracted work W (a), and efficiency η (b) of the thermalization protocol as a function of the temperature of the bath, $k_BT/(\hbar\omega)$, for different values of the coupling constant, g/ω.

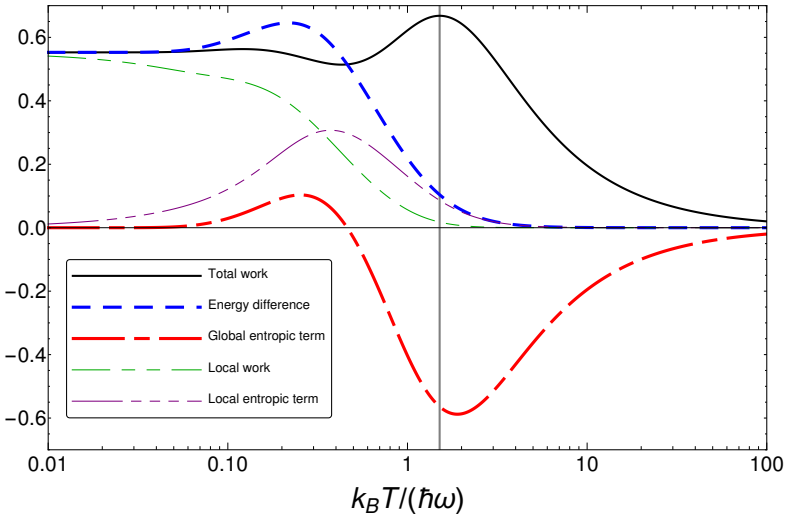

Figure 3.4: Two-qubit model: comparison of different quantities (each in units of $\hbar\omega$) as a function of the bath temperature for $g = 2\ \omega$. A grey vertical line is depicted in correspondence of the peak of the total work Wat $k_BT \simeq 1.51\ \hbar\omega$.

entropic term, $k_BT\left[S\left(\rho_S^{\text{th}}\right) - S\left(\rho_A^{\text{th}} \otimes \rho_B^{\text{th}}\right)\right]$, is important in that temperature region[13]. On the contrary, for lower values of T, the global entropic term reduces the amount of extracted work with respect to the energy difference $\langle H_0\rangle_{t_4} - \langle H_0\rangle_{t_1}$. On the local level, the local entropic term, $k_BT\left[S\left(\rho_A^{\text{rth}} \otimes \rho_B^{\text{rth}}\right) - S\left(\rho_A^{\text{th}} \otimes \rho_B^{\text{th}}\right)\right]$, always reduces the amount of work extracted, independently of the temperature. This difference of behavior between the local and non-local parts of the entropy explains the quantitative difference between the local and total extracted work.

3.4 Rabi model

Here, we consider the case in which S consists of a two-level system (subsystem A) interacting with a harmonic oscillator (subsystem B). The system is governed by the Rabi Hamiltonian [22]:

$$H_{\text{Rb}} = H_A + H_B + H_I, \tag{3.4.1}$$

where

$$H_A = \hbar\Delta\sigma_z, \quad H_B = \hbar\omega\hat{n}, \quad H_I = \hbar g\sigma_x\left(a^\dagger + a\right), \tag{3.4.2}$$

$\hbar\Delta$ is half of the energy distance[14] between the ground state $|g\rangle$ and the excited state $|e\rangle$ of A, ω is the frequency of B (typically $\omega \sim 2\Delta$), $\hat{n}$ is the number operator (with the number basis given by $\hat{n}\,|n\rangle = n\,|n\rangle$), $a^\dagger$ and a are the creation and annihilation operators and σ_z an σ_x are Pauli matrices.

Since the analytical solution of the Rabi model is given in terms of series that have to be truncated [152, 153, 161][15], from a numerical point of view, it is easier to directly do all the computations numerically without using the analytical solution. In this section, we report the results of these numerical simulations done with the Python package QuTiP [216, 217], only dealing with the resonant case $\Delta = \omega/2$. For the zero-temperature case, we use the analytical solution, checking that it coincides with the numerical simulations at very low temperatures. A detailed discussion about the ground state of the system, used for $T = 0$ case, can be found in Appendix 3.D.

Fig. 3.5 shows how the extracted work and the efficiency as a function of the coupling parameter g/ω for different values of the bath temperature. We notice a dissimilar behavior of the Rabi model with respect to the two-qubit one. Overall, the Rabi model attains a higher value of extracted work and higher efficiency. Contrarily to the two-qubit case, here increasing the interaction may increase the efficiency, which is always higher than one half.

As in the two-qubit case, also in the Rabi model, for a given value of the coupling constant, an ideal value of the temperature exists (see Fig. 3.6). Comparing Figs. 3.3 and 3.6 we notice that the best values of temperature in the Rabi model case are one order of magnitude lower. In general, given a value of the coupling constant g, there

[13] We recall that $\rho_S(t_3) = \rho_S^{\text{th}}$ while $\rho_S(t_1) = \rho_A^{\text{th}} \otimes \rho_B^{\text{th}}$.

[14] Here, we are following the notation of Ref. [152] instead of the usual one.

[15] See section 2.4.2 for the formal solutions of the Rabi model.

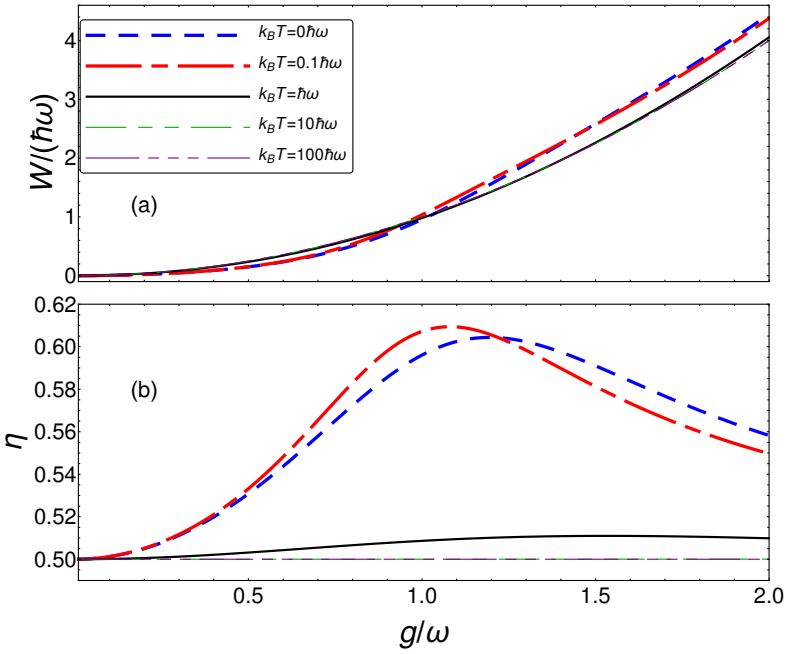

Figure 3.5: Rabi model: extracted work W (a) and efficiency η (b) of the thermalization protocol as a function of the coupling constant, g/ω, for different values of the bath temperature, $k_BT/(\hbar\omega)$.

exist a temperature sweet point where the work is nearly at its maximum and, close to which, the efficiency has its peak. Among the values reported in the plot, this does not hold for $g = 2\ \omega$. Moreover, the extracted work does not tend to zero for large temperatures as in the two-qubit case. This is due to the fact that the Rabi Hamiltonian contains a non-finite and not bounded system (the harmonic oscillator). This means that a temperature that makes all the levels equally populated so that the thermal state is practically the identity state does not exist. We also remark that both the work and the efficiency reach an asymptotic behavior for $k_BT \sim 10\ \hbar\omega$.

In Fig. 3.7 we show the extracted work and other relevant quantities as a function of the temperature (compare it with Fig. 3.4). Differently from the two-qubit case, here the peak of work extraction is not due to the entropic term but to the energy term. Indeed, the peak of work extraction (roughly at $k_BT \simeq 0.16\ \hbar\omega$ and marked with a grey vertical line in the figure) is near the peak of the energy difference term. As in the two-qubit case, the local work rapidly goes to zero starting from $k_BT \sim \hbar\omega$. In the present case, however, this is not due to the fact that the reduced thermal states are very similar to the thermal ones. In this case, the energy difference remains high and the local entropic term counterbalances it. Then, even if the global entropic term does not seem to play a significant role, its non-local component (the mutual information) does, by balancing the local entropic terms and thus avoiding that they take the total work down to zero in the high-temperature region.

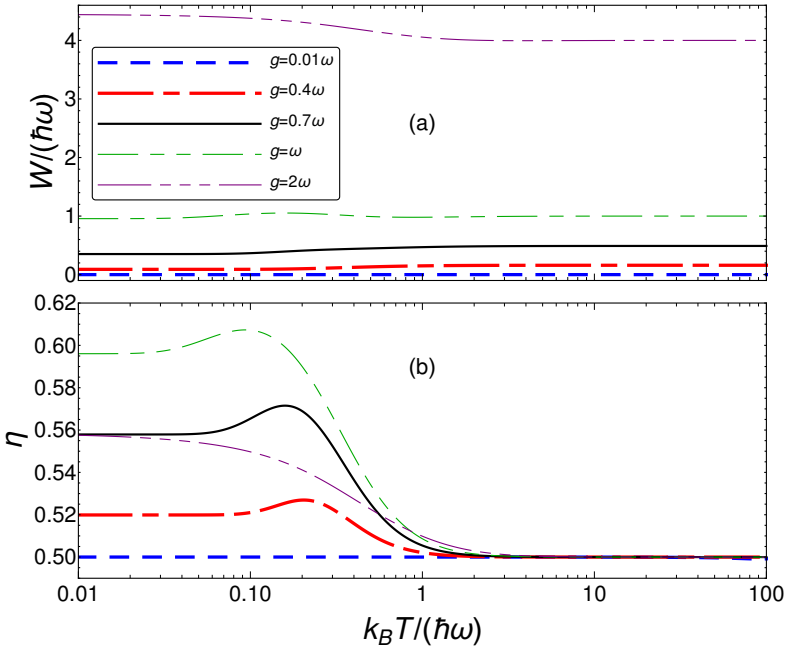

Figure 3.6: Rabi model: extracted work W (a) and efficiency η (b) of the thermalization protocol as a function of the bath temperature, $k_BT/(\hbar\omega)$, for different values of the coupling constant, g/ω.

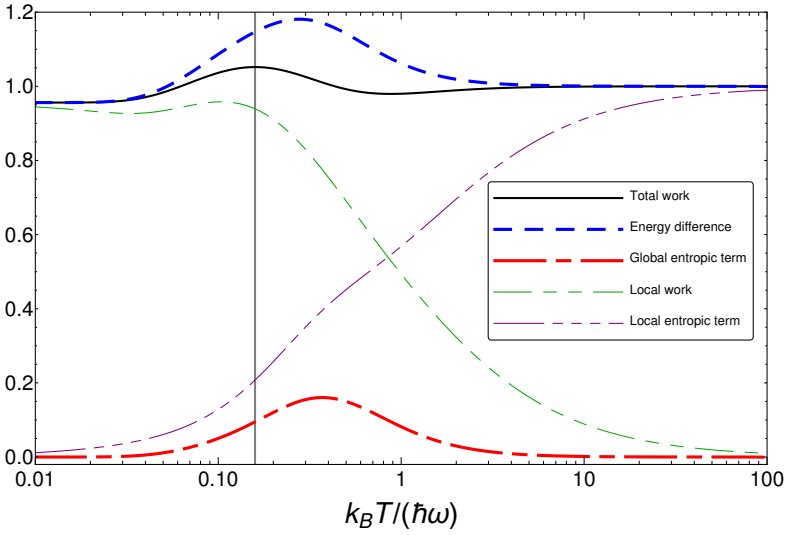

Figure 3.7: Rabi model: comparison of different quantities (each in units of $\hbar\omega$) as a function of the bath temperature for $g = \omega$. A grey vertical line is depicted in correspondence of the peak of the total work Wat $k_BT \simeq 0.16\ \hbar\omega$.

Charging a battery. — In general, the aim of work-extraction protocols is to realize something useful, e.g. a process that could be seen as the *charge of a battery*. Here, we propose a *transfer protocol* (for the zero-temperature case) that allows for storing the energy gained by system S into an external harmonic oscillator (system C) which plays the role of a battery, whose energy can be increased more and more through suitable cyclic interactions with system S.

The main idea is to imagine that system A is not just a two-level system, but a three-level system whose intermediate level does not participate to the interaction with system B. However, system C is resonant with the transition from this intermediate level to the excited one and interacts with system A through a Jaynes-Cummings Hamiltonian. In this way, whatever is the population of the ground level of system A, it can only give energy to system C but not receive it. Moreover, we use, as free resources, a certain number of systems having the same spectrum of system A, to transfer energy from B to C. Imagining the role of system R being played by the wave functions spatial part of each three-level system approaching and then leaving the harmonic oscillator (you could think of flying atoms and a cavity), we can clearly see that we could not charge system C by using directly the three-level systems in their initial state at $T = 0$ (ground state), i.e. without by first charging them through their interaction with system B. We observe that in this specific case, then, the resource would have a genuine quantum nature. An extensive description of this transfer protocol is reported in Appendix 3.E.

In a specific simulation of this transfer protocol (in the deep strong coupling regime, $g > \omega$, and for one hundred iterations) we obtain a final energy transferred to system C of the order of one hundred ω with a low standard deviation and a reasonable efficiency (see table 3.1 of Appendix 3.E).

3.5 Conclusions

In this chapter, we have proposed a work extraction protocol that consists of the thermalization of a storage bipartite system S by using a resource system R. Firstly, we have described the protocol in the general case without referring to a specific implementation. The protocol we have proposed should be easily implementable as it only requires to turn on and off the interaction between subsystems A and B of system S. This turning on/off has to happen quickly without changing the state of system S. Moreover, we have used thermodynamic resource theory results to define the extracted work W and the efficiency η. We point out that our results are not in contrast with the second law of thermodynamics. The work comes from the external resource R while the bath is used to enable the protocol itself.

Secondly, we have investigated the protocol performances in two models: two interacting qubits and the Rabi model. The entropic terms turn out to play an important role when the bath temperature (times the Boltzmann constant) is comparable with the subsystems energies. Indeed, the great difference between local and total extracted work is due to the correlations between A and B. The extracted work is comparable with the frequencies of the systems in both cases. Moreover, in the Rabi model case,

the efficiency we have obtained is always higher than one half. Both these applications show that simple processes like thermalization and switching on/off interactions between quantum systems can be fruitfully used for work extraction.

Thirdly, as a proof of principle, we have shown a specific example of how the energy extracted in the thermalization protocol can migrate to an external work storage system through a transfer process, making the complete protocol iterable. The whole protocol, composed of many thermalization protocol iterations plus the transfer protocol, realizes something like the *charge of a battery* in a realistic scenario and does not involve fine operations.

We deem interesting to generalize our study of the Rabi model to the N qubits scenario. This generalization will allow one to study if the qubits correlations lead to a greater work extraction. Further studies could suggest how to improve our transfer protocol, thus paving the way to proposals in specific physical scenarios.

3.A Work definition, heat and entropy production

Here, we make some comments on what could be the consequences of the adopted work quantifier [see Eq. (2.3.5)] on the definition of heat and on its connection with the entropy production. Let us assume that we can use $\Delta U = \mathrm{Tr}\{H'\rho'\} - \mathrm{Tr}\{H\rho\}$ as the internal energy change in the first law of thermodynamics, $\Delta U = Q + W$. It follows

$$Q = \mathrm{Tr}\left\{H'\rho'^{\mathrm{th}}\right\} - \mathrm{Tr}\left\{H\rho^{\mathrm{th}}\right\} + k_B T\left[S\left(\rho^{\mathrm{th}}\right) - S\left(\rho'^{\mathrm{th}}\right) + S\left(\rho'\right) - S(\rho)\right], \quad \text{(3.A.1)}$$

where ρ^{th} and ρ'^{th} are the thermal states corresponding, respectively, to H and H'. When only the system state changes we have:

$$\Delta U = \mathrm{Tr}\left\{H\left(\rho' - \rho\right)\right\}, \quad Q = k_B T\left[S\left(\rho'\right) - S(\rho)\right], \quad \text{(3.A.2)}$$

which seems reasonable as the heat is given by the change of entropy times $k_B T$, T being the temperature at which the process takes place. On the other hand, when only the Hamiltonian changes while the state of the system does not, ΔU and Q reduce to:

$$\Delta U = \mathrm{Tr}\left\{\left(H' - H\right)\rho\right\}, \quad Q = F\left(\rho'^{\mathrm{th}}, H'\right) - F\left(\rho^{\mathrm{th}}, H\right). \quad \text{(3.A.3)}$$

Let us comment now on a possible connection with the entropy production. During a thermal operation, system and bath together evolve unitarily so that the total entropy of both systems does not change and we can apply findings of Ref. [218]. There, the system under analysis is unitarily interacting with one or more thermal baths. To adapt the equations to our case we will use one single thermal bath. In particular we focus on a generic time interval with time-independent Hamiltonians, as from t_2 to t_3 in our thermalization protocol.

The system and the bath are considered to be in the state $\rho(0) = \rho_S(0) \otimes \rho^{\mathrm{th}}_{\mathrm{bath}}$ at time $t = 0$, as we also assume in our case during the thermalization step[16]. In particular, the entropy change in the system during the evolution can be decomposed as follows:

$$\Delta S(t) = \Delta_i S(t) + \Delta_e S(t), \quad \text{(3.A.4)}$$

where $\Delta_i S(t)$ is the entropy production and $\Delta_e S(t)$ represents the reversible contribution to the system entropy due to heat exchanges. More specifically [218], $\Delta_e S(t) = \beta Q_{\mathrm{bath}}(t)$, where $Q_{\mathrm{bath}}(t) \equiv \langle H_{\mathrm{bath}}\rangle_{t=0} - \langle H_{\mathrm{bath}}\rangle_t$ represents the heat flow from the reservoir (here $\beta = 1/k_B T$).

We are only interested to what happens at the end of the thermalization protocol, where TRT imposes the conservation of the total energy (see Appendix 2.3.1), therefore in this case $Q_{\mathrm{bath}}(t)$ is equal to $\Delta\langle H_S\rangle_t = \mathrm{Tr}\{H_S\rho_S(t)\} - \mathrm{Tr}\{H_S\rho_S(0)\}$. We recall that free energy is a decreasing monotone of thermal operations, that is $F(\rho_S(0), H_S) - F(\rho_S(t), H_S) \geq 0$. Then, we can show that $\Delta_i S(t) \geq 0$[17] as follows:

$$\begin{aligned}\Delta_i S(t) &= -\beta Q_{\mathrm{bath}}(t) + \Delta S(t) = \beta\left[-\Delta\langle H_S\rangle_t + \frac{1}{\beta}\Delta S(t)\right] \\ &= \beta\left[F(\rho_S(0), H_S) - F(\rho_S(t), H_S)\right] \geq 0.\end{aligned} \quad \text{(3.A.5)}$$

[16] With t_2 in place of $t = 0$.

[17] Notice that the positivity of entropy production verifies the second law of thermodynamics.

Notice that $\Delta_i S(t) = -\beta W(t)$, i.e., the entropy production exactly matches the loss of athermality of system S times the inverse temperature of the environment.

In the other steps of the protocol no entropy is produced because we assume ideal switchings (i.e., reversible processes) to define the ideal efficiency. Of course, some entropy is expected to be produced in a realistic implementation even during these operations.

3.B Work expense of system R

Here, we compute the amount of free energy that system R has to lose to turn on the interaction of system S. Considering the whole system $S+R$, before the action of system R we have:

$$\Delta F\left(\rho_R \otimes \rho_{AB}^{\text{th}}, H_R + H_0\right) = \Delta F\left(\rho_R, H_R\right), \tag{3.B.1}$$

where $\rho_{AB}^{\text{th}} = \rho_A^{\text{th}} \otimes \rho_B^{\text{th}}$. After the action of R, we have:

$$\Delta F\left(\rho'_{RAB}, H_R + H_0 + H_I\right) \geq \Delta F\left(\rho'_R, H_R\right) + \Delta F\left(\rho_{AB}^{\text{th}}, H_0 + H_I\right). \tag{3.B.2}$$

We consider the operation under consideration to be a catalytic Gibbs-preserving transition so that $\Delta F\left(\rho, H\right)$ has to decrease or to stay constant [137][18], therefore:

$$F\left(\rho'_R, H_R\right) - F\left(\rho_R, H_R\right) \leq \Delta F\left(\rho_{AB}^{\text{th}}, H_0 + H_I\right). \tag{3.B.3}$$

In the above equation, the equality holds in the best-case scenario. The work expense of R to perform the switching on is then given by Eq. (3.2.5) while, analogously, one can obtain Eq. (3.2.6) for the switching off.

3.C High temperature limit of extracted work in finite systems

If both A and B are finite, in the high temperature limit ($\beta \to 0$) it holds, at first order in β, the expansion:

$$e^{-\beta H} \simeq \mathbb{I} - \beta H, \tag{3.C.1}$$

where H is the Hamiltonian of the whole bipartite system and $\mathbb{I}$ is the identity in the whole Hilbert space. We call N_A the dimension of subsystem A and N_B the dimension of subsystem B while $N_S = N_A N_B$. Moreover, we use Eq. (3.2.11) written in the following way:

$$W = \frac{1}{\beta}\ln\left(Z_A Z_B\right) - \frac{1}{\beta}\ln(Z_S) - \langle H_I \rangle_{t_3}. \tag{3.C.2}$$

[18] See also section 2.3.1.

Then, expanding up to first order in β we get

$$\begin{aligned} Z_{A(B)} &\simeq N_{A(B)} - \beta \operatorname{Tr}_{A(B)} \left\{ H_{A(B)} \right\}, \\ Z_A Z_B &\simeq N_S - \beta \left(N_A \operatorname{Tr}_B \{H_B\} + N_B \operatorname{Tr}_A \{H_A\} \right), \\ \ln(Z_A Z_B) &\simeq \ln N_S - \frac{\beta}{N_S} \left(N_A \operatorname{Tr}_B \{H_B\} + N_B \operatorname{Tr}_A \{H_A\} \right). \end{aligned} \tag{3.C.3}$$

Similarly

$$\begin{aligned} Z_S &\simeq [Z_A Z_B]^{(1)} - \beta \operatorname{Tr}_S \{H_I\}, \\ \ln(Z_S) &\simeq [\ln (Z_A Z_B)]^{(1)} - \frac{\beta}{N_S} \operatorname{Tr}_S \{H_I\}, \end{aligned} \tag{3.C.4}$$

where the terms $[Z_A Z_B]^{(1)}$ and $[\ln(Z_A Z_B)]^{(1)}$ are the functions between brackets computed at first order in β. Lastly, to order zero in β:

$$\langle H_I \rangle_{t_3} = \operatorname{Tr}_S \left\{ H_I \frac{e^{-\beta(H_A+H_B+H_I)}}{Z_S} \right\} \simeq \frac{\operatorname{Tr}_S \{H_I\}}{N_S}. \tag{3.C.5}$$

Then, by considering all the contributions we obtain

$$\lim_{\beta \to 0} W = 0. \tag{3.C.6}$$

This result also implies

$$\lim_{\beta \to 0} \frac{1}{\beta} S(A:B) = 0, \tag{3.C.7}$$

because the global work is always higher or equal than the local one, but they are both positive and their difference is given by the correlation term.

3.D Rabi Hamiltonian ground state

In this Appendix, we study the ground state of the Rabi model in order to characterize the protocol at $T = 0$ for the Rabi model and compare our findings with the numerical simulations. Here, all the quantities with the tilde are in units of ω to lighten the notation ($\tilde{X} \equiv X/\omega$).

At $T = 0$, the entropy terms do not contribute to the free energies and, then, we can deal with average energies only. As a consequence, $W = W_l$, which takes the form

$$W = \langle H_A \rangle_{t_3} + \langle H_B \rangle_{t_3} + \hbar\Delta = \hbar\nu_0 - \langle H_I \rangle_{t_3} + \hbar\Delta, \tag{3.D.1}$$

where $\hbar\nu_0$ is the energy of the ground state of the Rabi model. The efficiency is given by

$$\eta = \frac{\langle H_A \rangle_{t_3} + \langle H_B \rangle_{t_3} + \hbar\Delta}{-\langle H_I \rangle_{t_3}}. \tag{3.D.2}$$

In order to calculate the quantities in Eqs. (3.D.1) and (3.D.2) we need to study the ground state and how it is decomposed in the bare basis. To this end we mainly

follow the approach and the formalism of Ref. [153]. These calculations allow us to compute numerically, but starting from the formal and analytical solutions, the amount of extracted work and the efficiency of the protocol.

Following Ref. [153], the ground energy $\hbar\nu_0$ of the ground state of the Rabi Hamitonian of Eq. (3.4.1) can be calculated by searching for the first zero of the Braak's function $G_-(x)$ [152, 153, 161], defined by:

$$G_\pm(x) = \sum_{n=0}^{\infty} \left(1 \mp \frac{\tilde{\Delta}}{x-n}\right) f_n \tilde{g}^n = 0, \tag{3.D.3}$$

where $x = \tilde{\nu} + \tilde{g}^2$. The factors f_n are calculated by recurrence through the following formulas:

$$\begin{aligned} f_n &= \frac{1}{n}\left[\Omega(n-1) f_{n-1} - f_{n-2}\right], \quad f_0 = 1,\ f_1 = \Omega(0), \\ \Omega(n) &= \frac{1}{2\tilde{g}}\left(n + 3\tilde{g}^2 - \tilde{\nu} - \frac{\tilde{\Delta}^2}{n - \tilde{g}^2 - \tilde{\nu}}\right). \end{aligned} \tag{3.D.4}$$

The values of ν for which the Braak's functions are zero are the eigenvalues of the Rabi Hamiltonian. The lowest of these eigenvalues is the ground energy of the system.

According to [153], after some easy but lengthy calculations the ground state can be written as follows:

$$|\psi_g\rangle = \frac{1}{2\sqrt{\mathcal{N}}}\left[|e\rangle\left(|\phi_1\rangle + |\phi_2\rangle\right) + |g\rangle\left(|\phi_1\rangle - |\phi_2\rangle\right)\right], \tag{3.D.5}$$

where $\mathcal{N}$ is a normalization constant,

$$\begin{aligned} \langle n|\phi_1\rangle &= e^{-\tilde{g}^2/2}\sqrt{n!}\sum_{m=0}^{\infty} m!\ e_m \left[\sum_{k=\max(0,n-m)}^{n} \frac{(-1)^k}{(m-(n-k))!(n-k)!k!}\tilde{g}^{m-(n-2k)}\right], \\ e_m &= -\frac{\tilde{\Delta}}{m - \tilde{g}^2 - \tilde{\nu}_0} f_m, \end{aligned} \tag{3.D.6}$$

and $\langle n|\phi_2\rangle$ is equal to $\langle n|\phi_1\rangle$ if one replaces in its expression e_m with f_m.

The parity operator $\Pi = -\sigma_z(-1)^{\hat{n}}$ commutes with H_{Rb}. Thus, it is easy to show that the ground state of the Rabi Hamiltonian has to be of the form

$$|\psi_g\rangle = \sum_{n=0}^{\infty} c_{2n}\,|g, 2n\rangle + \sum_{n=0}^{\infty} c_{2n+1}\,|e, 2n+1\rangle\,. \tag{3.D.7}$$

Indeed, for low values of $\tilde{g}$ the ground state has to contain the component $|g,0\rangle$ so that all the other components have to be of the same parity. Moreover, for every value of $\tilde{g}$ the ground eigenvalue does not cross with the others eigenvalues, therefore the ground state has the same parity for each value of $\tilde{g}$. By taking the scalar product of both sides

of Eq. (3.D.5) with $|n\rangle$, odd or even, and comparing with Eq. (3.D.7) one can easily infer the following equalities:

$$\sqrt{\mathcal{N}}c_n = \langle n|\phi_1\rangle = (-1)^{n+1}\langle n|\phi_2\rangle\,, \qquad \forall n. \tag{3.D.8}$$

Now we can easily calculate the reduced states and write down the quantities of interest. First of all, let us observe that

$$\rho_B^{\rm rth} = \mathrm{Tr}_A\left\{|\psi_g\rangle\langle\psi_g|\right\} = \frac{1}{2\mathcal{N}}\left(|\phi_1\rangle\langle\phi_1| + |\phi_2\rangle\langle\phi_2|\right). \tag{3.D.9}$$

Then, exploiting Eq. (3.D.8), the average energy of the harmonic oscillator can be written as follows:

$$\langle H_B\rangle_{t_3} = \frac{\hbar\omega}{\mathcal{N}}\sum_{n=0}^{\infty} n|\langle n|\phi_1\rangle|^2. \tag{3.D.10}$$

Similarly, the reduced state of the two-level system is found to be

$$\begin{aligned}\rho_A^{\rm rth} &= \mathrm{Tr}_B\left\{|\psi_g\rangle\langle\psi_g|\right\} = \frac{1}{\mathcal{N}}\left[\left(\sum_{n=0}^{\infty}|\langle 2n+1|\phi_1\rangle|^2\right)|e\rangle\langle e| + \left(\sum_{n=0}^{\infty}|\langle 2n|\phi_1\rangle|^2\right)|g\rangle\langle g|\right] \\ &= \left(\sum_{n=0}^{\infty}|c_{2n+1}|^2\right)|e\rangle\langle e| + \left(\sum_{n=0}^{\infty}|c_{2n}|^2\right)|g\rangle\langle g|\,,\end{aligned} \tag{3.D.11}$$

and the average energy is

$$\langle H_A\rangle_{t_3} = \hbar\Delta\left(2\sum_{n=0}^{\infty}|c_{2n+1}|^2 - 1\right). \tag{3.D.12}$$

Concerning the average of the interaction energy $\langle H_I\rangle_{t_3}$, it can be directly calculated with the formula:

$$\langle H_I\rangle_{t_3} = \frac{2\hbar g}{\mathcal{N}}\sum_{n=0}^{\infty}\sqrt{n+1}\,\langle n+1|\phi_1\rangle\,\langle n|\phi_1\rangle\,, \tag{3.D.13}$$

or, alternatively, it can be inferred from Eq. (3.D.1) as we already know $\langle H_A\rangle_{t_3}$ and $\langle H_B\rangle_{t_3}$ which we calculated through the knowledge of ν_0.

For very low values of g/ω the Jaynes-Cummings approximation can be used [12]. In this case Eq. (3.D.5) becomes $|\psi_g\rangle \simeq |g,0\rangle$. The Bloch-Siegert approximation holds good for higher values of g/ω (still $g/\omega \ll 1$) [155]. In this case, at resonance, $2\Delta = \omega$, Eq. (3.D.5) becomes [cf. Eq. (2.4.18)]

$$|\psi_g\rangle \simeq \left(1 - \frac{\Lambda^2}{2}\right)|g,0\rangle - \Lambda\,|e,1\rangle + \Lambda^2\sqrt{2}\,|g,2\rangle\,, \tag{3.D.14}$$

where $\Lambda = g/(2\omega)$.

3.E An example of transfer protocol

Here, we provide more details on the transfer protocol briefly described at the end of section 3.4, concerning the Rabi model in the case when the environment is at zero temperature. First, we suppose that system A, which we previously treated as a two-level system, is a three-level system whose intermediate third level $|u\rangle$ did not participate in the interaction with system B during the thermalization process. Then, the Hamiltonian of system A has to be written as follows:

$$H_A = \frac{\hbar\omega}{2}\,|e\rangle\langle e| - \hbar\gamma\,|u\rangle\langle u| - \frac{\hbar\omega}{2}\,|g\rangle\langle g|\,, \tag{3.E.1}$$

where $|\gamma| < \omega/2$. We also suppose to have at our disposal a number N_c of systems D_i, with the same spectrum of system A, in the ground state $|g\rangle$ (these copies are free resources because they are, initially, in the thermal state at $T = 0$)[19].

The main idea, depicted in figure 3.8, is to use system A and systems D_i to charge system C through interactions modeled with the Jaynes-Cummings Hamiltonian. The external harmonic oscillator is chosen to be resonant with the transition connecting states $|e\rangle$ and $|u\rangle$. The interaction with C will be assumed to involve only these states. By doing this and taking $|\gamma| < \omega/2$, we assure that $|u\rangle$ is never the ground state in each part of the thermalization protocol and that the interactions with system C are one-way energy transfers from systems A and D_i to system C.

The N_c systems D_i interact with system B through the Jaynes-Cummings Hamiltonian:

$$H_{\mathrm{JC}} = \hbar g_B \left(a\sigma_+ + a^\dagger\sigma_-\right), \tag{3.E.2}$$

where σ_+ and σ_- are, respectively, the raising and lowering Pauli operators. To analyze the simplest situation, each copy interacts with the harmonic oscillator for the same time t_B. Turning on this interaction does not require energy because the initial state of the three-level systems is the ground state and no energy is required also for turning off the interaction because H_{JC} commutes with the total Hamiltonian. By suitably choosing the time t_B, system B will be nearly depleted and the energy will be stored in the three-level systems.

Using Eqs. (3.D.5), (3.D.7), and (3.D.8), the reduced density matrix of system B after the thermalization protocol involving systems A and B can be rewritten as follows:

$$\rho_B^{\mathrm{rth}} = \sum_{n,m} \frac{c_n c_m}{2}\left[1 + (-1)^{n+m}\right]|n\rangle\langle m|\,. \tag{3.E.3}$$

Under the Jaynes-Cummings evolution, a two-level system and a harmonic oscillator in the state $|n+1\rangle$ undergo the following transformation [22]:

$$|g, n+1\rangle \to -i\sin\alpha_n\,|e, n\rangle + \cos\alpha_n\,|g, n+1\rangle\,, \quad \text{where} \quad \alpha_n = g_B t_B\sqrt{n+1}. \tag{3.E.4}$$

[19] In a realistic implementation, the assumption here is that the temperature T of the environment is very low with respect to the first energy gap of the systems. Then, they can be safely assumed to be, initially, in their ground state.

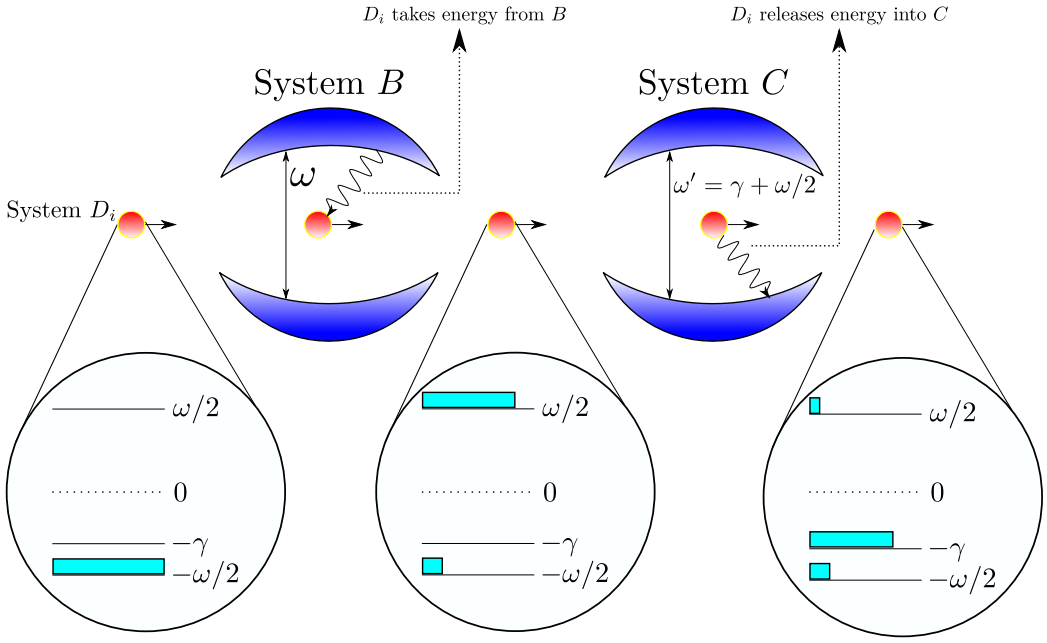

Figure 3.8: This figure shows the mechanism employing systems D_i to move energy from system B to the external battery, i.e., system C. The picture also shows the energy level scheme of systems A and D_i (we recall that systems D_i and system A have the same spectrum), while the light blue bars over the levels give a representation of how the populations of the different energy levels change during the transfer. Notice that the various coupling constants here involved are assumed to be zero before and after the interaction, and constant during it. This means that the transients of the coupling are assumed to happen in a very short time.

A simple calculation shows that, after the interaction, the three-level system D_i is in a mixed state without coherences:

$$\rho_{D_i} = \sum_n c_n^2 \Big(\sin^2 \alpha_{n-1} \, |e\rangle\langle e| + \cos^2 \alpha_{n-1} \, |g\rangle\langle g| \Big). \tag{3.E.5}$$

Moreover, the new state of the cavity is of the same form of Eq. (3.E.3), therefore none of the three-level systems acquires coherences in the energy basis.

In Fig. 3.9, we plot the efficiency of this energy transfer against the interaction time t_B, for $g = 1.6\ \omega$ and different values of N_c. This efficiency is defined as the ratio between the energy acquired by D_i and the energy, W_B, that was stored in system B, i.e., $\eta_1 = \left(\hbar\omega \sum_{i=1}^{N_c} p_i\right)/W_B$. Fig. 3.9 shows that a great part of W_B ($W_B \simeq 2.49\ \hbar\omega$) can be taken in this way by properly choosing the interaction time t_B. For comparison,

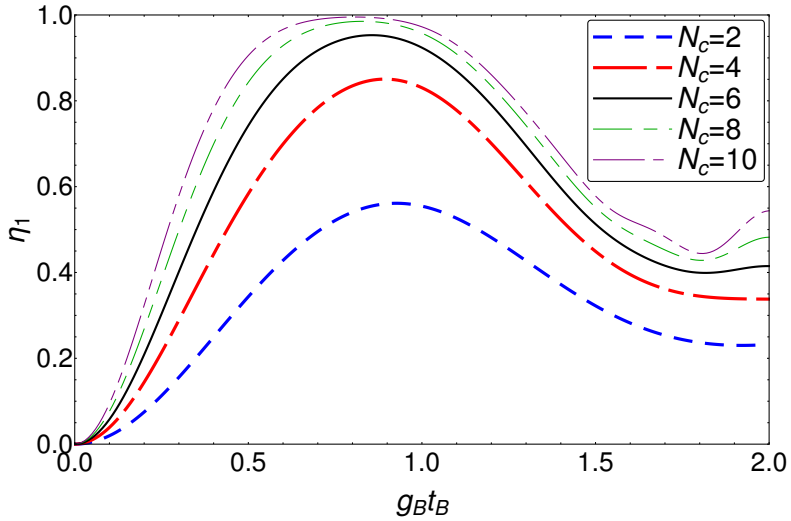

Figure 3.9: This graph shows the efficiency (η_1) of the extraction part of the transfer protocol as a function of the interaction time t_B for different values of N_c.

for a Rabi oscillation we have $g_B t_B = 2\pi$. This figure also suggests considering $N_c = 8$ in view of the fact that increasing this number raises the extracted energy by a very small amount. Moreover, the quantity of energy extracted in this way seems to be robust to little variations of t_B. We observe that in general the efficiency η_1 could be raised (and/or smaller values of N_c could be used) by choosing different interaction times for each of the three-level systems. The remaining energy of system B will be dissipated in the thermal bath.

In order to charge system C, we have then $N_c + 1$ three-level systems (the system A and the N_c systems D_i) with different excited populations. The system A and the systems D_i interact with system C through:

$$H'_{\mathrm{JC}} = \hbar g_C \left(c\sigma'_+ + c^\dagger \sigma'_- \right), \tag{3.E.6}$$

where c ($c^\dagger$) is the annihilation (creation) operator for C, which has Hamiltonian $H_C = \hbar\omega'\hat{n}_c$, with $\hat{n}_c = c^\dagger c$ and $\omega' = \omega/2 + \gamma$. We recall that this interaction with a system D_i can take place while another three-level system interacts with system B.

For every interaction with system C, the initial state of any D_i is of the kind

$$p_e \left|e\right\rangle\!\left\langle e\right| + 0 \left|u\right\rangle\!\left\langle u\right| + p_g \left|g\right\rangle\!\left\langle g\right|. \tag{3.E.7}$$

To compute the Jaynes-Cummings evolution under a time t_C, we can make use of the following transformation, concerning a two-level system in the excited state $|e\rangle$ and an harmonic oscillator in the state $|n\rangle$ [22]:

$$|e,n\rangle \to \cos\left(g_C t_C \sqrt{n+1}\right)|e,n\rangle - i \sin\left(g_C t_C \sqrt{n+1}\right)|u,n+1\rangle. \tag{3.E.8}$$

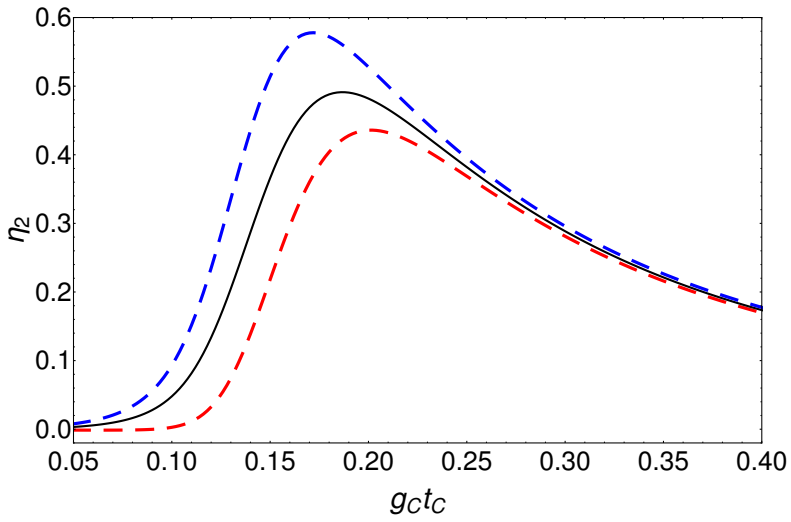

Figure 3.10: This graph shows the efficiency (η_2) of the charging part of the transfer protocol, for $N = 100$ iterations, as a function of the interaction time t_C for $N_c = 8$, $g_B t_B = 0.84$ and $\gamma = 0.4\ \omega$, which implies $\omega' = 0.9\ \omega$. In the graph, the solid line is the efficiency obtained using the average energy, while the dotted lines represent the efficiencies obtained using the average energy plus or minus the standard deviation.

Parameters	
$W_A = p_a\,\hbar\omega \simeq 0.44\ \hbar\omega$	$W_B \simeq 2.49\ \hbar\omega$
$N = 100$	$N_c = 8$
$g = 1.6\ \omega$	$\gamma = 0.4\ \omega$
Optimal interaction times and results	
$g_B t_B = 0.84$	$g_C t_C = 0.26$
$\eta_1 \simeq 0.985$	$\eta_2 \simeq 0.361$
$\eta_T \simeq 0.357$	$E_C \simeq (104.60 \pm 3.29)\,\hbar\omega$

Table 3.1: This table shows all the relevant values of the transfer protocol for a specific choice of the parameters.

It is then easy to show that each number state of the harmonic oscillator transforms as follows:

$$|n\rangle\langle n| \to \gamma_n\,|n\rangle\langle n| + (1-\gamma_n)\,|n+1\rangle\langle n+1|\,, \quad \gamma_n = p_e \cos^2\left(g_C t_C \sqrt{n+1}\right) + p_g. \tag{3.E.9}$$

Then, if the initial state of system C is a state with no coherences in its energy basis, it will never gain coherences from this interaction. In this case, the initial state of system C is the ground state $|0\rangle$.

Again, to analyze the simplest situation, each three-level system will interact with the harmonic oscillator for the same time t_C. Cycle after cycle, each three-level system meets system C in a different state, in general, so that the efficiency of this part of the whole

protocol depends on the number of cycles. After having interacted with system C, the three-level systems are reinitialized through thermalization and ready to start another cycle of the global protocol. The average efficiency per cycle of this energy transfer to system C is equal to the ratio of the energy stored in it after N cycles divided by N and the total transferable energy of the three-level systems before the interaction:

$$\eta_2 = \frac{E_C/N}{\hbar\omega\left(\sum_{i=1}^{N_c} p_i + p_a\right)} = \frac{\omega'}{\omega}\frac{\langle\hat{n}_C\rangle/N}{\left(\sum_{i=1}^{N_c} p_i + p_a\right)}, \tag{3.E.10}$$

where p_a is the excited population of system A at the end of the thermalization protocol[20].

In Fig. 3.10, we plot the efficiency of this part of the transfer protocol using the three-level systems of the previous part and one hundred iterations of the whole process as a function of t_C. The plot also shows the behavior of the standard deviation. As one can see, a maximum efficiency of the order of 50% can be achieved for $g_C t_C \simeq 0.18$. However, by choosing a larger value for t_C we can obtain smaller values for the standard deviation, thus improving the analogy between system C and an ordinary battery, since C is in a mixed state with a relatively high energy and small standard deviation, e.g., $E_C \simeq (104.60 \pm 3.29)\,\hbar\omega$ for $g_C t_C = 0.26$.

We think that $N = 100$ is a suitable compromise to show the iterability of the process while keeping reasonable (at least in principle) the assumption that the dissipation of system C is negligible. We have also considered other values of N (for example N=25 and N=1000), observing that the results for the efficiency and the standard deviation do not change qualitatively. We finally observe, from Fig. 3.10, that the optimal interaction time is much lower than the time of a Rabi oscillation ($g_C t_C = 2\pi$) and that the protocol is robust to small variations of t_C.

An interesting feature emerging from numerical simulations is that if we vary the populations p_i by keeping fixed their sum, the plot in Fig. 3.10 almost does not change, for N sufficiently high. This means that this result is solid with respect to the number of copies N_c and to variations of the populations.

The total efficiency of the complete transfer protocol can be calculated as follows:

$$\eta_T = \frac{W_A + \eta_1 W_B}{W_A + W_B} \times \eta_2. \tag{3.E.11}$$

In table 3.1 we report the efficiencies η_1, η_2 and η_T for some specific values of the relevant parameters, as well as the optimal interaction times (up to the second decimal digit) found through numerical simulations.

One can also estimate the minimum amount of time a cycle of the complete protocol takes when considering both the thermalization and the transfer protocol. By neglecting the A-B interaction switches, we get

$$T = (t_3 - t_2) + N_c \max\{t_B, t_C\}. \tag{3.E.12}$$

[20] See Eq. (3.D.11) for our specific model.

If $t_B > t_C$, this result is obtained by considering that when the last three-level system of a cycle ends its interaction with system B, system A can already be ready to start another thermalization process, i.e., the next cycle of the complete protocol. If $t_C > t_B$, the last of the copies has to wait N_c interactions of other three-level systems with system C. When its interaction begins, system A can already start the thermalization protocol. It follows that for N_c and N not too large, depending on the actual physical implementation, the dissipative processes of system C during its charge could be effectively negligible, as we assumed here.

Chapter 4

Thermodynamics protocols: thermal cycles

4.1 Introduction

As anticipated in section 2.3, much effort has been devoted to the tradeoff between power and efficiency, with power usually increased at the expense of efficiency. When studying the power of a discrete quantum heat device, i.e., operating with finite-time strokes, the time allocated for thermalization typically plays an important role often representing the main contribution to the waiting time between subsequent strokes. In most cases, such a waiting time can be so high that all the other cycle steps can be considered instantaneous [133, 134, 219]. On the other hand, there is an ongoing effort to reduce the thermalization times, especially within the quantum Carnot cycle [220–223], and to optimize the power output [224]. In some cases, however, the waiting time is assumed negligible compared to other times, as done in other proposals of the quantum Otto cycle employing shortcuts to adiabaticity [142–144], reducing the time necessary to vary the Hamiltonian of the working fluid.

In this chapter, we propose two quantum thermal machines based on two-stroke cycles. In both models, two collections of identical quantum systems with constant and evenly spaced energy levels are initially prepared in equilibrium by bringing them in contact with a cold and a hot thermal bath, respectively. In the first scheme we propose, a system of one collection interacts with a system of the other one, and then they thermalize. The presence of many copies in each collection can change the magnitude of the effective waiting time with respect to the interaction time. In the second scheme, the two collections do not interact directly anymore but by means of a mediator system. The mediator interacts alternately with some systems from one collection and then with some from the other one. While the mediator interacts with one collection, the systems of the other collection can interact with their own thermal bath, thus amortizing the waiting time.

Under the general assumption that the various interactions preserve the number of excitations, we show that the efficiencies of the two cycles depend only on the Bohr

frequencies of the two collections and are equal to the one of an "equivalent" Otto cycle[1]. Remarkably, this is obtained without the need for time intervals where these Bohr frequencies or energy gaps must be varied. With a specific choice of the interaction Hamiltonian, we investigate for both models the problem of power optimization, focusing on the case of qubits and harmonic oscillators. One of the novel aspects of our work is a detailed analysis of the role of the waiting time between consecutive interactions, especially in relation to the maximum achievable power, an aspect which has often been overlooked in the literature. For the first model, we also compare our results with those of "equivalent" Otto cycles. Concerning the second model, instead, we show that the presence of a mediator can bring a performance advantage for a specific range of the waiting time in the correspondent cycle without the mediator. Moreover, a machine with the mediator system could be more easily implemented, depending on the experimental platform.

This chapter is organized as follows. In section 4.2, we describe the model without the mediator, analyze its efficiency, and maximize its power. Then, in section 4.3, we perform a similar study for the model with the mediator and show that its presence can lead to performance advantages. In section 4.4, we compare the cycle without the mediator with quantum Otto cycles which make use of shortcuts to adiabaticity. Finally, in section 4.5, we briefly state the conclusions of our work, while we provide details of our analysis and calculations in several Appendices.

4.2 The model without mediator

In this model, depicted in Fig. 4.1, the thermal machine consists of two collections C_c and C_h of copies of, respectively, quantum systems S_c and S_h, with Hilbert space dimensions, respectively, N_c and N_h. The systems of the two collections, when non-interacting, are in contact with a cold bath at temperature T_c and a hot bath at temperature T_h, respectively. The systems S_c and S_h have evenly spaced energy levels so that they can be characterized, respectively, by the positive frequencies ω_c and ω_h as shown in Fig. 4.1. The machine cycle consists of the two following strokes.

1. One system S_c, initially at equilibrium at temperature T_c, interacts for a time τ with a system S_h, initially at equilibrium at temperature T_h.

2. After the interaction or collision, S_c and S_h thermalize again.

In realistic implementations of this kind of thermal machines, there could also be other times required, for example, to re-initialize the machine. We denote by t_w the waiting time between the end of a collision and the start of the following one. Then, each cycle lasts $\tau + t_w$. Depending on the physical realization, the time t_w can vary over a wide range, from being negligible compared to τ to being much larger than that. For example, Fig. 4.1 describes a situation similar to that of Refs. [133, 134, 225], in the

[1] See section 2.3.2.

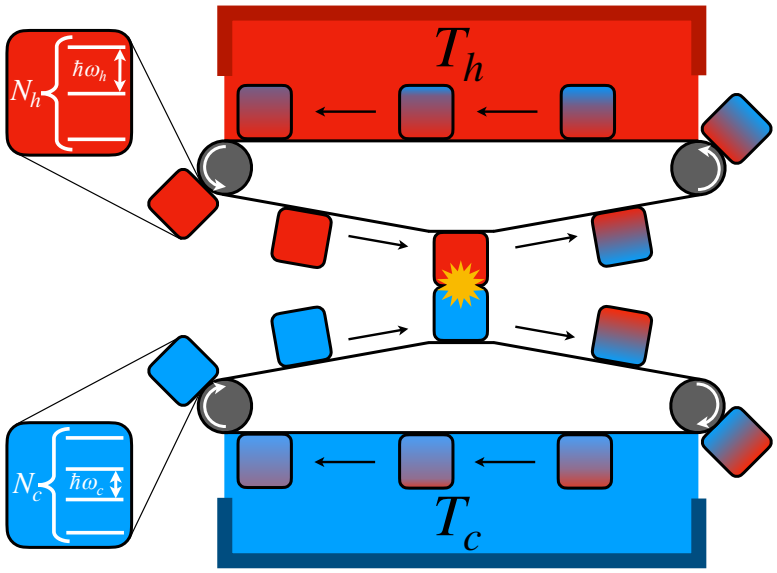

Figure 4.1: A scheme of the cycle with no mediator. Couples of systems belonging to each of the two collections interact for a time τ and then thermalize, sequentially. With enough couples, the thermalization of each one of them occurs during the collisions of other couples so that the waiting time t_w can be greatly amortized and can become even negligible compared to the interaction time τ.

case each collection is made of only one system and the interaction time between the machine systems is assumed to be negligible compared to the waiting time, which at least comprises the thermalization time. In the opposite case, we assume that both collections are made of many systems and the interaction between couples of systems is activated sequentially. Therefore, if there are enough couples, the systems of the first couple are already practically thermalized when the interaction of the last couple ends[2]. Even in the latter case, the waiting time t_w can not be deemed exactly zero since an unavoidable amount of time may be required for the machine between the end of a collision and the beginning of the following one. Having in mind this scenario, in our analysis we consider t_w as a parameter which can vary.

We notice that a model sharing some similarity with the one we propose in this section has been very recently investigated [225]. There, differently from here, the time allocated for the second stroke has a different physical origin being it connected to partial thermalization by means of a collisional bath.

The free Hamiltonians of the systems of each collection are given by

$$H_r = \hbar\omega_r n_r, \quad n_r = a_r^\dagger a_r, \tag{4.2.1}$$

[2]Strictly speaking, a system requires an infinite time to thermalize at the temperature of the heat bath it is weakly interacting with [12]. However, after a certain finite time, the system reaches a state which is practically indistinguishable from a thermal state.

	Engine	Refrigerator	Heat Pump	Thermal Accelerator
Conditions	$\omega_c < \omega_h < \omega_c\,(T_h/T_c)$	$\omega_h > \omega_c\,(T_h/T_c)$	$\omega_h > \omega_c\,(T_h/T_c)$	$\omega_h < \omega_c$
Work and Heat	$W<0,\ Q_h>0,\ Q_c<0$	$W>0,\ Q_h<0,\ Q_c>0$	$W>0,\ Q_h<0,\ Q_c>0$	$W>0,\ Q_h>0,\ Q_c<0$
Efficiency or COP	$-W/Q_h = 1-\omega_c/\omega_h$	$Q_c/W = \omega_c/(\omega_h-\omega_c)$	$-Q_h/W = \omega_h/(\omega_h-\omega_c)$	$-Q_c/W = \omega_c/(\omega_c-\omega_h)$

Table 4.1: Working regimes of the cycle. The conditions of the first line are valid when $N_c = N_h$ and $\min(\langle n_c\rangle_{\rm th}, \langle n_h\rangle_{\rm th}) \leq \langle n_r\rangle_\tau \leq \max(\langle n_c\rangle_{\rm th}, \langle n_h\rangle_{\rm th})$. Regarding the cycle with mediator (see section 4.3), we also require that $N_c = N_m$ and that $\min(\langle n_m\rangle_{u_r-1}, \langle n_r\rangle_{\rm th}) \leq \langle n_m\rangle_{u_r} \leq \max(\langle n_m\rangle_{u_r-1}, \langle n_r\rangle_{\rm th})\ \forall\ u_r > 0$, where N_m is the dimension of the mediator, n_m its number operator, and u_r the number of its collisions with systems S_r (see Appendix 4.B for more details). Notice that the efficiencies η and the COP do not depend on the dimensions of the systems and the conditions on the time evolution.

where $r = c, h$, depending on which kind of system we are describing. The operators a_r and $a_r^\dagger$ satisfy

$$\begin{aligned} a_r\,|n\rangle &= \sqrt{n}\,|n-1\rangle\,, & a_r^\dagger\,|n\rangle &= \sqrt{n+1}\,|n+1\rangle\,, \\ a_r\,|0\rangle &= 0, & a_r^\dagger\,|N_r-1\rangle &= 0. \end{aligned} \tag{4.2.2}$$

The use of the operators a_r and $a_r^\dagger$ allows us to have a unified formalism whatever the Hilbert space dimensions of the systems are, including qubits and harmonic oscillators as special cases. The commutator of a_r and $a_r^\dagger$ gives

$$\left[a_r, a_r^\dagger\right] = \mathbb{I} - d_r\,|d_r-1\rangle\langle d_r-1|\,, \tag{4.2.3}$$

where $\mathbb{I}$ is the identity operator in the Hilbert space of dimension N_r, $d_r = N_r$ for any finite-dimensional case[3], while the correct result for the harmonic oscillator case[4] is formally obtained by putting $d_r = 0$.

Regarding the interaction Hamiltonian for the collisions S_c-S_h, we use

$$H_I = \hbar g\left(a_c^\dagger a_h + a_c a_h^\dagger\right), \tag{4.2.4}$$

where, without loss of generality, the coupling constant g is assumed to be real and positive. This Hamiltonian, which can be described as "exchange" or "tight-binding" in solid state and condensed matter physics and as "beam-splitter" in quantum optics, is widely used in the literature [12, 22], for example, in the case of qubits [71, 226–228] and harmonic oscillators [229, 230]. Notice that the Hamiltonian of Eq. (4.2.4) preserves the total excitation number in the system $S_c + S_h$, i.e.,

$$[n_c + n_h, H_I] = 0. \tag{4.2.5}$$

During the interaction, systems S_c and S_h are considered isolated from the environments so that the external work W, required to switch on and off the interaction, is equal

[3]For example, the qubit case is obtained by choosing $d_r = N_r = 2$.

[4]In the case of harmonic oscillators, we recall that $\left[a_r, a_r^\dagger\right] = \mathbb{I}$.

to the difference in energy before and after the collision:

$$W = \hbar\,(\omega_h - \omega_c)\,(\langle n_h\rangle_\tau - \langle n_h\rangle_{\rm th})\,, \tag{4.2.6}$$

where $\langle n_r\rangle_\tau$ and $\langle n_r\rangle_{\rm th}$ are the average number of excitations of the system S_r, after the interaction and in the thermal state at temperature T_r for the free Hamiltonian of system S_r, respectively[5]. In particular, we have $\langle n_r\rangle_{\rm th} = {\rm Tr}\{\rho_r^{\rm th} n_r\}$, where we have defined the equilibrium thermal state $\rho_r^{\rm th} = Z_r^{-1}\exp[-H_r/(k_B T_r)]$, being $Z_r = {\rm Tr}\{\exp[-H_r/(k_B T_r)]\}$ the partition function, and k_B the Boltzmann constant. Eq. (4.2.6) clearly shows that W can be different from zero only when S_c and S_h are not resonant. We also notice that the number-conserving property of the interaction Hamiltonian implies $\langle n_h\rangle_\tau - \langle n_h\rangle_{\rm th} = \langle n_c\rangle_{\rm th} - \langle n_c\rangle_\tau$. We use the convention that the external work W is negative in the case of work extraction. Notice that this external work has to be provided by an external agent turning on and off the interaction. Taking as an example the picture of figure 4.1, this external agent could be represented by the conveyor belts.

After the interaction, the system S_r (with $r = c, h$) is put in contact with its thermal bath at temperature T_r and thermalizes again. In this case, the system exchanges exclusively heat with its bath equal to

$$Q_r = \hbar\omega_r\,(\langle n_r\rangle_{\rm th} - \langle n_r\rangle_\tau)\,. \tag{4.2.7}$$

An engine is realized when $W < 0$, a refrigerator or heat pump when $W > 0$ and $Q_c > 0$ while a thermal accelerator[6] is obtained for $W > 0$ and $Q_c < 0$, as summarized in Table 4.1. The consequence of choosing an interaction Hamiltonian preserving the total excitation number in the systems[7] is that the efficiencies and the coefficients of performance (COPs) of these thermal machines only depend on the frequencies of the systems S_c and S_h, as reported in Table 4.1. Moreover, under the assumption that $N_c = N_h$ and that $\min(\langle n_c\rangle_{\rm th}, \langle n_h\rangle_{\rm th}) \leq \langle n_r\rangle_\tau \leq \max(\langle n_c\rangle_{\rm th}, \langle n_h\rangle_{\rm th})$[8], the working regimes depend only on frequencies and temperatures. In fact, it suffices to notice that, when $N_c = N_h$,

$$\frac{\omega_c}{T_c} > \frac{\omega_h}{T_h} \iff \langle n_c\rangle_{\rm th} < \langle n_h\rangle_{\rm th}\,. \tag{4.2.8}$$

Notably, the efficiencies and COPs here are the same of the "equivalent" adiabatic Otto cycle [143, 144], described in section 4.4. We remark that Eqs. (4.2.6) and (4.2.7) and the results reported in Table 4.1 hold good for any interaction Hamiltonian satisfying Eq. (4.2.5).

[5] We point out that, in this chapter, the work is not defined as in chapter 3 since here we refer to a thermal cycle involving two baths at different temperatures. As a consequence, also the heat is defined differently here.

[6] In literature, a thermal accelerator is considered to be a machine which facilitates the natural heat flow from the hot bath to the cold bath.

[7] See Eq. (4.2.5).

[8] In the case of qubits and harmonic oscillators, we have verified that this condition and the analogous ones in the case with the mediator [see caption of Table (4.1)] are satisfied for Eq. (4.2.4).

4.2.1 Maximization of power

Here, we solve the problem of maximizing the power of the machine. We remark that all the maximizations in this chapter are performed at fixed temperatures and couplings. As a first step, we need to find the average number of excitations in the systems after the collision. This computation, performed in the Heisenberg picture, is detailed in Appendix 4.A and gives for a qubit-qubit collision or an oscillator-oscillator one

$$\langle n_h \rangle_\tau = \langle n_c \rangle_{\rm th} + \left(\langle n_h \rangle_{\rm th} - \langle n_c \rangle_{\rm th} \right) A, \tag{4.2.9}$$

with

$$A = \frac{2\delta^2 + g^2 \left[1 + \cos\left(2k\tau \right) \right]}{2k^2} = 1 - \frac{g^2}{k^2} \sin^2\left(k\tau \right), \tag{4.2.10}$$

where $\delta = \left(\omega_h - \omega_c \right)/2$ and $k = \sqrt{\delta^2 + g^2}$. Since the above formulas are exact only in the cases of qubit-qubit and oscillator-oscillator collisions, every detailed analysis in this chapter will be done for these cases. However, in all the other cases, we expect these formulas to be a good approximation when some appropriate conditions are fulfilled (see Appendix 4.A for more details).

By using Eqs. (4.2.9) and (4.2.10) in Eqs. (4.2.6) and (4.2.7), it is possible to cast the functional dependence of the power for the various working regimes into a product of a function $f(T_c, T_h, \omega_c, \omega_h)$ that depends solely on temperatures and frequencies and a coefficient V:

$$\begin{aligned}
P_E &= \frac{-W}{\tau + t_w} = \hbar \left(\omega_h - \omega_c \right) \left(\langle n_h \rangle_{\rm th} - \langle n_c \rangle_{\rm th} \right) V, \\
P_R &= \frac{Q_c}{\tau + t_w} = \hbar \omega_c \left(\langle n_c \rangle_{\rm th} - \langle n_h \rangle_{\rm th} \right) V, \\
P_H &= \frac{-Q_h}{\tau + t_w} = \hbar \omega_h \left(\langle n_c \rangle_{\rm th} - \langle n_h \rangle_{\rm th} \right) V, \\
P_A &= \frac{-Q_c}{\tau + t_w} = \hbar \omega_c \left(\langle n_h \rangle_{\rm th} - \langle n_c \rangle_{\rm th} \right) V,
\end{aligned} \tag{4.2.11}$$

where

$$V = \frac{1 - A}{\tau + t_w} = \frac{g^2}{k^2} \frac{\sin^2\left(k\tau \right)}{\tau + t_w}. \tag{4.2.12}$$

In the following, after a first study which applies to all the functioning regimes, we will deal with the general problem by focusing on the engine regime. In the case of qubits, we have checked that the qualitative results are the same when studying the figure of merit for refrigerators, which is the product of the cooling power P_R and of the COP, and is the quantity one usually tries to maximize when optimizing a refrigerator cycle [133, 231].

Maximization with fixed frequencies

We start our investigation on power maximization by studying the case in which both the temperatures and the frequencies of the systems are fixed, as commonly done in the

literature (see, for example, Refs. [133, 134, 142–144]). We also consider the coupling g and the waiting time t_w as given parameters and the optimization is performed only with respect to the collision time τ. In the next subsection, instead, the optimization will be done also with respect to the frequencies of the systems. Here, since τ only appears in the term V, we can maximize all the power functions at once by just maximizing V. Notice that when the frequencies are fixed, maximizing the cooling power is equivalent to maximizing the figure of merit since the COP only depends on the frequencies. With this first analysis, we show how much impact the waiting time has on the maximization of power and the optimal collision time for which it is realized.

The maximization of the term V of Eq. (4.2.12) with respect to the collision time τ has to be carried out numerically. In Fig. 4.2, we report the optimal value of $k\tau$ as a function of the quantity kt_w. We denote the optimal collision time as τ^* and the term V calculated for this collision time as $V_{\max}$. Moreover, the same plot also shows the value of Vk/g^2, which is a function of $k\tau$ and kt_w, in two cases: for $\tau = \tau^*$ and $k\tau = \pi/2$. The first case is the value of τ maximizing the power while the second one is the smallest value that maximizes the work per cycle[9]. When $t_w = 0$, the optimal collision time is given by the equation $k\tau^* = y^*$, where $y^* \simeq 1.16556$ is the value of y maximizing $\sin^2(y)/y$, the maximum being equal to $\alpha \simeq 0.724611$. On the other hand, in the limit $t_w \to \infty$, the maximum of V is simply obtained for $k\tau = \pi/2$ since the contribution of τ in the denominator od Eq. (4.2.12) becomes negligible in this limit. We also denote the time value for which $k\tau = \pi/2$ as the "swap time" since the states of the two systems S_c and S_h are practically swapped when $g \gg |\delta|$. Figure 4.2 shows that the optimal time drastically changes value when kt_w varies in the interval $[0.1, 10]$ and that up to $kt_w \sim 10$ the dimensionless optimal time $k\tau^*$ is substantially different from $\pi/2$. However, the advantage in power obtained by using the optimal time instead of the swap one is significant only up to $kt_w \sim 0.1$.

Remarkably, the power output is quite resilient to errors in the interaction time, as can be seen in Fig. 4.3. There, we show how $V/V_{\max}$ changes as a function of $k\tau$. Small uncertainties in the collision time around the optimal collision time τ^* lead to a small decrease in the output power. The plot also shows that the loss in power obtained by using the swap time instead of the optimal one increases when t_w decreases, becoming approximately 12% for $kt_w = 0.01$.

The perfect swap between two non-resonant systems[10] is often assumed to be a valid operation in a thermodynamic cycle. One could wonder about the power of a Hamiltonian capable of exactly implementing a perfect swap and its performance. We analyze this case in Appendix 4.C for the qubits case, finding that the "swap" Hamiltonian preserves the number of excitations in a collision, thus leading to the same efficiencies of our interaction Hamiltonian of Eq. (4.2.4). We compare the performance of the exchange and swap Hamiltonians by imposing that the difference between the highest and lowest eigenvalues is the same in the two Hamiltonians (for simplicity, this is done for $t_w = 0$). We find that the swap Hamiltonian performs better when it is possible to optimize the interaction

[9] The work per cycle is maximized when $k\tau = \pi/2 + m\pi$, where m is a natural number.

[10] For example, qubits in Ref. [134].

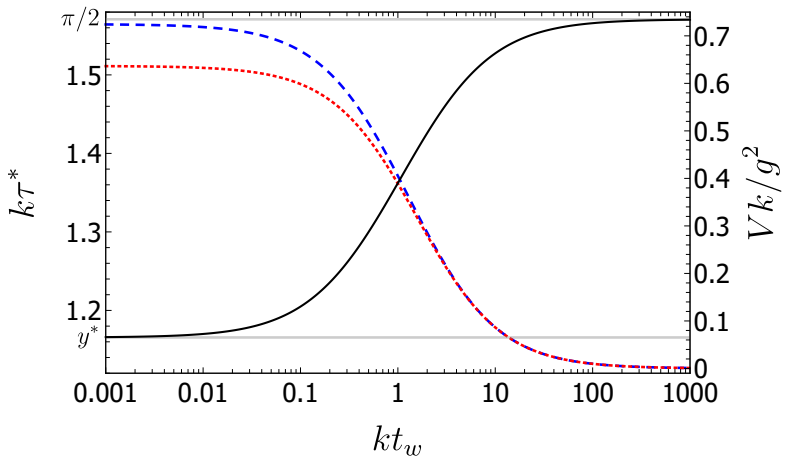

Figure 4.2: Optimal collision time τ^* (black continuous curve), $V_{\max}$, i.e., V calculated at the optimal time τ^* (blue dashed curve), and $V(k\tau = \pi/2)$, i.e., V calculated at the swap time (red dotted curve), as functions of the waiting time t_w for fixed frequencies and coupling. Each curve presents its greatest variation when kt_w varies in the interval $[0.1, 10]$. Regarding τ^*, the two limit values for $kt_w \to 0, \infty$ are, respectively, y^* and $\pi/2$.

time, while this is not always true if the swap Hamiltonian acts for the appropriate swap time. For this case, we find for which values of g the exchange Hamiltonian leads to higher power output than the swap one.

Maximization with respect to frequencies, qubits case

Here, we deal with the problem of maximizing the power output not only with respect to the collision time but also with respect to the frequencies of the two collections, assuming that both of them are composed of qubits. Contrary to the previous maximization of the term V at fixed frequencies, maximizing over frequencies impacts the efficiencies of the thermal machine and leads to different results for different working regimes. We choose to make this maximization in the engine case. Similar qualitative results are obtained by studying the figure of merit for refrigerators.

We start our analysis by observing that, for properly optimizing the power, it is not sufficient to maximize with respect to ω_c/ω_h. Therefore, since we cannot use ω_c as the unit frequency, we define the frequency $\nu_c = k_B T_c/\hbar$ as a unit measure for frequencies.

In Fig. 4.4, we show the behavior of the normalized maximum power as a function of the efficiency for different values of the waiting time. Noticeably, the power peaks are characterized by an efficiency larger than the Curzon-Ahlborn one[11] provided a high enough coupling is employed. Therefore, our model belongs to the class of systems that may surpass the Curzon-Ahlborn efficiency at maximum power [20, 127–129, 131–134]. Moreover, the curves corresponding to the high coupling limit do not change significantly

[11] See section 2.3 for a brief introduction to this quantity.

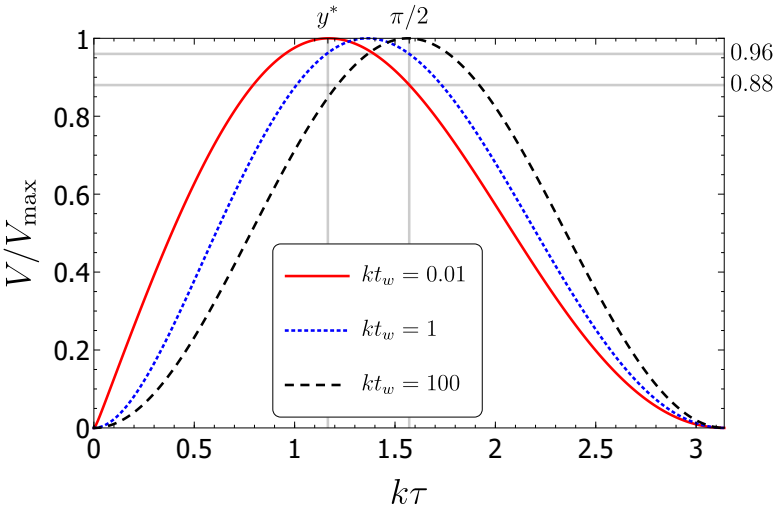

Figure 4.3: $V/V_{\max}$ as a function of the collision time τ for fixed frequencies and coupling. In this case, the ratio is only a function of $k\tau$ and kt_w. Small errors in the collision time around τ^* provoke only a small decrease of V.

when increasing the waiting time t_w while the other ones have their peak moving to the left.

We would like to comment on what the high coupling limit represents in this setting, where the frequencies can vary. The high coupling limit is obtained when $g \gg |\delta|$ so that $k \simeq g$. However, $|\delta| = |(\omega_h - \omega_c)/2|$ so that the magnitude of δ maximizing the power depends on T_h/T_c even if the temperatures do not directly appear in the term V. Our numerical simulations suggest that the optimal frequencies are roughly comprised in the range $[\nu_c, (T_h/T_c)\nu_c]$ (the upper bound can be slightly overcome for small values of η_E), hence a safe condition for the high coupling limit is $g \gg (T_h/T_c)\nu_c$.

Maximization with respect to frequencies, harmonic oscillators case

In the case of harmonic oscillators, the power peak is not obtained for some specific finite non-zero values of ω_c and ω_h, as shown in Appendix 4.D. There, the power is indeed shown to increase monotonically by decreasing the frequencies while keeping the temperatures and the efficiency fixed.

When searching for the maximum power, since it is obtained in the limit $\omega_c, \omega_h \to 0$, the high coupling condition ($g \gg |\delta|$) is always respected so that $V_{\max}$ is independent from the frequencies for any finite coupling[12]. For the same reason ($\omega_c, \omega_h \to 0$), the search for the maximum can be done in the mathematically equivalent high-temperature limit ($k_B T_r \gg \hbar\omega_r$). To find P_E of Eq. (4.2.11) in this case, let us write $\omega_h = \omega_c/(1-\eta_E)$ and $T_h = T_c/(1-\eta_C)$, where η_C is the Carnot efficiency. Then, after some straightforward

[12]See Eq. (4.D.8).

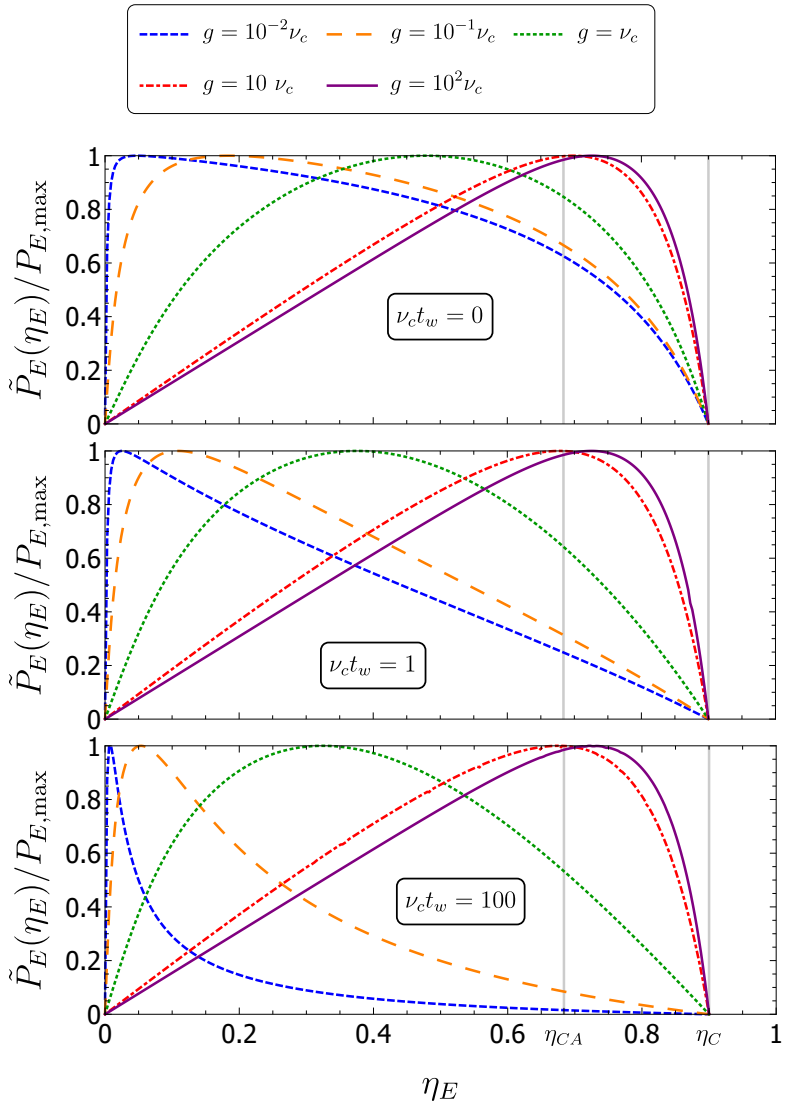

Figure 4.4: Normalized maximum power $\tilde{P}_E(\eta_E)/P_{E,\max}$ as a function of the efficiency $\eta_E = 1 - \omega_c/\omega_h$. For a given η_E, the maximization is done with respect to τ and ω_c, imposing $\omega_h = \omega_c/(1-\eta_E)$. Each plot shows the same curve for different values of the coupling g, while they differ for the value of t_w. Other parameters are: $N_c = N_h = 2$ and $T_h = 10T_c$. The two vertical lines indicate, from left to right, the Curzon-Ahlborn efficiency and the Carnot one. Noticeably, in the high coupling limit, the efficiency at maximum power is higher than the Curzon-Ahlborn one for every waiting time.

calculations, we obtain

$$P_E \simeq \frac{k_B T_c}{1-\eta_C} \frac{\eta_E(\eta_C-\eta_E)}{1-\eta_E} V. \tag{4.2.13}$$

When maximizing P_E in this limit, we recall that $V_{\max}$ is independent of the frequencies and, consequently, of the efficiency η_E. Then, one can just maximize $[\eta_E(\eta_C-\eta_E)]/(1-\eta_E)$ in Eq. (4.2.13) finding that the efficiency maximizing the power is the Curzon-Ahlborn one.

The distinct behavior between qubits and harmonic oscillators stems from the very different probability distribution of the populations in the thermal states, which, being both systems characterized by a single frequency, is entirely due to the difference in the number of levels. It follows that although the Heisenberg dynamics of the observables we are interested in during the collision is the same, a maximization over frequencies leads to different results. In particular, the monotonic increase of power obtained by decreasing the frequencies in the case of oscillators appears to be connected to their capacity of absorbing an unlimited number of excitations in the limit of vanishing frequencies, in contrast to finite dimensional systems.

4.3 The model with mediator

As we have seen in the previous section, when the number of couples S_c-S_h at disposal is large enough, the contribution of the thermalization to the effective waiting time t_w can be eliminated, greatly reducing t_w, whose final value will depend, for example, on the time required by the machine between a collision and the next one. However, for a small number of couples, the relaxation time cannot be neglected. In this situation, one could try to improve the setup by adding a mediator system S_m which alternately interacts with one of the two systems S_c and S_h in order to double the number of collisions, thus effectively extending the time allocated for the thermalization. This can practically eliminate the contribution of the thermalization time to the effective waiting time $t_{w,m}$ for a relatively large number of couples even when this number is not sufficient for the case without the mediator. Moreover, the addition of a mediator could also modify the part of the waiting time due to machine requirements. For example, if some amount of time is required between subsequent collisions, with the presence of the mediator this time could be suppressed because the interaction S_m-S_h can be turned on as soon as the S_m-S_c is turned off.

The new setup can be described as follows: we consider a machine composed of the same components as in the previous section, but with the addition of a central "mediator" system S_m characterized by the frequency ω_m. Moreover, we consider the possibility of grouping the systems of each collection in order to make the mediator interact, alternately, with sequences of systems of the same collection. Then, in the most general case, the cycle consists of the two following strokes.

1. The mediator interacts consecutively with u_c systems of the collection C_c, each collision lasting for a time τ_c through an interaction Hamiltonian like that of

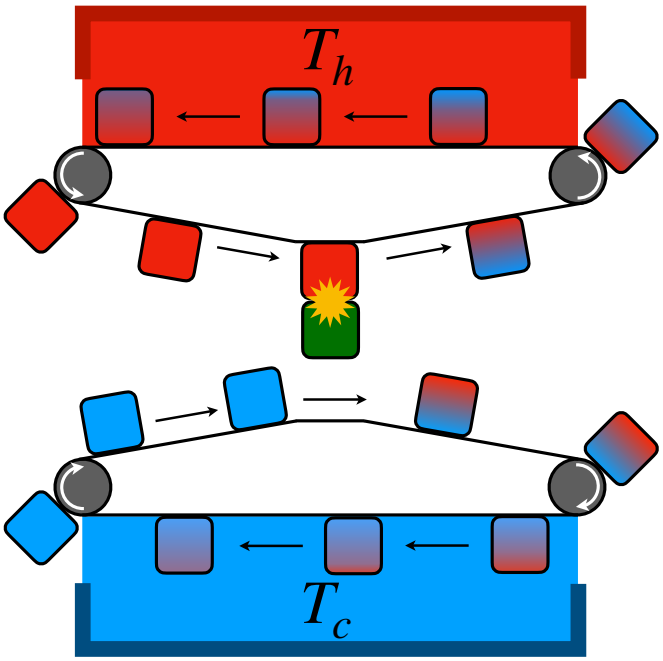

Figure 4.5: A scheme of the cycle with the mediator. Here, for each cycle, the mediator system interacts alternately with a system of collection C_c and then with a system of C_h (in the general case considered in the text, one can have u_r collisions).

Eq. (4.2.4) but with coupling g_c and operators a_m and $a_m^\dagger$[13] instead of, respectively, g, a_h, and $a_h^\dagger$.

2. The mediator interacts consecutively with u_h systems of the collection C_h, each collision lasting for a time τ_h through an interaction Hamiltonian like that of Eq. (4.2.4) but with coupling g_h and operators a_m and $a_m^\dagger$ instead of, respectively, g, a_c, and $a_c^\dagger$.

This model and its functioning are illustrated in Fig. 4.5 in the particular case $u_c = u_h = 1$, which we will argue to be the best performing case. We assume that, before the interaction with S_m, the state of the systems S_r[14] is always described by the corresponding thermal state and that the interacting systems are initially not correlated.

Ideally, as said above, the advantage of this scheme compared to the previous one is that the effective waiting time can be reduced even more. In particular, by comparing the two models in the case $u_c = u_h = 1$, we can expect that $t_{w,m} \simeq 0$ when $t_w \lesssim \tau_m^*$, where τ_m^* is the optimal collision time of the model with the mediator (computed in the case $t_{w,m} = 0$), since $t_{w,m} \simeq \max\{0, t_w - \tau_m^*\}$. For simplicity, within this model, we consider the cases when one can effectively neglect the waiting time, i.e., when $t_{w,m} = 0$.

[13] Operators a_m and $a_m^\dagger$ satisfy the same conditions of Eq. (4.2.2).
[14] As in the preceding section, r can stand both for c or h.

Besides a possible performance advantage, the addition of a mediator could make the experimental implementation of the model easier. In fact, with the mediator, one needs only to turn on and off the interactions between different systems and a single one, which is always the same, instead of doing it between systems taken from the two collections. For example, moving systems around can present some difficulties in some specific applications. By using the mediator, it is sufficient to move it from one collection to the other instead of always trying to move a different system from each collection.

Assuming excitation-preserving interactions, we obtain the same results for the efficiencies of the previous model[15]. If all the systems are of the same type and the conditions on the time evolution due to the collisions reported in Table 4.1 are fulfilled, the same conditions on the frequencies for the working regimes are obtained again.

4.3.1 Maximization of power

Maximization with fixed frequencies

Analogously to the analysis presented in section 4.2, we keep fixed the two bath temperatures and the coupling constants, and we start by maximizing the power output with respect to the collision time with fixed frequencies.

In Appendix 4.E we report the detailed calculations showing that the values of the power for the setup with the mediator are the same of Eq. (4.2.11) with the substitution $V \to V_m$ where

$$V_m = \frac{[1-(A_c)^{u_c}][1-(A_h)^{u_h}]}{(u_c\tau_c + u_h\tau_h)\,[1-(A_c)^{u_c}(A_h)^{u_h}]}, \tag{4.3.1}$$

and the quantities A_r, with $r = h, c$, are the equivalent of the quantity A of Eq. (4.2.10) with the substitutions $g \to g_r$, $\delta \to \delta_r = (\omega_r - \omega_m)/2$, $k \to k_r = \sqrt{g_r^2 + \delta_r^2}$, and $\tau \to \tau_r$. Each of these quantities concerns the collisions S_r-S_m and is analogous to those of the model without the mediator. However, despite this similarity, it is too difficult to maximize exactly Eq. (4.3.1) or to obtain a simple general numerical solution as for Eq. (4.2.12). To simplify the problem we assume that $u_c = u_h \equiv u_m$ and $g_c = g_h \equiv g_m$. In this case, numerical simulations show that the maximum of V_m is obtained for $\tau_c = \tau_h \equiv \tau_m$ and $\omega_m = \bar{\omega} \equiv (\omega_c + \omega_h)/2$, leading to $-\delta_c = \delta_h = \delta_m \equiv (\omega_h - \omega_c)/4$ and $\tau_c = \tau_h \equiv \tau_m$. With these assumptions, $A_c = A_h \equiv A_m$ and we can cast the term V_m in the simplified form

$$V_m = \frac{1-(A_m)^{u_m}}{2u_m\tau_m[1+(A_m)^{u_m}]}. \tag{4.3.2}$$

Numerical simulations show that the maximum power is achieved when system S_m makes just one collision with each collection corresponding to $u_m = 1$[16]. In this case, V_m further simplifies to

$$V_m = \frac{g_m^2 \sin^2(k_m\tau_m)}{2\tau_m\left[2k_m^2 - g_m^2\sin^2(k_m\tau_m)\right]}. \tag{4.3.3}$$

[15] See Table 4.1 for the results and Appendix 4.B for a detailed discussion on how to obtain them in the case with the mediator.

[16] See Appendix 4.E for additional considerations.

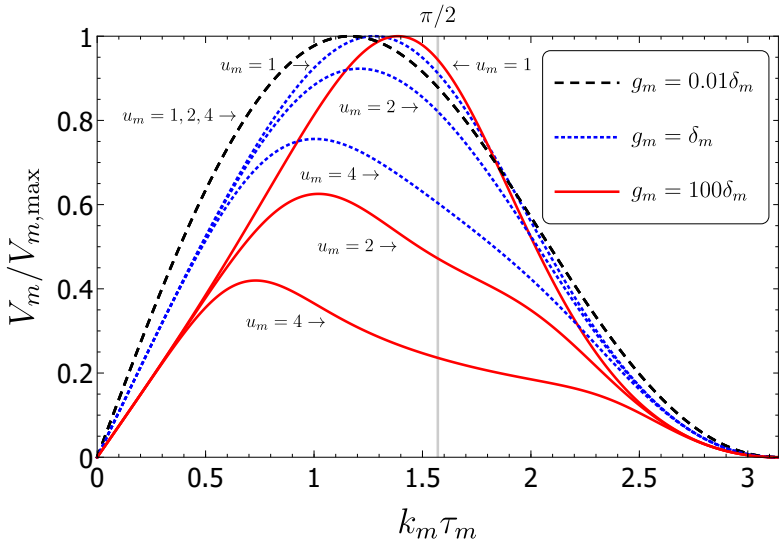

Figure 4.6: Normalized term $V_m/V_{m,\max}$, $V_{m,\max}$ being the maximum of V_m in the case $u_m = 1$ (for the same value of g_m), as a function of time for fixed frequencies and temperatures. The various curves refer to different values of the coupling g_m with respect to the detuning term $\delta_m = (\omega_h - \omega_c)/4$. Moreover, for each choice of g_m, we plot three times the term V_m with u_m assuming the values 1, 2, and 4 (curves with the same g_m are plotted with the same style). Increasing u_m always lowers the power of the machines. When $g_m = 0.01\delta_m$ the three curves practically coincide. We remark that the positions of the peaks move when the ratio g_m/δ_m varies.

We stress that in the following numerical study we always impose $g_c = g_h = g_m$ and $\tau_c = \tau_h = \tau_m$.

Figure 4.6 shows that, as in the no-mediator case, the protocol is resilient to small errors in the collision times. Differently from the no-mediator case, the optimal value of $k_m\tau_m$ cannot be made independent on g_m and δ_m because Eqs. (4.3.2) and (4.3.3) cannot be written as a single-variable function of $k_m\tau_m$. In fact, Figure 4.6 shows how the peak of V_m moves to the right with increasing g_m. Figure 4.6 also shows that multiple collisions decrease the performance and that when $g_m \ll |\delta_m|$ the loss in power for doing multiple collisions is negligible.

Hereafter, we only deal with the case $u_m = 1$, which seems to give the best performance. In the two limiting cases of small and large coupling, it is easy to see from Eq. (4.3.3) that the no-mediator (with $g = g_m$) cycle with $t_w = 0$ greatly outperforms the version with the mediator in terms of maximum power[17]. Moreover, numerical simulations confirm that this remains valid for any value of g_m. However, the cycle with the mediator can perform better when $t_w > 0$ but $t_{w,m} = 0$, as shown in Fig. 4.7. There, the term $V_{\max}$ is plotted against the waiting time t_w. We observe a parameter zone where $t_w \lesssim \tau_m^*$

[17]Compare with Eq. (4.2.12). We recall that, for this comparison, $t_{w,m} = t_w = 0$.

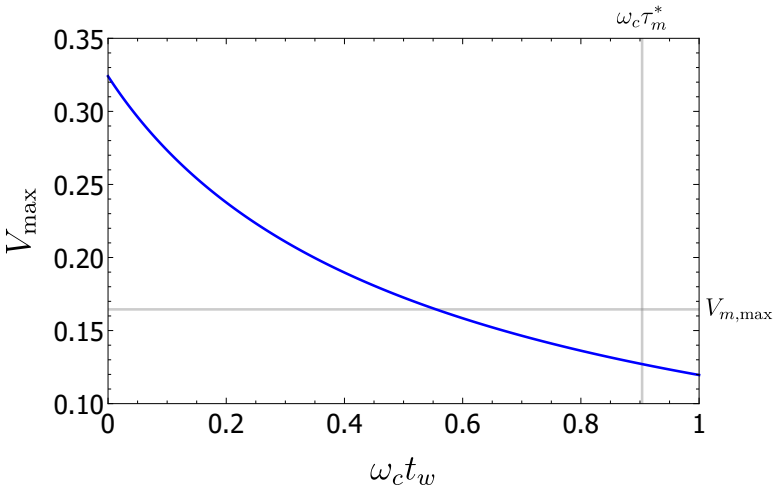

Figure 4.7: $V_{\max}$ of the model without mediator against the waiting time t_w with $\omega_h = 5\omega_c$ and $g = g_m = \omega_c$. The vertical line indicates the optimal interaction time in the model with the mediator, while the horizontal line indicates the term $V_{m,\max}$. The zone where $V_{\max}$ is lower than $V_{m,\max}$ and $t_w \lesssim \tau_m^*$ indicates a power advantage of the model with the mediator compared to the model without it (for $t_w > \tau_m^*$ the assumption $t_{w,m} = 0$ is not justified in general).

and $V_{m,\max} > V_{\max}$ in which the system with mediator performs better than the system without it. We recall that for $t_w > \tau_m^*$ the assumption $t_{w,m} = 0$ is not justified, in general.

Maximization with respect to frequencies, qubits case

In the previous section, we have seen with a specific example that there are configurations in which the cycle with the mediator can offer performance advantages compared to the cycle without it. However, we have observed this behavior by choosing specific frequencies for the collections. In this subsection, we show that the advantage remains if we maximize both cycles not only with respect to the collision time but also over the frequencies. To do so, we focus on the engine working regime in the case in which all the systems are qubits.

Figure 4.8 shows the variation of the efficiency in the optimal configuration of frequencies and collision times as a function of the coupling $g = g_m$, for the fixed temperature ratio $T_h/T_c = 10$. In this plot, the waiting time of the cycle without the mediator is assumed equal, for each value of g, to the optimal time of the cycle with the mediator, i.e., $t_w = \tau_m^*$. Under this assumption, the efficiency of the system with the mediator is always larger than or equal to that of the cycle without it. Regarding the power output, the top-left inset shows the ratio of the two power maximum outputs, $P_{E,\max}^{(m)}/P_{E,\max}$, where $P_{E,\max}^{(m)}$ is the maximum power in the model with the mediator. We can see that around $g = \nu_c$ the cycle with the mediator also outputs more power than

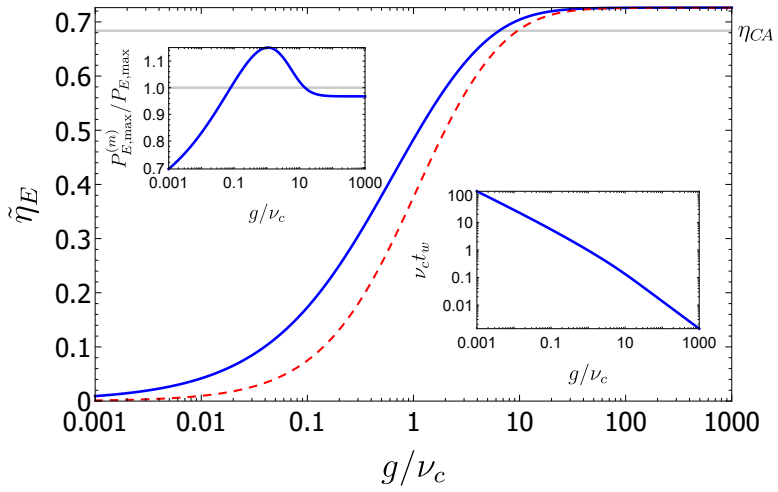

Figure 4.8: The continuous blue line refers to the efficiency at maximum power, $\tilde{\eta}_E$, as a function of the coupling g ($g = g_m$ in this plot) for the cycle with the mediator. The maximization is over frequencies and collision time. The frequency $\nu_c = k_B T_c/\hbar$ is the measure unit and $T_h = 10T_c$. The horizontal line indicates the Curzon-Ahlborn efficiency for the given temperatures. The red dashed line refers to the efficiency at maximum power in the same case of the continuous blue line but for the cycle without the mediator and $t_w = \tau_m^*$. The top-left inset shows the ratio of the maximum power in the cycle with the mediator over the maximum power in the cycle without the mediator (here too with $t_w = \tau_m^*$). The bottom-right inset shows t_w or, equivalently for this plot, τ_m^* as a function of the coupling g. The graph shows that there can be performance advantages in using the mediator when $t_w \sim \tau_m^*$.

the cycle without it, thus providing a complete performance advantage. The bottom-right inset shows the optimal time of the collision in the cycle with the mediator as a function of the coupling[18].

In Fig. 4.9, we analyze more in detail the case with $g = g_m = \nu_c$ by letting t_w vary. Regarding the efficiency at maximum power, the cycle with the mediator provides an appreciably higher value provided that the waiting time in the cycle without the mediator is not negligible. Regarding the power, instead, the waiting time t_w has to be a significant fraction of τ_m^* in order to provide an advantage. As before, it must be taken into consideration that for $t_w > \tau_m^*$ the assumption $t_{w,m} = 0$ is not justified, in general.

[18]Equivalently, it shows the waiting time used for the cycle without the mediator as a function of the coupling.

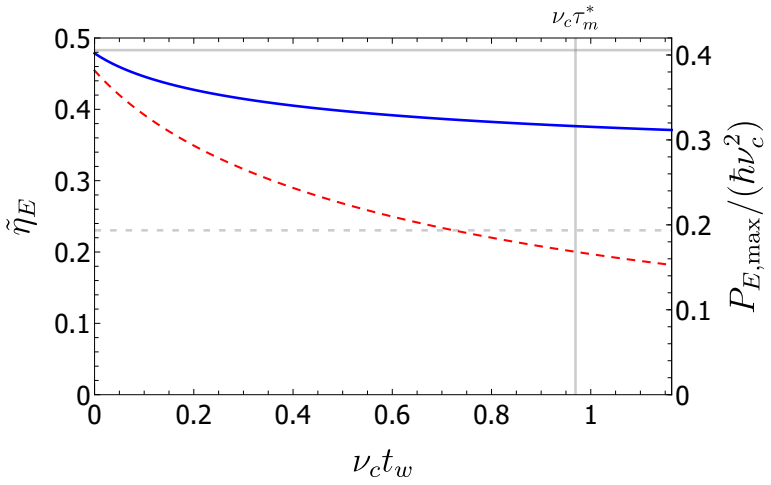

Figure 4.9: Efficiency at maximum power $\tilde{\eta}_E$ (continuous blue line) and maximum power $P_{E,\max}$ (dashed red line) of the model without the mediator as a function of the waiting time t_w with $T_h = 10T_c$ and $g = g_m = \nu_c$ (we recall that $t_{w,m} = 0$). The vertical line indicates the optimal collision time in the model with the mediator, while the horizontal lines indicate, respectively, the efficiency at maximum power (continuous line) and the maximum power (dashed line) in the same model. The plot shows that the model with the mediator can have performance advantages.

4.4 Comparison with the quantum Otto cycle

In this section, we compare the power of the cycle we have studied in section 4.2 with that of another cycle intensely studied in the literature, the so-called quantum Otto cycle [113, 232–234], described in section 2.3.2.

To compare it with our model without the mediator, we denote $\hbar\omega_c$ the energy separation of the eigenstates of the system when it is in contact with the cold thermal bath and $\hbar\omega_h$ when in contact with the hot thermal bath. If the expansion and compression strokes can be performed adiabatically[19], the efficiency of the Otto cycle is given by the same formulas of Table 4.1 for engines and refrigerators [113, 143, 144]. However, in real applications, the expansion and compression strokes last a finite driving time so that the cycle cannot be performed perfectly adiabatically: the states of the system at the end of the expansion and compression strokes are not the same as in the adiabatic case. Therefore, the power output and the efficiency decrease. To counter this limitation, various techniques called shortcuts to adiabaticity (STA) have been applied during finite-time expansion and compression stages to maintain constant the populations of the energy eigenstates [142–144]. However, the STA require an additional cost which increases as the driving time decreases [142–145, 235–237]. In the two Otto cycles we consider below, the cost for the STA implementation is computed differently in the two

[19] Requiring, then, an infinite time.

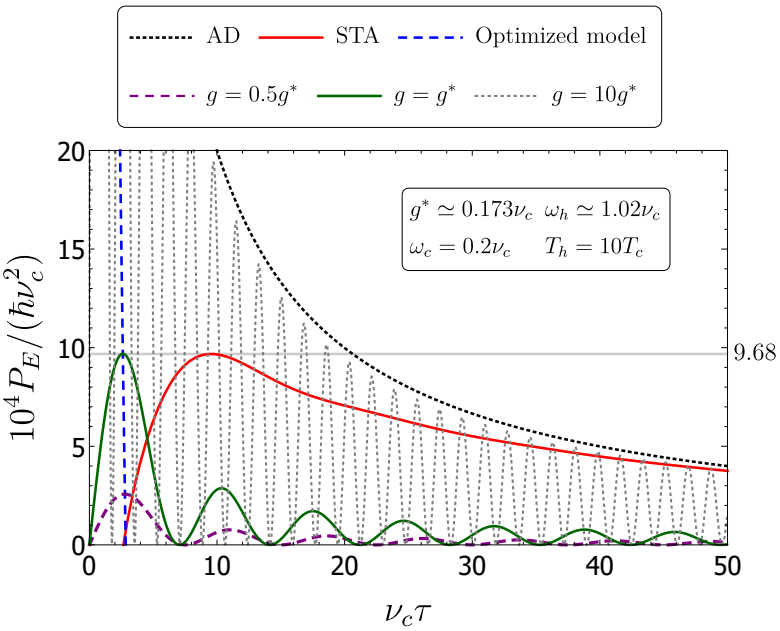

Figure 4.10: Power P_E as a function of the total cycle time, which is equal to the collision time τ in our model without the mediator and to twice the driving time in Ref. [143] (t_w is assumed to be negligible compared to τ), for the parameters given in the inset and in the legend, in the case of qubits. The continuous red line is the power obtained in the Otto cycle with STA. The dotted black line is the power in an ideal Otto cycle without friction, i.e., an Otto cycle in which one makes the adiabatic approximation (AD line). The dashed purple line, the continuous green line, and the dotted grey line (all three oscillating) refer to the power obtained with our model without the mediator, for various fixed coupling strengths g. The dashed blue line is the ensemble of the peaks of the oscillating lines for all the values of g (see text). The maximum power of the Otto cycle with STA ($\simeq 9.68 \cdot 10^{-4}\hbar\nu_c^2$, indicated in the plot by a continuous horizontal line) can be obtained in our model for $g \simeq 0.173\nu_c$.

cases, according to the original works, which can be found, respectively, in Refs. [143] and [144].

The same efficiency of the ideal Otto cycle has been found also in other cycles comprising working substances made of non-resonant components, see for example [134, 230, 238]. Before comparing the Otto cycle and our cycle without the mediator we comment on what could physically motivate the fact that the ideal Otto cycle and our cycle have the same efficiency. As shown in Sec. 4.2, the efficiency of our cycle only depends on the frequencies ω_c and ω_h. If we consider the limit in which the interaction g goes to infinity and $g\tau = \pi/2$, the collision gives place to a swap between the particles. Therefore, the state of the system belonging to collection C_c goes to the system of collection C_h and viceversa. This is equivalent to performing at once the expansion and

compression strokes adiabatically because, in this case, the states remain unaltered while the Hamiltonian changes. In our case, instead, the two Hamiltonians are not altered but the corresponding systems swap the states. After the collision, in our cycle, both systems thermalize, thus performing at once the equivalent of the two isothermal strokes of the Otto cycle. To conclude, since there is a region of parameters in which the ideal Otto cycle and our cycle give rise to the same "dynamics of the states", they give rise to the same efficiency. Then, since this efficiency, in our cycle, is dependent only on the frequencies, the equality holds also when the two models are not so directly correspondent. Overall, the connection between the two models can be then linked to the conversion or exchange of excitations through the Hamiltonian of Eq. (4.2.4) between non-resonant systems at frequencies ω_c and ω_h.

We start by comparing a qubit-powered engine fixing the same energy separations and temperatures of Ref. [143]. Fig. 4.10 shows various curves of power as functions of the total cycle time, which we denote with τ since, being the waiting times assumed to be negligible for all the curves[20], it coincides with the collision time τ. With respect to the model of Ref. [143], τ corresponds to twice the driving time. The continuous red line shows the power of the non-adiabatic quantum Otto engine improved by the STA developed in Ref. [143]. Instead, the dotted black line is the power that one would obtain if the adiabatic approximation worked even for finite times (AD line). The dashed purple line, the continuous green line, and the dotted grey line (all three oscillating) give, respectively, the power P_E of our cycle without mediator[21] as a function of τ for different values of the coupling g. The quantity g^* is obtained by searching for the value of g such that the peak of power in our model is roughly equal to that of the STA cycle. Finally, the dashed blue line represents the collection of the maximum values of the oscillating lines for all coupling strengths. In other words, it is the parametric curve $(\tau^*(g), P_{E,\max}(g))$, reported in the plot with appropriate units, where $\tau^*(g)$ is the optimal collision time given the coupling g, satisfying $k\tau^*(g) = y*$[22].

This plot shows that in our model one does not need to have $g \gg \omega_c, \omega_h$ to make the maximum power comparable with that of the quantum Otto cycle. Indeed, in this example, when $g \simeq 0.173\nu_c$, our cycle gives roughly the same peak of power output of the Otto cycle while maintaining the efficiency of an ideal Otto cycle. Moreover, our design does not require the control of time-dependent Hamiltonians, needed to implement Otto cycles with STA.

Figure 4.10 also shows that for large values of g, the local peaks of the power approach the values obtainable in the adiabatic limit. This stems from the fact that the power of the ideal Otto Cycle without friction[23] is equal to that of Eq. (4.2.11) with $V = 1/\tau$ [143] and that, when $k\tau = \pi/2 + m\pi$, where m is a natural number, $V = g^2/(k^2\tau)$[24].

Figure 4.11 shows the same kind of comparison in the refrigerator case but for harmonic oscillators, as in Ref. [144]. Instead of the power, we have plotted the figure of

[20] As done in Ref. [143].
[21] Compare with Eq. (4.2.11).
[22] See section 4.2.1.
[23] Without friction here indicates an Otto cycle which we treated as adiabatic even for finite times.
[24] Compare with Eq. (4.2.12), recalling that here $t_w = 0$.

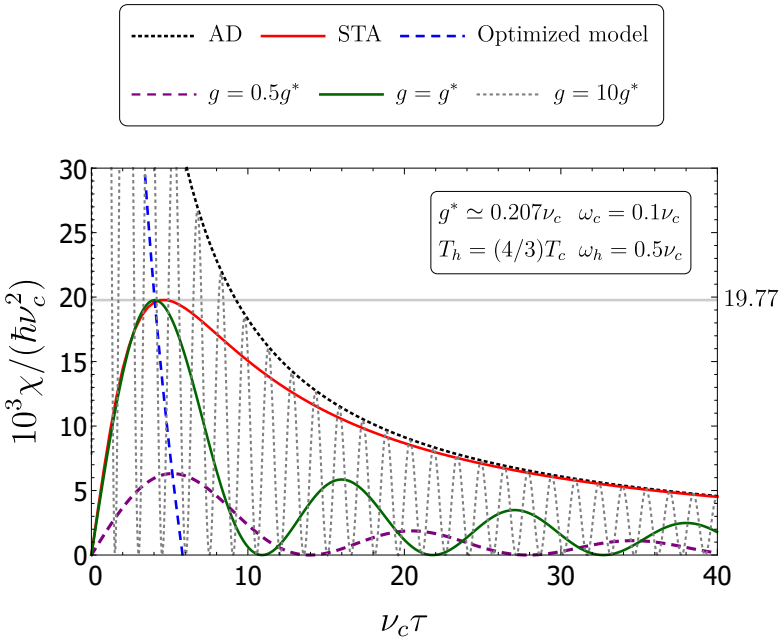

Figure 4.11: Figure of merit χ as a function of the total cycle time, which is equal to the collision time τ in our model without the mediator and to twice the driving time in Ref. [144] (t_w is assumed to be negligible compared to τ), for the parameters given in the inset and in the legend, in the case of quantum harmonic oscillators. The continuous red line is the figure of merit obtained in the Otto cycle with STA. The dotted black line is the figure of merit in an ideal Otto cycle without friction, i.e., an Otto cycle in which one makes the adiabatic approximation (AD line). The dashed purple line, the continuous green line, and the dotted grey line (all three oscillating) refer to the figure of merit obtained with our model without the mediator, for various fixed coupling strengths g. The dashed blue line is the ensemble of the peaks of the oscillating lines for all the values of g [see part of the text concerning the same line in Fig. 4.10]. The maximum figure of merit of the Otto cycle with STA ($\simeq 19.77 \cdot 10^{-3}\hbar\nu_c^2$, indicated in the plot by a continuous horizontal line) can be obtained in our model for $g \simeq 0.207\nu_c$.

merit $\chi = \epsilon_R P_R$, where ϵ_R is the COP and $P_R = Q_c/\tau$ is the cooling power. Analogously to the previous comparison, the condition $g \gg \omega_c, \omega_h$ is not needed to obtain the same peak value of χ obtained in the quantum Otto cycle. Note that for $g \geq \sqrt{\omega_c \omega_h} \simeq 0.224\nu_c$ the interaction Hamiltonian between two harmonic oscillators leads to an instability[25].

4.5 Conclusions

In this chapter, we have considered two different versions of a two-stroke quantum thermal machine. In both versions of the machine, two collections of identical systems with evenly spaced energy levels can be put in contact, respectively, with a cold and a hot thermal bath. Since the energy levels are evenly spaced, we can characterize each system by using a single frequency. In the first version we have examined, a collection system interacts with a system of the other collection, and then they both thermalize. In the second version, we have added a mediator system that interacts alternately with one or more systems of each collection.

Under the assumption that the interaction Hamiltonian conserves the total excitation number, we have proved that the efficiency depends only on the two collection frequencies in both versions of the cycle.

In section 4.2, we have investigated the problem of power maximization in the cycle without the mediator. In particular, we have explored the effect of the waiting time on the optimal collision time and the optimal frequencies. Maximizing over the frequencies has shown that exceeding the Curzon-Ahlborn efficiency is possible when using qubits while it is not with harmonic oscillators.

In section 4.3, we have added the mediator. We have shown that its addition can bring performance advantages when the corresponding cycle waiting time, without the mediator, is of the same order as the collision time. In most other cases, the cycle without the mediator performs better. However, there could be experimental platforms where the implementation of the cycle without the mediator results to be easier.

Finally, in section 4.4, our cycle without the mediator is compared to two examples of Otto cycles enhanced by shortcuts to adiabaticity. This investigation has shown that high coupling ($g \gg \omega_c, \omega_h$) is not needed in our model to obtain a power output comparable to that of the Otto cycle with shortcuts to adiabaticity at maximum power.

[25] See Appendix 4.F.

4.A Dynamics of a collision

In this Appendix, we describe in detail the dynamics of a collision between two systems governed by the Hamiltonian $H_T = H_c + H_h + H_I$, equal to

$$H_T = \hbar \left[\omega_c n_c + \omega_h n_h + g \left(a_c^\dagger a_h + a_c a_h^\dagger \right) \right]. \tag{4.A.1}$$

To this aim we compute, in the Heisenberg picture, the time evolution of the number operator for a system S_h, which we denote as $(n_h)_H(t)$. In order to do this, we first calculate the commutators of the following operators

$$\begin{aligned} n_h &= a_h^\dagger a_h, & n_c &= a_c^\dagger a_c, \\ A_+ &= a_h a_c^\dagger + a_h^\dagger a_c, & A_- &= a_h a_c^\dagger - a_h^\dagger a_c, \end{aligned} \tag{4.A.2}$$

obtaining

$$\begin{aligned} [n_h, A_+] &= -A_-, \qquad [n_c, A_+] = A_-, \\ [n_h, A_-] &= -A_+, \qquad [n_c, A_-] = A_+, \\ [A_+, A_-] &= 2 \left[n_h \left(1 - d_c B_c \right) - n_c \left(1 - d_h B_h \right) \right], \end{aligned} \tag{4.A.3}$$

where $B_r = |N_r - 1\rangle\langle N_r - 1|$. Notice that when $d_c = d_h = 0, 2$ (two-harmonic oscillator and two-qubit cases) one finds $[A_+, A_-] = 2 \left(n_h - n_c \right)$, which gives rise to a closed algebra of commutators. In the following, we solve the dynamics analytically using this form of the commutator $[A_+, A_-]$. However, we will give some comments about the validity of the solutions in the general case. We observe that the commutator $[A_+, A_-]$ has not the above simplified form in the case of the Jaynes-Cumming model where a qubit interacts with a harmonic oscillator so that the analytic solution of the dynamics presented in the remainder of this Appendix cannot be applied to this case.

By using $[A_+, A_-] = 2 \left(n_h - n_c \right)$ and by rewriting the total Hamiltonian of the system as

$$H_T = \hbar \left(\omega_c n_c + \omega_h n_h + g A_+ \right), \tag{4.A.4}$$

we obtain the following commutators

$$\begin{aligned} [H_T, n_h]/\hbar &= g A_-, \quad [H_T, n_c]/\hbar = -g A_-, \\ [H_T, A_+]/\hbar &= \left(\omega_c - \omega_h \right) A_-, \\ [H_T, A_-]/\hbar &= \left(\omega_c - \omega_h \right) A_+ + 2g \left(n_h - n_c \right). \end{aligned} \tag{4.A.5}$$

Within this assumption, the operator $(n_h)_H(t)$ in the Heisenberg picture can be expressed by

$$(n_h)_H(t) = f_h(t) n_h + f_c(t) n_c + f_+(t) A_+ + f_-(t) A_-, \tag{4.A.6}$$

where $f_h(0) = 1$ and $f_c(0) = f_+(0) = f_-(0) = 0$. The evolution of a generic operator O in the Heisenberg picture is given by the Heisenberg formula

$$\dot{O}_H(t) = (i/\hbar)[H_T, O_H(t)], \tag{4.A.7}$$

where the corresponding operator O is a time-independent operator in the Schrödinger picture. By inserting Eq. (4.A.6) into Eq. (4.A.7) we obtain the following system of differential equations

$$\begin{cases} \dot{f}_h(t) &= 2igf_-(t), \\ \dot{f}_c(t) &= -2igf_-(t), \\ \dot{f}_+(t) &= -2i\delta f_-(t), \\ \dot{f}_-(t) &= -2i\delta f_+(t) + ig\left[f_h(t) - f_c(t)\right], \end{cases} \tag{4.A.8}$$

which together with the boundary conditions given just after Eq. (4.A.6) have the solutions

$$\begin{cases} f_h(t) &= \frac{2\delta^2+g^2[1+\cos(2kt)]}{2k^2}, \\ f_c(t) &= \frac{g^2[1-\cos(2kt)]}{2k^2}, \\ f_+(t) &= \frac{g\delta[1-\cos(2kt)]}{2k^2}, \\ f_-(t) &= i\frac{g\sin(2kt)}{2k}, \end{cases} \tag{4.A.9}$$

where we recall that $\delta = (\omega_h - \omega_c)/2$ and $k = \sqrt{g^2+\delta^2}$.

Now, we can calculate the value of $\langle (n_h)_H(t=\tau)\rangle = \langle n_h\rangle_\tau$ after the interaction time τ. In particular, we focus on the case treated in the main text of this chapter, where both systems are initially in a thermal state. It follows that at the beginning of the collision $\langle A_+\rangle_0 = \langle A_-\rangle_0 = 0$ and we get

$$\langle n_h\rangle_\tau = f_h(\tau)\langle n_h\rangle_{\text{th}} + f_c(\tau)\langle n_c\rangle_{\text{th}}. \tag{4.A.10}$$

Noticing that $f_c(\tau) = 1 - f_h(\tau)$ and denoting $A \equiv f_h(\tau)$, we can write

$$\langle n_h\rangle_\tau = \langle n_c\rangle_{\text{th}} + (\langle n_h\rangle_{\text{th}} - \langle n_c\rangle_{\text{th}})\, A. \tag{4.A.11}$$

Let us now comment on the approximate validity of the above solution when $[A_+, A_-] \neq 2(n_h - n_c)$ (i.e., when the condition one of the two conditions $d_c = d_h = 0$ or $d_c = d_h = 2$ is not satisfied). In fact, we expect that when a system with evenly spaced energy levels is big enough and its higher energy levels are approximately empty during the dynamics, this system should be a good approximation of a harmonic oscillator. Then, if both systems satisfy this requirement, we expect that the solution found above describes the dynamics of the operators quite well. However, one situation in which the above dynamics is surely wrong is when $\delta = 0$ and $\max(\langle n_c\rangle_{\text{th}}, \langle n_h\rangle_{\text{th}}) > \min(N_c, N_h)$ because at some point we would have a system with more excitations than levels, which is absurd. In general, we expect that the dynamics of Eq. (4.A.11) is a good description if $\langle B_r\rangle \simeq 0$ during the whole evolution.

4.B Functioning regimes and efficiency of the cycle with mediator

In this Appendix, we analyze the efficiencies and energy fluxes of the cycle with the mediator described in section 4.3. This is done directly for the steady cycle.

After u_r[26] collisions with systems S_r, the difference in internal energy of system S_m is given by the change of its average excitation number multiplied by the energy gap, i.e.,

$$\Delta U_r = \hbar\omega_m \left(\langle n_m \rangle_{u_r} - \langle n_m \rangle_{0_r} \right), \tag{4.B.1}$$

where $\langle n_m \rangle_{u_r}$ is the average number of excitations in system S_m after u_r collisions with systems S_r while $\langle n_m \rangle_{0_r}$ is the same quantity before the first collision. The internal energy change of systems S_r can be regarded as heat because, after their collision, these systems will thermalize again by being in contact with one thermal bath. By considering the heat positive when energy flows from the bath to the system and taking into account the conservation of the total excitation number, heat is given by

$$Q_r = -\hbar\omega_r \sum_{i=1}^{u_r} \left(\langle n_r \rangle_{i_r} - \langle n_r \rangle_{\text{th}} \right) = \frac{\omega_r}{\omega_m} \Delta U_r, \tag{4.B.2}$$

where $\langle n_r \rangle_{i_r}$ is the average excitation number of system S_r after the collision with system S_m, which has already done $i_r - 1$ collisions, and $\langle n_r \rangle_{\text{th}}$ is the same quantity in the thermal state at temperature T_r, ρ_r^{th}. Finally, by exploiting the first law of thermodynamics, we find that the work done in u_r collisions is given by

$$W_r = \Delta U_r - Q_r = \hbar \left(\omega_m - \omega_r \right) \left(\langle n_m \rangle_{u_r} - \langle n_m \rangle_{0_r} \right). \tag{4.B.3}$$

Then, by using $\langle n_m \rangle_{0_c} = \langle n_m \rangle_{u_h}$ and $\langle n_m \rangle_{0_h} = \langle n_m \rangle_{u_c}$, the total work in a cycle is given by

$$W = W_c + W_h = \hbar \left(\omega_c - \omega_h \right) \left(\langle n_m \rangle_{u_h} - \langle n_m \rangle_{u_c} \right). \tag{4.B.4}$$

Alternatively, since in a cycle $\Delta U_c + \Delta U_h = 0$, we can write

$$Q_c = -\frac{\omega_c}{\omega_h} Q_h, \quad W = -\left(1 - \frac{\omega_c}{\omega_h} \right) Q_h, \tag{4.B.5}$$

from which it is easy to obtain the efficiencies of Table 4.1.

Regarding the frequency conditions, to obtain them we must also impose two conditions for the collisions S_m-S_r. On the one hand, the system S_m has to acquire excitations if it has less than S_r and vice versa. On the other hand, the system which had less excitations cannot have, after the collision, more than the other one had. In this case, it holds $\langle n_m \rangle_{u_h} > \langle n_m \rangle_{u_c} \iff \langle n_h \rangle_{\text{th}} > \langle n_c \rangle_{\text{th}}$. Then, if $N_c = N_h$, the sign of Eq. (4.B.4) is completely determined by the value of the ratios ω_c/T_c and ω_h/T_h since the number of excitations in the mediator system has to be between $\langle n_c \rangle_{\text{th}}$ and $\langle n_h \rangle_{\text{th}}$ once the steady cycle has been reached.

[26] As always, $r = c, h$.

4.C Comparison with a perfect swap Hamiltonian

In our setting, when the parameter g is very high ($g \gg \delta$), the collision between two systems approximately results in a swap operation. One could wonder if a Hamiltonian that generates the swap operation outperforms the exchange one proposed in section 4.2. In this Appendix, we investigate this question for the case of two qubits.

In order to find a swap Hamiltonian, we first write a swap operation. Using the basis $\{|1_c, 1_h\rangle, |1_c, 0_h\rangle, |0_c, 1_h\rangle, |0_c, 0_h\rangle\}$, where $|1_r\rangle$ is the excited state of qubit r and $|0_r\rangle$ is the ground one, we choose the following swap operator:

$$U_{\text{SWAP}} = \begin{pmatrix} 1 & 0 & 0 & 0 \\ 0 & 0 & 1 & 0 \\ 0 & 1 & 0 & 0 \\ 0 & 0 & 0 & 1 \end{pmatrix}. \tag{4.C.1}$$

The Hamiltonian which generates this unitary evolution after a swap time $t = t_S$ is

$$H_{\text{SWAP}} = \frac{i\hbar}{t_S} \ln(U_{\text{SWAP}}) = \frac{\pi\hbar}{2t_S} \begin{pmatrix} 0 & 0 & 0 & 0 \\ 0 & -1 & 1 & 0 \\ 0 & 1 & -1 & 0 \\ 0 & 0 & 0 & 0 \end{pmatrix}, \tag{4.C.2}$$

which has spectrum $\sigma(H_{\text{SWAP}}) = \{-\pi\hbar/t_S, 0, 0, 0\}$ and commutes with the total number operator, thus implying the same efficiencies of the exchange Hamiltonian (for the same frequencies) even when not performing a complete swap. Notice that we assume that during the collision the free Hamiltonian of the colliding systems are suppressed and the dynamics is governed only by the Hamiltonian H_{SWAP}. After a collision lasting τ_S, the swap Hamiltonian leads to the new populations

$$\begin{aligned} \langle n_c \rangle_{\tau_S} &= \langle n_c \rangle_{\text{th}} \cos^2\left(\frac{\pi\tau_S}{2t_S}\right) + \langle n_h \rangle_{\text{th}} \sin^2\left(\frac{\pi\tau_S}{2t_S}\right), \\ \langle n_h \rangle_{\tau_S} &= \langle n_h \rangle_{\text{th}} \cos^2\left(\frac{\pi\tau_S}{2t_S}\right) + \langle n_c \rangle_{\text{th}} \sin^2\left(\frac{\pi\tau_S}{2t_S}\right). \end{aligned} \tag{4.C.3}$$

By inserting the above equations into Eqs. (4.2.6) and (4.2.7) we get the same formulas of Eq. (4.2.11) but with the term V substituted by

$$V_S = \frac{1}{\tau_S + t_w} \sin^2\left(\frac{\pi\tau_S}{2t_S}\right). \tag{4.C.4}$$

To make a fair comparison we choose the parameter t_S of the swap Hamiltonian so that the difference between maximum and minimum eigenvalues are equal to the same quantity in the case of the Hamiltonian of Eq. (4.A.1), which has matrix form

$$H_T = \hbar \begin{pmatrix} 2\bar{\omega} & 0 & 0 & 0 \\ 0 & \omega_c & g & 0 \\ 0 & g & \omega_h & 0 \\ 0 & 0 & 0 & 0 \end{pmatrix}, \tag{4.C.5}$$

and the spectrum of which is $\sigma(H_T) = \{2\hbar\bar{\omega}, \hbar(\bar{\omega}+k), \hbar(\bar{\omega}-k), 0\}$, where we recall that $\bar{\omega} = (\omega_c + \omega_h)/2$, $k = \sqrt{\delta^2 + g^2}$, and $\delta = (\omega_h - \omega_c)/2$. The difference between maximum and minimum eigenvalues for the swap Hamiltonian is just $\pi\hbar/t_S$ while for our Hamiltonian is $2\hbar\bar{\omega}$ if $g \leq \sqrt{\omega_c\omega_h}$ and $2\hbar k$ if $g \geq \sqrt{\omega_c\omega_h}$. Then, for the two cases, we have $t_S = \pi/(2\bar{\omega})$ and $t_S = \pi/(2k)$, respectively. In both cases, if the collision time of the swap Hamiltonian can be optimized, the swap interaction outperforms the exchange one since, for $|\delta| > 0$, if $t_S = \pi/(2\bar{\omega})$, which occurs when $\bar{\omega} > k$,

$$\frac{k^2}{g^2}\max_{\tau} V = \frac{\sin^2(k\tau^*)}{\tau^* + t_w} < \frac{\sin^2(k\tau^*)}{(k/\bar{\omega})\tau^* + t_w} = \frac{\sin^2(\bar{\omega}\tau')}{\tau' + t_w} \leq \max_{\tau_S}\frac{\sin^2(\bar{\omega}\tau_S)}{\tau_S + t_w} = \max_{\tau_S} V_S, \tag{4.C.6}$$

where $\tau' = (k/\bar{\omega})\tau^*$, while, if $t_S = \pi/(2k)$,

$$\max_{\tau_S} V_S = \max_{\tau_S}\frac{\sin^2(k\tau_S)}{\tau_S + t_w} > \frac{g^2}{k^2}\max_{\tau}\frac{\sin^2(k\tau)}{\tau + t_w} = \max_{\tau} V. \tag{4.C.7}$$

With respect to a perfect swap situation with switching time $\tau_S = t_S$, the time-optimized exchange Hamiltonian can give a higher power output. We show this in the case $t_w = 0$. In the case $t_S = \pi/(2\bar{\omega})$, one gets that $V_{\max} > V_S(\tau_S = t_S)$ implies

$$g > \frac{\sqrt{2\bar{\omega}\left(\bar{\omega} + \sqrt{\bar{\omega}^2 + \alpha^2\pi^2\delta^2}\right)}}{\alpha\pi}, \tag{4.C.8}$$

where α is the maximum value of $\sin^2(x)/x$, i.e., $\alpha \simeq 0.7246$. Numerically, one can see that the condition $g \leq \sqrt{\omega_c\omega_h}$ can be satisfied together with the above one only when ω_h/ω_c roughly lies in the interval $[0.4832, 2.0697]$. Regarding the ratio $V_{\max}/V_S(\tau_S = t_S)$, recalling that $t_S = \pi/(2\bar{\omega})$ for $g \leq \sqrt{\omega_c\omega_h}$, one gets

$$\frac{V_{\max}}{V_S(\tau_S = t_S)} = \frac{\alpha\pi}{2}\frac{g^2}{k\bar{\omega}} \leq \alpha\pi\frac{\omega_c\omega_h}{2\bar{\omega}^2}. \tag{4.C.9}$$

Regarding the case $t_S = \pi/(2k)$, one gets

$$V_{\max} > V_S(\tau_S = t_S) \iff g > \sqrt{\frac{2}{\alpha\pi - 2}}|\delta| \simeq 2.6898|\delta|, \tag{4.C.10}$$

and

$$\frac{V_{\max}}{V_S(\tau_S = t_S)} = \frac{\alpha\pi}{2}\frac{g^2}{k^2} \simeq 1.1382\frac{g^2}{k^2}. \tag{4.C.11}$$

4.D The power of a harmonic oscillator couple is not frequency bounded

In this Appendix, we show, for the case of harmonic oscillators, that the power increases monotonically by decreasing the frequencies while keeping fixed their ratio and the

temperatures. In order to do this, we start by writing $\omega_h = \omega_c/(1-\eta_E)$ and $T_h = T_c/(1-\eta_C)$ so that we can write the maximum power for the engine for a given ω_c as

$$\tilde{P}_E = k_B T_c \frac{\eta_E}{1-\eta_E} f(x) V_{\max}, \tag{4.D.1}$$

where

$$f(x) = x\left[\coth(lx) - \coth(x)\right], \tag{4.D.2}$$

$x = \hbar\omega_c/(2k_B T_c)$, and $l = (1-\eta_C)/(1-\eta_E)$.

In order to show that the maximum power is obtained in the limit $x \to 0$, we prove that $\partial_x \tilde{P}_E < 0 \ \forall\ x > 0$. The derivative of $\tilde{P}_E$ takes the form

$$\partial_x \tilde{P}_E = k_B T_c \frac{\eta_E}{1-\eta_E}\left[\left(\partial_x f(x)\right) V_{\max} + f(x)\partial_x V_{\max}\right]. \tag{4.D.3}$$

We start by analyzing the term

$$\partial_x f(x) = \coth(lx) - \coth(x) + x\left[\operatorname{csch}^2(x) - l\operatorname{csch}^2(lx)\right], \tag{4.D.4}$$

which can be shown to be negative for every $x > 0$. Indeed, we can rewrite the above function as

$$\partial_x f(x) = b(lx) - b(x), \quad b(x) = \frac{\sinh(x)\cosh(x) - x}{\sinh^2(x)}. \tag{4.D.5}$$

Since $0 \le l \le 1$ we can find the sign of $\partial_x f(x)$ by understanding the behavior of $b(x)$. If $b(x)$ is always increasing, it follows that $\partial_x f(x)$ is always negative. Then, we calculate the derivative of $b(x)$:

$$\partial_x b(x) = \frac{2}{\sinh^2(x)}\left[x\coth(x) - 1\right], \tag{4.D.6}$$

which is always positive because

$$x\coth(x) - 1 > 0, \quad \forall\ x > 0. \tag{4.D.7}$$

Thus, since $V_{\max} > 0$, we have shown that the first term in the square brackets of Eq. (4.D.3) is negative.

Concerning the second term in the square brackets of Eq. (4.D.3), since $f(x) > 0\ \forall\ x > 0$, we could show that it is negative by proving that $\partial_x V_{\max} < 0\ \forall\ x > 0$. Writing $\omega_h = \omega_c/(1-\eta_E)$, the quantity k can be cast in the form

$$k = \sqrt{g^2 + \left(\frac{\omega_c}{2}\frac{\eta_E}{1-\eta_E}\right)^2}, \tag{4.D.8}$$

which makes evident that k increases when ω_c does, i.e., $\partial_x k > 0\ \forall x > 0$. Then, we can just study[27]

$$\partial_k V_{\max} = \partial_k\left(\frac{g^2}{k}\frac{\sin^2(z)}{z + kt_w}\right), \tag{4.D.9}$$

[27] See Eq. (4.2.12).

where $z = k\tau^*$ is the value for which V is maximized for given k and t_w. For $t_w = 0$, $z = y^*$[28] so that $\partial_k z = 0$ and the disequality $\partial_k V_{\max} < 0$ reduces to $-\sin^2(y^*) < 0$ which is, indeed, true. For $t_w > 0$ we can write

$$\partial_k V_{\max} = -\frac{g^2}{k^2}\frac{\sin^2(z)}{z + kt_w} + \frac{g^2}{k}\partial_k\left(\frac{\sin^2(z)}{z + kt_w}\right), \tag{4.D.10}$$

where the first term is negative since $k > 0$ and $y^* < z < \pi/2$. The second term can be rewritten as

$$\frac{g^2 t_w}{k}\partial_{(kt_w)}\left(\frac{\sin^2(z)}{z + kt_w}\right), \tag{4.D.11}$$

and one can numerically check that is negative for $kt_w > 0$. Then, $\partial_k V_{\max} < 0$ follows and, being $\partial_x \tilde{P}_E$ composed by the sum of two negative quantities multiplied by a positive one, it also follows that $\partial_x \tilde{P}_E < 0 \;\forall\; x > 0$.

4.E Maximization of power in the cycle with the mediator

In this Appendix, we deal with the problem of maximizing the power of the cycle with the mediator, when the frequencies of the collections, the temperatures, and the couplings are fixed. To this aim, we must first find the stationary values of the average excitation number of system S_m in the steady cycle.

We already know, from Appendix 4.A that the result of each collision between system S_m and system S_r is described by the analogous of Eq. (4.A.11) if $\langle A_- \rangle_0 = \langle A_+ \rangle_0 = 0$ at the beginning of the collision under examination (we recall that this solution is exact only for the cases of qubits and harmonic oscillators).

We notice that this condition is always satisfied since systems S_r are in a thermal state before their collision. Then, one can easily prove by induction that for u_r collisions of the same duration the evolution is given by

$$\langle n_m \rangle_{u_r} = \langle n_r \rangle_{\text{th}} + \left(\langle n_m \rangle_{0_r} - \langle n_r \rangle_{\text{th}}\right) A_r^{u_r}, \tag{4.E.1}$$

where A_r is defined below Eq. (4.3.1). If the duration time of the collisions can vary, the term $A_r^{u_r}$ becomes

$$A_r^{u_r} \longrightarrow \prod_{i=1}^{u_r} A_r\left(\tau_{r,i}\right), \tag{4.E.2}$$

where $\tau_{r,i}$ denotes the duration of the i-th collision.

Turning back to the case of equal-time collisions, we can find the steady cycle values of $\langle n_m \rangle_{u_h}$ and $\langle n_m \rangle_{u_c}$ by solving the following simultaneous equations:

$$\begin{aligned} \langle n_m \rangle_{u_h} &= \langle n_h \rangle_{\text{th}} + \left(\langle n_m \rangle_{u_c} - \langle n_h \rangle_{\text{th}}\right) A_h^{u_h}, \\ \langle n_m \rangle_{u_c} &= \langle n_c \rangle_{\text{th}} + \left(\langle n_m \rangle_{u_h} - \langle n_c \rangle_{\text{th}}\right) A_c^{u_c}, \end{aligned} \tag{4.E.3}$$

[28] See section 4.2.1.

which lead to Eq. (4.3.1) using Eqs. (4.2.11) and (4.B.4).

Even if we cannot provide an analytical proof that one collision is the best option, performance-wise, we can provide an argument for why we strongly believe so. In the cycle with the mediator, the work is connected to the change of internal energy of system S_m [cf. Eqs. (4.B.1), (4.B.2), and (4.B.3)]. Then, instead of showing that $u_c = u_h = 1$ is optimal for maximizing Eq. (4.3.1) we show that the maximization of $|\Delta U_r|/(u_r\tau_r)$ is obtained for $u_r = 1$. From Eqs. (4.B.1) and (4.E.1) we get

$$\frac{|\Delta U_r(1)|}{\tau_r} - \frac{|\Delta U_r(u_r)|}{u_r\tau_r} = \hbar\omega_m \left|\langle n_r\rangle_{\text{th}} - \langle n_m\rangle_{0_r}\right| \left(\frac{1-A_r}{\tau_r} - \frac{1-A_r^{u_r}}{u_r\tau_r}\right), \tag{4.E.4}$$

where $u_r \geq 2$ and $\Delta U_r(u_r)$ indicates ΔU_r after u_r collisions. If $A_r = 0$, the above quantity is positive, while it is zero for $A_r = 1$. By deriving the above quantity with respect to A_r, we can see that the derivative is always non-positive for $A_r \in [0, 1]$[29]. This means that when all the other parameters are fixed, the energy exchange rate with one collision is maximized for $u_r = 1$. We remark that the above argument refers only to one stroke of the cycle, and then it is not a proof that the maximization of the entire cycle involving a proper maximization of the term V_m [Eq. (4.3.1)] is obtained for $u_c = u_h = 1$. However, Fig. 4.6 and other numerical simulations suggest that this is indeed the case.

We finally remark, in the case of qubits and harmonic oscillators[30], that in the limit case of a great number of collisions between the mediator and systems of a collection, the mediator steady state has the same average number of excitations of the thermal state of the collection systems[31]. It is also possible to show that these states have the same populations level by level, as already predicted for harmonic oscillators in Ref. [239].

4.F Coupling limit for quantum harmonic oscillators

Here, we discuss the physical limit with respect to the coupling of the total Hamiltonian in the case of harmonic oscillators.

When considering the interaction of two harmonic oscillators, the term g cannot be too high because, otherwise, one of the so-called normal frequencies becomes negative and this translates into a total Hamiltonian not bounded from below [148, 240]. Referring to the Gaussian formalism [148], this translates into the requirement of positive definiteness for the "Hamiltonian matrix". Assuming the exchange interaction of Eq. (4.2.4), the total Hamiltonian is given by Eq. (4.A.1) and its "Hamiltonian matrix"[32] reads

$$\hbar \begin{pmatrix} \omega_h & 0 & g & 0 \\ 0 & \omega_h & 0 & g \\ g & 0 & \omega_c & 0 \\ 0 & g & 0 & \omega_c \end{pmatrix}. \tag{4.F.1}$$

[29] This is the interval where A_r is confined. See Eq. (4.2.10) and the comment below Eq. (4.3.1).

[30] Here, we implicitly assume systems of the same kind both for the mediator and the collection.

[31] Compare with Eq. (4.E.1).

[32] The Hamiltonian matrix is given with respect to the quadrature operators, see Ref. [148] and section 2.4.1.

The doubly degenerate eigenvalues of the above matrix are

$$\frac{\lambda_{\pm}}{\hbar} = \frac{\omega_h + \omega_c}{2} \pm \sqrt{\delta^2 + g^2}, \tag{4.F.2}$$

thus leading to the condition $g < \sqrt{\omega_c \omega_h}$ to avoid non-positive normal frequencies. However, if the two systems are not real harmonic oscillators but many-level ones, the highest levels of which are practically unoccupied during the whole dynamics, they are very well approximated by harmonic oscillators and this problem can be avoided.

Chapter 5

Driven quantum harmonic oscillator in a non-Markovian collisional environment

In this chapter, we analyze the non-Markovian dynamics of a driven harmonic oscillator in a collisional environment[1]. The reservoir is composed of harmonic oscillators with frequency ω_B and all of the bath units are described by the covariance matrix $\boldsymbol{\sigma}_B$[2]. Furthermore, we assume that the variation timescale of the open system frequency is large compared to the timescale of a collision so that each collision occurs between two time-independent harmonic oscillators, i.e., the open system frequency is assumed constant during a collision. Notice that the results of this chapter are still preliminary.

5.1 Description of the system

The collision model (CM) considered in this chapter works as that described in section 2.2.3. Here, both the system of interest (system S) and the bath units (systems B_i) are harmonic oscillators.

The Hamiltonian of the harmonic oscillator constituting the open quantum system of interest is

$$H_S = \frac{p_S^2}{2m_S} + \frac{1}{2} m_S \omega_S^2(t) x_S^2, \tag{5.1.1}$$

where p_S is the momentum operator, m_S is the mass, x_S is the position operator and $\omega_S(t)$ is the time-dependent frequency[3]. We can rewrite it using the so-called quadrature operators $X_S(t)$ and $P_S(t)$ and use them to define the annihilation and creation ladder

[1] See section 2.2.3.
[2] See section 2.4.1.
[3] We recall that the canonical commutation relation (CCR) reads $[x_S, p_S] = i\hbar$.

operators a and $a^\dagger$:

$$X_S(t) = \sqrt{\frac{m_S\omega_S(t)}{\hbar}}x_S, \qquad P_S(t) = \sqrt{\frac{1}{\hbar m_S\omega_S(t)}}p_S, \qquad a(t) = \frac{X_S(t) + iP_S(t)}{\sqrt{2}}. \tag{5.1.2}$$

Notice that the canonical commutation relation (CCR) for the quadrature operators assumes the form $[X_S(t), P_S(t)] = i$ and that these operators are time-dependent. The Hamiltonian of Eq. (5.1.1) can now be rewritten as

$$H_S = \frac{\hbar\omega_S(t)}{2}\left(X_S^2(t) + P_S^2(t)\right), \tag{5.1.3}$$

and the time-dependence of the quadrature operators can be cast in the form

$$X_S(t') = \sqrt{\frac{\omega_S(t')}{\omega_S(t)}}X_S(t), \quad P_S(t') = \sqrt{\frac{\omega_S(t)}{\omega_S(t')}}P_S(t). \tag{5.1.4}$$

We also write the form of the operators L_S and C_S. The former is the Lagrangian while the latter is the position-momentum correlation [234]. Together, they can be used to quantify the coherence $\mathcal{C}_S$ of the harmonic oscillator [234]

$$L_S = \frac{\hbar\omega_S(t)}{2}\left(P_S^2(t) - X_S^2(t)\right), \quad C_S = \frac{\hbar\omega_S(t)}{2}\{P_S(t), X_S(t)\},$$
$$\mathcal{C}_S = \frac{1}{\hbar\omega_S(t)}\sqrt{\langle L_S^2\rangle + \langle C_S^2\rangle}. \tag{5.1.5}$$

The Hamiltonian $H_{B,n}$ of the n-th bath harmonic oscillator is

$$H_{B,n} = \frac{\hbar\omega_B}{2}\left(X_{B,n} + P_{B,n}\right), \tag{5.1.6}$$

where $X_{B,n}$ and $P_{B,n}$ are the quadrature operators of the n-th bath harmonic oscillator and ω_B is their frequency. Finally, for the interaction Hamiltonian between S and B_n we choose a beam-splitter interaction:

$$H_{I,n} = \hbar g\left(X_S(t)X_{B,n} + P_S(t)P_{B,n}\right), \tag{5.1.7}$$

where $X_{B,n}$ and $P_{B,n}$ are the quadrature operators for the n-th unit of the bath. A similar interaction describes the intra-bath collisions with the substition of g with g_B, $X_S(t)$ with $X_{B,n-1}$, and $P_S(t)$ with $P_{B,n-1}$.

We assume that both the system and the bath units can be fully described within the Gaussian state formalism and that they have zero first moment. Therefore, covariance matrices are sufficient to describe their states.

5.2 Dynamics of a collision

In this section, we analyze the dynamics of a collision. Since the interaction Hamiltonians have the same form both for S-B_n and B_{n-1}-B_n collisions[4], we omit the subscript n and analyze a generic S-B collision. Moreover, since we assume that the driving of system S is slow compared to the timescale of a collision, we use as value for $\omega_S(t)$ its value at the start of the collision and denote it simply by ω_S[5].

We can directly write (we will omit the subscript zero and others to lighten the notation) the whole Hamiltonian as

$$H = H_S + H_B + H_I = \frac{1}{2}\boldsymbol{R}^\intercal \boldsymbol{H} \boldsymbol{R}, \tag{5.2.1}$$

where

$$\boldsymbol{H} = \hbar \begin{pmatrix} \omega_S & 0 & g & 0 \\ 0 & \omega_S & 0 & g \\ g & 0 & \omega_B & 0 \\ 0 & g & 0 & \omega_B \end{pmatrix}, \qquad \boldsymbol{R} = \begin{pmatrix} X_S \\ P_S \\ X_B \\ P_B \end{pmatrix}. \tag{5.2.2}$$

In order to simplify calculations it is better to rewrite the Hamiltonian matrix $\boldsymbol{H}$ as follows

$$\boldsymbol{H} = \hbar\omega \mathbb{I}_4 + \hbar \begin{pmatrix} \delta & g \\ g & -\delta \end{pmatrix} \otimes \mathbb{I}_2, \tag{5.2.3}$$

where $\omega = (\omega_S + \omega_B)/2$ and $\delta = (\omega_S - \omega_B)/2$. The doubly degenerate eigenvalues of this matrix are $\hbar\lambda_\pm$ with $\lambda_\pm = \omega \pm \sqrt{\delta^2 + g^2}$. Therefore, to be a positive definite matrix we must impose $\omega^2 > \delta^2 + g^2$. We recall that[6], given an Hamiltonian matrix $\boldsymbol{H}$, the equation of motion for the covariance matrix $\boldsymbol{\sigma}(t)$ is given by:

$$\frac{\partial}{\partial t}\boldsymbol{\sigma}(t) = \boldsymbol{D}\sigma(t) + \sigma(t)\boldsymbol{D}^\intercal, \tag{5.2.4}$$

where $\boldsymbol{D} = \boldsymbol{\Omega}\boldsymbol{H}/\hbar$[7]. Notice that, when $\boldsymbol{H}$ is symmetric, $\boldsymbol{D}$ is antisymmetric if and only if $[\boldsymbol{\Omega}, \boldsymbol{H}] = 0$. In our case, this condition is satisfied.

Starting the dynamics at $t = 0$, the formal solution of Eq. (5.2.4) at time $t = \tau$ can be immediately written as

$$\boldsymbol{\sigma}(\tau) = e^{\tau \boldsymbol{D}} \boldsymbol{\sigma}(0) e^{\tau \boldsymbol{D}^\intercal}. \tag{5.2.5}$$

In general, however, Eq. (5.2.5) cannot be easily calculated because the matrix $\boldsymbol{D}$ is not diagonal. Notice that assuming ω_S to be time-independent during the collision is not equivalent to assuming that we can expand $e^{\tau \boldsymbol{D}}$ in a Taylor series.

[4] The B_{n-1}-B_n collisions will be used to introduce non-Markovianity in the model.

[5] In the same vein, we write X_S and P_S without the explicit time dependence.

[6] See Eq. (2.4.9)

[7] The matrix $\boldsymbol{\Omega}$ is what we call the standard symplectic matrix. In two dimensions $\boldsymbol{\Omega} = \Omega_2 = \begin{pmatrix} 0 & 1 \\ -1 & 0 \end{pmatrix}$, while in four dimensions $\boldsymbol{\Omega} = \Omega_2 \oplus \Omega_2 = \mathbb{I}_2 \otimes \Omega_2$. See section 2.4.1 for more details.

One standard way to perform the calculation required by Eq. (5.2.5) by means of symplectic diagonalization can be found in Ref. [148]. Here, we follow instead another route. We write the drift matrix $\boldsymbol{D}$ as:

$$\boldsymbol{D} = \omega\boldsymbol{\Omega} + g\boldsymbol{X} + \delta\boldsymbol{Z}, \quad \boldsymbol{\Omega} = \mathbb{I}_2 \otimes \Omega_2, \quad \boldsymbol{X} = \sigma_x \otimes \Omega_2, \quad \boldsymbol{Z} = \sigma_z \otimes \Omega_2, \quad \Omega_2 = \begin{pmatrix} 0 & 1 \\ -1 & 0 \end{pmatrix}, \tag{5.2.6}$$

where σ_x and σ_z are the standard Pauli operators. By also defining $\boldsymbol{Y} = \sigma_y \otimes \Omega_2$, where σ_y is the standard Pauli operator, and recalling that $[A \otimes B, C \otimes B] = [A, C] \otimes B^2$ one can get the following relations:

$$[\boldsymbol{X}, \boldsymbol{Y}] = 2i\boldsymbol{Z}\boldsymbol{\Omega}, \quad [\boldsymbol{Y}, \boldsymbol{Z}] = 2i\boldsymbol{X}\boldsymbol{\Omega}, \quad [\boldsymbol{Z}, \boldsymbol{X}] = 2i\boldsymbol{Y}\boldsymbol{\Omega}. \tag{5.2.7}$$

Moreover, matrices $\boldsymbol{X}$, $\boldsymbol{Y}$, and $\boldsymbol{Z}$ commute with $\boldsymbol{\Omega}$. Then, let use define the matrix $\boldsymbol{A} = (g/k)\boldsymbol{X} + (\delta/k)\boldsymbol{Z}$ where $k = \sqrt{g^2 + \delta^2}$. Since $\boldsymbol{A}^2 = -\mathbb{I}_4$ we can compute the exponential:

$$e^{\tau k \boldsymbol{A}} = \mathbb{I}_4 \cos(\tau k) + \boldsymbol{A} \sin(\tau k). \tag{5.2.8}$$

Lastly, since $[\boldsymbol{A}(t), \boldsymbol{\Omega}] = 0$ and $\boldsymbol{D} = \omega\boldsymbol{\Omega} + k\boldsymbol{A}$ we get:

$$\boldsymbol{K}(\tau) \equiv e^{\tau \boldsymbol{D}(t)} = [\cos(\omega\tau)\mathbb{I}_4 + \sin(\omega\tau)\boldsymbol{\Omega}] \times [\cos(k\tau)\mathbb{I}_4 + \sin(k\tau)\boldsymbol{A}]\,. \tag{5.2.9}$$

The above matrix can be rewritten by composing 2×2 blocks[8], i.e.,

$$\boldsymbol{K}(\tau) = \begin{pmatrix} K_+(\tau) & K_1(\tau) \\ K_1(\tau) & K_-(\tau) \end{pmatrix}, \quad K_1(\tau) = -\frac{g}{k}\left(a(\tau)\mathbb{I}_2 - b(\tau)\Omega_2\right), \tag{5.2.10}$$

$$K_+(\tau) = \left(c(\tau) - \frac{\delta}{k}a(\tau)\right)\mathbb{I}_2 + \left(d(\tau) + \frac{\delta}{k}b(\tau)\right)\Omega_2, \tag{5.2.11}$$

$$K_-(\tau) = \left(c(\tau) + \frac{\delta}{k}a(\tau)\right)\mathbb{I}_2 + \left(d(\tau) - \frac{\delta}{k}b(\tau)\right)\Omega_2, \tag{5.2.12}$$

where

$$\begin{aligned} a(\tau) &= \sin(\omega\tau)\sin(k\tau), & b(\tau) &= \cos(\omega\tau)\sin(k\tau), \\ c(\tau) &= \cos(\omega\tau)\cos(k\tau), & d(\tau) &= \sin(\omega\tau)\cos(k\tau). \end{aligned} \tag{5.2.13}$$

When the two colliding oscillators are resonant, i.e., $\delta = 0$, one has that $\boldsymbol{A} = \boldsymbol{X}$ and the operator $\boldsymbol{K}(\tau)$ greatly simplifies. In particular, for $g\tau = \pi/2$ one gets

$$\boldsymbol{K}(\pi/(2g)) = [\cos(\pi\omega/(2g))\mathbb{I}_4 + \sin(\pi\omega/(2g))\boldsymbol{\Omega}]\,\boldsymbol{X}, \tag{5.2.14}$$

which is, up to local rotation matrices, a swap operator[9]. We can also derive the free evolution of system S by setting $g = 0$. Lengthy but straightforward calculations lead to $U_S(\tau) \equiv K_+(\tau) = \cos(\omega_S\tau)\mathbb{I}_2 + \sin(\omega_S\tau)\Omega_2$.

[8] Doing this requires lengthy but straightforward calculations.

[9] The standard swap can be obtained by setting also $\omega = g$.

5.3 Markovian dynamics in the continuous limit

Here we derive the Markovian master equation for the dynamics of system S, therefore we do not consider the intra-bath collisions. The map describing the evolution of system S during a collision is given by[10]

$$\begin{aligned}\sigma_S(t+\tau) &= \mathrm{Tr}_B\left\{\boldsymbol{K}(t,\tau)\left(\sigma_S(t)\oplus\sigma_B\right)\boldsymbol{K}(t,\tau)^\intercal\right\},\\ &= K_+(t,\tau)\sigma_S(t)K_+^\intercal(t,\tau)+K_1(t,\tau)\sigma_B K_1^\intercal(t,\tau),\end{aligned}\tag{5.3.1}$$

where $\sigma_S(t)$ and σ_B are, respectively, the covariance matrix of system S at the start of the collision and the initialized state of each bath unit. If we want to keep into account the fact that $\omega_S(t)$ is time-dependent we must update the frequency by applying a suitable operator to $\sigma_S(t)$. If we consider this update to happen *after* the collision, i.e., this update is the last operation in a step of the CM, we can see that this is done by

$$\sigma_S(t+\tau)\to T(t,\tau)\sigma_S(t+\tau)T(t,\tau),\quad \text{where}\quad T(t,\tau)=\begin{pmatrix}\sqrt{\frac{\omega_S(t+\tau)}{\omega_S(t)}} & 0\\ 0 & \sqrt{\frac{\omega_S(t)}{\omega_S(t+\tau)}}\end{pmatrix},\tag{5.3.2}$$

by checking Eq. (5.1.4). Then, the entire step is given by

$$\sigma_S(t+\tau)=\mathrm{Tr}_B\left\{\boldsymbol{T}(t,\tau)\boldsymbol{K}(t,\tau)\left(\sigma_S(t)\oplus\sigma_B\right)\boldsymbol{K}(t,\tau)^\intercal\boldsymbol{T}(t,\tau)\right\}.\tag{5.3.3}$$

where $\boldsymbol{T}(t,\tau)=T(t,\tau)\oplus\mathbb{I}_2$. Alternatively, one could consider to do the update *before* the next collision. In this case, the entire step would be described by

$$\sigma_S(t+\tau)=\mathrm{Tr}_B\left\{\boldsymbol{K}(t,\tau)\boldsymbol{T}(t-\tau,\tau)\left(\sigma_S(t)\oplus\sigma_B\right)\boldsymbol{T}(t-\tau,\tau)\boldsymbol{K}(t,\tau)^\intercal\right\}.\tag{5.3.4}$$

A common trick [230] to obtain a continuous master equation from a CM is to substitute the interaction coupling g with $\sqrt{h/\tau}$ and then make the limit $\lim_{\tau\to0}(\sigma_S(t+\tau)-\sigma_S(t))/\tau$[11]. Expanding up to first order in τ the quantities $K_+(t,\tau)$, $K_1(t,\tau)$, and $T(t,\tau)$ one obtains[12]

$$\dot\sigma_S=\omega_S(t)[\Omega_2,\sigma_S(t)]+\frac{\partial_t\omega_S(t)}{2\omega_S(t)}\{\sigma_z,\sigma_S(t)\}-h\sigma_S(t)-h\Omega_2\sigma_B\Omega_2.\tag{5.3.5}$$

Here, the origin of the term $\partial_t\omega_S(t)/\omega_S(t)$ comes from including the matrices $T(t,\tau)$ in the derivation. The result is the same if we consider doing the update both after the collision or before. Since in this limit each collision is practically instantaneous, the requirement that $\omega_S(t)$ does not change during a collision should be always satisfied. Then, we could think that Eq. (5.3.5) is a nonadiabatic Markovian master equation.

[10] In this section we write the explicit temporal dependence of the various quantities such as $\boldsymbol{K}(t,\tau)$.

[11] Notice that, in this way, g is a function of the collision duration τ while h is not.

[12] For completeness, we report here $K_1(t,\tau)\simeq\sqrt{h\tau}\Omega_2$, $K_+(t,\tau)\simeq\mathbb{I}_2+\omega_S(t)\tau\Omega_2-(h/2)\tau\mathbb{I}_2$, and $T(t,\tau)\simeq\mathbb{I}_2+\tau\partial_t\omega_S(t)/(2\omega_S(t))\sigma_z$.

Indeed, if $\omega_S(t)$ varies slowly, the term $\partial_t\omega_S(t)/\omega_S(t)$ should be negligible. When this is not true, the dynamics of the system changes quite sensibly, as we will show in section 5.5.

From Eq. (5.3.5) we can also directly derive the equation for the average number of excitations, $\langle n(t)\rangle$, in the harmonic oscillator[13]. We get

$$\langle \dot{n}_S(t)\rangle = h\left[\langle n_B\rangle - \langle n_S(t)\rangle\right] + \frac{\partial_t\omega_S(t)}{4\omega_S(t)}\,\mathrm{Tr}\{\sigma_z\sigma_S(t)\}. \tag{5.3.6}$$

The equation above shows that if we can neglect the nonadiabatic term the dynamics of the average excitation number is independent of the frequency $\omega_S(t)$ and the actual bath units state. For example, if σ_B would describe a pure squeezed state with the same average excitation number of a certain thermal state, the dynamics of $\langle n_S(t)\rangle$ would be exactly the same. We have checked numerically that this is not true when the time-dependent term is considered.

Notice that in the time-independent case, Eq. (5.3.5) has the same structure of the one reported in Ref. [148] for a diffusive Gaussian dynamics[14] and that when $\sigma_B = (2\overline{n}+1)\mathbb{I}_2$, i.e., the bath units are in a thermal state, the master equation reduces to

$$\dot{\sigma}_S = \omega_S[\Omega_2, \sigma_S(t)] - h\sigma_S(t) + h(2\overline{n}+1)\mathbb{I}_2, \tag{5.3.7}$$

which is the equation for thermal diffusion [148]. Moreover, when the bath is thermal, calculating thermodynamic quantities from the master equation becomes easy. In fact, since the interaction Hamiltonian of Eq. (5.1.7) preserves the total number of excitations, the heat flux can be calculated as $\dot{Q} = \hbar\omega_B\langle\dot{n}_S(t)\rangle$[15]. Indeed, in the Markovian case, the energy variations of the bath units are reabsorbed in the bath itself after the interaction. Regarding the rate of internal energy variation, it is given by

$$\frac{\mathrm{d}}{\mathrm{d}t}\left(\hbar\omega_S(t)\langle n_S(t)\rangle\right) = \hbar\omega_S(t)\left[\langle\dot{n}_S(t)\rangle + \frac{\dot{\omega}_S(t)}{\omega_S(t)}\langle n_S(t)\rangle\right]. \tag{5.3.8}$$

Therefore, by exploiting the first law of thermodynamics, $W = U - Q$, we find

$$\dot{W} = \hbar(\omega_S(t) - \omega_B)\langle\dot{n}_S(t)\rangle + \dot{\omega}_S(t)\langle n_S(t)\rangle. \tag{5.3.9}$$

Another way to find a master equation starting from a CM is to find a Lindbladian interpolating the discrete CPTP map induced by the CM [239, 241, 242]. This method, however, has been developed assuming time-independent CMs. Following Ref. [242], we start from Eq. (5.3.1) and we must expand to second order in τ, around $\tau = 0$, the matrices $P = K_+(\tau)$ and $R = K_1(\tau)\sigma_B K_1^\intercal(\tau)$ so that we can write them as $P \simeq \mathbb{I}_2 + \tau P_1 + \tau^2 P_2$ and $R \simeq 0_2 + \tau R_1 + \tau^2 R_2$[16]. This is done in Appendix 5.A. Then, we can calculate the following matrices at first order in τ:

$$A \simeq P_1 + \tau(P_2 - (1/2)P_1^2), \quad C \simeq R_1 + \tau\left[R_2 - (1/2)(P_1R_1 + R_1P_1^\intercal)\right]. \tag{5.3.10}$$

[13] The average number of excitations is given by $\langle n_S(t)\rangle = (\mathrm{Tr}\{\sigma_S(t)\} - 2)/4$. See section 2.4.1.
[14] See page 144 of Ref. [148]. In particular, using its notation, $A = \omega_S\Omega_2 - h/2$.
[15] This is true even if $\omega_S(t)$ varies in time.
[16] We denote by 0_n the zero square matrix of dimension n.

The explicit form of these matrices is

$$A \simeq \omega_S \Omega_2 + \frac{\tau}{2} g^2 \mathbb{I}_2, \qquad C \simeq -\tau g^2 \Omega_2 \sigma_B \Omega_2. \tag{5.3.11}$$

Finally, the master equation is [242]:

$$\dot{\sigma}_S(t) = A\sigma_S(t) + \sigma_S(t)A^\intercal + C = \omega_S[\Omega_2, \sigma_S(t)] - \tau g^2 \sigma_S(t) - \tau g^2 \Omega_2 \sigma_B \Omega_2, \tag{5.3.12}$$

which is equal to the time-independent case of Eq. (5.3.5) by setting $g^2\tau = h$.

If we abuse of the formalism developed in Refs. [239, 241, 242], we can also calculate the time-dependent case. The difference is that now $P \equiv T(t,\tau)K_+(t,\tau)$. Calculations are detailed in Appendix 5.A while the final result is

$$A \simeq \omega_S \Omega_2 + \frac{\dot{\omega}_S}{2\omega_S}\sigma_z + \frac{\tau}{2}\left[\dot{\omega}_S \sigma_x - \left(\frac{\dot{\omega}_S^2}{4\omega_S^2} + g^2\right)\mathbb{I}_2 + M_2(t)\right], \quad C \simeq -\tau g^2 \Omega_2 \sigma_B \Omega_2. \tag{5.3.13}$$

The matrix $M_2(t)$ is given in Appendix 5.A and contains second derivatives of the frequency $\omega_S(t)$. In this case, one can obtain Eq. (5.3.5) by setting again $g^2\tau = h$ and performing, only then, the limit $\tau \to 0$.

5.4 Non-Markovian dynamics

Here we study a non-Markovian version of the CM studied in the preceding section. Non-Markovianity is introduced by allowing intra-bath interactions preceding the collision with system S, as explained in section 2.2.3. In order to analyze this non-Markovain dynamics, we will make use of the Markovian embedding technique described in section 2.2.3.

We denote by $\boldsymbol{\sigma}_L$ the covariance matrix of system L, comprising subsystems S and B_1, while we denote by $\boldsymbol{\sigma}_{L,n}$ the covariance matrix including also the n-th bath unit involved in the dynamics in a given moment. Since B_1 will not be discarded because of the Markovian embedding, we rename it A, standing for ancilla. The starting state of L is then given by $\sigma_S(0) \oplus \sigma_A(0) = \sigma_S(0) \oplus \sigma_B$. After the first collision of duration τ, i.e., the S-A collision and the frequency update, the state is described by

$$\boldsymbol{\sigma}_L(\tau) = \boldsymbol{T}(0,\tau)\boldsymbol{K}(0,\tau)\boldsymbol{\sigma}_L(0)\boldsymbol{K}^\intercal(0,\tau)\boldsymbol{T}(0,\tau). \tag{5.4.1}$$

Then, for the second and subsequent steps of the CM we must first consider the intra-bath collision, whose duration and coupling strength we denote by, respectively, τ_B and g_B. These steps are described by

$$\boldsymbol{\sigma}_L(t+\tau_B+\tau) = \mathrm{Tr}_B\left\{\boldsymbol{\Phi}(t,\tau_B,\tau)\left(\boldsymbol{\sigma}_L(t)\oplus\sigma_B\right)\boldsymbol{\Phi}^\intercal(t,\tau_B,\tau)\right\}, \tag{5.4.2}$$

with

$$\boldsymbol{\Phi}(t,\tau_B,\tau) = \boldsymbol{T}(t+\tau_B,\tau)\left(\boldsymbol{K}(t+\tau_B,\tau)\oplus\mathbb{I}_2\right)\boldsymbol{T}(t,\tau_B)\left(\mathbb{I}_2\oplus\boldsymbol{S}\right)\left(U_S(t,\tau_B)\oplus\boldsymbol{K}_B(t,\tau_B)\right), \tag{5.4.3}$$

where $\boldsymbol{K}_B(t,\tau)$ is the same of $\boldsymbol{K}(t,\tau)$ with the substitution of g with g_B and $\omega_S(t)$ with ω_B[17], and $\boldsymbol{S}$ implements the swap between A and the bath unit after their interaction[18].

[17] Notice that this is a resonant interaction so that what we would call δ_B is zero.

[18] See section 2.2.3. Here, the explicit form of $\boldsymbol{S}$ is $\boldsymbol{S} = \sigma_x \otimes \mathbb{I}_2$.

Notice that $\boldsymbol{\sigma}_L(t)$ can contain correlations between the subsystems S and A. We write

$$\boldsymbol{\sigma}_L(t) = \begin{pmatrix} \sigma_S(t) & \sigma_C(t) \\ \sigma_C^\intercal(t) & \sigma_A(t) \end{pmatrix}, \tag{5.4.4}$$

where $\sigma_C(t)$, a 2×2 matrix, is zero only for uncorrelated states [150].

The explicit form of Eq. (5.4.3) is derived in Appendix 5.B and is

$$\boldsymbol{\sigma}_L(t+\tau_B+\tau) = \boldsymbol{U}(t,\tau_B,\tau)\boldsymbol{\sigma}_L(t)\boldsymbol{U}^\intercal(t,\tau_B,\tau) + \boldsymbol{\Phi}_B(t,\tau_B,\tau)\begin{pmatrix} \sigma_B & \sigma_B \\ \sigma_B & \sigma_B \end{pmatrix}\boldsymbol{\Phi}_B^\intercal(t,\tau_B,\tau), \tag{5.4.5}$$

where, with $t' = t + \tau_B$ and 0_2 being the 2×2 null matrix,

$$\boldsymbol{U}(t,\tau_B,\tau) = \boldsymbol{T}(t',\tau)\boldsymbol{K}(t',\tau)\boldsymbol{T}(t,\tau_B)\begin{pmatrix} U_S(t,\tau_B) & 0_2 \\ 0_2 & K_1^B(t,\tau_B) \end{pmatrix}, \tag{5.4.6}$$

and

$$\boldsymbol{\Phi}_B(t,\tau_B,\tau) = \begin{pmatrix} T(t',\tau)K_1(t',\tau)K_-^B(t,\tau_B) & 0_2 \\ 0_2 & K_-(t',\tau)K_-^B(t,\tau_B) \end{pmatrix}. \tag{5.4.7}$$

The evolution of system L is more complex than that of S in the Markovian case, even if the dynamics of L is Markovian too. However, if the bath is thermal and $\omega_S(t)$ is time-independent, we can easily see that the $\boldsymbol{\sigma}_L = \sigma_B \oplus \sigma_B$ is a fixed point of the map. Indeed, the intra-bath interaction gives rise to no dynamics at all and the swap operation swaps to equal states. Then, the same is true for the S-A interaction. Therefore, since all parts of one step do not change anything, we conclude that $\boldsymbol{\sigma}_L(t) = \sigma_B \oplus \sigma_B$ implies $\boldsymbol{\sigma}_L(t+\tau_B+\tau) = \boldsymbol{\sigma}_L(t)$.

In order to obtain a Markovian continuous master equation for $\boldsymbol{\sigma}_L$, the trick of making the interaction dependent on the collision duration does not work because of divergent terms for $\tau \to 0$. We could also think of applying the formalism of Ref. [242], neglecting that here we would not obtain $P_0 = \mathbb{I}_4$ and $R_0 = 0$. We tried this route and even this did not work. Therefore, at the moment, we can just describe the discrete dynamics.

The discrete dynamics described by Eq. (5.4.5) is Markovian for the enlarged system L. We can quantify how much it is non-Markovian on system S by using the Gaussian quantifier defined in Ref. [101] for continuous Gaussian maps and adapted for discrete ones in Ref. [102]. In order to do this, we write the state of L after n steps. We define $t_0 = 0$, $t_1 = \tau$, and $t_n = \tau + (n-1)(\tau + \tau_B)$[19]. Then we recast the evolution of $\boldsymbol{\sigma}_L(t)$ as

$$\boldsymbol{\sigma}_L(t_n) = \boldsymbol{X}_n\boldsymbol{\sigma}_L(0)\boldsymbol{X}_n^\intercal + \boldsymbol{Y}_n, \tag{5.4.8}$$

in order to obtain a similar equation for σ_S[20]:

$$\sigma_S(t_n) = \mathcal{X}_n\sigma_S(0)\mathcal{X}_n^\intercal + \mathcal{Y}_n. \tag{5.4.9}$$

[19] We must distinguish between the first step and the others because in the first step there is no intra-bath interaction and swap.

[20] The step-wise equivalent of Eq. (2.4.8).

First, we introduce the symbols

$$\boldsymbol{U}_0 = \boldsymbol{T}(0,\tau)\boldsymbol{K}(0,\tau), \quad \boldsymbol{U}_n = \boldsymbol{U}(\tau + n(\tau+\tau_B),\tau,\tau_B), \quad \boldsymbol{U}_{n\to m} = \boldsymbol{U}_{m-1}\boldsymbol{U}_{m-2}\ldots\boldsymbol{U}_n, \tag{5.4.10}$$

with $\boldsymbol{U}_{n\to m} = \mathbb{I}_4$ when $m \leq n$. Then, we can write

$$\boldsymbol{X}_0 = \mathbb{I}_4, \quad \boldsymbol{X}_1 = \boldsymbol{U}_0, \quad \boldsymbol{X}_n = \boldsymbol{U}_{1\to n}\boldsymbol{U}_0 \tag{5.4.11}$$

and

$$\boldsymbol{Y}_0 = \boldsymbol{Y}_1 = 0, \qquad \boldsymbol{Y}_n = \sum_{i=2}^{n}\left[\boldsymbol{U}_{i\to n}\boldsymbol{\Phi}_B(t_{n-1},\tau_B,\tau)\begin{pmatrix}\sigma_B & \sigma_B\\ \sigma_B & \sigma_B\end{pmatrix}\boldsymbol{\Phi}_B^{\intercal}(t_{n-1},\tau_B,\tau)\boldsymbol{U}_{i\to n}^{\intercal}\right]. \tag{5.4.12}$$

Finally, since $\boldsymbol{\sigma}_L(0) = \sigma_S(0)\oplus\sigma_B$, we get

$$\mathcal{X}_n = (\boldsymbol{X}_n)_{1,1}, \quad \mathcal{Y}_n = (\boldsymbol{X}_n)_{1,2}\sigma_B\left[(\boldsymbol{X}_n)_{2,1}\right]^{\intercal} + (\boldsymbol{Y})_{1,1}, \tag{5.4.13}$$

where the subscripts refer to the 2×2 block matrices. For example, $[(\boldsymbol{X}_n)_{2,1}]^{\intercal}$ is the transpose of the lower right block matrix of $\boldsymbol{X}_n$.

Now, following Ref. [102] we can quantify the non-Markovianity of the process by finding the eigenvalues of the Hermitian matrix Λ_n:

$$\begin{aligned}\Lambda_n &= \mathcal{Y}_{n,n-1} - \frac{i}{2}\Omega + \frac{i}{2}\mathcal{X}_{n,n-1}\Omega\mathcal{X}_{n,n-1}^{\intercal},\\ \mathcal{X}_{n,n-1} = \mathcal{X}_n\mathcal{X}_{n-1}^{-1}, &\qquad \mathcal{Y}_{n,n-1} = \mathcal{Y}_n - \mathcal{X}_{n,n-1}\mathcal{Y}_{n-1}\mathcal{X}_{n,n-1}^{\intercal}.\end{aligned} \tag{5.4.14}$$

Naming $\lambda_{n,\pm}$ the eigenvalues of Λ_n we have that the punctual non-Markovianity at step n is given by

$$\mathcal{N}_n = \sum_{\pm}\frac{|\lambda_{n,\pm}| - \lambda_{n,\pm}}{2}. \tag{5.4.15}$$

while the total one is $\mathcal{N}_T(n) \equiv \sum_{i=1}^{n}\mathcal{N}_n$.

5.5 Analysis of the dynamics

In this section, we analyze the various dynamics found in the previous sections.

We start by investigating the role of the nonadiabatic time-dependent term in Eq. (5.3.5), by also comparing the resulting master equation with the original discrete dynamics. This is done for the average number of excitations in Fig. 5.1 when the bath unit state is thermal. There, we can see that including the nonadiabatic time-dependent term in the Markovian continuous master equation is necessary to fit well the discrete curve calculated by using Eq. (5.3.3). Moreover, the difference between the complete form of the dynamics computed through Eq. (5.3.13) and the dynamics given by Eq. (5.3.5) is not very high for the case here shown. However, if we change the parameters the accord between interpolating curves and the discrete points can get worse. We remark that for the average excitation number the actual form of the bath unit state is not important in

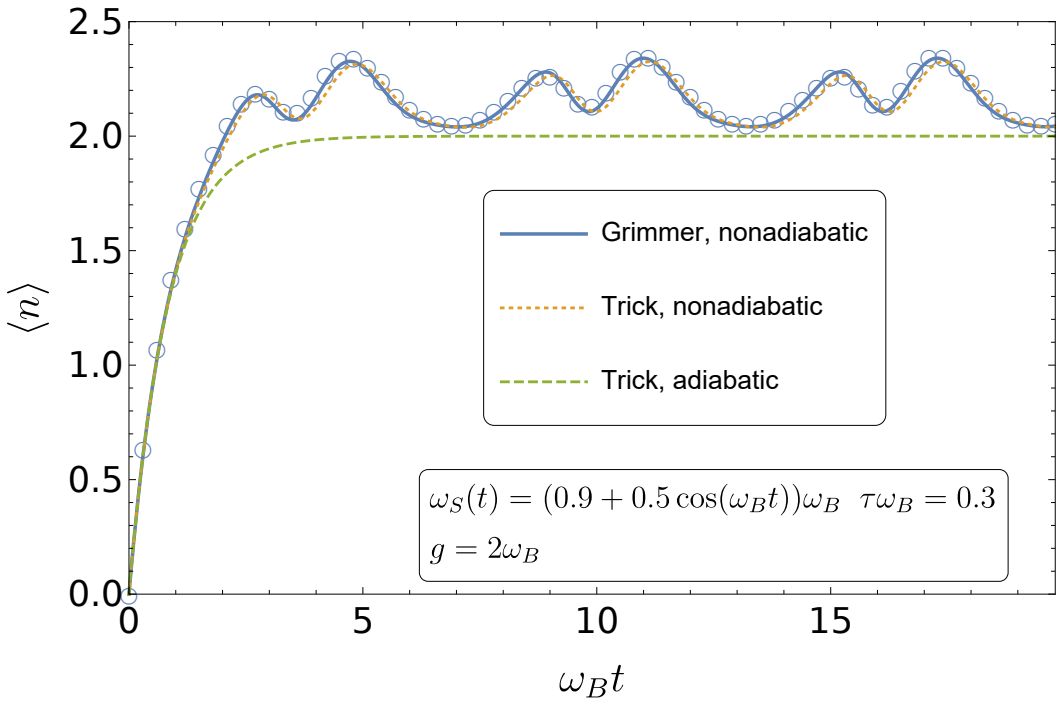

Figure 5.1: Average number of excitations as a function of time. Bath units are in the thermal state with two average excitations, i.e., $\sigma_B = 5\mathbb{I}_2$. The blues circles indicate the dynamics given by the discrete model of Eq. (5.3.3). The "Trick, nonadiabatic" dashed curve is obtained by numerically solving the master equation of Eq. (5.3.5) while "Trick, adiabatic" is obtained by solving the same equation without considering the nonadiabatic term $\partial_t\omega_S(t)/(2\omega_S(t))\{\sigma_z, \sigma_S(t)\}$. The curve denoted by "Grimmer, nonadiabatic" is obtained by numerically solving Eq. (5.3.12), using the coefficients given in Eq. (5.3.13). Here, the agreement between continous curves and discrete dynamics is good. However, if we employ a non-thermal bath and consider a time-dependent $\omega_S(t)$ the agreement is worse.

the time-independent case, as shown in Eq. (5.3.6). However, it is if one considers the nonadiabatic time-dependent term and, for some reasons that we do not understand yet, when the bath is not in a thermal state, the agreement between the continuous equations and the discrete dynamics is not good as when the bath is thermal.

In the same vein, we plot in Fig. 5.2 the purity of system S as a function of time. As in Fig. 5.1, there is a good agreement between the continuous curves with the time-dependent term and the discrete points calculated iteratively through Eq. (5.3.3). However, variations for purity are much lower with respect to the average excitation number case. Moreover, as for the average excitation number, when the bath is not thermal and we consider the time-dependent term, the agreement between continous and discrete dynamics is not so good anymore.

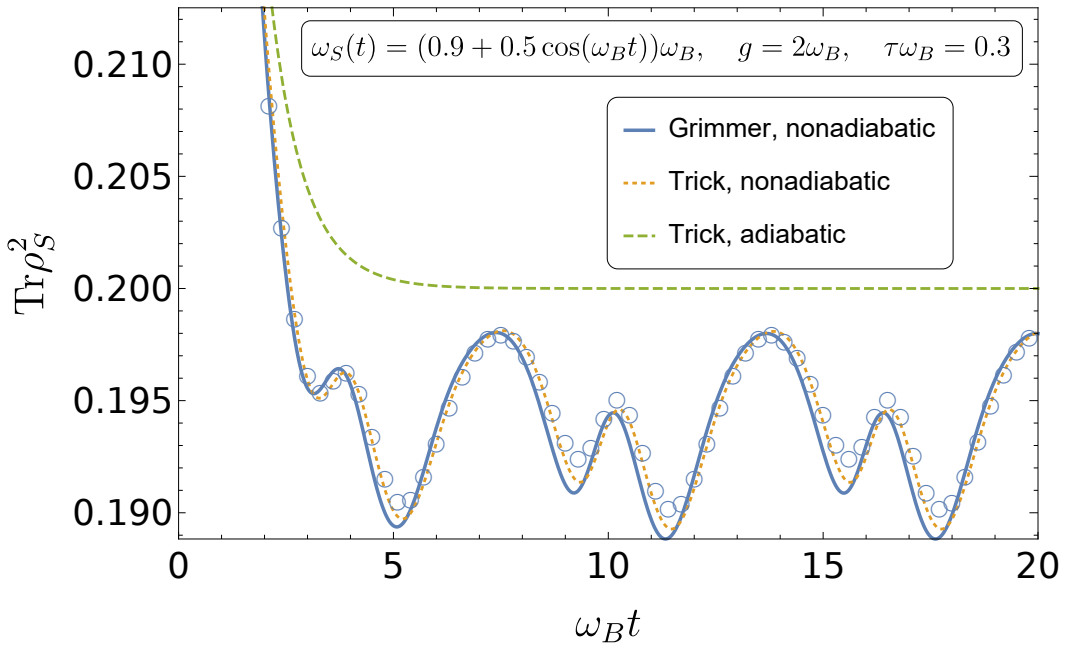

Figure 5.2: Purity as a function of time. Bath units are in the thermal state with two average excitations, i.e., $\sigma_B = 5\mathbb{I}_2$. The blues circles indicate the dynamics given by the discrete model of Eq. (5.3.3). The "Trick, nonadiabatic" dashed curve is obtained by numerically solving the master equation of Eq. (5.3.5) while "Trick, adiabatic" is obtained by solving the same equation without considering the nonadiabatic term $\partial_t\omega_S(t)/(2\omega_S(t))\{\sigma_z, \sigma_S(t)\}$. The curve denoted by "Grimmer, nonadiabatic" is obtained by numerically solving Eq. (5.3.12), using the coefficients given in Eq. (5.3.13). The same comments of Fig. 5.1 regarding the agreement between continuous and discrete dynamics apply here.

Regarding the non-Markovian case, we start by analyzing a situation in which $\omega_S(t)$ is time-independent, in order to focus on the non-Markovian effects. One could think that the higher is the product $g_B\tau_B$ the higher the non-Markovianity is. However, since the interaction gives rise to a complete swap[21] of the colliding particles when $g_B\tau_B = \pi/2 + n\pi$ with $n \in \mathbb{N}$[22], the maximum of non-Markovianity is attained for these values. Then, the effect of non-Markovianity can be seen by observing for different values of $g_B\tau_B$ ranging from zero to $\pi/2$. Moreover, in order to solely focus on the effect of the non-Markovianity we choose $\tau_B = 0.01\tau$ so that the time used for the intra-bath collision is negligible and serves only to the purpose of giving rise to the non-Markovian effects

Figs. 5.3 and 5.4 show, respectively, the average excitation number and purity of system S as a function of time. As for the Markovian case, we choose the state of the bath

[21] We recall that the intra-bath collision is resonant.
[22] We include the case $n = 0$.

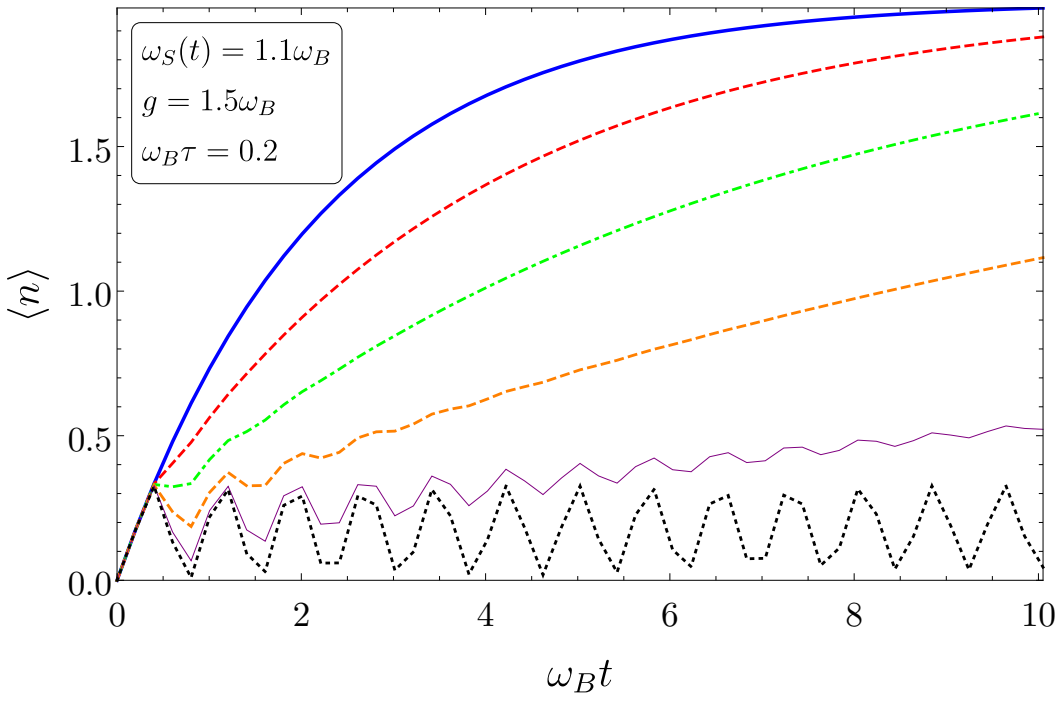

Figure 5.3: Average number of excitations as a function of time for various values of $g_B\tau_B$, with $\omega_B\tau_B = 0.001$. The blue continuous and thick curve corresponds to $g_B\tau_B = 0.001$, the dashed red one to $g_B\tau_B = 0.5$, the dot-dashed green one to $g_B\tau_B = 0.75$, the more dashed orange one to $g_B\tau_B = 1$, the thin purple one to $g_B\tau_B = 1.25$, and the black dotted one to $g_B\tau_B = 1.5$. As expected, the more $g_B\tau_B$ approaches $\pi/2$, the more the dynamics shows non-Markovian oscillations. Notice that the overall effect of increasing $g_B\tau_B$ is to increase the relaxation time.

units to be thermal. We notice that, for thermal bath, the steady state of $\sigma_S(t)$ is the same of the Markovian dynamics, i.e., σ_B. This stems from the fact that $\boldsymbol{\sigma}_L = \sigma_B \oplus \sigma_B$ is a fixed point of the discrete map and that we have checked numerically that the dynamics makes σ_L converge to that state. The two figures show the typical fluctuations due to non-Markovian dynamics for high enough $g_B\tau_B$. Moreover, we observe that the overall effects of increasing the non-Markovian nature of the dynamics is to effectively raise the relaxation time of the system. This becomes intuitive by considering that in the case $g_B\tau_B = \pi/2$ the effective dynamics of system L is unitary so that system S cannot have a steady state. Therefore, the more $g_B\tau_B$ approaches $\pi/2$ the more system S will take to reach its steady state.

Finally, Fig. 5.5 shows the plot of the non-Markoviniaty quantifier defined in Eq. (5.4.15) as a function of time, again for a thermal bath. By comparing it with Figs. 5.3 and 5.4 we see that the peaks of non-Markovianity corresponds to the fluctuations. These graphs confirm the presence of non-Markovianity in the map and are independent of the

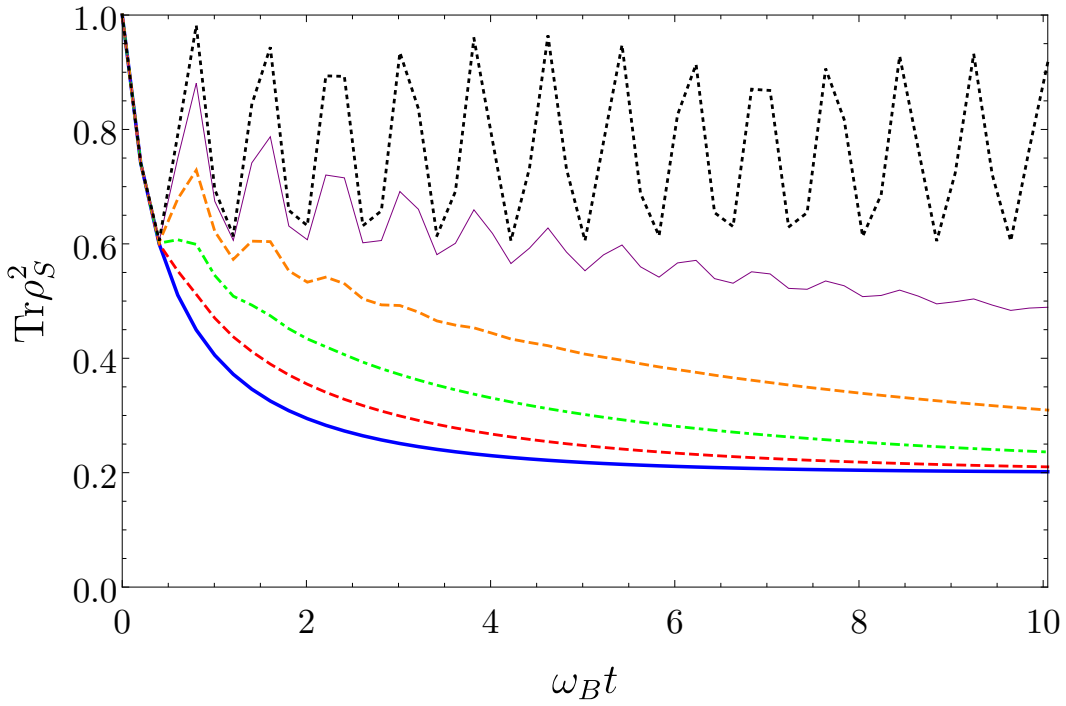

Figure 5.4: Purity as a function of time for various values of $g_B\tau_B$, with $\omega_B\tau_B = 0.001$. This plot legend and the parameters we have used are the same of Fig. 5.3.

initial state chosen for S. If, for example, we had chosen $\sigma_S(t=0) = \sigma_B$ we would not have a dynamics at all since σ_S is already in the steady state and, therefore, we would see no fluctuations. Nevertheless, Fig. 5.5 would show these non-zero non-Markovianity values, indicating that there exist initial states for which it is possible to see the typical non-Markovianity induced fluctuations. This property will be useful in the case of time-dependent non-Markovian dynamics in order to discriminate between fluctuations induced by non-Markovianity and those induced by the variation of $\omega_S(t)$.

5.6 Conclusions

In this chapter, we have firstly described through the Gaussian formalism the Markovian dynamics of a harmonic oscillator, denoted by S, in contact with a collisional environment made of harmonic oscillators. Using the collision model, we have derived a time-dependent continuous master equation containing a nonadiabatic term, the study of which seems to be promising. We have also checked that similar results are obtained using two different methods to derive this continuous master equation.

Secondly, we have studied the system in the non-Markovian case by introducing the non-Markovianity through intra-bath collisions. In order to study the system dynamics,

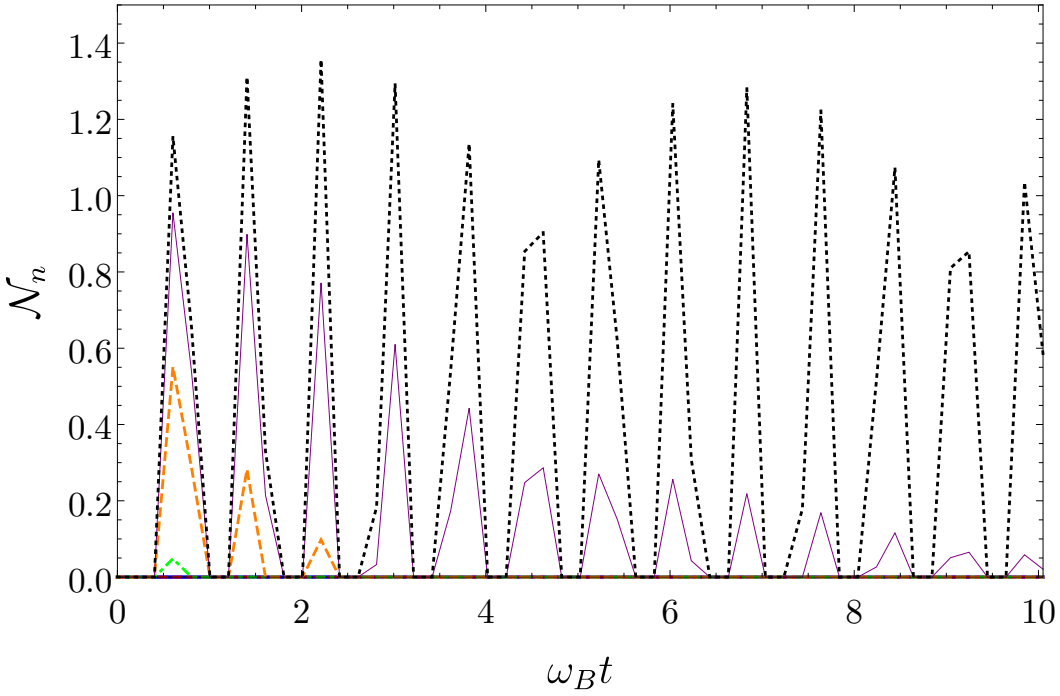

Figure 5.5: Quantifier of non-Markovianity as a function of time for various values of $g_B\tau_B$, with $\omega_B\tau_B = 0.001$. This plot legend and the parameters we have used are the same of Fig. 5.3.

we have made use of the Markovian embedding technique, thus studying the Markovian dynamics of an enlarged system L comprising system S and an ancilla A. At the moment, we have been able to compute only the discrete dynamics of system L.

Lastly, we have studied different properties of the dynamics induced by the equations found for the Markovian and the non-Markovian cases. We have verified the goodness of the techniques employed for the Markovian dynamics and found the typical signatures of non-Markovianity for the non-Markovian dynamics. On the one hand, our plots for the Markovian case show that the time-dependent term obtained in the continuous equation is necessary to well interpolate the discrete dynamics even if the same techniques do not work as well when the state of the bath is not thermal. On the other hand, we have argued about how the non-Markovianity quantifier could be used in the time-dependent non-Markovian case to discriminate between effects induced by non-Markovianity and those induced by the temporal variations of system S frequency.

We deem that these first preliminary results are encouraging. Indeed, the collision models let us to explore dynamics regimes which are usually difficult to deal with.

In addition to what we exposed in this chapter, we are currently working with Gabriele De Chiara and Heather Leitch at Queen's University Belfast to study a similar setup in which there are two collisional reservoirs: one cold and one hot. The aim is to study

a continuous thermal machine whose working fluid is made of one or more harmonic oscillators with time-dependent frequencies. Although we are just dealing with Markovian dynamics in this case, when we will have completed the study of the non-Markovian dynamics in the setup exposed in this chapter, i.e., a single harmonic oscillator in contact with a single collisional bath, we could try to extend the study of the above described thermal machine to the non-Markovian regime.

5.A Taylor expansions of the collision matrices

In this section, we give details about the perturbative expansion of the matrix $\boldsymbol{K}(\tau)$, defined in Eq. (5.2.10), up to second order in τ for $\tau \to 0$. We first analyze the time-independent case and fix the starting time of the collision at $t = 0$. Then, with an abuse of the methods described in Ref. [242], we also treat the expansion of the time-dependent terms in Eq. (5.3.3).

First of all, we expand all the coefficients defined in Eq. (5.2.13):

$$a(\tau) \simeq \omega k \tau, \quad b(\tau) \simeq k\tau, \quad c(\tau) \simeq 1 - \frac{\omega^2 + k^2}{2}\tau^2, \quad d(\tau) \simeq \omega\tau. \tag{5.A.1}$$

Then, we can easily calculate the matrices at second order:

$$\begin{aligned} K_1(\tau) &\simeq g\tau\Omega_2 - \omega g \tau^2 \mathbb{I}_2, \\ K_+(\tau) &\simeq \mathbb{I}_2 + \omega_S \tau \Omega_2 - \left(\omega_S^2 + g^2\right)\frac{\tau^2}{2}\mathbb{I}_2, \\ K_-(\tau) &\simeq \mathbb{I}_2 + \omega_B \tau \Omega_2 - \left(\omega_B^2 + g^2\right)\frac{\tau^2}{2}\mathbb{I}_2. \end{aligned} \tag{5.A.2}$$

Finally, we can expand to second order Eq. (5.3.1). We get

$$\begin{aligned} K_+(\tau)\sigma_S K_+^\intercal(\tau) &\simeq \sigma_S + \omega_S\tau[\Omega_2, \sigma_S] - \left(\omega_S^2 + g^2\right)\tau^2\sigma_S - \omega_S^2\tau^2\Omega_2\sigma_S\Omega_2, \\ K_1(\tau)\sigma_B K_1^\intercal(\tau) &\simeq -g^2\tau^2\Omega_2\sigma_B\Omega_2. \end{aligned} \tag{5.A.3}$$

Now, we can write the rate of variation of σ_S during a collision, up to second order in τ:

$$\frac{\sigma(\tau) - \sigma_S(0)}{\tau} \simeq \omega_S[\Omega_2, \sigma_S] - \left(\omega_S^2 + g^2\right)\tau\sigma_S - \omega_S^2\tau\Omega_2\sigma_S\Omega_2 - g^2\tau\Omega_2\sigma_B\Omega_2. \tag{5.A.4}$$

We obtain the time-independent version of Eq. (5.3.5) if we set $g^2\tau = h$ and, *then*, we take the limit $\tau \to 0$.

When adding the time-dependent terms to the calculations, i.e., by considering also the matrices $T(t,\tau)$, to obtain the interpolated master equation we must only modify the expansion of $K_+(\tau)$ into the expansion of $T(t,\tau)K_+(t,\tau)$. The expansion of $T(t,\tau)$ gives

$$T(t,\tau) \simeq \mathbb{I}_2 + \tau\frac{\dot{\omega}_S(t)}{2\omega_S(t)}\sigma_z + \frac{\tau^2}{2}M_2(t), \tag{5.A.5}$$

where

$$M_2(t) = \frac{1}{4\omega_S^2(t)}\begin{pmatrix} 2\omega_S(t)\ddot{\omega}_S(t) - \dot{\omega}_S^2(t) & 0 \\ 0 & 3\dot{\omega}_S^2(t) - 2\omega_S(t)\ddot{\omega}_S(t) \end{pmatrix}. \tag{5.A.6}$$

Therefore, we obtain

$$T(t,\tau)K_+(t,\tau) \simeq \mathbb{I}_2 + \tau\left(\omega_S(t)\Omega_2 + \frac{\dot{\omega}_S(t)}{2\omega_S(t)}\sigma_z\right) + \frac{\tau^2}{2}\left(\dot{\omega}_S(t)\sigma_x - \left(\omega_S^2(t) + g^2\right)\mathbb{I}_2 + M_2(t)\right). \tag{5.A.7}$$

Finally, the matrix A can be now calculated and is reported in Eq. (5.3.13).

5.B Computation of a full non-Markovian step

In this section, we give some details about the calculation to obtain Eq. (5.4.5).

First, performing the explicit matrix multiplication of Eq. (5.4.3), we find the explicit form of $\mathbf{\Phi}(t,\tau_B,\tau)$, which is

$$\begin{pmatrix} T(t',\tau)K_+(t',\tau)U'_S(t,\tau_B) & T(t',\tau)K_1(t',\tau)K_1^B(t,\tau_B) & T(t',\tau)K_1(t',\tau)K_-^B(t,\tau_B) \\ K_1(t',\tau)U'_S(t,\tau_B) & K_-(t',\tau)K_1^B(t,\tau_B) & K_-(t',\tau)K_-^B(t,\tau_B) \\ 0_2 & K_+^B(t,\tau_B) & K_1^B(t,\tau_B) \end{pmatrix}, \tag{5.B.1}$$

where $t'=t+\tau_B$ and $U'_S(t,\tau_B)=T(t,\tau_B)U_S(t,\tau_B)$. Now, we rewrite $\mathbf{\Phi}(t,\tau_B,\tau)$ as

$$\mathbf{\Phi}(t,\tau_B,\tau)=\begin{pmatrix} a & b & c \\ d & e & f \\ 0_2 & g & h \end{pmatrix}, \tag{5.B.2}$$

and calculate Eq. (5.4.2):

$$\begin{aligned}
\boldsymbol{\sigma}_L(t+\tau_B+\tau)_{1,1} &= a\sigma_S a^\intercal + b\sigma_L b^\intercal + c\sigma_B c^\intercal + a\sigma_C b^\intercal + b\sigma_C^\intercal a^\intercal, \\
\boldsymbol{\sigma}_L(t+\tau_B+\tau)_{1,2} &= a\sigma_S d^\intercal + b\sigma_L e^\intercal + c\sigma_B f^\intercal + a\sigma_C e^\intercal + b\sigma_C^\intercal d^\intercal, \\
\boldsymbol{\sigma}_L(t+\tau_B+\tau)_{2,1} &= d\sigma_S a^\intercal + e\sigma_L b^\intercal + f\sigma_B c^\intercal + d\sigma_C b^\intercal + e\sigma_C^\intercal a^\intercal, \\
\boldsymbol{\sigma}_L(t+\tau_B+\tau)_{2,2} &= d\sigma_S d^\intercal + e\sigma_L e^\intercal + f\sigma_B f^\intercal + d\sigma_C e^\intercal + e\sigma_C^\intercal d^\intercal.
\end{aligned} \tag{5.B.3}$$

The exact same result can be obtained by calculating

$$\boldsymbol{\sigma}_L(t+\tau_B+\tau)=\begin{pmatrix} a & b \\ d & e \end{pmatrix}\boldsymbol{\sigma}_L(t)\begin{pmatrix} a^\intercal & d^\intercal \\ b^\intercal & e^\intercal \end{pmatrix}+\begin{pmatrix} c & 0_2 \\ 0_2 & f \end{pmatrix}\begin{pmatrix} \sigma_B & \sigma_B \\ \sigma_B & \sigma_B \end{pmatrix}\begin{pmatrix} c^\intercal & 0_2 \\ 0_2 & f^\intercal \end{pmatrix}. \tag{5.B.4}$$

We can substitute back the correct entries for $\mathbf{\Phi}(t,\tau_B,\tau)$ and rearrange the term to obtain

$$\boldsymbol{\sigma}_L(t+\tau_B+\tau)=\boldsymbol{U}(t,\tau_B,\tau)\boldsymbol{\sigma}_L(t)\boldsymbol{U}^\intercal(t,\tau_B,\tau)+\mathbf{\Phi}_B\mathcal{Q}\sigma_B\mathbf{\Phi}_B^\intercal, \tag{5.B.5}$$

where $\mathcal{Q}\sigma\equiv\sigma\otimes(\mathbb{I}_2+\sigma_x)$,

$$\boldsymbol{U}(t,\tau_B,\tau)=\boldsymbol{T}(t',\tau)\boldsymbol{K}(t',\tau)\begin{pmatrix} U'_S(t,\tau_B) & 0_2 \\ 0_2 & K_1^B(t,\tau_B) \end{pmatrix}, \tag{5.B.6}$$

and

$$\mathbf{\Phi}_B=\begin{pmatrix} T(t',\tau)K_1(t',\tau)K_-^B(t,\tau_B) & 0_2 \\ 0_2 & K_-(t',\tau)K_-^B(t,\tau_B) \end{pmatrix}. \tag{5.B.7}$$

Chapter 6

Two-photon interaction effects in the bad-cavity limit

In section 2.4.2, we discussed about the importance and relevance of the Dicke model in actual experimental platforms and technological setups. In particular, we also argued about the recent applications of the two-photon Dicke model and some of its different features compared to the usual dipolar one. We also discussed about the application of the adiabatic elimination for the dipolar Dicke model in the bad-cavity limit.

In this chapter, we deal with the two-photon Dicke model by studying the dynamics of a damped harmonic oscillator (HO) interacting with an ensemble of qubits in the bad-cavity limit and, as already said, in the case of a two-photon coupling. By applying a recently-developed approach to perform adiabatic elimination in open quantum systems [32, 33][1], we derive an effective master equation for the qubits that takes into account the coupling with finite-temperature baths as well as coherent and incoherent optical drivings. Our analytical and numerical analysis of the time evolution and steady-state behavior unveils a novel collective phenomenology induced by nondipolar light-matter interactions. Compared to the dipolar case, the two-photon coupling introduces the possibility to enhance the absorption and emission processes, and leads to a higher resilience of sub and superradiance with respect to the baths temperature.

6.1 Physical models

We study a system composed of a damped HO interacting via a resonant Jaynes-Cummings Hamiltonian with N qubits in the bad cavity limit [33, 106, 107], comparing the one-photon (1ph) and two-photon (2ph) interaction cases. The two models are described by the Hamiltonians

$$H_l = \hbar\omega a^\dagger a + \frac{l\hbar\omega}{2} J_z + \hbar g \left[a^l J_+ + \left(a^\dagger\right)^l J_- \right], \tag{6.1.1}$$

[1] See also section 2.2.4.

where $l = 1$ for the 1ph case and $l = 2$ for the 2ph one, ω is the frequency of the HO and $l\omega$ the one of the qubits[2], g is the coupling parameter between the HO and the qubits, a and $a^\dagger$ are the usual annihilation and creation operators of a HO, while $J_z = \sum_{i=1}^{N} \sigma_z^{(i)}$ and $J_\pm = \sum_{i=1}^{N} \sigma_\pm^{(i)}$, where σ_z, σ_-, and σ_+ are, respectively, the z-Pauli, the lowering, and the raising operators of a qubit. The ground and the excited energy levels of each qubit are indicated, respectively, by $|g\rangle$ and $|e\rangle$. In Appendix 6.A, we provide an example of a possible implementation with superconducting circuits of the Hamiltonian of Eq. (6.1.1) for the case $l = 2$, by generalizing the study done in Ref. [243] to the case of more than one qubit.

Moreover, we suppose that the HO and each qubit are each in contact with an independent thermal bath at temperature T (equal for all baths) and that a resonant coherent pumping on the HO and an incoherent local pumping on the qubits are available. In the interaction picture, using a phenomenological approach [12, 244, 245], the master equation for the global density matrix ρ_G is

$$\dot{\rho}_G = -ig\left[a^l J_+ + \left(a^\dagger\right)^l J_-, \rho_G\right] + \mathcal{L}_{\mathrm{HO}}(\rho_G) + \mathcal{L}_Q(\rho_G), \tag{6.1.2}$$

where $\mathcal{L}_{\mathrm{HO}}(\bullet)$ and $\mathcal{L}_Q(\bullet)$ are dissipators acting, respectively, on the HO and on the qubits, given by

$$\begin{aligned}
\mathcal{L}_{\mathrm{HO}}(\bullet) &= -i\left[\left(\beta^* a + \beta a^\dagger\right), \bullet\right] + k\left[(1+\bar{n}_{\omega,T})\,\mathcal{D}_a(\bullet) + \bar{n}_{\omega,T}\mathcal{D}_{a^\dagger}(\bullet)\right], \\
\mathcal{L}_Q(\bullet) &= \sum_{i=1}^{N}\left[\gamma_{\mathrm{loc}}(1+\bar{n}_{l\omega,T})\,\mathcal{D}_{\sigma_-^{(i)}}(\bullet) + (\gamma_{\mathrm{loc}}\bar{n}_{l\omega,T} + P)\,\mathcal{D}_{\sigma_+^{(i)}}(\bullet)\right],
\end{aligned} \tag{6.1.3}$$

where $\mathcal{D}_X(\bullet) = X \bullet X^\dagger - \frac{1}{2}\{X^\dagger X, \bullet\}$, k and γ_{loc} are the relaxation rates of, respectively, the HO and each qubit due the local couplings with their own thermal baths (γ_{loc} is assumed to be the same for all the qubits), β characterizes the interaction between the HO and the coherent field, P quantifies the action of the incoherent pumping on each qubit, and $\bar{n}_{\omega,T} = [e^{\hbar\omega/(k_B T)} - 1]^{-1}$, k_B being the Boltzmann constant. Moreover, the coherent pumping is treated in the rotating-wave approximation, being $|\beta| \ll \omega$. The phenomenological approach is justified because we consider the qubits and the HO weakly coupled ($g \ll \omega$) [12], the HO weakly coupled to its bath ($k \ll \omega$) [12], and the external coherent field resonant with the HO [244].

6.2 Adiabatic Elimination

By applying a recently-introduced adiabatic elimination technique [32, 33] we have been able to derive an effective master equation for the reduced density matrix of the qubits, $\rho = \mathrm{Tr}_{\mathrm{HO}}\{\rho_G\}$[3]:

$$\dot{\rho} = -ig\left[\alpha^l J_+ + (\alpha^*)^l J_-, \rho\right] + \mathcal{L}_Q(\rho) + \gamma_l\left[n_l \mathcal{D}_{J_+}(\rho) + (1+n_l)\,\mathcal{D}_{J_-}(\rho)\right], \tag{6.2.1}$$

[2] Because of the two different values of l, the interaction is resonant in both cases.

[3] See section 2.2.4 for a resume of this technique and Appendix 6.B for the detailed derivation

where we recall that $l = 1$ for the 1ph case and $l = 2$ for the 2ph one, and

$$\alpha = -\frac{2i\beta}{k},\ \gamma_1 = \frac{4g^2}{k},\ n_1 = \bar{n}_{\omega,T},\ \gamma_2 = \gamma_1\left(1 + 2n_1 + 4|\alpha|^2\right),\ n_2 = n_1\frac{n_1 + 4|\alpha|^2}{1 + 2n_1 + 4|\alpha|^2}. \tag{6.2.2}$$

As expected, even in the 2ph case the adiabatic elimination gives rise to collective dissipative terms[4]. Notice that, although Eq. (6.2.1) retains its formal structure when changing l, the effective parameters α^l, γ_l, and n_l coming from the adiabatic elimination depend differently in the two models on the physical parameters g, β, k, ω, and T [see Eq. (6.2.2)]. This results in profound physical differences between the 1ph case and the 2ph one, leading to novel effects specific to the 2ph case. In particular, we can identify three main modifications. A first evident difference regards the dependence of the unitary driving term on α, which is linear in the 1ph case and quadratic in the 2ph one. An even more striking difference concerns the collective relaxation rate γ_l which, only in the 2ph case, depends on the parameters characterizing the state of the HO at order zero, n_1 and α[5]. Finally, the coherent pumping increases the temperature of the effective collective bath seen by the qubits, generated by the adiabatic elimination of the HO. In particular, setting $n_2 = \bar{n}_{2\omega,T^*} = [e^{2\hbar\omega/(k_B T^*)} - 1]^{-1}$, the temperature of this collective bath is

$$T^* = \frac{2\hbar\omega}{k_B}\left[\log\left(\frac{e^{2\hbar\omega/(k_B T)} - 2}{1 + 4|\alpha|^2\left(e^{\hbar\omega/(k_B T)} - 1\right)} + 2\right)\right]^{-1}. \tag{6.2.3}$$

Notice that when $\alpha = 0$ the temperature of this collective bath would be the same of the original bath of the HO ($T^* = T$). The peculiar form of γ_2 and n_2, especially their quadratic dependence on $|\alpha|$, can be useful to manipulate the dynamics of the qubits, possibly enhancing their absorption and emission processes.

The equivalence of the master equation mathematical structure for the two models, highlighted by Eq. (6.2.1), can be made explicit. In particular, given the physical parameters in the 2ph model

$$g, \quad \beta, \quad k, \quad \omega, \quad T, \quad P, \quad \gamma_{\rm loc}, \tag{6.2.4}$$

contained in the effective parameters $\alpha,\ n_1, n_2, \bar{n}_{2\omega,T}$, the dynamics to which they give rise can be obtained in the 1ph model by different proper choices of the physical parameters. Denoting with an apex the effective quantities for this "simulation" in the 1ph model we get

$$\frac{g'}{\sqrt{k'}} = \frac{g\sqrt{1 + 2n_1 + 4|\alpha|^2}}{\sqrt{k}}, \qquad n_1' \equiv \bar{n}_{\omega',T'} = n_2, \quad \gamma_{\rm loc}' = \gamma_{\rm loc}\frac{1 + \bar{n}_{2\omega,T}}{1 + n_2},$$
$$\alpha'\sqrt{k'} = \frac{\alpha^2\sqrt{k}}{\sqrt{1 + 2n_1 + 4|\alpha|^2}}, \qquad P' = P - (n_2 - \bar{n}_{2\omega,T})\frac{\gamma_{\rm loc}}{1 + n_2}. \tag{6.2.5}$$

[4]The dissipative terms due to adiabatic elimination are those containing γ_l in Eq. (6.2.1).

[5]Notice that the state of the HO is a thermal coherent state at order zero. See Appendix 6.B.

We remark, however, that this mapping between the two models is a mathematical mapping and that there are situations in which the dynamics obtained in one model is not obtainable in the other one. For example, when the incoherent pumping is absent in the 2ph model, since $n_2 > \bar{n}_{2\omega,T}$ [see Eqs. (6.2.3) and (6.B.30)], in the 1ph model we could need $P' < 0$ to simulate the 2ph model, and this does not correspond to the case of an incoherent pumping term. Indeed, the physical reason for this incompatibility is the temperature-modifying effect of the coherent driving taking place only in the 2ph model [cf. Eq. (6.2.3)].

We finally comment on the validity of the adiabatic elimination approximation which, in our setting, relies on the much higher rate of losses of the HO compared to its exchanges with the qubits and requires stronger conditions than just $g \ll k$. For example, for the 1ph coupling with one qubit, if the HO is in a Fock state with $\tilde{n}$ excitations and the qubit is in the ground state, the "Rabi oscillations" have angular frequency $g\sqrt{\tilde{n}}$, leading to the condition $g\sqrt{\tilde{n}} \ll k$ while, in the 2ph case, the same reasoning leads to $g\sqrt{\tilde{n}(\tilde{n}-1)} \ll k$. In our dynamics and at order zero[6], the HO is in a thermal coherent state with an average number of excitations $\bar{n} = |\alpha|^2 + \bar{n}_{\omega,T}$. Then, we can roughly estimate the validity of the adiabatic elimination by using this value for $\tilde{n}$ in the above conditions. In general, we expect the approximation to not work properly also when $P \gtrsim k$ since in this case the qubits emission would compete with the HO losses.

In the following, we discuss the physical consequences of the differences between the 1ph and 2ph models. In order to check the validity of the adiabatic elimination, we will show in several figures numerical simulations of the full model of Eq. (6.1.2).

6.3 Coherent driving effects: faster dynamics and robust steady-state coherence

In order to focus on the effects due to the coherent pumping on the HO, let us consider the case of zero temperature and no local incoherent pumping on the qubits. For $T = 0$ and $P = 0$, Eq. (6.2.1) simplifies and $\gamma_2 = \gamma_1(1 + 4|\alpha|^2)$. Then, the quadratic dependence of γ_2 on $|\alpha|$ can be exploited to make the system reach much faster its steady state in the 2ph case. This is shown in Fig. 6.1, comparing the dynamics of a one qubit system for the two models.

Turning back to the general case with finite T and P, in the case when system B consists of just one qubit, its dynamics is described by the master equation

$$\dot{\rho} = -ig\left[\alpha^l \sigma_+ + \alpha^{*l}\sigma_-, \rho\right] + \left[\Gamma_l^{(-)}\mathcal{D}_{\sigma_-}(\rho) + \Gamma_l^{(+)}\mathcal{D}_{\sigma_+}(\rho)\right], \tag{6.3.1}$$

where $\Gamma_l^{(-)} = \gamma_{\rm loc}(1 + \bar{n}_{l\omega,T}) + \gamma_l(1 + n_l)$ and $\Gamma_l^{(+)} = \gamma_{\rm loc}\bar{n}_{l\omega,T} + \gamma_l n_l + P$. The density

[6] See Eqs. (6.B.5) and (6.B.6).

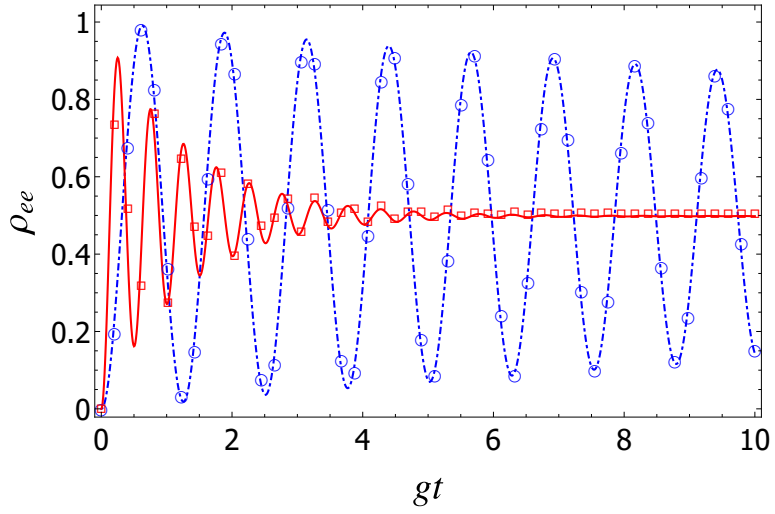

Figure 6.1: Time evolution of the excited state population of one qubit, ρ_{ee}, with physical parameters $\beta = 1.25k$ (so that $|\alpha| = 2.5$), $\gamma_{\rm loc} = 0$, $g = 0.01k$, $T = 0$, and $P = 0$. The dot-dashed blue line and the continuous red line are the curves obtained by using the effective model of Eq. (6.2.1) for, respectively, the 1ph and 2ph models. Empty markers show discrete points obtained from the numerical simulation of the full model of Eq. (6.1.2). These empty markers closely follow the corresponding continuous curve. In the 2ph model the steady state is clearly reached much faster.

matrix elements of the steady state $\rho^{\rm st}$ are found to be[7]

$$\rho_{ee}^{\rm st} = \frac{4g^2|\alpha|^{2l} + \Gamma_l^{(+)}\left(\Gamma_l^{(-)} + \Gamma_l^{(+)}\right)}{8g^2|\alpha|^{2l} + \left(\Gamma_l^{(-)} + \Gamma_l^{(+)}\right)^2}, \quad \rho_{eg}^{\rm st} = \frac{2ig\alpha^l\left(\Gamma_l^{(+)} - \Gamma_l^{(-)}\right)}{8g^2|\alpha|^{2l} + \left(\Gamma_l^{(-)} + \Gamma_l^{(+)}\right)^2}, \tag{6.3.2}$$

being for any ρ, $\rho_{gg} = 1 - \rho_{ee}$ and $\rho_{ge} = \rho_{eg}^*$.

An interesting limit case is obtained when $|\alpha|$ is high enough that every term not containing it can be safely neglected. In the 1ph case, the result of this operation is

$$\rho_{ee}^{\rm st} = \frac{1}{2}, \quad \rho_{eg}^{\rm st} = 0. \tag{6.3.3}$$

In the 2ph case, this limit leads to

$$\Gamma_2^{(-)} \simeq 16(1+n_1)|\alpha|^2 g^2/k, \qquad \Gamma_2^{(+)} \simeq 16 n_1 |\alpha|^2 g^2/k, \tag{6.3.4}$$

so that

$$\rho_{ee}^{\rm st} = \frac{1 + 64 n_1 (1+2n_1)(g/k)^2}{2 + 64(1+2n_1)^2(g/k)^2}, \qquad \rho_{eg}^{\rm st} = e^{i\left(2\phi - \frac{\pi}{2}\right)} \frac{4g/k}{1 + 32(1+2n_1)^2(g/k)^2}, \tag{6.3.5}$$

[7] Hereafter, we use the notation $\langle x|\rho|y\rangle = \rho_{xy}$.

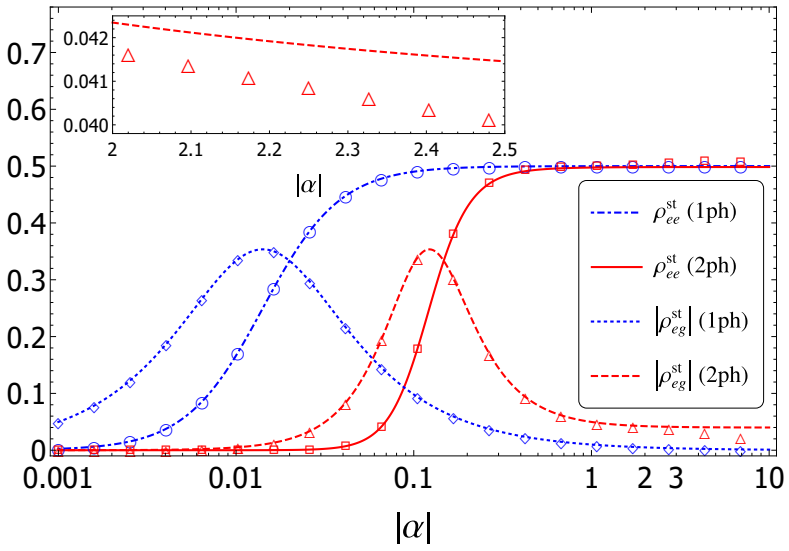

Figure 6.2: Steady state excited populations and coherences of one qubit as functions of $|\alpha|$ with $\gamma_{\rm loc} = 0$, $g = 0.01k$, $T = 0$, and $P = 0$. The various empty markers show discrete points computed with the full model of Eq. (6.1.2). These empty markers closely follow the corresponding continuous curve, even if, as predicted, the error induced by the effective model increases as $|\alpha|$ increases. The inset shows a zoom of the 2ph steady-state coherence for $2 \leq |\alpha| \leq 2.5$. Both the full and the effective model predict a very low variation of the coherence in this range of $|\alpha|$.

where we have used the notation $\alpha = |\alpha| e^{i\phi}$. The case represented in Fig. 6.2 is the zero-temperature and no pumping one[8], for which Eq. (6.3.5) becomes

$$\rho_{ee}^{\rm st} = \frac{1}{2 + 64(g/k)^2}, \quad \rho_{eg}^{\rm st} = e^{i\left(2\phi - \frac{\pi}{2}\right)} \frac{4g/k}{1 + 32(g/k)^2}. \tag{6.3.6}$$

In this case, the maximum of $\left|\rho_{eg}^{\rm st}\right|$ is obtained for $g/k = 1/(4\sqrt{2}) \simeq 0.177$. However, for this value of g/k we are not anymore in the bad-cavity limit.

Fig. 6.2 and Eqs. (6.3.2) and (6.3.5) show that non-diagonal steady states in the bare basis, that is presenting coherences, can be obtained. In particular, for the case analyzed in Fig. 6.2, non negligible coherences are obtained when g is sufficiently high[9]. By comparing the two models, one can see that great differences arise for $|\alpha| \gtrsim 1$. In this regime, indeed, the 2ph interaction allows one to generate steady states in much shorter time, as one can evince from Fig. 6.1, and with higher coherences. Moreover, the steady state does not change much for little variations of α when $|\alpha|$ is high enough. This is

[8] In formulas, $T = 0$ and $P = 0$.

[9] Indeed, g has to be not so high to move the model outside of the validity range of the adiabatic elimination.

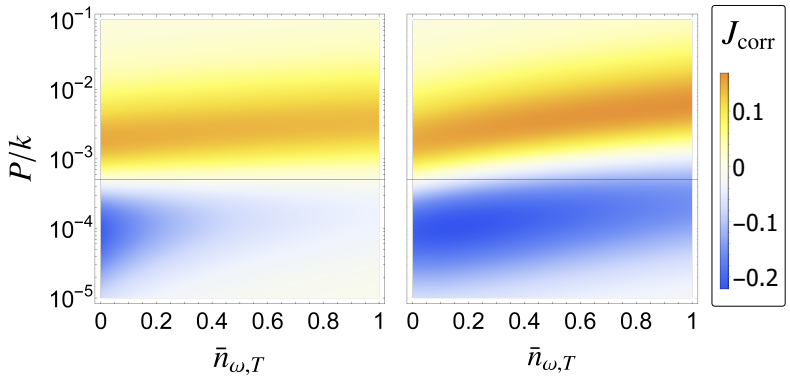

Figure 6.3: $J_{\rm corr}$ of the steady state of two qubits as a function of T ($\bar{n}_{\omega,T}$ in the plot) and P/k in the 1ph and 2ph cases for $g = 0.01k$, $\gamma_{\rm loc} = 10^{-4}k$, and $\alpha = 0$. The horizontal lines correspond to the value $P = P^* \equiv \gamma_{\rm loc} + \gamma_1 = 5 \times 10^{-4}k$, where both models give exactly $J_{\rm corr} = 0$ at zero temperature. The 2ph model exhibits a richer dependence on temperature including stronger subradiance and superradiance at higher temperatures. Note that the extremal values that $J_{\rm corr}$ may assume in the two-qubit case are -1 and 1.

due to the fact that when $\gamma_{\rm loc}$ is negligible, the steady state depends only on the ratio $\gamma_l/(g|\alpha|^l)$, which in the 2ph case does not tend to zero but to $16g/k$ [cf. Eq. (6.3.4)]. For example, when $\gamma_{\rm loc} = 0$ and $g = 0.01k$, the steady state coherences for $2 \leq |\alpha| \leq 2.5$ are very close, as shown in the inset of Fig. 6.2. Therefore, it is possible to rapidly generate non-diagonal steady states resilient to intensity fluctuations of the coherent driving. We stress that the generation of steady-state coherence is relevant since, in general, it is considered as a resource for quantum technologies [246]. In particular, it has been recently shown that non-diagonal steady states can find applications in quantum metrology protocols that can be enhanced by generating these states faster [247, 248].

6.4 Temperature resilience of collective phenomena

Let us now consider the case of no coherent pumping, in order to focus on the emergence of correlations due to the collective dissipative terms. For $\alpha = 0$, in Eq. (6.2.1) the unitary term disappears, $\gamma_2 = \gamma_1(1 + 2n_1)$, and $n_2 = n_1^2/(1 + 2n_1) = 1/[e^{2\hbar\omega/(k_B T)} - 1]$. This particular setting has been used [167, 168] to study the emergence of sub and superradiant steady states as functions of the incoherent pumping parameter P when $T = 0$. The quantity $J_{\rm corr} = \langle J_+ J_- \rangle - \sum_{i=1} \langle \sigma_+^{(i)} \sigma_-^{(i)} \rangle$ is used to characterize these collective phenomena. In particular, $J_{\rm corr} > 0$ indicates the occurrence of superradiance while $J_{\rm corr} < 0$ of subradiance.

Let us start by studying the steady state of two qubits in the case $\alpha = 0$. The

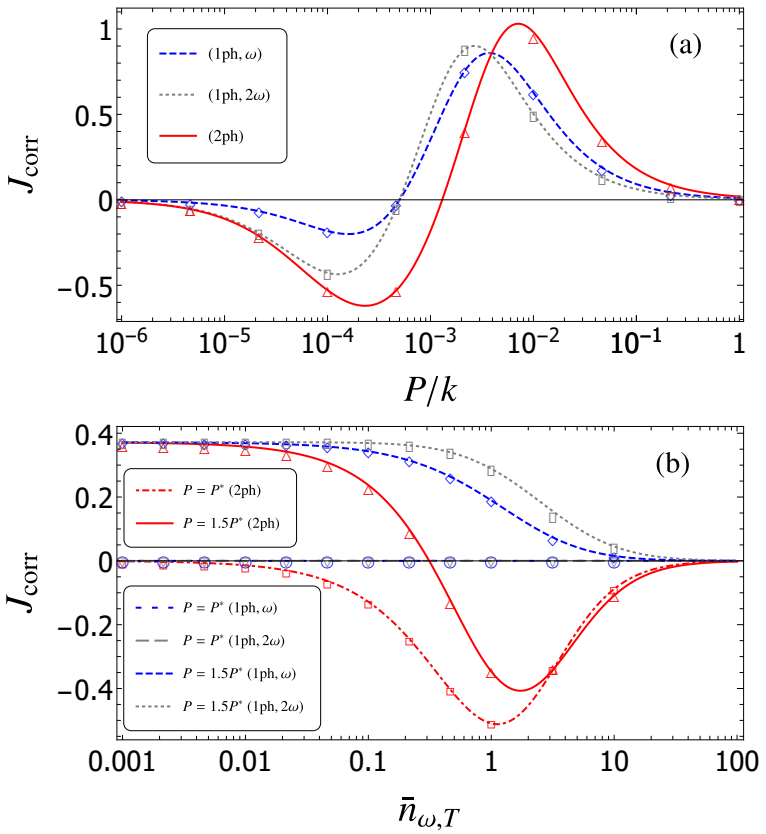

Figure 6.4: (a) $J_{\rm corr}$ of the steady state of four qubits as a function of P, for $g = 0.01k$, $\gamma_{\rm loc} = 10^{-4}k$, T such that $\bar{n}_{\omega,T} = 1$, and $\alpha = 0$. Here, $J_{\rm corr}$ is plotted for the 1ph (for both ω and 2ω) and 2ph cases. (b) Steady $J_{\rm corr}$ of four qubits as a function of T ($\bar{n}_{\omega,T}$ in the plot), for $g = 0.01k$, $\gamma_{\rm loc} = 10^{-4}k$, and $\alpha = 0$, for $P = P^* \equiv \gamma_{\rm loc} + \gamma_1 = 5 \times 10^{-4}k$ and $P = 1.5P^*$ (see legend). The 1ph (ω and 2ω) and 2ph cases are compared. In both plots, $J_{\rm corr}$ is always zero for $P = P^*$ in the 1ph case and the various empty markers indicate discrete points computed with the full model of Eq. (6.1.2), i.e., without performing the adiabatic elimination. These empty markers closely follow the corresponding continuous curve. Note that the extremal values that $J_{\rm corr}$ may assume in the four-qubit case are -2 and 4.

analytical form of $J_{\rm corr}$ is[10]:

$$J_{\rm corr} = \frac{P\gamma_l(1+R_l)(P-\gamma_l-\gamma_{\rm loc})}{(P+\gamma_{\rm loc}R_l)^3 + 3\gamma_l R_l\,(P+\gamma_{\rm loc}R_l)^2 + \gamma_l^2\left[2\gamma_{\rm loc}R_l^3 + P\left(1+R_l+2R_l^2\right)\right]}, \quad (6.4.1)$$

where $R_l = 1+2n_l$. The sign of $J_{\rm corr}$ in Eq. (6.4.1) depends only on $P-\gamma_l-\gamma_{\rm loc}$, which is temperature dependent only in the 2ph case. When $T=0$, there is no difference between the 1ph and the 2ph models because $\gamma_2=\gamma_1$. In contrast, the two models behave very differently for $T\neq 0$, as shown in Fig. 6.3 where we plot the steady value of $J_{\rm corr}$ in the two models as functions of the incoherent pumping and the baths temperature in the case of two qubits, for $g=0.01k$ and $\gamma_{\rm loc}=10^{-4}k$. A more varied dependence of the collective phenomena on temperature in the 2ph case is observed due to the increase of the collective dissipation rate γ_2 with the temperature. In particular, remarkable differences are observed when P is close to $P^*\equiv\gamma_1+\gamma_{\rm loc}$, since for this value of P, in the 1ph case, $J_{\rm corr}=0$ for any T, while this is not the case in the two 2ph case [cf. Eq. (6.4.1)]. This behavior of the sign of $J_{\rm corr}$ has been confirmed in all the other simulations that we have done (up to six qubits). This means that for $P=P^*$, since γ_2 increases with temperature, subradiance is observed for any temperature different from zero in the 2ph case. One could wonder if part of these differences arise just because the qubits in the 2ph model have frequency 2ω so that, for the same temperature, they interact with local baths by means of a lower average excitation number. To check the extent of this effect we have also looked at the same plot using the frequency 2ω for the qubits and the HO for the 1ph case finding only a partial reduction of the differences between the two models. An example of this issue is treated for a specific example in Fig. 6.4.

A different behavior of collective phenomena is still present in the case of a larger number of qubits, as exhibited in Fig. 6.4(a), where the plot of $J_{\rm corr}$ in the steady state as a function of the incoherent pumping for four qubits at a fixed temperature ($\bar{n}_{\omega,T}=1$) clearly shows relevant differences in the two models, especially for the subradiance. In particular, in the 2ph case, a higher peak of both super and subradiance can be reached, even when the frequency of the qubits and of the HO in 1ph case is set equal to 2ω. A more striking different behavior of the two models can be obtained by studying the dependence of the steady value $J_{\rm corr}$ on T for specific values of the pump, as shown in Fig. 6.4(b). For $P=P^*$ no subradiance nor superradiance are visible in the 1ph case, while in the 2ph case a strong subradiance may be observed. An even more interesting case is obtained for $P>P^*$. In this case, the system displays superradiance at $T=0$ in both models while it follows very different paths, depending on the model, when the temperature increases. In the 1ph model, $J_{\rm corr}$ is always positive and tends to zero for increasing temperature whereas, in the 2ph model, there is a temperature T' such that $P<\gamma_2+\gamma_{\rm loc}$ for $T>T'$. Therefore, in the 2ph model, the system can go into a subradiant zone inaccessible through the 1ph interaction at fixed pumping.

[10]The same quantity with $\alpha>0$ can be found analytically. In particular, using MATHEMATICA, we have found the analytical form of the two-qubits steady state. However, since the resulting formula for $J_{\rm corr}$ is very cumbersome we do not report it here.

6.5 Conclusions

In this chapter, we have studied a setup composed of a damped harmonic oscillator (HO) interacting with N qubits via a two-photon coupling in the bad-cavity limit. Moreover, we have considered the presence of finite temperature baths, a coherent pumping on the HO, and an incoherent pumping on the qubits, comparing the two-photon coupling case to the one-photon one. We have successfully applied a novel adiabatic elimination technique in the two-photon model to obtain a reduced master equation governing the qubits collective evolution.

The effective master equation governing the qubits dynamics presents two fundamental differences compared to the dipolar case. The first one consists of an enhancement of the spontaneous-like emission rate, which includes a thermal contribution and a quadratic term in the coherent driving. The second one consists of an increased temperature of the effective bath experienced by the qubits.

We have individuated two main consequences of this novel phenomenology. First, it makes it possible to accelerate the generation of non-diagonal steady states. Second, we can observe a drastic change in the temperature-dependent behavior of quantum collective phenomena, leading to a stronger resilience of these phenomena to high temperatures.

We remark that the models here studied can be feasibly implemented with both atomic and solid-state existing quantum technologies, as discussed in section 2.4.2. In particular, in Appendix 6.A we provide an example of a possible implementation with superconducting circuits of the two-photon coupling Hamiltonian of Eq. (6.1.1) for the case $l = 2$.

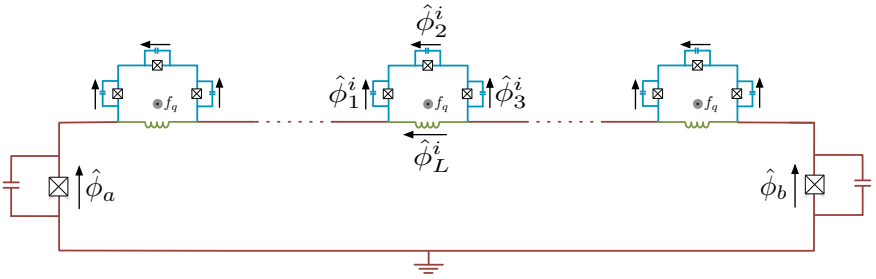

Figure 6.5: (a) Sketch of the circuit QED scheme: a SQUID resonator (brown), coupled through linear inductive elements (green) with flux qubits (cyan). An arbitrary number of flux qubits can in principle be coupled with the SQUID resonator. For the sake of simplicity, the variables $\hat{\phi}_1^i$, $\hat{\phi}_2^i$ and $\hat{\phi}_3^i$, of the elements composing the flux qubits are explicitly shown only for the qubit in the middle.

6.A Circuit model

In this section, we provide a detailed description of a superconducting quantum circuit scheme that can implement the two-photon Jaynes-Cumming Hamiltonian used in Eq. (6.1.1) for $l = 2$. Indeed, in the framework of circuit QED [249] it is possible to engineer artificial atoms that are nonlinearly coupled with a single-mode quantum resonator [185, 243]. We follow the derivation proposed in Ref. [243] for the case of one qubit, generalizing it to the multiqubit case. Our scheme is depicted in Fig. 6.5 and it consists of an arbitrary number of flux qubits [250, 251] coupled to a single superconducting quantum interference device (SQUID) resonator. For each qubit the coupling is realized via an inductance and the values of the coupling inductances are assumed to be the same for all the qubits. The SQUID is used in the linear regime so that, for the considered energy scales, it supports a quantum harmonic resonator mode. However, as shown in the following, the intrinsic nonlinearity of the device can lead to a dynamics governed by a two-photon coupling between the artificial atoms and the resonator. We will first derive an effective Lagrangian model of the circuit, and we will then quantize the corresponding Hamiltonian.

6.A.1 Lagrangian

Our starting point is the Lagrangian of the system [249],

$$\mathcal{L}_{\mathrm{TOT}} = \mathcal{L}_{\mathrm{SQUID}} + \sum_i \left[\mathcal{L}_{\mathrm{FQ}}^i + \mathcal{L}_{\mathrm{L}}^i\right], \tag{6.A.1}$$

where the index i runs over the flux qubits and where the different contributions of the SQUID, the flux qubits (FQ), and the coupling inductances (L) are given by

$$\mathcal{L}_{\mathrm{SQUID}} = \frac{C}{2}\dot{\phi}_a^2 + \frac{C}{2}\dot{\phi}_b^2 + E_J\left[\cos\left(\frac{\phi_a}{\phi_0}\right) + \cos\left(\frac{\phi_b}{\phi_0}\right)\right], \tag{6.A.2}$$

$$\mathcal{L}^i_{\rm FQ} = \frac{\widetilde{C}}{2}\left[(\dot{\phi}^i_1)^2 + (\dot{\phi}^i_3)^2\right] + \frac{\eta\widetilde{C}}{2}(\dot{\phi}^i_2)^2 + \widetilde{E}_J\left[\cos\left(\frac{\phi^i_1}{\phi_0}\right) + \cos\left(\frac{\phi^i_3}{\phi_0}\right) + \eta\cos\left(\frac{\phi^i_2}{\phi_0}\right)\right], \tag{6.A.3}$$

$$\mathcal{L}^i_{\rm L} = -\frac{(\phi^i_L)^2}{2L}. \tag{6.A.4}$$

Here, E_J denotes the Josephson energy and C the capacitance of the Josephson junctions (JJ) a and b composing the SQUID, which are assumed to be identical. As for the flux qubits, $\tilde{E}_J$ and $\tilde{C}$ are the Josephson energy and capacitance of the JJs labeled by 1 and 3, while η is a parameter, smaller than one, used to quantify the corresponding values $\eta\tilde{E}_J$ and $\eta\tilde{C}$ for the second JJ. The coupling inductances between each flux qubit and the SQUID are also assumed to be identical with value L. Finally, all the variables denoted with a ϕ are the generalized fluxes associated to each element of the circuit [249], and we have defined the reduced magnetic flux quantum as $\phi_0 = \Phi_0/(2\pi) = \hbar/(2e)$, where e is the electron charge.

We now define symmetric and anti-symmetric SQUID variables as $\phi_+ = \frac{\phi_a+\phi_b}{2}$ and $\phi_- = \frac{\phi_a-\phi_b}{2}$ and apply the flux-quantization rule [249, 252] to the SQUID loop, obtaining $\phi_a - \phi_b = \sum_i \phi^i_L + \phi^{\rm ext}_s$, where $\phi^{\rm ext}_s$ is the external magnetic flux flowing through the SQUID loop. We can then rewrite the anti-symmetric variable in terms of the phases ϕ^i_L of the coupling inductances obtaining $\phi_- = \sum_i \frac{\phi^i_L}{2} + \frac{\phi^{\rm ext}_s}{2}$. We consider a constant external flux implying $\dot{\phi}^{\rm ext}_s = 0$. Straightforward calculations allow us to rewrite the SQUID Lagrangian as,

$$\mathcal{L}_{\rm SQUID} = C\dot{\phi}^2_+ + \frac{C}{4}(\dot{\phi}^{\rm tot}_L)^2 + 2E_J\cos\left(\frac{\phi^{\rm tot}_L + \phi^{\rm ext}_s}{2\phi_0}\right)\cos\left(\frac{\phi_+}{\phi_0}\right), \tag{6.A.5}$$

where we have defined $\phi^{\rm tot}_L = \sum_i \phi^i_L$. Now, we turn our focus on the circuit elements composing the flux qubits, and we define $\phi^i_p = \frac{\phi^i_1+\phi^i_3}{2}$ and $\phi^i_m = \frac{\phi^i_1-\phi^i_3}{2}$. We denote with $\phi^{\rm ext}_q$ the external flux on each qubit, which is taken to be the same for all flux qubits, and which is defined in the opposite direction with respect to $\phi^{\rm ext}_s$. The flux-quantization rule for the qubit loop, $\phi^i_1 - \phi^i_2 - \phi^i_3 = -\phi^i_L - \phi^{\rm ext}_q$, allows us to eliminate the phase variable of the second junction of each qubit: $\phi^i_2 = 2\phi^i_m + \phi^i_L + \phi^{\rm ext}_q$. We take also the external flux biasing the flux qubit to be constant implying $\dot{\phi}^{\rm ext}_q = 0$, so we can write

$$\begin{aligned}\mathcal{L}^i_{\rm FQ} = {} & \widetilde{C}(\dot{\phi}^i_p)^2 + \widetilde{C}(\dot{\phi}^i_m)^2 + \frac{\eta\widetilde{C}}{2}\left(2\dot{\phi}^i_m + \dot{\phi}^i_L\right)^2 + \\ & \widetilde{E}_J\left[2\cos\left(\frac{\phi^i_p}{\phi_0}\right)\cos\left(\frac{\phi^i_m}{\phi_0}\right) + \eta\cos\left(\frac{2\phi^i_m + \phi^i_L + \phi^{\rm ext}_q}{\phi_0}\right)\right].\end{aligned} \tag{6.A.6}$$

We now take a perturbative approach based on the assumption that the coupling inductances are chosen to be so small that the following approximations are justified. In particular, we perform two main approximations: (1) we linearize the Lagrangian with respect to the coupling-inductance phase variables divided by ϕ_0, that is we expand to first

order in ϕ_L^i/ϕ_0, and then (2) we perform an adiabatic elimination of the corresponding degrees of freedom. Notice that this adiabatic elimination concerns only the detail of the circuit design and it is not related with the adiabatic elimination performed on the quantum model considered in the main text of this chapter. To simplify the notation, let us define the gauge-invariant phase variables $\varphi_j = \phi_j/\phi_0$, where ϕ_j denotes generically the flux variable of any circuit element. We also define the frustration parameters $f_s = \phi_s^{\rm ext}/\phi_0$ and $f_q = \phi_q^{\rm ext}/\phi_0$.

(1) First, we assume that the flux variables ϕ_L^i are small with respect to the reduced magnetic flux quantum, so that Eq.(6.A.5) and Eq.(6.A.6) can be linearized with respect to the variables φ_L^i. Thus, from Eq. (6.A.5) we obtain

$$\mathcal{L}_{\rm SQUID} = C\dot{\phi}_+^2 + \frac{C}{4}\left(\dot{\phi}_L^{\rm tot}\right)^2 + 2E_J\left[\cos\left(\frac{f_s}{2}\right) - \sin\left(\frac{f_s}{2}\right)\frac{\varphi_L^{\rm tot}}{2}\right]\cos\left(\varphi_+\right). \tag{6.A.7}$$

Then, by linearizing Eq.(6.A.6) with respect to each φ_L^i we obtain,

$$\mathcal{L}_{\rm FQ}^i = \mathcal{L}_{\rm qubit}^i + \frac{\eta\widetilde{C}}{2}\left[\left(\dot{\phi}_L^i\right)^2 + 4\dot{\phi}_L^i\dot{\phi}_m^i\right] + \eta\widetilde{E}_J\sin\left(2\varphi_m^i + f_q\right)\varphi_L^i, \tag{6.A.8}$$

where $\mathcal{L}_{\rm qubit}^i$ denotes the standard Lagrangian of the i-th flux qubit [250, 251],

$$\mathcal{L}_{\rm qubit}^i = \widetilde{C}\left(\dot{\phi}_p^i\right)^2 + (1+2\eta)\,\widetilde{C}\left(\dot{\phi}_m^i\right)^2 + \widetilde{E}_J\left[2\cos\left(\varphi_p^i\right)\cos\left(\varphi_m^i\right) + \eta\cos\left(2\varphi_m^i + f_q\right)\right]. \tag{6.A.9}$$

(2) Now, we perform the adiabatic elimination on the degrees of freedom of the coupling inductances. These inductances appear in the following terms of the total Lagrangian [see Eqs. (6.A.4), (6.A.7), and (6.A.8)]:

$$\begin{aligned}\frac{1}{2}\Bigg[\left(\frac{C+2\eta\widetilde{C}}{2}\right)\sum_i\left(\dot{\phi}_L^i\right)^2 - \frac{1}{L}\sum_i\left(\phi_L^i\right)^2 + \frac{C}{2}\sum_{i\neq j}\dot{\phi}_L^i\dot{\phi}_L^j\Bigg] \\ -E_J\sin\left(\frac{f_s}{2}\right)\sum_i\phi_L^i\cos\left(\varphi_+\right) \\ +2\eta\widetilde{C}\sum_i\dot{\phi}_L^i\dot{\phi}_m^i + \eta\widetilde{E}_J\sum_i\varphi_L^i\sin\left(2\varphi_m^i + f_q\right).\end{aligned} \tag{6.A.10}$$

The first line corresponds to N interacting harmonic oscillators. Given the high symmetry of the coefficients, it is easy to find the normal frequencies [253], which are given by

$$\omega_L^- = \sqrt{\frac{1}{L\left(\eta\widetilde{C} + NC/2\right)}}, \qquad \omega_L^+ = \sqrt{\frac{1}{L\eta\widetilde{C}}}, \tag{6.A.11}$$

where the frequency ω_L^+ has degeneracy $N-1$. Here, L is assumed to be so small that the frequency ω_L^- (which is clearly smaller than ω_L^+) is much larger than the relevant characteristic frequencies of the other elements of the circuit. Moreover, the interaction

of the inductances with the other elements of the circuit is such that, if L is small enough, we can adiabatically eliminate the variables corresponding to the inductances by setting $\dot{\phi}_L^i = 0$.

To simplify the notation let us define the following parameters:

$$S = E_J \sin\left(\frac{f_s}{2}\right), \quad \Omega_m^i = -\eta \widetilde{E}_J \sin\left(2\varphi_m^i + f_q\right). \tag{6.A.12}$$

Imposing $\dot{\phi}_L^i = 0$ in the Euler-Lagrange equation

$$\frac{\partial}{\partial \phi_L^i}\mathcal{L}_{\mathrm{TOT}} - \frac{\mathrm{d}}{\mathrm{d}t}\frac{\partial}{\partial \dot{\phi}_L^i}\mathcal{L}_{\mathrm{TOT}} = 0, \tag{6.A.13}$$

we obtain the dependence of ϕ_L^i on the remaining dynamic variables,

$$\varphi_L^i = \frac{\phi_L^i}{\phi_0} = -\frac{1}{2E_L}\left[S\cos(\varphi_+) + \Omega_m^i\right], \tag{6.A.14}$$

where $E_L = \phi_0^2/(2L)$. Therefore,

$$\varphi_L^{\mathrm{tot}} = \frac{1}{\phi_0}\sum_i \phi_L^i = -\frac{1}{2E_L}\left[SN\cos(\varphi_+) + \sum_i \Omega_m^i\right], \tag{6.A.15}$$

where N is the total number of TLSs.

Before replacing the variables, in order to simplify the expressions, we also define

$$K = 2E_J \cos\left(\frac{f_s}{2}\right). \tag{6.A.16}$$

Within the above approximations, the total Lagrangian is then obtained adding Eqs. (6.A.7), (6.A.8) and (6.A.4), and it can be written as,

$$\mathcal{L}_{\mathrm{TOT}} = C\dot{\phi}_+^2 + \left[K - S\varphi_L^{\mathrm{tot}}\right]\cos\left(\varphi_+\right) + \sum_i \left[\mathcal{L}_{\mathrm{qubit}}^i - \Omega_m^i\varphi_L^i - E_L(\varphi_L^i)^2\right].$$

Finally, by replacing φ_L^i and φ_L^{tot} by means of, respectively, Eqs. (6.A.14) and (6.A.15) we obtain,

$$\begin{aligned}\mathcal{L}_{\mathrm{TOT}} = C\dot{\phi}_+^2 + K\cos\left(\varphi_+\right) + \frac{NS^2}{4E_L}\cos^2(\varphi_+) \\ + \frac{S\cos(\varphi_+)}{2E_L}\sum_i \Omega_m^i + \frac{1}{4E_L}\sum_i \left(\Omega_m^i\right)^2 + \sum_i \mathcal{L}_{\mathrm{qubit}}^i.\end{aligned} \tag{6.A.17}$$

6.A.2 Hamiltonian

The system Hamiltonian $\mathcal{H}_{\rm TOT}$ can be derived implementing the Legendre transformation, i.e.,

$$H_{\rm TOT} = \dot{\varphi} p_+ + \sum_j \dot{\varphi}_p^j p_p^j + \sum_j \dot{\varphi}_m^j p_m^j - \mathcal{L}_{\rm TOT}, \tag{6.A.18}$$

where we use the standard definition of conjugate variables

$$\begin{aligned} p_+ &= \partial \mathcal{L}_{\rm TOT}/\partial \dot{\varphi}_+ = 2C\phi_0^2 \dot{\varphi}_+, \\ p_p^j &= \partial \mathcal{L}_{\rm TOT}/\partial \dot{\varphi}_p^j = 2\tilde{C}\phi_0^2 \dot{\varphi}_p^j, \\ p_m^j &= \partial \mathcal{L}_{\rm TOT}/\partial \dot{\varphi}_m^j = 2(1+2\eta)\tilde{C}\phi_0^2 \dot{\varphi}_p^j. \end{aligned} \tag{6.A.19}$$

We replace now the classical variables with quantum operators and we start using the hat formalism to avoid confusion. The total Hamiltonian can be written as

$$\hat{H}_{\rm TOT} = \hat{H}_{\rm SQUID} + \sum_i \hat{H}_{\rm FQ}^i + \hat{H}_I. \tag{6.A.20}$$

The SQUID Hamiltonian is given by

$$\hat{H}_{\rm SQUID} = \frac{\hat{p}_+^2}{4C\phi_0^2} - K\cos(\hat{\varphi}_+) - \frac{NS^2}{4E_L}\cos^2(\hat{\varphi}_+). \tag{6.A.21}$$

The Hamiltonian $\hat{H}_{\rm FQ}^i$ is given by the standard flux qubit Hamiltonian $\hat{H}_{\rm FQ}^{i,\rm st}$, plus a correction proportional to the small parameter L [since $E_L = \phi_0^2/(2L)$],

$$\hat{H}_{\rm FQ}^i = \hat{H}_{\rm FQ}^{i,\rm st} - \frac{(\hat{\Omega}_m^i)^2}{4E_L}, \tag{6.A.22}$$

where

$$\hat{H}_{\rm FQ}^{i,\rm st} = \frac{(\hat{p}_p^i)^2}{4\widetilde{C}\phi_0^2} + \frac{(\hat{p}_m^i)^2}{4\widetilde{C}\phi_0^2(1+2\eta)} - \widetilde{E}_J\left[2\cos\left(\hat{\varphi}_p^i\right)\cos\left(\hat{\varphi}_m^i\right) + \eta\cos\left(2\hat{\varphi}_m^i + f_q\right)\right].$$

It is well known that the standard flux qubit Hamiltonian has a strongly nonlinear eigenspectrum [250, 251]. As a result, for the relevant energy scale, the system dynamics is constrained in the lowest two-level subspace [250, 251]. In the next section we discuss the role of the additional term $-(\hat{\Omega}_m^i)^2/(4E_L)$, and we show that it does not induce state leakage outside the low-energy subspace so that each flux qubit can be considered as a two-level system (TLS). In the following, the two states of the low-energy subspace for the i-th TLS are denoted as $|0\rangle_i$ and $|1\rangle_i$ and the Hamiltonian of each TLS is $\hbar\omega_q\hat{\sigma}_z^i/2$, where ω_q is the common transition frequency of the TLSs and $\hat{\sigma}_z^i$ is the usual z-Pauli operator.

The last term in Eq. (6.A.20) corresponds to the nondipolar coupling Hamiltonian:

$$\hat{H}_I = -\frac{S}{2E_L}\cos(\hat{\varphi}_+)\sum_i \hat{\Omega}_m^i. \tag{6.A.23}$$

We show in the following that, in a broad regime of parameters, such nondipolar coupling can be reduced to a two-photon interaction plus an additional correction to the flux qubit Hamiltonian.

6.A.3 Effective model

We now assume that the phase of the SQUID junctions is small compared to the reduced magnetic flux quantum, $\varphi_+ = \phi_+/\phi_0 \ll 1$. This is a standard approximation [249] which is valid when the SQUID operates in the linear regime, that is in the limit of large Josephson energy for the two Josephson junctions, a and b, of the SQUID. Expanding up to second order the cosines and discarding constant terms in Eq. (6.A.21) we obtain,

$$\hat{H}_{\mathrm{SQUID}} = \frac{\hat{p}_+^2}{4\phi_0^2 C} + \left(K + \frac{NS^2}{2E_L}\right)\frac{\hat{\varphi}_+^2}{2}, \tag{6.A.24}$$

Similarly, we obtain from Eq. (6.A.23)

$$\hat{H}_I = -\frac{S}{2E_L}\sum_i \hat{\Omega}_m^i + \frac{S}{2E_L}\frac{\hat{\varphi}_+^2}{2}\sum_i \hat{\Omega}_m^i, \tag{6.A.25}$$

where the first term is a free energy term of the qubit, while the second term is the origin of the nondipolar coupling.

We now introduce the standard ladder operators $\hat{a}$ and $\hat{a}^\dagger$ of the quantum harmonic oscillator corresponding to the SQUID Hamiltonian of Eq. (6.A.24) in

$$\hat{\varphi}_+ = \sqrt{\frac{\hbar\omega_c L_{\mathrm{eff}}}{2\phi_0^2}}\left(\hat{a}^\dagger + \hat{a}\right), \quad \hat{p}_+ = i\sqrt{\frac{\hbar\phi_0^2}{2\omega_c L_{\mathrm{eff}}}}\left(\hat{a}^\dagger - \hat{a}\right), \tag{6.A.26}$$

where we have defined

$$L_{\mathrm{eff}} = \frac{\phi_0^2}{\left(K + \frac{NS^2}{2E_L}\right)}, \qquad \omega_c = \sqrt{\frac{1}{2CL_{\mathrm{eff}}}} = \frac{1}{\hbar}\sqrt{4E_C\left(K + \frac{NS^2}{2E_L}\right)}, \tag{6.A.27}$$

and where we have introduced the charging energy $E_C = e^2/(2C)$ [we recall that $\phi_0 = \hbar/(2e)$]. Equation (6.A.24) can be then rewritten as

$$\hat{H}_{\mathrm{SQUID}} = \hbar\omega_c \hat{a}^\dagger\hat{a}, \tag{6.A.28}$$

where we have used $[\hat{a}, \hat{a}^\dagger] = 1$ and we have again disregarded constant terms.

Now, we redefine the total free Hamiltonian of a flux qubit as the sum of Eq. (6.A.22) and of the i-th element of the first term in Eq. (6.A.25),

$$\hat{H}_{\mathrm{FQ}}^i = \hat{H}_{\mathrm{FQ}}^{i,\mathrm{st}} - \left[\frac{1}{4E_L}\left(\hat{\Omega}_m^i\right)^2 + \frac{S}{2E_L}\hat{\Omega}_m^i\right], \tag{6.A.29}$$

which corresponds to the standard Hamiltonian of a flux qubit plus two corrections. In the first two energy levels subspace we can write [250, 251]

$$\hat{\Omega}_m^i = -\eta\widetilde{E}_J \langle 0|_i \sin\left(2\hat{\varphi}_m^i + f_q\right)|1\rangle_i \hat{\sigma}_x^i = -\eta\widetilde{E}_J T(f_q)\hat{\sigma}_x^i, \tag{6.A.30}$$

where $\hat{\sigma}_x^i$ is the usual x-Pauli operator and the transition amplitude $T(f_q)$ is the same for all the qubits because we have set a homogeneous f_q and the operator $\hat{\varphi}_m^i$ has the same form for all qubits. Notice that the first correction, proportional to $(\hat{\Omega}_m^i)^2$, corresponds to a constant energy offset, since $(\hat{\Omega}_m^i)^2 \propto \mathbb{I}$ in the two-level subspace, being $\mathbb{I}$ the identity operator in a two-dimensional Hilbert space, and can be then disregarded. The second one, proportional to $\hat{\Omega}_m^i$, can be compensated by a small adjustment of the frustration parameter f_q leading to a renormalization of the qubit-cavity coupling [250, 251]. Therefore, these additional terms do not modify the behavior of the flux qubit, and so the latter can be faithfully modelized as a TLS. In this limit, the Hamiltonian of a flux qubit is then redefined as

$$\hat{H}_{\mathrm{FQ}}^i = \frac{\hbar\omega_q}{2}\hat{\sigma}_z^i. \tag{6.A.31}$$

Finally, we redefine the interaction Hamiltonian as given by only the second term in Eq. (6.A.25), which corresponds to the nondipolar interaction Hamiltonian between the TLSs and the resonator mode,

$$\hat{H}_I = \hbar g_2 \left(\hat{a}^\dagger + \hat{a}\right)^2 \sum_i \hat{\sigma}_x^i, \tag{6.A.32}$$

where we have defined the two-photon coupling strength g_2 as

$$g_2 = \frac{S}{4\hbar E_L}\sqrt{\frac{E_C}{\left(K + \frac{NS^2}{2E_L}\right)}}\eta\widetilde{E}_J T(f_q). \tag{6.A.33}$$

Now, we consider the resonant case by setting $\omega \equiv \omega_c = \omega_q/2$ and we redefine for this case the total system Hamiltonian $\hat{H}_{\mathrm{TOT}}$ up to second order in $\hat{\varphi}_+$ as the sum of Eqs. (6.A.28), (6.A.31), and (6.A.32), obtaining

$$\hat{H}_{\mathrm{TOT}} = \hbar\omega\hat{a}^\dagger\hat{a} + \hbar\omega\hat{J}_z + \hbar g\left(\hat{a} + \hat{a}^\dagger\right)^2\left(\hat{J}_+ + \hat{J}_-\right), \tag{6.A.34}$$

where $g \equiv g_2$, $\hat{J}_z = \sum_i \hat{\sigma}_z^{(i)}$, and $\hat{J}_\pm = \sum_i \hat{\sigma}_\pm^{(i)}$, as in the main text of this chapter, being $\hat{\sigma}_+^{(i)}$ and $\hat{\sigma}_-^{(i)}$ the usual raising and lowering operators for a TLS. Notice that, as shown in Ref. [243], the fourth-order corrections here neglected have a negligible impact on the system dynamics and spectral features.

Going to the interaction picture through the unitary operator $\hat{U}_0 = \exp\left\{-i\hat{H}_0 t/\hbar\right\}$, where $\hat{H}_0 = \hbar\omega\hat{a}^\dagger\hat{a} + \hbar\omega\hat{J}_z$, the interaction Hamiltonian becomes $\hat{H}_{I,\mathrm{int}} = \hat{U}_0^\dagger\hat{H}_I\hat{U}_0$, with

$$\begin{aligned}\hat{H}_{I,\mathrm{int}}/(\hbar g) = &\left(\hat{a}^\dagger\right)^2\hat{J}_- + \hat{a}^2\hat{J}_+ + \\ &+ e^{2i\omega t}\left[\left(2\hat{a}^\dagger\hat{a}+1\right)\hat{J}_+\right] + e^{-2i\omega t}\left[\left(2\hat{a}^\dagger\hat{a}+1\right)\hat{J}_-\right] + \\ &+ e^{4i\omega t}\left(\hat{a}^\dagger\right)^2\hat{J}_+ + e^{-4i\omega t}\hat{a}^2\hat{J}_-.\end{aligned} \tag{6.A.35}$$

For the regime of the parameters we explore in the main text of this chapter (where $g \ll \omega$), the ubiquitous rotating-wave approximation (RWA) can be applied to Eq. (6.A.34) and

Qubit parameters			
$\tilde{E}_J/h = 200$ GHz	$\tilde{E}_C/h = \tilde{E}_J/(80h) = 2.5$ GHz	$\eta = 0.8$	$f_q/(2\pi) = 0.485$
Resonator and inductances parameters			
$E_J/h = 13$ GHz	$E_C/h = 1$ GHz	$E_L/h = 2.5 \times 10^4$ GHz	$f_s/(2\pi) = 0.1$
Resulting parameters			
$\omega_c/(2\pi) \approx 10$ GHz	$\omega_q/(2\pi) \approx 20$ GHz	$g_2 \approx 10^{-4}\omega_c$	$\omega_L^-/(2\pi) \approx 415$ GHz

Table 6.1: This table reports an example of circuit parameters able to implement the two-photon coupling model of the main text of this chapter in the case of four TLSs, i.e., for $N = 4$ [we have defined $\tilde{E}_C = e^2/(2\tilde{C})$]. The resulting parameters are also reported. Notice the use of the non-reduced Planck's constant h for quantifying energies. The parameters chosen for the flux qubit have been taken from an example of Ref. [250] on the basis of the standard flux qubit Hamiltonian $\hat{H}_{\rm FQ}^{i,\rm st}$. Notice that, because of the two additional terms in Eq. (6.A.29) with respect to $\hat{H}_{\rm FQ}^{i,\rm st}$, the parameter values should be slightly calibrated in a real experimental realization in order to obtain the resonance $\omega_q = 2\omega_c$. Regarding the number $T(f_q)$ which appears in the formula for g_2 of Eq. (6.A.33), we have used $T(f_q) = 0.8$. This value has been calculated for similar circuit parameters in the code used for Ref. [243]. We remark that, to implement our model, only the order of magnitude of g_2 is important, not its exact value.

(6.A.35), neglecting all the terms oscillating in the interaction picture. We can thus redefine the total Hamiltonian as the two-photon Jaynes-Cumming Hamiltonian used in Eq. (6.1.1) for $l = 2$ (we remark that in the main text of this chapter and in the following sections of the Appendices of this chapter the operators are not anymore marked by the "hat"):

$$\hat{H}_{\rm TOT} = \hbar\omega\hat{a}^\dagger\hat{a} + \hbar\omega\hat{J}_z + \hbar g\left[\hat{a}^2\hat{J}_+ + \left(\hat{a}^\dagger\right)^2\hat{J}_-\right]. \tag{6.A.36}$$

An analysis of the RWA in an analogous context can be found in [187].

To conclude this section, let us provide an example of a set of physical parameters that matches the required regime. We consider a system composed of 4 TLSs, as in the case of Fig. 6.4. Notice that all model parameters can be analytically derived, except for the flux qubit frequency which has been taken by an example of Ref. [250], where the same values for the flux qubit circuit parameters have been used. The values of the various parameters are summarized in Table 6.1, which has been constructed as follows. First, we have taken the flux qubit circuit parameters from Ref. [250], where the resulting frequency of the flux qubit is also given, $\omega_q/(2\pi) \approx 20$ GHz. Then, we have searched for a configuration of the resonator and inductances parameters (E_J, E_C, E_L, and f_s) giving us leading to $\omega_c/(2\pi) \approx 10$ GHz for the harmonic oscillator, well within

the working range of circuit QED devices [249]. For the number $T(f_q)$ appearing in the expression for g_2 of Eq. (6.A.33), we have used the value $T(f_q) = 0.8$, which has been calculated for similar circuit parameters in the code used for Ref. [243]. Regarding the inductances, from Eq. (6.A.14) one can estimate by excess the expectation value of the operator associated to the variable φ_L^i finding in modulus ≈ 0.0026, which is consistent with the linearization procedure we have performed with respect to the variables φ_L^i. Morevoer, this choice of the circuit parameters leads to a value of the lowest inductances characteristic frequency ω_L^- well above the relevant energy scale, being ω_L^- more than 20 times larger than the flux qubits frequency [11]. It follows that the adiabatic elimination we have made concerning the variables ϕ_L^i, $\dot{\phi}_L^i = 0$, is well justified. Finally, we have $g_2 \approx 10^{-4}\omega_c$, that is $g_2 \approx 0.01k$ (this is the value considered in all the figures of the main text of this chapter) if we take $k = 0.01\omega_c$, where k is the dissipation rate of the harmonic oscillator due to the interaction with its environment.

Concerning the flux qubits, the parameters are taken from Ref. [250] on the basis of the standard flux qubit Hamiltonian $\hat{H}_{\rm FQ}^{i,\rm st}$, i.e., the Hamiltonian of Eq. (6.A.29) without the two additional terms. It follows that the parameter values should be slightly calibrated in a real experimental realization in order to obtain the resonance $\omega_q = 2\omega_c$. However, the engineering of flux qubit is a well-developed area of research and their effective frequency can be finely tuned in various ways, also adding additional elements to the circuit [249]. Even if the values of Table 6.1 do not exactly match those that would be used for our circuit, are a good indicator of the experimental values that would be in fact necessary, especially considering that $g_2 \ll \omega_c, \omega_q$ so that the interaction does not sensibly modify the frequency of the flux qubits.

We stress out that the values used in Table 6.1 are commonly implemented in nowadays experiments [249] and that the proposed circuit design does not require any further improvement over standard circuit-QED technology.

6.B Adiabatic elimination of the harmonic oscillator

Here, we apply the general method described in section 2.2.4 to the one-photon (1ph) and the two-photon (2ph) models considered in section 6.1. In particular, the starting point for this application is Eq. (6.1.2), which describes the global dynamics of the two models and is given in the interaction picture. In the Schrödinger picture, the models are described by the equation

$$\dot{\rho}_{G,S} = -\frac{i}{\hbar}[H_l, \rho_{G,S}] + \mathcal{L}_{\rm HO,S}(\rho_{G,S}) + \mathcal{L}_{Q,S}(\rho_{G,S}), \tag{6.B.1}$$

[11] For convenience of the reader, we report in this note the formulas for the inductances normal frequencies in terms of the energetic circuit parameters:

$$\omega_L^- = \frac{4\sqrt{2}}{\hbar}\sqrt{\frac{E_C\tilde{E}_C E_L}{N\tilde{E}_C + 2\eta E_C}}, \quad \omega_L^+ = \frac{4}{\hbar}\sqrt{\frac{\tilde{E}_C E_L}{\eta}}.$$

These formulas are equivalent to those of Eq. (6.A.11).

where $\rho_{G,S}$ is the global density matrix in the Schrödinger picture, $l = 1$ for the 1ph case and $l = 2$ for the 2ph one, H_l is given in Eq. (6.1.1), and

$$\begin{aligned}\mathcal{L}_{\mathrm{HO},S}(\bullet) &= -i\left[\left(\beta^* a e^{i\omega t} + \beta a^\dagger e^{-i\omega t}\right), \bullet\right] + k\left[\left(1+\bar{n}_{\omega,T}\right)\mathcal{D}_a(\bullet) + \bar{n}_{\omega,T}\mathcal{D}_{a^\dagger}(\bullet)\right], \\ \mathcal{L}_{Q,S}(\bullet) &= \sum_{i=1}^{N}\left[\gamma_{\mathrm{loc}}\left(1+\bar{n}_{l\omega,T}\right)\mathcal{D}_{\sigma_-^{(i)}}(\bullet) + \left(\gamma_{\mathrm{loc}}\bar{n}_{l\omega,T} + P\right)\mathcal{D}_{\sigma_+^{(i)}}(\bullet)\right]. \end{aligned} \tag{6.B.2}$$

The passage from the Schrödinger picture to the interaction one is, indeed, necessary to apply the adiabatic elimination method since the bare dynamics of both the qubits and the harmonic oscillator (HO) is much faster than all other dynamics so that to separate the system into a fast and a slow part is not possible. Moreover, neglecting the interaction between the two subsystems, the steady state of the HO does not exist because of the time dependent part in the Hamiltonian describing the action of the coherent driving. The unitary operator used to move from the Schrödinger picture to the interaction one [i.e., from Eq. (6.B.1) to Eq. (6.1.2)] is

$$U_l(t) = e^{\frac{i}{\hbar}H_{0,l}t}, \tag{6.B.3}$$

where

$$H_{0,l} = \hbar\omega a^\dagger a + \frac{l\hbar\omega}{2}J_z. \tag{6.B.4}$$

In this section, we denote the reduced density matrix of the HO with ρ_A in order to maintain the notation of section 2.2.4, while we call the reduced density matrix of the qubits ρ, without suffixes, in order to have the same notation of section 6.2.

As explained in section 2.2.4, we first need to obtain the steady state of the HO when it does not interact with the qubits. This steady state is equal to [33]

$$\rho_A^{\mathrm{st}} = D(\alpha)\rho_A^{\mathrm{th}}D(-\alpha), \tag{6.B.5}$$

where $D(\alpha) = e^{\alpha a^\dagger - \alpha^* a}$, $\alpha = -\frac{2i\beta}{k}$, and

$$\rho_A^{\mathrm{th}} = \frac{1}{1+\bar{n}_{\omega,T}}\sum_{n=0}^{\infty}\left(\frac{\bar{n}_{\omega,T}}{1+\bar{n}_{\omega,T}}\right)^n |n\rangle\langle n|. \tag{6.B.6}$$

In other words, ρ_A^{st} is a thermal coherent state obtained by applying to the thermal state with energy $\hbar\omega\bar{n}_{\omega,T}$ the displacement operator corresponding to the coherent state in which the HO would be at zero temperature.

We choose to use as perturbative parameter ϵ the quantity g/k so that $\epsilon = g/k$. With this choice, we can write

$$H_{\mathrm{int}} = \hbar k\left[a^l J_+ + \left(a^\dagger\right)^l J_-\right], \tag{6.B.7}$$

where $c = k$ [cf. Eq. (2.2.18)]. Moreover, $\mathcal{L}_Q = \epsilon\mathcal{L}_B$. Therefore, at first order in g/k we get[12]

$$\epsilon\mathcal{L}_{S,1}(\rho) = -ig\left[\alpha^l J_+ + (\alpha^*)^l J_-, \rho\right] + \mathcal{L}_Q(\rho), \tag{6.B.8}$$

[12] See Eq. (2.2.22) with $A_1 = a^l$, $A_2 = \left(a^\dagger\right)^l$, $B_1^\dagger = J_+$, and $B_2^\dagger = J_-$.

since, using $aD(\alpha) = \alpha D(\alpha) + D(\alpha)a$,

$$\begin{aligned}
\mathrm{Tr}\left\{a^l \rho_A^{\mathrm{st}}\right\} &= \mathrm{Tr}\left\{\alpha a^{l-1}\rho_A^{\mathrm{st}} + D(\alpha)a\rho_A^{\mathrm{th}}D(-\alpha)\right\} \\
&= \mathrm{Tr}\left\{\alpha a^{l-1}\rho_A^{\mathrm{st}}\right\} + \mathrm{Tr}\left\{a\rho_A^{\mathrm{th}}\right\} \\
&= \mathrm{Tr}\left\{\alpha^2 a^{l-2}\rho_A^{\mathrm{st}}\right\} + \alpha\,\mathrm{Tr}\left\{a\rho_A^{\mathrm{th}}\right\} \\
&= \vdots \\
&= \alpha^l, \\
\mathrm{Tr}\left\{\left(a^\dagger\right)^l \rho_A^{\mathrm{st}}\right\} &= \left(\mathrm{Tr}\left\{a^l\rho_A^{\mathrm{st}}\right\}\right)^* = (\alpha^*)^l\,.
\end{aligned} \tag{6.B.9}$$

To obtain the second order dynamics we need the super-operators F_k. In this case, there are only two of them:

$$F_1\left(\rho_A^{\mathrm{st}}\right) = \int_0^\infty e^{t\mathcal{L}_A}\left[\left(a^l - \alpha^l\right)\rho_A^{\mathrm{st}}\right]\mathrm{d}t\,, \quad F_2\left(\rho_A^{\mathrm{st}}\right) = \int_0^\infty e^{t\mathcal{L}_A}\left[\left(\left(a^\dagger\right)^l - (\alpha^*)^l\right)\rho_A^{\mathrm{st}}\right]\mathrm{d}t\,. \tag{6.B.10}$$

In order to calculate the matrix elements $X_{i,j}$ and $Y_{i,j}$ of Eq. (2.2.25) we just need to compute terms like $\mathrm{Tr}\left\{F_1\rho_A^{\mathrm{st}}\left(a^\dagger\right)^l\right\}$ so that finding the explicit form of the operators F_k is not necessary. Since $\mathrm{Tr}\left\{F_i\left(\rho_A^{\mathrm{st}}\right)\right\} = 0$, one can, for example, write

$$\begin{aligned}
\mathrm{Tr}\left\{F_1\rho_A^{\mathrm{st}}\left(a^\dagger\right)^l\right\} &= \mathrm{Tr}\left\{\left(a^\dagger\right)^l\int_0^\infty e^{t\mathcal{L}_A}\left[(a^l-\alpha^l)\rho_A^{\mathrm{st}}\right]\mathrm{d}t\right\} \\
&= \mathrm{Tr}\left\{\left[\left(a^\dagger\right)^l - (\alpha^*)^l\right]\int_0^\infty e^{t\mathcal{L}_A}\left[(a^l-\alpha^l)\rho_A^{\mathrm{st}}\right]\mathrm{d}t\right\} \\
&= \mathrm{Tr}\left\{\left[(a^l-\alpha^l)\rho_A^{\mathrm{st}}\right]\int_0^\infty e^{t\mathcal{L}_A^\dagger}\left[\left(a^\dagger\right)^l - (\alpha^*)^l\right]\mathrm{d}t\right\},
\end{aligned} \tag{6.B.11}$$

where $\mathcal{L}_A^\dagger$ is the adjoint Lindblad operator [12, 33][13]. In the same way, one obtains the following quantities

$$\begin{aligned}
\mathrm{Tr}\left\{F_1\rho_A^{\mathrm{st}}\left(a^\dagger\right)^l\right\} &= \mathrm{Tr}\left\{\left[(a^l-\alpha^l)\rho_A^{\mathrm{st}}\right]\int_0^\infty e^{t\mathcal{L}_A^\dagger}\left[\left(a^\dagger\right)^l - (\alpha^*)^l\right]\mathrm{d}t\right\}, \\
\mathrm{Tr}\left\{F_1\rho_A^{\mathrm{st}}a^l\right\} &= \mathrm{Tr}\left\{\left[(a^l-\alpha^l)\rho_A^{\mathrm{st}}\right]\int_0^\infty e^{t\mathcal{L}_A^\dagger}\left(a^l-\alpha^l\right)\mathrm{d}t\right\}, \\
\mathrm{Tr}\left\{F_2\rho_A^{\mathrm{st}}\left(a^\dagger\right)^l\right\} &= \mathrm{Tr}\left\{\left[\left(\left(a^\dagger\right)^l - (\alpha^*)^l\right)\rho_A^{\mathrm{st}}\right]\int_0^\infty e^{t\mathcal{L}_A^\dagger}\left[\left(a^\dagger\right)^l - (\alpha^*)^l\right]\mathrm{d}t\right\}, \\
\mathrm{Tr}\left\{F_2\rho_A^{\mathrm{st}}a^l\right\} &= \mathrm{Tr}\left\{\left[\left(\left(a^\dagger\right)^l - (\alpha^*)^l\right)\rho_A^{\mathrm{st}}\right]\int_0^\infty e^{t\mathcal{L}_A^\dagger}\left(a^l-\alpha^l\right)\mathrm{d}t\right\}.
\end{aligned} \tag{6.B.12}$$

The above formulas (and the resulting master equation) are valid for any l but, from now on, we will deal explicitly with the $l = 1, 2$ cases because otherwise calculations

[13] See also Eq. (2.2.8).

become needlessly cumbersome. The result obtained in the case $l = 1$ is already known in literature [33]. Nevertheless, we think that reporting here its derivation with this method can be helpful.

6.B.1 The 1ph case

For $l = 1$ it is possible to write $e^{t\mathcal{L}_A^\dagger} a = f_0(t) + f_1(t)a$, with $f_0(0) = 0$ and $f_1(0) = 1$. The adjoint master equation for the operator $e^{t\mathcal{L}_A^\dagger} a$ reads [12, 33]

$$\frac{\mathrm{d}}{\mathrm{d}t} f_0(t) + \frac{\mathrm{d}}{\mathrm{d}t} f_1(t) a = -\frac{k}{2} f_1(t) a + \alpha \frac{k}{2} f_1(t), \tag{6.B.13}$$

whose solution, $f_0(t) = \alpha \left(1 - e^{-\frac{k}{2}t}\right)$ and $f_1(t) = e^{-\frac{k}{2}t}$, implies

$$e^{t\mathcal{L}_A^\dagger} (a - \alpha) = e^{-\frac{k}{2}t} (a - \alpha) . \tag{6.B.14}$$

We recall that $e^{t\mathcal{L}_A^\dagger} r = r$, where r is a constant. Analogously, we can write $e^{t\mathcal{L}_A^\dagger} a^\dagger = \tilde{f}_0(t) + \tilde{f}_1(t) a^\dagger$ and solve the associated differential equations. The solutions are equal to the ones for $f_0(t)$ and $f_1(t)$ with the substitution $\alpha \to \alpha^*$. It follows that

$$e^{t\mathcal{L}_A^\dagger} \left(a^\dagger - \alpha^*\right) = e^{-\frac{k}{2}t} \left(a^\dagger - \alpha^*\right) . \tag{6.B.15}$$

Now, we can calculate the elements of the X and Y matrices. Using Eqs. (6.B.14) and (6.B.15) in Eq. (6.B.12), we obtain for $l = 1$ (hereafter $n_1 = \bar{n}_{\omega,T} = [e^{\hbar\omega/(k_B T)} - 1]^{-1}$)

$$\mathrm{Tr}\left\{F_1 \rho_A^{\mathrm{st}} a^\dagger\right\} = \frac{2}{k} n_1, \ \mathrm{Tr}\left\{F_1 \rho_A^{\mathrm{st}} a\right\} = 0, \ \mathrm{Tr}\left\{F_2 \rho_A^{\mathrm{st}} a^\dagger\right\} = 0, \ \mathrm{Tr}\left\{F_2 \rho_A^{\mathrm{st}} a\right\} = \frac{2}{k} (1 + n_1) . \tag{6.B.16}$$

By inserting Eq. (6.B.16) in Eq. (2.2.25), we then have

$$X = 4k \begin{pmatrix} n_1 & 0 \\ 0 & 1 + n_1 \end{pmatrix}, \quad Y = \begin{pmatrix} 0 & 0 \\ 0 & 0 \end{pmatrix}. \tag{6.B.17}$$

We can set $\Lambda = \sqrt{X}$ thus obtaining in Eq. (2.2.27):

$$L_1 = \Lambda_{1,1}^* J_+ + \Lambda_{2,1}^* J_- = \sqrt{4kn_1} J_+, \quad L_2 = \Lambda_{1,2}^* J_+ + \Lambda_{2,2}^* J_- = \sqrt{4k\,(1 + n_1)} J_- . \tag{6.B.18}$$

Eventually, using Eqs. (2.2.26) and (6.B.8), we obtain as equation for the second order dynamics of the qubits

$$\dot{\rho} = -ig[\alpha J_+ + \alpha^* J_-, \rho] + \mathcal{L}_Q(\rho) + \gamma_1 \left[n_1 \mathcal{D}_{J_+}(\rho) + (1 + n_1)\, \mathcal{D}_{J_-}(\rho)\right] , \tag{6.B.19}$$

where $\gamma_1 = 4g^2/k$.

6.B.2 The 2ph case

The derivation of the reduced dynamics for $l = 2$ proceeds analogously to the $l = 1$ case, but it is more involved. We can write $e^{t\mathcal{L}_A^\dagger} a^2 = h_0(t) + h_1(t)a + h_2(t)a^2$, with $h_0(0) = h_1(0) = 0$ and $h_2(0) = 1$. The adjoint master equation for the operator $e^{t\mathcal{L}_A^\dagger} a^2$ reads

$$\frac{\mathrm{d}}{\mathrm{d}t}h_0(t) + \frac{\mathrm{d}}{\mathrm{d}t}h_1(t)a + \frac{\mathrm{d}}{\mathrm{d}t}h_2(t)a^2 = \frac{\alpha k}{2}h_1(t) + \left[\alpha k h_2(t) - \frac{k}{2}h_1(t)\right] a - k h_2(t) a^2, \quad \text{(6.B.20)}$$

whose solution, $h_0(t) = \alpha^2 e^{-kt}\left(e^{\frac{k}{2}t} - 1\right)^2$, $h_1(t) = 2\alpha e^{-kt}\left(e^{\frac{k}{2}t} - 1\right)$, and $h_2(t) = e^{-kt}$, implies

$$e^{t\mathcal{L}_A^\dagger}\left(a^2 - \alpha^2\right) = e^{-kt}\left(a - \alpha\right)^2 + e^{-\frac{k}{2}t}\left[2\alpha\left(a - \alpha\right)\right]. \quad \text{(6.B.21)}$$

Analogously, we can write $e^{t\mathcal{L}_A^\dagger}(a^\dagger)^2 = \tilde{h}_0(t) + \tilde{h}_1(t)a^\dagger + \tilde{h}_2(t)(a^\dagger)^2$ and solve the associated differential equations. The solutions are equal to the ones for $h_0(t)$, $h_1(t)$, and $h_2(t)$ with the substitution $\alpha \to \alpha^*$:

$$e^{t\mathcal{L}_A^\dagger}\left[\left(a^\dagger\right)^2 - (\alpha^*)^2\right] = e^{-kt}\left(a^\dagger - \alpha^*\right)^2 + e^{-\frac{k}{2}t}\left[2\alpha^*\left(a^\dagger - \alpha^*\right)\right]. \quad \text{(6.B.22)}$$

Now, we can calculate the elements of the X and Y matrices. After straightforward but lengthy calculations, using Eqs. (6.B.21) and (6.B.22) in Eq. (6.B.12) and the following equalities

$$\begin{aligned}
D(-\alpha)(a - \alpha) &= aD(-\alpha), & D(-\alpha)(a^\dagger - \alpha^*) &= a^\dagger D(-\alpha),\\
\left(a^2 - \alpha^2\right) D(\alpha) &= D(\alpha)\left(a + 2\alpha\right) a, & \left[\left(a^\dagger\right)^2 - (\alpha^*)^2\right] D(\alpha) &= D(\alpha)\left(a^\dagger + 2\alpha^*\right) a^\dagger,\\
\mathrm{Tr}\left\{\left(a^\dagger\right)^2 a^2 \rho_A^{\mathrm{th}}\right\} &= 2(n_1)^2, & \mathrm{Tr}\left\{a^2\left(a^\dagger\right)^2 \rho_A^{\mathrm{th}}\right\} &= 2(1 + n_1)^2, \quad \text{(6.B.23)}
\end{aligned}$$

we obtain, for $l = 2$,

$$\begin{aligned}
\mathrm{Tr}\left\{F_1 \rho_A^{\mathrm{st}}\left(a^\dagger\right)^2\right\} &= \frac{2}{k}\left[(n_1)^2 + 4|\alpha|^2 n_1\right], \quad \mathrm{Tr}\left\{F_1 \rho_A^{\mathrm{st}} a^2\right\} = \mathrm{Tr}\left\{F_2 \rho_A^{\mathrm{st}}\left(a^\dagger\right)^2\right\} = 0,\\
\mathrm{Tr}\left\{F_2 \rho_A^{\mathrm{st}} a^2\right\} &= \frac{2}{k}\left[(1 + n_1)^2 + 4|\alpha|^2\left(1 + n_1\right)\right]. \quad \text{(6.B.24)}
\end{aligned}$$

Then, the X and Y matrices are easily obtained by inserting Eq. (6.B.24) in Eq. (2.2.25):

$$X = 4k\begin{pmatrix} (n_1)^2 + 4|\alpha|^2 n_1 & 0 \\ 0 & (1 + n_1)^2 + 4|\alpha|^2\left(1 + n_1\right) \end{pmatrix}, \quad Y = \begin{pmatrix} 0 & 0 \\ 0 & 0 \end{pmatrix}. \quad \text{(6.B.25)}$$

Eventually, using Eq. (2.2.26) and setting $\Lambda = \sqrt{X}$ as in the 1ph case, the second order dynamics of the qubits reads

$$\begin{aligned}
\dot{\rho} = &-ig\left[\alpha^2 J_+ + (\alpha^*)^2 J_-, \rho\right] + \mathcal{L}_Q(\rho)\\
&+ \gamma_1\left[\left(4|\alpha|^2 n_1 + (n_1)^2\right)\mathcal{D}_{J_+}(\rho) + \left(4|\alpha|^2\left(1 + n_1\right) + (1 + n_1)^2\right)\mathcal{D}_{J_-}(\rho)\right]. \quad \text{(6.B.26)}
\end{aligned}$$

The above equation can be rewritten by operating the following substitutions

$$\begin{aligned}\gamma_1\left[4|\alpha|^2 n_1+(n_1)^2\right]&\to\gamma_2 n_2\\ \gamma_1\left[4|\alpha|^2(1+n_1)+(1+n_1)^2\right]&\to\gamma_2(1+n_2),\end{aligned}\tag{6.B.27}$$

where

$$n_2=n_1\frac{n_1+4|\alpha|^2}{1+2n_1+4|\alpha|^2},\qquad \gamma_2=\gamma_1\left(1+2n_1+4|\alpha|^2\right).\tag{6.B.28}$$

In this way, the 2ph model reduced master equation becomes

$$\dot\rho=-ig\left[\alpha^2 J_+ +(\alpha^*)^2 J_-,\rho\right]+\mathcal{L}_Q(\rho)+\gamma_2\left[n_2\mathcal{D}_{J_+}+(1+n_2)\mathcal{D}_{J_-}\right]\rho.\tag{6.B.29}$$

Notice that the quantity n_2 can also be written as

$$n_2=\bar n_{2\omega,T}+\frac{4n_1|\alpha|^2}{1+2n_1+4|\alpha|^2}\frac{1+n_1}{1+2n_1},\tag{6.B.30}$$

which is another way to display what is shown in Eq. (6.2.3), i.e., the fact that the effective temperature of the collective bath as seen by the qubits is higher than the actual temperature T due to the action of the external coherent field on the harmonic oscillator.

Chapter 7

Minimum energy entangled states

As detailed in section 2.1, many quantum information processes rely on entanglement. Their energetic efficiency can be improved by studying the connection between entanglement and energy. In addition to the potential application, a connection between these two quantities can be of interest in itself.

In this chapter, we investigate for an arbitrary finite bipartite system the connection between local energy and entanglement in the case of discrete local Hamiltonians. Firstly, for any given amount of entanglement, we look for the range of possible values for the local energy and search for quantum states that reach, respectively, the lower and the upper bounds on the local energy and we denote them, respectively, by *minimum energy entangled states* (MEES) and *maximum energy entangled states* (MaxEESs). The search for these extremal states[1] is first conducted for pure states and, then, the obtained results are extended to mixed states. Secondly, we point out the formal connection between MEESs and MaxEESs and thermal states, we show how MEESs naturally appear as ground states of some many-body systems and that both MEESs and MaxEESs are LOCC-connected. Then, we present various proposals to generate MEESs efficiently, through unitary or dissipative dynamics. Indeed, MEESs are the cheapest states to generate unitarily but we also show that the energetic cost generation of MEESs is practically the minimum one for all classes of dissipative dynamics we study. Finally, we show how the utilization of MEESs in some quantum information protocols can decrease their energetic cost.

The chapter is organized as follows. Firstly, in section 7.1 we find the form of MEESs and MaxEESs. Secondly, in section 7.2 we show that they are extremal states even when considering mixed states. We do this by using some general properties of entanglement quantifiers for mixed states. Thirdly, section 7.3 explores the connection of these entangled states with thermodynamics, many-body physics, and LOCC transformations. Then, in section 7.4, unitary transformation approaches to the generation of MEESs are discussed

[1] Both MEESs and MaxEESs.

while, in section 7.5, different approaches based on zero-temperature thermalization processes are explored. In section 7.6 we present a detailed comparison of the various methods based on zero-temperature thermalization focusing on a 3×4 system. Finally, in section 7.7 we provide examples of how MEESs can be used to decrease the energetic cost of some quantum information protocols and, in section 7.8, we give some conclusive remarks. We provide details of our analysis and explicit calculations in several Appendices.

7.1 Pure states saturating entanglement energy bounds

7.1.1 Definition of the problem

We consider a bipartite system A-B composed of two arbitrary quantum systems A and B, with local Hamiltonian $H = H_A + H_B$, where N_A and N_B are the dimensions of, respectively, H_A and H_B, being $N_A \leq N_B$. H_A and H_B can be written as

$$H_X = \sum_{n=0}^{N_X-1} X_n \left|X_n\right\rangle\!\left\langle X_n\right|, \quad X = A, B, \tag{7.1.1}$$

where $X_0 \leq X_1 \leq \cdots \leq X_{N_X-1}$. The above local Hamiltonian H suitably describes systems at the start and at the end of most quantum protocols, in which the possible interaction between the subsystems takes place only during the protocol.

We will first consider the case of pure states. In order to quantify the degree of entanglement of a pure state $|\psi\rangle$ of system A-B, we use the entropy of entanglement, that is regarded as the standard entanglement measure for pure states [91, 92] and is equal to the Von Neumann entropy of one of the reduced states, i.e., $\mathcal{E}(|\psi\rangle) = S(\mathrm{Tr}_{A(B)}\{|\psi\rangle\langle\psi|\})$, where $S(\rho) = -\,\mathrm{Tr}\{\rho \ln \rho\}$[2].

Every pure state of system A-B can be rewritten according to its Schmidt decomposition[3] as [10]

$$|\psi\rangle = \sum_{i=0}^{N_A-1} \sqrt{\lambda_i}\, |a_i b_i\rangle\,, \tag{7.1.2}$$

where $\langle a_i|a_j\rangle = \langle b_i|b_j\rangle = \delta_{ij}$, $\sum_{i=0}^{N_A-1} \lambda_i = 1$, and $0 \leq \sqrt{\lambda_{N_A-1}} \leq \cdots \leq \sqrt{\lambda_1} \leq \sqrt{\lambda_0} \leq 1$. Accordingly, $\mathcal{E}\left(|\psi\rangle\right) = -\sum_i \lambda_i \ln \lambda_i$.

7.1.2 Minimum energy entangled states (MEESs)

For each value of entanglement, $\mathcal{E}$, multiple sets of squared Schmidt coefficients such that the correct amount of entanglement is attained can be found. Therefore, let us concentrate on one of these sets, $\vec{\lambda} \equiv \{\lambda_i\}_{i=0}^{N_A-1}$. In Appendix 7.A, we prove the following theorem.

[2] See also section 2.1.3.
[3] See also Appendix 2.A.2.

Theorem 7.1.1. *For any bipartite system with Hamiltonians H_A and H_B of the form of Eq. (7.1.1), given a fixed set of squared Schmidt coefficients $\vec{\lambda} \equiv \{\lambda_i\}_{i=0}^{N_A-1}$ with $\lambda_i \leq \lambda_j$ for $i > j$, no pure state can have less energy than the state*

$$\left|\psi_{\vec{\lambda}}\right\rangle = \sum_{i=0}^{N_A-1} \sqrt{\lambda_i}\,|A_iB_i\rangle = \sum_{i=0}^{N_A-1} \sqrt{\lambda_i}\,|E_i\rangle\,, \qquad (|E_i\rangle \equiv |A_iB_i\rangle). \tag{7.1.3}$$

Moreover, if both H_A and H_B do not have degeneracies and $\lambda_i < \lambda_j$ for $i > j$, the above state is the only pure state with that energy up to phase factors on the basis kets.

The main idea of the above theorem proof is that, being $|\psi\rangle = \sum_{i=0}^{N_A-1} \sqrt{\lambda_i}|a_ib_i\rangle$ any other pure state with the same Schmidt coefficients of $|\psi_{\vec{\lambda}}\rangle$, it holds

$$\langle\psi|H|\psi\rangle - \left\langle\psi_{\vec{\lambda}}\right|H\left|\psi_{\vec{\lambda}}\right\rangle = \sum_{i=0}^{N_A-1} \lambda_i\Delta_i \geq 0, \tag{7.1.4}$$

where $\Delta_i = \langle a_ib_i|H|a_ib_i\rangle - \langle A_iB_i|H|A_iB_i\rangle$.

Now that we have found the states having minimum energy for a given set of Schmidt coefficients, we can search for the MEESs. The state given in Eq. (7.1.3) has energy equal to

$$E_{\vec{\lambda}} \equiv \left\langle\psi_{\vec{\lambda}}\right|H\left|\psi_{\vec{\lambda}}\right\rangle = \sum_{i=0}^{N_A-1} \lambda_iE_i, \qquad E_i = A_i + B_i. \tag{7.1.5}$$

To minimize $E_{\vec{\lambda}}$ by varying $\vec{\lambda}$, we use the following bijection[4]:

$$\left|\psi_{\vec{\lambda}}\right\rangle = \sum_{i=0}^{N_A-1} \sqrt{\lambda_i}\,|E_i\rangle \leftrightarrow \tilde{\rho}_{\vec{\lambda}} = \sum_{i=0}^{N_A-1} \lambda_i\,|E_i\rangle\langle E_i|\,, \tag{7.1.6}$$

from which we get $\mathcal{E}(|\psi_{\vec{\lambda}}\rangle) = S(\tilde{\rho}_{\vec{\lambda}})$. Moreover, after introducing

$$\tilde{H} = \sum_{i=0}^{N_A-1} E_i\,|E_i\rangle\langle E_i|\,, \tag{7.1.7}$$

we can express the average energy in terms of the density operator $\tilde{\rho}_{\vec{\lambda}}$ because $\langle\psi_{\vec{\lambda}}|H|\psi_{\vec{\lambda}}\rangle = \mathrm{Tr}\{\tilde{H}\tilde{\rho}_{\vec{\lambda}}\}$. Thus, the problem of minimizing $E_{\vec{\lambda}}$ with respect to $\vec{\lambda}$ for a given degree of entanglement $\mathcal{E}$ is equivalent to find the diagonal density matrix $\tilde{\rho}_g$ that minimizes energy when its entropy $S = \mathcal{E}$ is fixed.

Let us suppose that the ground energy level of $\tilde{H}$ is degenerate with degeneration d_g. Then, trivially, when the entropy is lower or equal to $\ln d_g$, the minimum energy of $\tilde{\rho}_g$ is E_0 so that the corresponding MEES has to be found inside the degenerate subspace of energy E_0. In the other case, i.e., $\mathcal{E} > \ln d_g$, we show in the following that the solution is given by

$$\tilde{\rho}_g = \frac{e^{-\beta_g\tilde{H}}}{Z_g}, \quad \text{where} \quad Z_g = \mathrm{Tr}\left\{e^{-\beta_g\tilde{H}}\right\}, \tag{7.1.8}$$

[4]The bijection is valid up to phase factors on the kets $|E_i\rangle$.

and β_g is the non-negative solution of the equation:

$$\left(-\beta_g \frac{\partial}{\partial \beta_g} + 1\right) \ln Z_g = \mathcal{E}. \tag{7.1.9}$$

Suppose that it exists a state $\tilde{\sigma}_g$ with the same entropy of $\tilde{\rho}_g$ but lower energy. To each state ρ we can associate a functional formally equivalent to the free energy[5]:

$$F(\rho, \tilde{H}, \beta_g) = \mathrm{Tr}\left\{\tilde{H}\rho\right\} - \frac{1}{\beta_g} S(\rho). \tag{7.1.10}$$

Then, it holds

$$F(\tilde{\sigma}_g, \tilde{H}, \beta_g) - F(\tilde{\rho}_g, \tilde{H}, \beta_g) = \mathrm{Tr}\left\{\tilde{H}\tilde{\sigma}_g\right\} - \mathrm{Tr}\left\{\tilde{H}\tilde{\rho}_g\right\} < 0, \tag{7.1.11}$$

but also, as $\tilde{\rho}_g$ is the thermal state with inverse temperature β_g,

$$F(\tilde{\sigma}_g, \tilde{H}, \beta_g) - F(\tilde{\rho}_g, \tilde{H}, \beta_g) = \frac{1}{\beta_g} S(\tilde{\sigma}_g || \tilde{\rho}_g) > 0, \tag{7.1.12}$$

where $S(\rho||\sigma) = \mathrm{Tr}\left\{\rho\left(\ln\rho - \ln\sigma\right)\right\}$[6], which is always positive for $\sigma \neq \rho$ [12]. Therefore, $\tilde{\sigma}_g$ cannot exist.

It is straightforward to prove that Eq. (7.1.9) always has a unique non-negative solution, because entropy is a continuous and strictly decreasing function of β_g[7], and, moreover, the thermal state assumes the minimum and maximum values of entropy in the two limit cases $\beta_g = 0$ ($\mathcal{E} = \ln N_A$) and $\beta_g \to \infty$ ($\mathcal{E} \to \ln d_g$).

On the basis of Eqs. (7.1.6) and (7.1.8), we finally get:

$$|\psi_g\rangle = \frac{1}{\sqrt{Z_g}} \sum_{i=0}^{N_A-1} e^{-\frac{\beta_g}{2}E_i} |A_i B_i\rangle\,, \tag{7.1.13}$$

as one possible MEES. Its energy can be easily calculated as $E_g = -\partial_{\beta_g} \ln Z_g$. Note that a whole family of pure states with this amount of local energy and this entropy of entanglement can be easily constructed from Eq. (7.1.13) by multiplying kets by single phase factors:

$$\frac{1}{\sqrt{Z_g}} \sum_{i=0}^{N_A-1} e^{-\frac{\beta_g}{2}E_i} e^{i\theta_i} |A_i B_i\rangle\,, \quad \text{with} \quad \theta_i \in [0, 2\pi[. \tag{7.1.14}$$

Because of the theorem 7.1.1, we can say that this family comprehends all the lowest energy pure states if the two local Hamiltonians H_A and H_B have no degeneracies[8]. If at least one of the Hamiltonians has degeneracies, other states are valid. For example, suppose that $A_m = A_{m+1}$. Then, the state obtained from Eq. (7.1.13) by swapping $|A_m\rangle$

[5] See Eq. (2.A.3).

[6] This is the relative entropy defined in Appendix 2.A.1.

[7] This is shown later in Eq. (7.2.4).

[8] We recall that $\lambda_i = \exp\left\{-\beta_g E_i\right\}/Z_g$, therefore the condition $\lambda_i > \lambda_j$ for $i < j$ is satisfied.

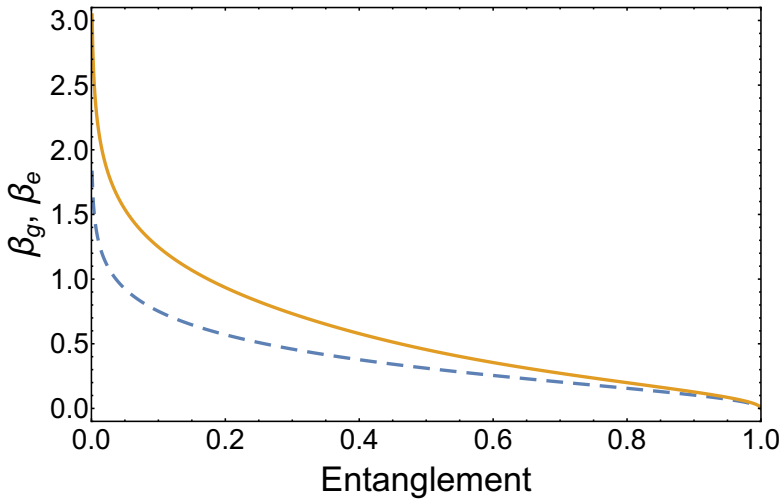

Figure 7.1: β_g (orange solid line) and β_e (blue dashed line) as functions of the entropy of entanglement (normalized), in the inversed arbitrary units of the local Hamiltonians, whose spectra are: $\sigma(H_A) = \{0, 2, 4\}$ and $\sigma(H_B) = \{0, 1, 6, 9\}$.

with $|A_{m+1}\rangle$ is still a MEES. In general, every state that can be obtained from the state of Eq. (7.1.13) through the application of energy preserving unitary operators of the form $U_A \otimes U_B$ is one of the lowest energy states.

We stress that Eq. (7.1.9) can be solved numerically in a straightforward way and that, in the two-qubit case, analytical expressions can be found[9]. Moreover, we remark that our treatment is valid for every finite N_A and N_B, even immensely large. Therefore, on a physical ground, we conjecture that our analysis holds good even for discrete Hilbert spaces of infinite dimensions, as in the case of two harmonic oscillators.

7.1.3 Maximum energy entangled states

MaxEESs can be easily obtained by searching for the MEESs when considering the Hamiltonians $\bar{H}_{A(B)} = -H_{A(B)}$. Hence, if $\mathcal{E} > \ln d_e$, where d_e is the lowest of the degeneracies of the maximum eigenvalues of H_A and H_B, a maximum energy state is given by

$$|\psi_e\rangle = \frac{1}{\sqrt{Z_e}} \sum_{i=0}^{N_A-1} e^{\frac{\beta_e}{2}(A_i + B_{i+\Delta})} |A_i B_{i+\Delta}\rangle \,, \tag{7.1.15}$$

where $\Delta = N_B - N_A$, $Z_e = \sum_{i=0}^{N_A-1} e^{\beta_e(A_i+B_{i+\Delta})}$, and β_e is the positive solution of the equation $(-\beta_e \partial_{\beta_e} + 1) \ln Z_e = \mathcal{E}$. Similarly to the minimum energy case, the energy of $|\psi_e\rangle$ can be easily calculated as $E_e = \partial_{\beta_e} \ln Z_e$. Moreover, the same considerations made for the minimum energy case about the uniqueness of the state hold good here. If

[9] We will do this explicitly later in this section.

$\mathcal{E} \leq \ln d_e$, then the maximum energy is $A_{N_A-1} + B_{N_B-1}$ and a maximum energy pure state can be searched in the eigenspace of the highest possible energy.

In general, β_g and β_e are different, as can be seen in Fig. 7.1, where we plot β_g and β_e as functions of $\mathcal{E}$, for a specific 3×4 system. However, it is possible to show that $\beta_g = \beta_e$ when the local spectra eigenvalues are symmetric with respect to a rotation[10]. This symmetry is automatically satisfied in the case of two qubits examined later in this section.

We finally observe that the minimization (maximization) process we have developed can be easily extended to any other couple of local observables. Indeed, whatever is the local operator $O = O_A + O_B$ we want to minimize (maximize) for an assigned value of entanglement, we can simply assume that $H_X = O_X$.

7.1.4 Closed expressions for a two-qubit system

Here, we apply our general results to the case of two qubits, i.e., to the case $N_A = N_B = 2$. By using the purity P[11] of one of the reduced states instead of the entropy of entanglement $\mathcal{E}$ as entanglement quantifier, it is possible to obtain through straightforward calculations closed analytical expressions both for the MEESs and MaxEESs and for the energy bounds using Eqs. (7.1.13) and (7.1.15). This is possible thanks to the fact that for a two-qubit system the von Neumann entropy and the purity can be bijectively connected. Starting from $|\psi_g\rangle = \sqrt{\lambda}|E_0\rangle + \sqrt{1-\lambda}|E_1\rangle$ and imposing $(1-\lambda)/\lambda = \exp[-\beta_g(E_1 - E_0)]$, one can easily obtain

$$\beta_g = -\frac{\ln[(1-\lambda)/\lambda]}{E_1 - E_0}, \quad \text{where} \quad \lambda = (1 + \sqrt{2P-1})/2. \tag{7.1.16}$$

Analogously, one can find $\beta_e = \beta_g$. Moreover, we can express the energy bounds as $E_g = \lambda E_0 + (1-\lambda)E_1$ and $E_e = (1-\lambda)E_0 + \lambda E_1$.

7.2 Extension to mixed states

We now show that the bounds derived in section 7.1 are still valid even when we extend the analysis to mixed states.

First, we need to prove that the lowest energy as a function of the entanglement $\mathcal{E}$ is monotonically increasing and convex[12]. In the following, $\langle H \rangle = \langle \psi_g | H | \psi_g \rangle = E_g$ and all the other expectation values refer to the state $|\psi_g\rangle$ as a function of β_g. Moreover, we consider $\beta_g > 0$ as the case $\beta_g = 0$ is obtained only in the extremal case $\mathcal{E} = \ln N_A$. Then, in the following we consider $\ln d_g < \mathcal{E} < \ln N_A$. First of all, we calculate

$$\frac{\partial}{\partial \beta_g} \langle H \rangle = \frac{\left(\partial_{\beta_g} Z_g\right)^2}{Z_g^2} - \frac{\partial^2_{\beta_g} Z_g}{Z_g}. \tag{7.2.1}$$

[10] In other words, a real constant C exists such that the spectra $\sigma\{H_{A(B)}\} = -\sigma\{H_{A(B)}\} + C$.
[11] The purity of a state ρ is equal to $P(\rho) = \mathrm{Tr}\{\rho^2\}$, see also Eq. 2.1.8.
[12] Indeed, we will also prove analogous properties for the highest energy.

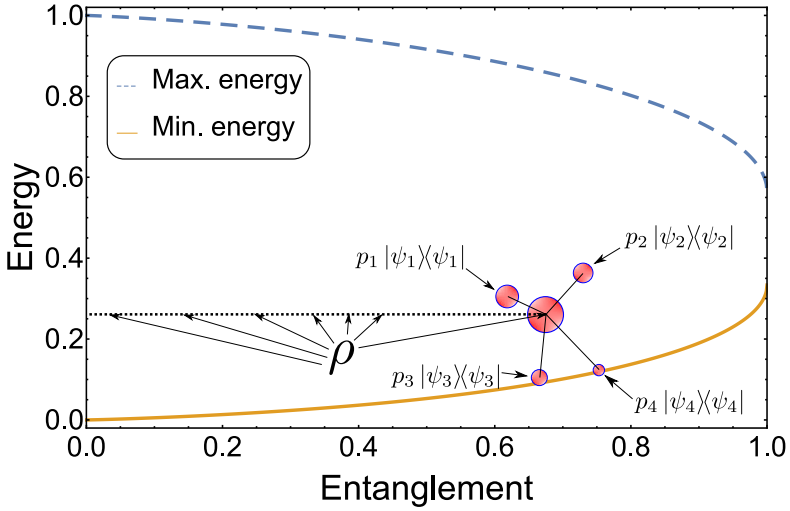

Figure 7.2: Representation of the energy-entanglement relation for a mixed state obtained as a convex sum of four pure states. The assigned energy value (obtained as the average of the energies of the pure states) and the possible values of entanglement (from zero to the average of the entanglement values of the single pure states) identify a segment. This segment always lies between the curves of minimum and maximum energy because of their monotonicity and convexity properties.

One can easily check that

$$\frac{\partial^n_{\beta_g} Z_g}{Z_g} = (-1)^n \langle H^n \rangle . \tag{7.2.2}$$

Then,

$$\frac{\partial}{\partial \beta_g} \langle H \rangle = \langle H \rangle^2 - \left\langle H^2 \right\rangle < 0, \tag{7.2.3}$$

since the states $|\psi_g\rangle$ are never eigenstates of H for the consider interval of $\mathcal{E}$. If we derive Eq. (7.1.9) with respect to β_g we thus obtain

$$\partial_{\beta_g} \mathcal{E} = \beta_g \partial_{\beta_g} \langle H \rangle < 0. \tag{7.2.4}$$

This means that $\mathcal{E}(\beta_g)$ is invertible for $\mathcal{E} > \ln d_g$. Then, we can use the theorem on the derivative of the inverse function to show that $\langle H \rangle$ is a monotone function of $\mathcal{E}$:

$$\partial_{\mathcal{E}} \langle H \rangle = \partial_{\beta_g} \langle H \rangle \times \partial_{\mathcal{E}} \beta_g = \frac{\partial_{\beta_g} \langle H \rangle}{\partial_{\beta_g} \mathcal{E}} = \frac{1}{\beta_g} > 0. \tag{7.2.5}$$

We can now calculate the second derivative of $\langle H \rangle$ respect to $\mathcal{E}$:

$$\partial^2_{\mathcal{E}} \langle H \rangle = \partial_{\mathcal{E}} \left(\frac{1}{\beta_g} \right) = -\frac{1}{\beta_g^2} \times \partial_{\mathcal{E}} \beta_g > 0. \tag{7.2.6}$$

Concerning the maximum energy decreasing monotonicity and concavity with respect to the entanglement, they follow from the fact that the maximum energy is found as the minimum for the Hamiltonian $-(H_A + H_B)$.

Contrarily to the pure state case, a standard entanglement quantifier does not exist [34]. However, as reported in section 2.1.3, it is generally required that the convexity property is satisfied [91, 92], i.e., for any arbitrary quantifier $\mathcal{E}_m$

$$\rho = \sum_i p_i \rho_i \implies \mathcal{E}_m(\rho) \leq \sum_i p_i \mathcal{E}_m(\rho_i), \tag{7.2.7}$$

where $p_i \geq 0 \ \forall i$ and $\sum_i p_i = 1$. In addition, we make the standard assumption that $\mathcal{E}_m$ applied to pure states is equal to the entropy of entanglement [92].

Every mixed state can be written as a combination of pure states, $\rho = \sum_i p_i |\psi_i\rangle\langle\psi_i|$. Thus, every mixed state has energy equal to $\mathrm{Tr}\{H\rho\} = \sum_i p_i \langle\psi_i|H|\psi_i\rangle$ and entanglement $\mathcal{E}_m(\rho) \leq \sum_i p_i \mathcal{E}_i$, where $\mathcal{E}_i = \mathcal{E}_m(|\psi_i\rangle)$. Since we proved that the curve $E_g(\mathcal{E})$ ($E_e(\mathcal{E})$) is increasing and convex (decreasing and concave), the following chain of relations holds:

$$\mathrm{Tr}\{H\rho\} \geq \sum_i p_i E_g(\mathcal{E}_i) \geq E_g\left(\sum_i p_i \mathcal{E}_i\right) \geq E_g(\mathcal{E}_m(\rho)). \tag{7.2.8}$$

Analogously, it holds that $\mathrm{Tr}\{H\rho\} \leq E_e(\mathcal{E}_m(\rho))$. It follows that, in an energy-entanglement graph, every mixed state can be found on a segment that is entirely between the minimum and maximum energy curves. In Fig. 7.2 an example of this situation is clearly shown.

We finally observe that our analysis extends to other entanglement quantifiers with the following properties[13]:

1. they are in a one-to-one relation with the entropy of entanglement when the domain of application is restricted to pure states;
2. they have the convexity property[14];
3. the minimum (maximum) energy curve is monotonically increasing (decreasing) and convex (concave).

This claim becomes intuitive if one thinks that all these requirements let one make the same reasoning done before, with the substitution of the quantifier $\mathcal{E}$ with $\mathcal{E}_m$ when applied to pure states, i.e., calculating the energy curves with respect to $\mathcal{E}(\mathcal{E}_m)$. Indeed, considering as new quantifier $\mathcal{E}_m$ a bijective function of the quantifier $\mathcal{E}$ is equivalent to apply a transformation along the x-axis to the energy-entanglement graphs. Therefore, the results on the mixed states obtained with the standard assumptions still apply if this transformation conserves the convexity and concavity of the two energy curves[15] and the chain of relations of Eq. (7.2.8) becomes:

$$\mathrm{Tr}\{H\rho\} \geq \sum_i p_i E_g(\mathcal{E}(\mathcal{E}_i)) \geq E_g\left(\sum_i p_i \mathcal{E}(\mathcal{E}_i)\right) \geq E_g(\mathcal{E}(\mathcal{E}_m(\rho))). \tag{7.2.9}$$

[13] Notice that all these properties together are a weaker version of the standard assumptions made before.

[14] See Eq. (7.2.7).

[15] That is, point 3 in the list of properties.

7.3 Connections with thermodynamics, entanglement Hamiltonian, and LOCC

In this section, we comment about connections MEESs and MaxEESs have with thermodynamics, many-body physics, and local operations and classical communication (LOCC) theory.

7.3.1 Connection with thermodynamics

MEESs and MaxEESs are characterized by coefficients that can be directly linked to the Boltzmann factors of a fictitious thermal state and, as a consequence, their energy can be calculated through their fictitious partition function. This is worth mentioning because entanglement and thermodynamics are believed to be conceptually connected in the context of typicality [110, 254] and they have various formal analogies when treated within resource theories such as LOCC and thermodynamic resource theory (TRT) [34, 120, 255]. In fact, a connection with thermodynamics has been also found in the study conducted in Ref. [78]. There, the authors dealt with the problem of creating the maximum amount of correlations[16] by employing a limited amount of energy, through the application of a unitary operator. They considered non-interacting bipartite systems starting from thermal product states. Since the mutual information is twice the entropy of entanglement in the zero temperature limit, their problem coincides with our search for the MEESs. Indeed, they have found that to maximize the correlations one has to generate states of the form of Eq. (7.1.13). Their proof relies on the concept of passive states[17], thus providing an additional link between our results and the field of thermodynamics.

It is also interesting to consider the limit case of Eq. (7.1.13) when $B_{N_A-1} = B_{N_A-2} = \cdots = B_0$. In this case, the reduced state of A, $\rho_g^A \equiv \mathrm{Tr}_B\{|\psi_g\rangle\langle\psi_g|\}$, is equal to

$$\rho_g^A = \frac{1}{Z_g} \sum_{i=0}^{N_A-1} e^{-\beta_g A_i} |A_i\rangle\langle A_i|, \quad Z_g = \sum_{i=0}^{N_A-1} e^{-\beta_g A_i}, \tag{7.3.1}$$

which is a thermal state with respect to H_A at temperature $T = 1/(k_B\beta_g)$, where k_B is the Boltzmann constant. This result can be easily obtained without using Eq. (7.1.13) since in this limit the problem reduces to find the minimum energy state for a fixed entropy of subsystem A.

7.3.2 Many-body systems with minimal energy states as ground states

Our results also present connections with some studies based on the entanglement Hamiltonian formalism, which has been proved to be useful to get various insights in

[16] Quantified by mutual information, as explained in section 2.1.

[17] States the energy of which cannot be lowered by unitary operations.

solid-state physics research [256–260]. It consists of writing the full-rank density matrix[18] of a system as $\rho = \exp(-\mathcal{H})$, where $\mathcal{H}$ is called "entanglement Hamiltonian" [258, 259]. In our case, in fact, when $N_A = N_B$, the reduced states of $|\psi_g\rangle$ are[19]

$$\rho_g^{A(B)} = \frac{1}{Z_g} e^{-\beta_g \operatorname{Tr}_{B(A)}\{\tilde{H}\}}. \tag{7.3.2}$$

Thus, the reduced states have been easily written in the entanglement Hamiltonian formalism with $\mathcal{H}_{A(B)} = \beta_g \operatorname{Tr}_{B(A)}\{\tilde{H}\}$[20]. In addition, whenever the first N_A eigenvalues of Hamiltonian H_B are simply connected with the eigenvalues of H_A, it is easy to write down the entanglement Hamiltonian form of subsystem A only in terms of H_A when the system is in a MEES. For example, when $H_B = \alpha H_A$, the entanglement Hamiltonian is given by $\mathcal{H}_A = \beta_g(1+\alpha)H_A$.

Now, we prove that some relevant many-body systems have ground states[21] belonging to the family of MEESs. Following Ref. [258], we consider a bipartite system with Hamiltonian $H_T = H_A + H_B + H_I$, where H_I is the interaction Hamiltonian between subsystems A and B and we suppose that $H_I \gg H_A + H_B$, so that the local Hamiltonian $H_A + H_B$ can be treated as a perturbation. If H_I has a non-degenerate ground state $|\psi_0\rangle$, perturbation theory gives

$$|\psi_0'\rangle = |\psi_0\rangle - \sum_{k=1}^{N_A N_B - 1} |\psi_k\rangle \frac{\langle\psi_k|(H_A + H_B)|\psi_0\rangle}{V_k - V_0}, \tag{7.3.3}$$

where $|\psi_0'\rangle$ is the perturbed ground eigenstate of H_T at first order, $|\psi_k\rangle$ are the eigenstates of H_I, and V_k the eigenvalues. In Ref. [258], the following result has been proved. If:

1. there is only one positive energy Δ such that $\langle\psi_k|(H_A + H_B)|\psi_0\rangle = 0$ except when $V_k - V_0 = \Delta$,
2. $\langle\psi_k|H_A|\psi_0\rangle = \langle\psi_k|H_B|\psi_0\rangle$ for each k,
3. $\operatorname{Tr}_B\{|\psi_0\rangle\langle\psi_0|\} \propto I$ (this requires $N_A \leq N_B$ and implies that $|\psi_0\rangle$ is maximally entangled),

then

$$\rho_A' = \operatorname{Tr}_B\{|\psi_0'\rangle\langle\psi_0'|\} = \frac{e^{-\mathcal{H}_A}}{Z} = \frac{1}{Z}\exp\left(-\frac{4}{\Delta}H_A\right), \tag{7.3.4}$$

where $Z = \operatorname{Tr}_A\{e^{-\mathcal{H}_A}\}$ assures correct normalization.

[18] A full-rank density matrix has every eigenvalue strictly higher than zero.

[19] We define $\rho_g^B \equiv \operatorname{Tr}_A\{|\psi_g\rangle\langle\psi_g|\}$.

[20] This can be done for ρ_g^A even when $N_A < N_B$ by limiting the trace on B to the first N_A basis vectors $|B_i\rangle$.

[21] More precisely, these ground states are not exact since they are obtained by making certain assumptions and approximations.

The systems analyzed in Ref. [258], indeed, satisfy the above conditions, but also have the same dimension and $H_A = H_B$. Therefore, a MEES on these systems takes the form

$$|\psi_g\rangle = \frac{1}{\sqrt{Z_g}} \sum_{i=0}^{N_A-1} e^{-\beta_g A_i} |A_i B_i\rangle \,, \tag{7.3.5}$$

since $E_i = A_i + B_i = 2A_i$. The reduced state of system A is then given by

$$\rho_A = \frac{1}{Z_g} \exp(-2\beta_g H_A). \tag{7.3.6}$$

By comparing the above equation with Eq. (7.3.4), one sees that the ground states of these systems are MEESs with $\beta_g = 2/\Delta$. This can be seen also using in Eq. (7.3.2) the fact that $\mathrm{Tr}_{B(A)}\{\tilde{H}\} = 2H_{A(B)}$.

7.3.3 Minimum (maximum) energy entangled states are LOCC-connected

Here, we show that MEESs are connected by LOCC operations and that the same holds for MaxEESs. Nielsen's theorem[22] states that a pure state $|\psi\rangle$ can be converted to a pure state $|\phi\rangle$ through LOCC if and only if $\vec{\lambda}^{\psi} \prec \vec{\lambda}^{\phi}$[23], where $\vec{\lambda}^{\psi}$ is the vector of the eigenvalues of one of the reduced states of the subsystems for a given state of the total bipartite system [10]. In other words, putting the eigenvalues in non-increasing order, for every $N \leq N_A$

$$\sum_{j=0}^{N-1} \lambda_i^{\psi} \leq \sum_{j=0}^{N-1} \lambda_i^{\phi}. \tag{7.3.7}$$

We now show that the above majorization condition is satisfied between two MEESs[24] when the starting one has not less entanglement than the final one. If the two MEESs have the same entanglement, then they have the same parameter β_g. In this case the majorization condition is trivially satisfied. Then, let us analyze the case when the two states have a different β_g.

We define as follows the sum of the first N elements of the vector $\vec{\lambda}^{\psi_g}(\beta_g)$:

$$\lambda_N(\beta_g) = \frac{\sum_{i=0}^{N-1} e^{-\beta_g E_i}}{Z_g}, \tag{7.3.8}$$

[22] We introduced Nielsen's theorem in section 2.1.2. However, we restate it here for the reader's convenience.

[23] One says that $\vec{\lambda}^{\phi}$ majorizes $\vec{\lambda}^{\psi}$, see section 2.1.2.

[24] See Eq. (7.1.13).

where, we recall, $E_i = A_i + B_i$. Then, we can show that $\partial_\beta \lambda_N(\beta_g) \geq 0 \ \forall N$:

$$\begin{aligned} Z_g^2 \partial_{\beta_g} \lambda_N(\beta_g) &= \left(\sum_{i=0}^{N-1} e^{-\beta_g E_i}\right)\left(\sum_{j=0}^{N_A-1} E_j e^{-\beta_g E_j}\right) - \left(\sum_{j=0}^{N_A-1} e^{-\beta_g E_j}\right)\left(\sum_{i=0}^{N-1} E_i e^{-\beta_g E_i}\right) \\ &= \left(\sum_{i=0}^{N-1} e^{-\beta_g E_i}\right)\left(\sum_{j=0}^{N-1} E_j e^{-\beta_g E_j} + \sum_{j=N}^{N_A-1} E_j e^{-\beta_g E_j}\right) + \\ &\quad - \left(\sum_{j=0}^{N-1} e^{-\beta_g E_j} + \sum_{j=N}^{N_A-1} e^{-\beta_g E_j}\right)\left(\sum_{i=0}^{N-1} E_i e^{-\beta_g E_i}\right) \\ &= \left(\sum_{i=0}^{N-1} e^{-\beta_g E_i}\right)\left(\sum_{j=N}^{N_A-1} E_j e^{-\beta_g E_j}\right) - \left(\sum_{j=N}^{N_A-1} e^{-\beta_g E_j}\right)\left(\sum_{i=0}^{N-1} E_i e^{-\beta_g E_i}\right) \\ &= \sum_{i=0}^{N-1}\sum_{j=N}^{N_A-1} (E_j - E_i)\, e^{-\beta_g (E_i + E_j)} \geq 0, \end{aligned} \tag{7.3.9}$$

where the last equality holds because $E_j \geq E_i$ by definition. This means that $\beta_g > \beta_g' \implies \lambda_N(\beta_g) \geq \lambda_N(\beta_g') \ \forall N$, thus proving the majorization condition[25]. We recall that β_g increases as the entanglement decreases. Analogously, one can show that MaxEESs can be obtained from one another through LOCC if the starting state has not less entanglement than the final one.

This result has an immediate consequence: for any arbitrary pure state of the bipartite system one can easily individuate a family of LOCC-connected pure states including the state at hand. Every pure state can be written as follows

$$|\psi\rangle = \sum_{i=0}^{r-1} \sqrt{\lambda_i}\, |a_i b_i\rangle\,, \quad \lambda_0 \geq \lambda_1 \geq \ldots \lambda_{r-1} > 0, \tag{7.3.10}$$

where we used the Schmidt decomposition of $|\psi\rangle$ having Schmidt rank r. Since Nielsen's theorem does not depend on the space containing the two states we want to connect by LOCC [10], we can consider two local Hermitian operators O_A and O_B of dimension r such that:

$$|\psi\rangle = \frac{1}{\sqrt{Z_O}} \sum_{i=0}^{r-1} e^{-\frac{\beta_g}{2}(a_i + b_i)}\, |a_i b_i\rangle\,, \tag{7.3.11}$$

where $a_i(b_i)$ are the eigenvalues of the local operator $O_{A(B)}$ with eigenstates $|a(b)_i\rangle$, and $1/\sqrt{Z_O}$ is a normalization factor. These Hermitian operators have eigenstates determined by the Schmidt decomposition of $|\psi\rangle$, but their eigenvalues are only constrained by the condition

$$a_i + b_i = -\frac{1}{\beta_g}\left(\ln \lambda_i + \ln Z_O\right). \tag{7.3.12}$$

[25] The equality sign holds only when $E_0 = E_1 = \cdots = E_{N_A-1}$

By also requiring that O_A and O_B have non-decreasing eigenvalues, the state $|\psi\rangle$ can be regarded as a state analogous to a MEES, in an Hilbert space of dimension r^2, with respect to the average of an entire family of operators $O = O_A + O_B$. It is easy to see that the same state can be considered as a state analogous to a MaxEES with respect to the average of operators $O' = -O$.

Since we have shown that MEESs and MaxEESs are, respectively, LOCC-connected among themselves, this also holds for the states minimizing and maximizing the average of O or O'. It follows that, for any given pure state, one can immediately write down a family of states that are connected to it. For example, starting from the state of Eq. (7.3.10), corresponding to a given β_g, one can obtain through LOCC the following states

$$\left|\psi'(\beta'_g)\right\rangle = \frac{1}{\sqrt{Z_O}} \sum_{i=0}^{r-1} e^{-\frac{\beta'_g}{2}(a_i+b_i)} |a_i b_i\rangle \,, \tag{7.3.13}$$

where $\beta'_g > \beta_g$. On the other hand, the state of Eq. (7.3.10) can be obtained by the above states with $\beta'_g < \beta_g$.

The family of states LOCC-connected to an arbitrary state is unique[26]. Indeed, changing the value of β_g or adding additive constants to the Hermitian operators O_A and O_B does not change the family of reachable states[27]. Moreover, seeing the state $|\psi\rangle$ as a MaxEES determines the exact same family of LOCC-connected states as seeing it as a MEES since every MEES of Eq. (7.3.13) can be seen as a MaxEES because $O' = -O$.

Another consequence of the fact that MEESs are LOCC-connected is that if two distant parties share a MEES having more entanglement than needed, they can recover, with certainty, the maximum amount of local energy compatible with the needed entanglement.

7.4 Unitary generation of MEESs

In this section, we provide three explicitly constructed unitary operators which implement the transition $|E_0\rangle \to |\psi_g\rangle$[28]. These operators can be easily decomposed into other ones. Despite the fact that these three operators share a similar mathematical structure, they strongly differ in their physical implementation because the first one, U_S, can be decomposed as a product of non-local simple operators while the other two, $\tilde{U}_A$ and $\tilde{U}_B$, are compositions of simple local unitary operators and a single generalized CNOT gate [62] applied as last operation.

Before stating the explicit forms of these unitary operators, it is worth commenting about the energy distribution of the pure states corresponding to the same amount of entanglement. We have made several numerical simulations finding, in all the studied

[26] Up to local unitary operators.

[27] See Eqs. (7.3.11) and (7.3.13).

[28] The state $|E_0\rangle$ is the most natural choice for the starting state since, in many cases, it can be easily obtained as the result of an approximate zero-temperature thermalization. Indeed, if the energy gaps between the ground and the first excited level of the Hamiltonian $H_A + H_B$ is much higher than $k_B T$, where T is the temperature of the bath, the steady state of the dynamics, i.e., the thermal state at temperature T is a very good approximation of the ground state.

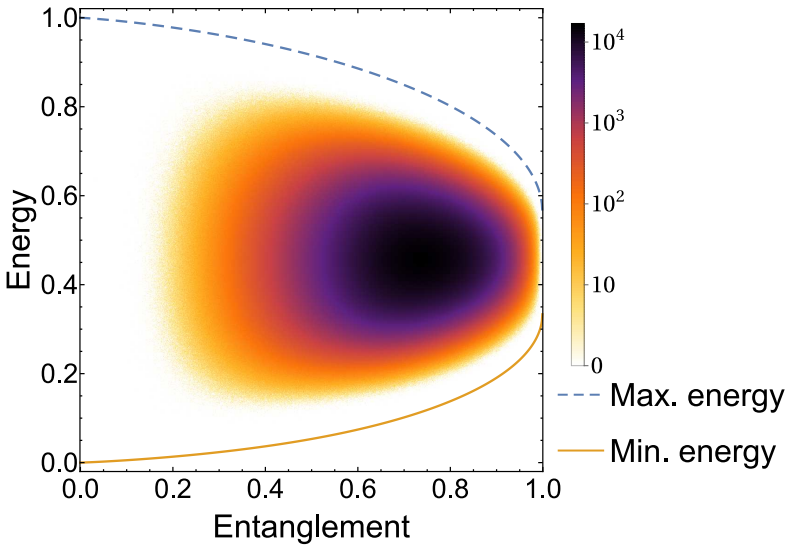

Figure 7.3: Distribution of 10^9 randomly generated pure states with respect to the entropy of entanglement and the local energy in a 1000×1000 grid. The Hamiltonians have spectra: $\sigma(H_A) = \{0, 2, 4\}$ and $\sigma(H_B) = \{0, 1, 6, 9\}$ in arbitrary units. Both the entanglement and the energy are normalized with respect to their maxima.

configurations, that the density of states in the proximity of the bounding curves is extremely low, except for the two-qubit case and highly degenerate cases. In fact, the main part of the states occupy the intermediate region, and the discrepancy between the peripheral and central densities becomes higher and higher as the dimensionality of the systems increases. We report here, as an example, the density of states corresponding to two local Hamiltonians having spectra given by $\sigma(H_A) = \{0, 2, 4\}$ and $\sigma(H_B) = \{0, 1, 6, 9\}$ in arbitrary units. In particular, in Fig. 7.3 we show the two curves defining the energy bounds for assigned entanglement and the distribution of a large number of randomly generated pure states [261][29]. It is well visible that the majority of the states lies in the central zone, while none of the generated states is very close to the bounding curves. This circumstance allows one to better appreciate the relevance of MEESs and unitary operators able to generate them. Indeed, in an entanglement generation process, one can choose to generate the state $|\psi_g\rangle$ having the lowest energy for the desired amount of entanglement, instead of any of all the other states which require more energy. We finally observe that the randomly generated states numerically satisfy the known theoretical expected averages both in entanglement and energy [110, 262, 263].

7.4.1 A global unitary transformation

We obtain the operator U_S as a change of basis between the eigenbasis of the Hamiltonian H_0 and a new basis obtained by applying the Gram-Schmidt orthogonalization process to

[29] The behavior of β_g and β_e for the same system is shown in Fig. 7.1.

the set of linearly independent vectors $\{|\phi\rangle, |E_1\rangle, \ldots, |E_{N_A-1}\rangle\}$, where $|\phi\rangle$ has the form

$$|\phi\rangle = \sum_{i=0}^{N_A-1} e^{i\theta_i}\sqrt{\lambda_i}\,|E_i\rangle\,. \tag{7.4.1}$$

The rest of the basis, i.e., all the vectors $|A_iB_j\rangle$ with $i \neq j$, are left unchanged. By varying the state $|\phi\rangle$, a family of unitary operators is obtained. This procedure, presented in detail in Appendix 7.B for a more general case, here leads to the vectors

$$\left|\phi_k^S\right\rangle = \frac{\gamma_k\,|E_k\rangle - e^{i(\theta_0-\theta_k)}\sqrt{\lambda_0\lambda_k}\,|E_0\rangle - \sum_{i=k+1}^{N_A-1} e^{i(\theta_i-\theta_k)}\sqrt{\lambda_k\lambda_i}\,|E_i\rangle}{\sqrt{\gamma_k\gamma_{k-1}}}, \tag{7.4.2}$$

where $1 \leq k \leq N_A - 1$, $\gamma_k = 1 - \sum_{i=1}^{k}\lambda_i$, and $\gamma_0 = 1$.

Denoting $\left|\phi_0^S\right\rangle = |\phi\rangle$, the unitary operator U_S takes the form

$$U_S = \sum_{k=0}^{N_A-1}\left|\phi_k^S\right\rangle\!\langle E_k| + \sum_{i=0}^{N_A-1}\sum_{j=0,j\neq i}^{N_B-1}|A_iB_j\rangle\!\langle A_iB_j|\,. \tag{7.4.3}$$

By choosing $|\phi\rangle = |\psi_g\rangle$, this family of operators provides an explicit construction for an operator making the $|E_0\rangle \to |\psi_g\rangle$ transition.

Interestingly, the operator U_S can be decomposed as the product of simple non-local operators[30]

$$U_S = \prod_{i=1}^{N_A-1} U_{S,i}, \tag{7.4.4}$$

where, for $1 \leq i < N_A$,

$$U_{S,i} = \sqrt{\frac{\gamma_i}{\gamma_{i-1}}}\,(|E_0\rangle\!\langle E_0| + |E_i\rangle\!\langle E_i|) + \sqrt{\frac{\lambda_i}{\gamma_{i-1}}}\left(e^{i\theta_i}\,|E_i\rangle\!\langle E_0| - e^{-i\theta_i}\,|E_0\rangle\!\langle E_i|\right) + \mathbb{I}_{\perp,i}, \tag{7.4.5}$$

while, for $i = N_A$,

$$U_{S,N_A} = e^{i\theta_0}\,|E_0\rangle\!\langle E_0| + \mathbb{I} - |E_0\rangle\!\langle E_0|\,, \tag{7.4.6}$$

being $\mathbb{I}$ the identity operator on the whole Hilbert space and

$$\mathbb{I}_{\perp,i} = \sum_{j\neq 0,i}|E_j\rangle\!\langle E_j| + \sum_{i=0}^{N_A-1}\sum_{j=0,j\neq i}^{N_B-1}|A_iB_j\rangle\!\langle A_iB_j| \tag{7.4.7}$$

the identity operator on the subspace perpendicular to the one spanned by $|E_0\rangle$ and $|E_i\rangle$. From a practical point of view, this may not be the best way to decompose the operator U_S, as it implies the application of $N_A - 1$ two-qudit gates, followed by a phase change. However, a similar decomposition is very fruitful for the MSSG unitary operators described in the next subsection. Since each component of the above decomposed form

[30] See Appendix 7.B for the proof.

of the operator U_S acts on the whole Hilbert space of system S, we refer to it also as the global unitary operator, as opposed to the MSSG[31] ones.

Even if in this section we concentrate on the generation of MEESs for a fixed entanglement, we remark that by applying the Gram-Schmidt procedure to the set $\{|\psi\rangle, |A_0B_1\rangle, |A_0B_2\rangle, \ldots, |A_{N_A-1}B_{N_B-1}\rangle\}$, the resulting family of operators can describe any transition from $|E_0\rangle$ to almost any state $|\psi\rangle$ of the Hilbert space of system S. A solvable exception is the case when the target state is orthogonal to the initial state $|E_0\rangle$[32]. Anyway, the simple form of the MEESs allow the unitary operators to be simpler when connecting $|E_0\rangle$ to one of them compared to when the target state is arbitrary. Indeed, the Schmidt decomposition of a MEES involves only the states $|E_i\rangle$, as in Eq. (7.4.1), where every coefficient λ_i is a simple function of the same parameter β_g. Moreover, the target MEES can be chosen with all the phases equal to zero. In general, in the case of an arbitrary target state the resulting unitary operator will be represented by a $N_S \times N_S$ matrix of non-trivial elements as opposed to the smaller number of non-trivial $N_A \times N_A$ elements of the matrix associated to Eq. (7.4.3) which holds for target states like those of Eq. (7.4.1). The possibility to generate practically every state will be used in section 7.5 to compare the behavior of the MEESs to all the other states in the zero-temperature thermalization approach.

7.4.2 Mostly single-system gates (MSSG) unitary transformations

Another unitary transformation mapping $|E_0\rangle$ to an arbitrary state $|\phi\rangle$ of the form of Eq. (7.4.1) is the one composed as follows[33]. A local unitary operator U_A acts as the previous operator U_S of Eq. (7.4.3) but on system A, i.e.,

$$U_A = \sum_{k=0}^{N_A-1} \left|\phi_k^A\right\rangle\!\left\langle A_k\right|, \tag{7.4.8}$$

where each $\left|\phi_k^A\right\rangle$ is equal to $\left|\phi_k^S\right\rangle$ of Eq. (7.4.2) with the substitution $|E_i\rangle \to |A_i\rangle$. Applying U_A to $|A_0\rangle$ induces the following transition

$$|A_0\rangle \to |A_g\rangle = \sum_{i=0}^{N_A-1} e^{i\theta_i}\sqrt{\lambda_i}\,|A_i\rangle\,. \tag{7.4.9}$$

Exactly like U_S, even U_A can be decomposed as a sequence of elementary two-dimensional rotations followed by a local phase change,

$$U_A = \prod_{i=1}^{N_A} U_{A,i}, \tag{7.4.10}$$

[31] We recall that MSSG stands for mostly single-system gates.

[32] The states which have zero projection on $|E_0\rangle$ can indeed be obtained by means of simple modifications of the method. See the relevant discussion in Appendix 7.B.

[33] The particular case $|\phi\rangle = |\psi_g\rangle$ is obtained when $\sqrt{\lambda_i} = e^{-\frac{\beta_g}{2}E_i}/\sqrt{Z_g}$.

where, for $1 \leq i < N_A$,

$$U_{A,i} = \sqrt{\frac{\gamma_i}{\gamma_{i-1}}}\left(|A_0\rangle\langle A_0| + |A_i\rangle\langle A_i|\right) + \sqrt{\frac{\lambda_i}{\gamma_{i-1}}}\left(e^{i\theta_i}\,|A_i\rangle\langle A_0| - e^{-i\theta_i}\,|A_0\rangle\langle A_i|\right) + \sum_{j\neq 0,i}|A_j\rangle\langle A_j|\,, \tag{7.4.11}$$

while, for $i = N_A$,

$$U_{A,N_A} = e^{i\theta_0}\,|A_0\rangle\langle A_0| + \sum_{i=1}^{N_A-1}|A_i\rangle\langle A_i|\,. \tag{7.4.12}$$

After having obtained $|A_g\rangle$, a single instance of the generalized CNOT gate [62] can be applied to obtain $|\phi\rangle$. For the CNOT gate we use the following form[34],

$$U_{G_A} = \sum_{i,j=0}^{N_A-1}|A_iB_{i\oplus j}\rangle\langle A_iB_j| + \sum_{i=0}^{N_A-1}\sum_{j=N_A}^{N_B-1}|A_iB_j\rangle\langle A_iB_j|\,, \tag{7.4.13}$$

where $i \oplus j = (i+j) \mod N_A$. Therefore, the final unitary operator is given by $\tilde{U}_A = U_{G_A}U_A$. The main advantage of using this technique is that, being U_A local, only a single standard two-qudit gate has to be used to construct $\tilde{U}_A$. Moreover, we have provided an explicit decomposition of U_A in terms of elementary operations.

A similar procedure can be implemented by applying on system B a local unitary operator U_B acting on system B analogously to how U_A acts on system A[35] and then using a CNOT gate, U_{G_B}, defined analogously to U_{G_A} by reversing the role of qudits A and B for the first N_A levels of both systems, i.e.,

$$U_{G_B} = \sum_{i,j=0}^{N_A-1}|A_{i\oplus j}B_j\rangle\langle A_iB_j| + \sum_{i=0}^{N_A-1}\sum_{j=N_A}^{N_B-1}|A_iB_j\rangle\langle A_iB_j|\,. \tag{7.4.14}$$

In this case, the final unitary operator is given by $\tilde{U}_B = U_{G_B}U_B$. We remark that, contrarily to U_S[36], the operators $\tilde{U}_A$ and $\tilde{U}_B$ do not allow to move from $|E_0\rangle$ to any other state. In fact, by construction only states such as those of Eq. (7.4.1) can be obtained[37].

The implementation of $\tilde{U}_A$ and $\tilde{U}_B$ in quantum circuits is expected to be largely simplified by the fact that they are given in terms of simple two-level local rotations and a local change of phase on a subsystem, and, subsequently, of a generalized CNOT gate on the bipartite system.

We finally observe that the decompositions of the three unitary operators provided in this section are given in terms of operators that never lower the energy of system S. This

[34] In Ref. [62] the CNOT gate is given for a bipartite system composed of two qudits with the same dimensions. Here, we have used what seemed to us the most natural extension of the CNOT gate operator, i.e., using system B as a qudit of dimension N_A. Therefore, we apply the CNOT gate such that it involves only the first N_A levels of both systems.

[35] In particular, the operator U_B acts as U_A on the first N_A levels of system B, while leaving unvaried the others.

[36] Or its modified form for target states orthogonal to $|E_0\rangle$, detailed in Appendix 7.B.

[37] In this case too, the procedure should be modified in the case of target states orthogonal to $|E_0\rangle$.

could be useful towards an efficient implementation of these operators since the apparatus implementing the unitary operators never has to recover energy from system S during the process. Moreover, we remark that these unitary protocols can be used even if the starting state ρ is not exactly the ground state $|E_0\rangle$ but a good approximation of it, i.e., such that the fidelity $F(\rho, |E_0\rangle\langle E_0|)$ is very near one. The fidelity for an arbitrary mixed state σ and an arbitrary pure state $|\varphi\rangle\langle\varphi|$ is equal to $F = \langle\varphi|\sigma|\varphi\rangle$. Indeed, one can easily check that for any suitable unitary operator U generating the required state $U|E_0\rangle$, the final fidelity is equal to the initial one since $F(U\rho U^\dagger, U|E_0\rangle\langle E_0|U^\dagger) = F(\rho, |E_0\rangle\langle E_0|)$.

7.5 MEESs generation through zero-temperature thermalization

In this section, we consider a different way to generate the states $|\psi_g\rangle$ exploiting a zero-temperature thermalization protocol. This protocol consists in turning on a suitable interaction between systems A and B, each of which had already thermalized to its own thermal state, while they are also weakly coupled to a common bath at zero temperature. Since $T = 0$ and we consider the ground level to be non-degenerate the thermal states correspond to the respective ground states. After the thermalization takes place, the coupling with the bath is suppressed and the interaction between A and B is turned off. In particular, here we make the assumption that the phases of turning on and off the interaction are so rapid that the state of the system is practically constant during the corresponding time intervals.

We considered this kind of protocols in the thermodynamic context of work extraction from a resource in chapter 3, where the efficiency of such protocols has been discussed. At zero temperature, the ideal efficiency and the expended energy of this protocol is given by

$$\eta = \frac{\langle\psi|H_0|\psi\rangle - E_0}{E_{\text{exp}}}, \quad E_{\text{exp}} = \langle E_0|H_I|E_0\rangle - \langle\psi|H_I|\psi\rangle\,, \tag{7.5.1}$$

where H_I is the interaction term that we turn on and off and $|\psi\rangle$ is the ground state of the Hamiltonian $H = H_0 + H_I$. In the above formula for η, the numerator represents the energy stored in system S at the end of the protocol minus the initial one, while the denominator is the minimum amount of expended energy to turn on and off the interaction. Therefore, we can call the denominator alone E_{exp}, standing for "expended energy". If our only concern is to maximize the entanglement production with respect to the used energy, then it is more important to minimize E_{exp} instead of maximizing η. We stress that this quantity represents the minimum energy required to perform the thermalization protocol. It corresponds to the actual amount of expended energy only in the ideal case when all energy losses take place only during the thermalization of the system.

To produce a MEES, $|\psi_g\rangle$, we need to find an interaction Hamiltonians H_I making $|\psi_g\rangle$ the ground state of the Hamiltonian $H = H_0 + H_I$. As an example, let us do this

by hand in the case of two qubits. The two-qubit Hamiltonian is

$$H_0 = \frac{\hbar\omega_A}{2}\sigma_z^A + \frac{\hbar\omega_B}{2}\sigma_z^B, \tag{7.5.2}$$

where σ_z^X is the z-Pauli matrix of qubit X ($X = A, B$). As basis for H_0 we use $|00, 01, 10, 11\rangle$, where, for each qubit, $\sigma_z^X |1\rangle = |1\rangle$ and $\sigma_z^X |0\rangle = -|0\rangle$. We choose an interaction term such that new Hamiltonian $H = H_0 + H_I$ is given by:

$$H = \frac{\hbar\omega_A}{2}\sigma_z^A + \frac{\hbar\omega_B}{2}\sigma_z^B + \frac{\hbar g}{2}\left(\sigma_x^A\sigma_x^B - \sigma_y^A\sigma_y^B\right). \tag{7.5.3}$$

Let us define $\omega = (\omega_A + \omega_B)/2$ and $\delta_A = (\omega_A - \omega_B)/2$, then the matrix of the Hamiltonian H in the basis $\{|00\rangle, |01\rangle, |10\rangle, |11\rangle\}$ is

$$H = \hbar\begin{pmatrix} -\omega & 0 & 0 & g \\ 0 & -\delta_A & 0 & 0 \\ 0 & 0 & \delta_A & 0 \\ g & 0 & 0 & \omega \end{pmatrix}. \tag{7.5.4}$$

The eigenstates and the corresponding eigenvalues are:

$$\begin{aligned} |\psi_e\rangle &= \sin\gamma\,|00\rangle + \cos\gamma\,|11\rangle, & \lambda_e &= \hbar\sqrt{\omega^2 + g^2}, & |\psi_+\rangle &= |10\rangle, & \lambda_+ &= \hbar\delta_A, \\ |\psi_g\rangle &= \cos\gamma\,|00\rangle - \sin\gamma\,|11\rangle, & \lambda_g &= -\hbar\sqrt{\omega^2 + g^2}, & |\psi_-\rangle &= |01\rangle, & \lambda_- &= -\hbar\delta_A, \end{aligned} \tag{7.5.5}$$

where $\tan\gamma = \frac{g}{\omega + \sqrt{\omega^2 + g^2}}$. The state $|\psi_g\rangle$ has always the lowest energy. By properly choosing g, one can obtain any linear combination[38] of $|11\rangle$ and $|00\rangle$ desired, i.e., one can obtain a MEES at any given entanglement.

In the following two subsections, we deal with the problem of finding some suitable interaction Hamiltonians leading to the desired ground state through methods that can work for any bipartite system.

7.5.1 A simple and a modified simple approach

The easiest total Hamiltonian leading to the desired MEES through a zero-temperature thermalization is

$$H_S^{\text{si}} = -V_S\,|\psi_g\rangle\langle\psi_g|, \tag{7.5.6}$$

where $V_S > 0$. This Hamiltonian has $|\psi_g\rangle$ as non-degenerate ground state and a degenerate excited subspace of dimension $N_S - 1$. The interaction term needed to obtain this Hamiltonian is

$$H_I^{\text{si}} = -V_S\,|\psi_g\rangle\langle\psi_g| - H_0. \tag{7.5.7}$$

From the mathematical point of view, the parameter V_S can assume any positive value. However, absolute zero temperature is never physically attainable. Therefore, V_S

[38] Up to phase factors.

must be high enough so that, for a sufficiently low temperature, the energy gap between the ground state and the excited states is high enough to make good the zero-temperature approximation. In particular, with this Hamiltonian one also has to consider the high-degeneration of the excited level. In the thermal state, the population ratio between the ground state and the degenerate excited level is

$$\frac{p_e}{p_g} = (N_S - 1)e^{-\beta V_S}, \tag{7.5.8}$$

where $\beta = 1/(k_B T)$ is the inverse temperature, k_B is the Boltzmann constant, and T is the temperature of the bath. Therefore, the larger the subsystems A and B are the higher V_S has to be in order to make the above ratio sufficiently small, consistently with the zero-temperature approximation.

The Hamiltonian of Eq. (7.5.6) can be improved by considering that $|\psi_g\rangle$ has not all the components in the bare basis, but only N_A components. For simplicity, let us consider that $A_0 = B_0 = 0$ and $A_1, B_1 > 0$. Then, one could use the following interaction term:

$$\tilde{H}_I^{\text{si}} = -V_M \, |\psi_g\rangle\langle\psi_g| - \sum_{i=0}^{N_A-1} E_i \, |E_i\rangle\langle E_i| \,, \tag{7.5.9}$$

where $V_M > 0$. By using this interaction term, the total Hamiltonian $H_M^{\text{si}} = H_0 + \tilde{H}_I^{\text{si}}$ has again $|\psi_g\rangle$ as its ground state but the degeneracy of the first excited level is only $N_A - 1$.

Let us define $\Delta = \min(A_1, B_1)$. Now, we make the assumption that the first excited level of H_0 is non-degenerate and that the other excited levels are enough higher than the first one so that the condition $e^{-\beta\Delta} \ll 1$ implies that the zero-temperature approximation for H_0 is valid. The value of V_X[39] such that the population ratio between the ground and first excited level is the same for H_0 and for H_X^{si}[40] results equal to

$$V_X \simeq \Delta \left[1 + \frac{\ln(N_X - 1)}{\beta\Delta}\right], \tag{7.5.10}$$

where N_S has already been defined as $N_S = N_A N_B$ and $N_M = N_A$. When V_X has such value, we can be certain that the zero-temperature approximation holds also after having turned on the interaction term.

When using this interaction term to enable the protocol[41], its efficiency and the expended energy for the generation of a MEES $|\psi_g\rangle$ are easily obtained from Eq. (7.5.1) as

$$\eta = \frac{E_g}{E_{\text{exp}}}, \qquad E_{\text{exp}} = E_g + V_X \, (1 - \lambda_0) \,, \tag{7.5.11}$$

where we recall that the energy of the MEESs, E_g, is given under Eq. (7.1.13) and where λ_0 can be computed from Eq. (7.1.14). For the generation of states $|\phi\rangle$ having the form

[39] Where $X = S, M$ depending on which case is analyzed.
[40] Compare with Eq. (7.5.8).
[41] Again with $A_0 = B_0 = 0$ for simplicity.

of Eq. (7.4.1), Eq. (7.5.11) holds by replacing E_g with the energy of the state $|\phi\rangle$ and using for λ_0 its actual value for this state.

We notice that, using Eq. (7.5.7), any arbitrary state of system S can be generated as the result of the thermalization by replacing $|\psi_g\rangle$ with the desired state $|\psi\rangle$. Therefore, it is possible to compare how MEESs behave with respect to all the other states. We already know from section 7.1.2 that, for a fixed amount of entanglement, $\langle\psi|H_0|\psi\rangle$ is minimized by $|\psi_g\rangle$. On the other hand, for a fixed entanglement, $V_X\,(1-\lambda_0)$ is minimized by taking the largest possible value of λ_0. Therefore, from a mathematical point of view, the states which minimize E_{exp} for a given entanglement are not the MEESs. However, in all the simulations we have run, as in the example shown in section 7.6, the E_{exp} associated to the MEESs result to be very close to the real minima of E_{exp} so that in practical applications one can directly choose to generate the MEESs if the aim is to minimize the expended energy. Specializing to the case of Eq. (7.5.9), we have been able to find the analytical solution for the states minimizing E_{exp}, as shown in Appendix 7.C. We also remark that using this simple modified approach, only states like those of Eq. (7.4.1) can be obtained by replacing $|\psi_g\rangle$ with $|\phi\rangle$ in Eq. (7.5.9).

7.5.2 A unitary transformation approach

Another way to obtain a new Hamiltonian having $|\psi_g\rangle$ as its ground state is to apply a transformation of the kind $UH_0U^\dagger$ to the original Hamiltonian H_0, with a unitary operator U such that $U|E_0\rangle = |\psi_g\rangle$. This has the advantage that when both systems A and B can be considered in their ground state, i.e., the zero-temperature approximation is well satisfied for both of them, then it will be valid also after the turning on of the interaction term since a unitary transformation does not change the spectrum of the Hamiltonian H_0. It follows that the zero-temperature thermalization will bring the system to the new ground state $|\psi_g\rangle$. Within this approach, the interaction term assumes the form:

$$H_I = UH_0U^\dagger - H_0. \tag{7.5.12}$$

We already know three different unitary operators assuring the requested transition, $U|E_0\rangle = |\psi_g\rangle$, from section 7.4. In the next two subsections we describe the interaction Hamiltonians that they generate.

H_I from the global unitary operator

Applying the unitary operator U_S of Eq. (7.4.3) in Eq. (7.5.12), one can obtain the explicit form of H_I[42]. Here, we report the results in the case of target states of the form of Eq. (7.4.1) by only focusing on the $N_A \times N_A$ terms that are non trivial, i.e., all the terms of the kind $|A_iB_i\rangle\langle A_jB_j|$. The remaining part of the matrix is just filled with zeroes. Denoting $X_0 = \langle E_0|H_I|E_0\rangle\,/\lambda_0$, where

$$\langle E_0|H_I|E_0\rangle = E_0(\lambda_0 - 1) + \lambda_0 \sum_{i=1}^{N_A-1} \frac{\lambda_i E_i}{\gamma_i \gamma_{i-1}}, \tag{7.5.13}$$

[42]This is done in Appendix 7.D for a general target state $|\psi\rangle$.

$$X_i \equiv E_0 - \frac{E_i}{\gamma_{i-1}} + \sum_{k=1}^{i-1} \frac{\lambda_k E_k}{\gamma_k \gamma_{k-1}}, \quad \text{for} \quad 1 \leq i \leq N_A - 1, \tag{7.5.14}$$

and $\Lambda_{i,j} = e^{i(\theta_i - \theta_j)} \sqrt{\lambda_i \lambda_j}$, we arrive at the matrix of H_I,

$$H_I = \begin{pmatrix} \Lambda_{0,0}X_0 & \Lambda_{0,1}X_1 & \Lambda_{0,2}X_2 & \dots & \Lambda_{0,n}X_n \\ \Lambda_{1,0}X_1 & \Lambda_{1,1}X_1 & \Lambda_{1,2}X_1 & \dots & \Lambda_{1,n}X_1 \\ \Lambda_{2,0}X_2 & \Lambda_{2,1}X_1 & \Lambda_{2,2}X_2 & \dots & \Lambda_{2,n}X_2 \\ \vdots & \vdots & \vdots & \ddots & \vdots \\ \Lambda_{n,0}X_n & \Lambda_{n,1}X_1 & \Lambda_{n,2}X_2 & \dots & \Lambda_{n,n}X_n \end{pmatrix}, \tag{7.5.15}$$

where $n = N_A - 1$.

Using Eqs. (7.4.2), (7.4.3), (7.5.1), and (7.5.12), and setting $E_0 = 0$, the efficiency of the thermalization protocol for target states like those of Eq. (7.4.1) results to be equal to[43]

$$\eta = \frac{\sum_{i=1}^{N_A-1} \lambda_i E_i}{E^S_{\text{exp}}}, \qquad E^S_{\text{exp}} = \sum_{i=1}^{N_A-1} \lambda_i E_i \left[1 + \frac{\lambda_0}{\gamma_i \gamma_{i-1}}\right]. \tag{7.5.16}$$

One can also show that the expended energy E^S_{exp} cannot be higher than $2E_{N_A-1}$[44].

H_I from the MSSG unitary operators

Other two interaction terms can be obtained by the application of the local unitaries U_A and U_B of section 7.4.2, together with the, respective, generalized CNOT gate. Since the two MSSG operations have the same structure, we will concentrate on the case of $\tilde{U}_A$.

The operator U_A acts on $|A_i\rangle$ as U_S acts on $|E_i\rangle$, therefore one can write the matrix $U_A H_A U_A^\dagger + H_B$ as[45]

$$\sum_{i,j=0}^{N_A-1} \sum_{k=0}^{N_B-1} \left[\delta_{i,j} \left(A_i + B_k\right) + \Lambda_{i,j} X^A_{i,j}\right] |A_i B_k\rangle\langle A_j B_k| \,, \tag{7.5.17}$$

where $X^A_{i,j}$ refers to the correspondent X_α of the matrix of Eq. (7.5.15) with all the E_i replaced by A_i[46], $\delta_{i,j}$ is the Kronecker delta, and

$$\alpha = \begin{cases} \max(i,j), & \text{if} \quad ij = 0, \\ \min(i,j), & \text{if} \quad ij \neq 0. \end{cases} \tag{7.5.18}$$

[43] For more details, see Appendix 7.E, where the computation is performed for an arbitrary state $|\psi\rangle$.
[44] See Appendix 7.E for the derivation of this inequality in a more general case.
[45] See Eqs. (7.5.12) and (7.5.15).
[46] The coefficients λ_i remain the same, even for the case of a MEES [Eq. (7.1.13)].

Then, applying the generalized CNOT gate U_{G_A} and subtracting the original Hamiltonian H_0, we obtain

$$H_I = \sum_{i,j,k=0}^{N_A-1} \left\{ \left[\delta_{i,j} \left(B_k - B_{i\oplus k} \right) + \Lambda_{i,j} X_{i,j}^A \right] |A_i B_{i\oplus k}\rangle\langle A_j B_{j\oplus k}| \right\} + \sum_{i,j=0}^{N_A-1} \sum_{k=N_A}^{N_B-1} \Lambda_{i,j} X_{i,j}^A \, |A_i B_k\rangle\langle A_j B_k| \, . \tag{7.5.19}$$

Even for this approach, we can calculate the efficiency of the thermalization protocol and the expended energy for target states like those of Eq. (7.4.1)[47]. Setting $A_0 = B_0 = 0$, we get

$$\eta = \frac{\sum_{i=1}^{N_A-1} \lambda_i E_i}{E_{\text{exp}}^A}, \quad E_{\text{exp}}^A = \sum_{i=1}^{N_A-1} \left[\lambda_i \left(E_i + \frac{\lambda_0 A_i}{\gamma_i \gamma_{i-1}} \right) \right]. \tag{7.5.20}$$

Notice that the MSSG approach based on $\tilde{U}_A$ is always more efficient than the global one when aiming at the same state, since

$$E_{\text{exp}}^S - E_{\text{exp}}^A = \lambda_0 \sum_{i=1}^{N_A-1} \frac{\lambda_i B_i}{\gamma_i \gamma_{i-1}} \geq 0, \tag{7.5.21}$$

while the numerators of the efficiencies are the same in the two cases. This conclusion also holds for the MSSG approach based on $\tilde{U}_B$, for which a formula analogous to the one of Eq. (7.5.20) applies, where the quantities A_i and B_i are swapped.

With regard to which approach is more efficient between the two possible MSSG approaches, the answer is model dependent, as it strongly depends on the spectra of both local Hamiltonians. In this case, the difference is given by

$$E_{\text{exp}}^B - E_{\text{exp}}^A = \lambda_0 \sum_{i=1}^{N_A-1} \frac{\lambda_i \left(B_i - A_i \right)}{\gamma_i \gamma_{i-1}}. \tag{7.5.22}$$

As we will see in the example of section 7.6, which of the two approaches requires more energy depends also on how much entanglement is demanded.

7.6 Analysis of the zero-temperature thermalization protocols for a three by four system

The simpler system to which we could apply the thermalization protocol is a system composed of two qubits. However, the two-level structure makes most results trivial and not meaningful in general so that the analysis of this section is devoted to a bigger system case. For completeness, in Appendix 7.G we report all the explicit formulas for a two-qubit system.

[47] See Appendix 7.F for the calculations.

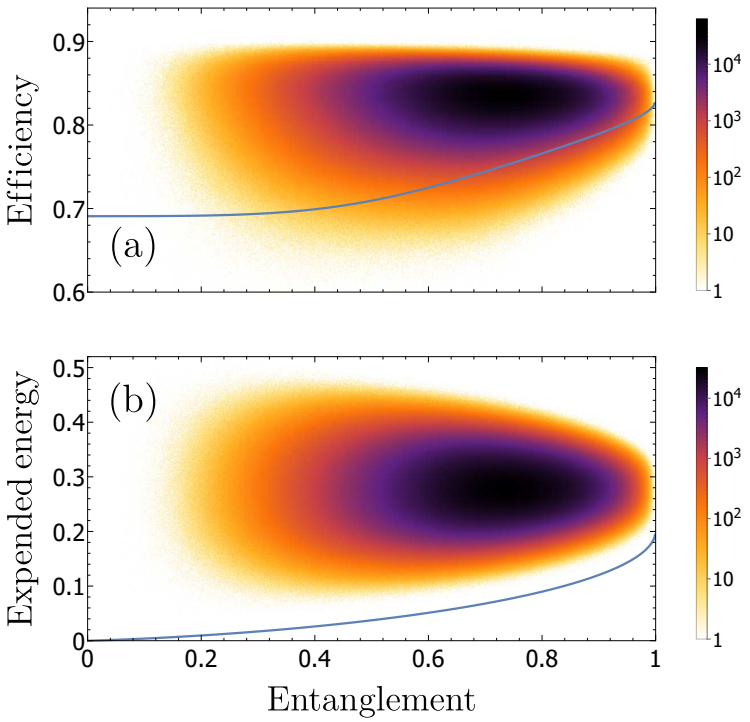

Figure 7.4: Distribution of randomly generated pure states with respect to the entropy of entanglement, $\mathcal{E}$, and the efficiency of the protocol (a) or the amount of energy used to create them (b). For these plots, the thermalization protocol is based on the simple approach. The relevant Hamiltonians have spectra: $\sigma(H_A) = \{0, 2, 4\}$ and $\sigma(H_B) = \{0, 1, 6, 9\}$ in arbitrary units. Both the entanglement and the expended energy are normalized to one, respectively, with respect to $\ln(3)$ and $2 \max \sigma(H_0)$. Each graph is the result of an interpolation of 10^9 random states distributed in a 1000×1000 grid, which covers the whole range of values (even those not shown on the graph; e.g., the grid of efficiency goes from zero to one). The colors correspond to $\log_{10}(1 + c)$, where c is the number of states in each grid element. In the bar legend, we report the value of $1 + c$, so that, e.g., 1 corresponds to the case of counting equal to zero. The blue lines give the position of the MEESs. Regarding the efficiency, we notice that it is quite high for every state and that the MEESs are among the worst ones. However, regarding the expended energy, they are much cheaper than the vast majority of all the possible pure states that can be generated.

In section 7.4 we analyzed a 3×4 system with spectra $\sigma(H_A) = \{0, 2, 4\}$ and $\sigma(H_B) = \{0, 1, 6, 9\}$ in arbitrary units. Here, we analyze the thermalization protocol applied to the same system, focusing on the behaviour of the MEESs with respect to all the other states that every specific interaction Hamiltonian we devised could produce.

Let us start from analyzing the simple case interaction of Eq. (7.5.7). Since in

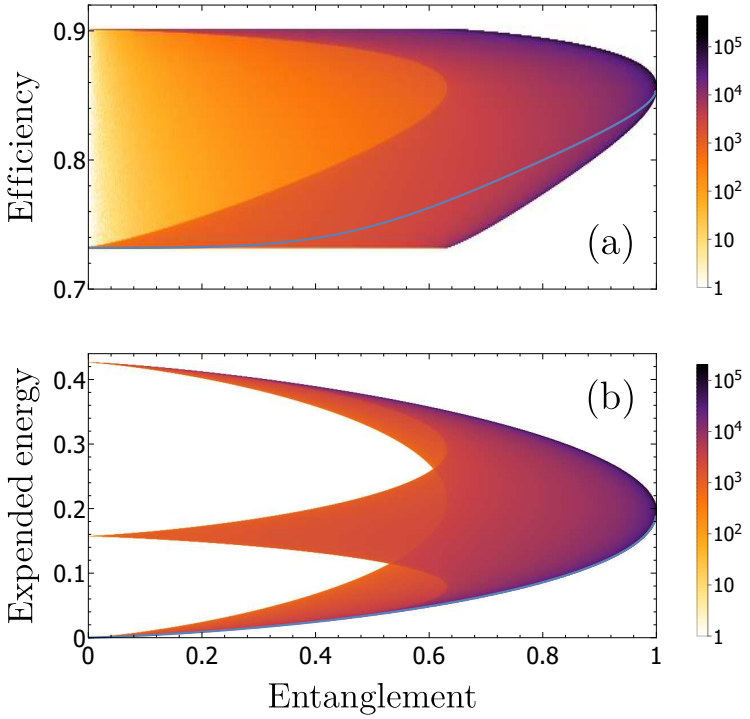

Figure 7.5: Same plots of Fig. 7.4 but with the thermalization protocol based on the modified simple approach. Here, we have used a different set of states with respect to the case of Fig. 7.4, since the modified simple approach cannot generate all the states but only those having the form of Eq. (7.4.1). In particular, we have randomly generated 10^9 pure states of this latter kind. As in Fig. 7.4, the efficiency is quite high for every generated state, with the MEESs being among the worst ones but also costing less than the vast majority of all the possible pure states that can be obtained.

Eq. (7.5.6) $|\psi_g\rangle$ can be replaced by any pure state of system S, any state can be obtained through a zero-temperature thermalization associated to H_S^{si}. Fig. 7.4 shows two plots relating the entanglement of 10^9 randomly generated pure states to, respectively, their generation efficiency η and their energy cost E_{exp}. The MEESs, represented by the blue lines, are not the best ones with respect to the efficiency, but, in general, they cost much less than the vast majority of all the possible pure states that can be generated. In effect, even if they are not the states mathematically minimizing the expended energy, numerical solutions of the minimization problem show, in all systems that we have simulated, that they are very close to them.

With the interaction Hamiltonian of the modified simple approach of Eq. (7.5.9), since $V_M < V_S$[48], we get an higher efficiency compared to the one we could get by reaching

[48] See Eq. (7.5.10)

the same states with the non-modified simple approach[49]. However, the modified simple approach lets us to obtain only states like those of Eq. (7.4.1). Fig. 7.5 shows the same two plots of Fig. 7.4 but using a sample of 10^9 randomly generated states that can be obtained through the modified simple approach. Indeed, the difference of the sample set is the main responsible for the great difference between the distributions of Fig. 7.4 and Fig. 7.5. Even in this case, the MEESs, represented by the blue lines, are not the best ones with respect to the efficiency. Regarding the expended energy, they are still among the cheapest states, but the distribution accumulates on the boundaries contrarily to the case of Fig. 7.4(b). By zooming enough in the graph[50], it is possible to see that some of the generated states are cheaper than the MEESs. We recall that, in this case only, we were able to find a simple analytical solution of the minimization problem, reported in Appendix 7.C. As in the simple approach case of Fig. 7.4, the solutions of the minimization problem show, in all systems that we have simulated, that MEESs are very close to the states minimizing the expended energy. We also notice that the maximum value of the efficiency with respect to the normalized entanglement starts to change around $\ln(2)/\ln(3) \simeq 0.631$. This is probably due to the fact that to obtain a certain degree of entanglement without involving all three states ($|E_0\rangle$, $|E_1\rangle$, and $|E_2\rangle$) is not possible when $\mathcal{E} > \ln(2)$[51].

Moving to the results of the unitary approach, Fig. 7.6 shows the same two plots of Fig. 7.4 but in the case when the interaction Hamiltonian is obtained through U_S. Notice how the state distribution of Fig. 7.6 is qualitatively similar to that of Fig. 7.4. This is due to the fact that the plots in the two figures have been made based on the same kind of sample set. In general, a comparison with all the other figures of this section suggests that the global unitary approach is the less performing.

Fig. 7.7 shows the same plots of previous figures in the case when the interaction is obtained through $\tilde{U}_A$. As for the modified simple approach, only states with a Schmidt decomposition in the $|E_i\rangle$ basis can be obtained through this approach[52]. Indeed, again for this reason, the distribution is completely different with respect to approaches that can give any state as result. In general, the efficiencies are higher compared to the ones obtained with the global approach. This is probably connected to the fact, proved analytically, that when the MSSG and global unitary approaches generate the same state, the MSSG ones are more efficient[53]. However, even in this case, the MEESs are not among the best ones but they lie very near the lower border of the E_{exp}-$\mathcal{E}$ distribution.

The same plots for the unitary approach on system B, reported in Fig. 7.8, give different results for the efficiency but similar for the expended energy. We can deal with this case by using directly the operator $\tilde{U}_B$ derived in section 7.4.2, even if we did not report explicitly the interaction Hamiltonian needed for implementing the thermalization protocol in section 7.5.2. In this case, for low entanglement, the efficiencies of the MEESs are practically the highest ones. Other simulations suggest that this probably depends

[49] See Eq. (7.5.11).
[50] And using a thinner line for the MEESs.
[51] We recall that, in the plot, the entanglement value is normalized to one.
[52] See Eq. (7.4.1).
[53] See Eq. (7.5.21) and the comment below it regarding the same approach but based on $\tilde{U}_B$.

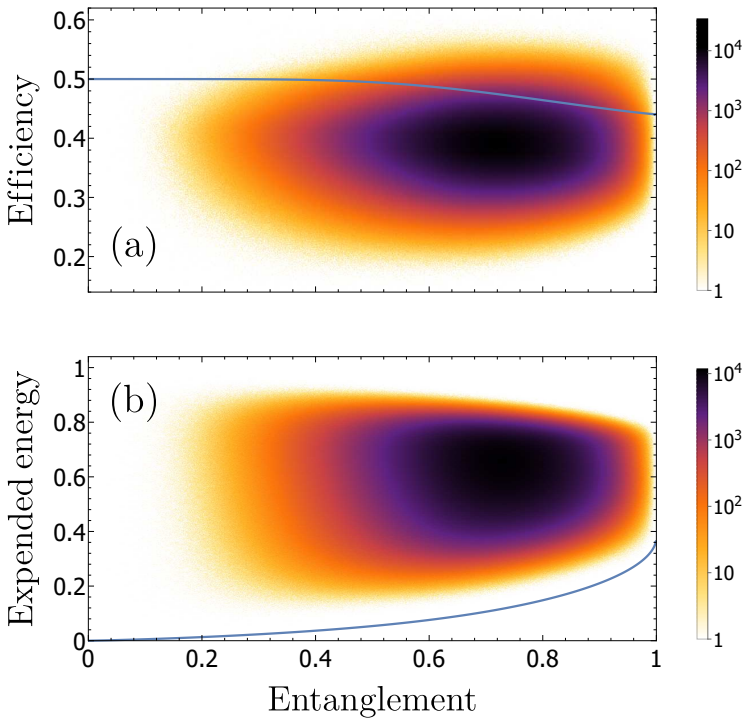

Figure 7.6: Same plots of Fig. 7.4 but with the thermalization protocol based on the transformation of H_0 through U_S. Here, the same states of Fig. 7.4 have been used. Compared to Fig 7.4, the efficiency is remarkably lower, but in this case the MEESs are among the best ones. As in all the other figures, they are cheaper than the vast majority of all the possible pure states that can be generated.

on the fact that between the two subsystems A and B, system B is the one with the lowest energy gap between the ground and the first excited state and the highest energy gap between the first and the second excited states. In fact, within the MSSG unitary approaches, the energy spectrum of the local system of interest is more important than the energy spectrum of the other one[54]. Since for low entanglement, two states in the decomposition are approximately sufficient, we can (heuristically) expect that the weight of the third state has to be marginal. Indeed, considering the spectrum of system B and the weights implied by a thermal distribution, the second excited state in MEESs is very low populated for low entanglement, thus leading to high efficiencies. As for the modified simple approach, we can also see in Fig. 7.7 and 7.8 that the maximum of the efficiency with respect to the entanglement starts declining roughly at $\ln(2)/\ln(3)$, we think, for the same reasons given in the case of Fig. 7.5.

Finally, Fig. 7.9 shows both efficiency and expended energy for all of the analyzed processes but focusing only on the generation of MEESs. Here, we can see that at low

[54]See Eq. (7.5.20).

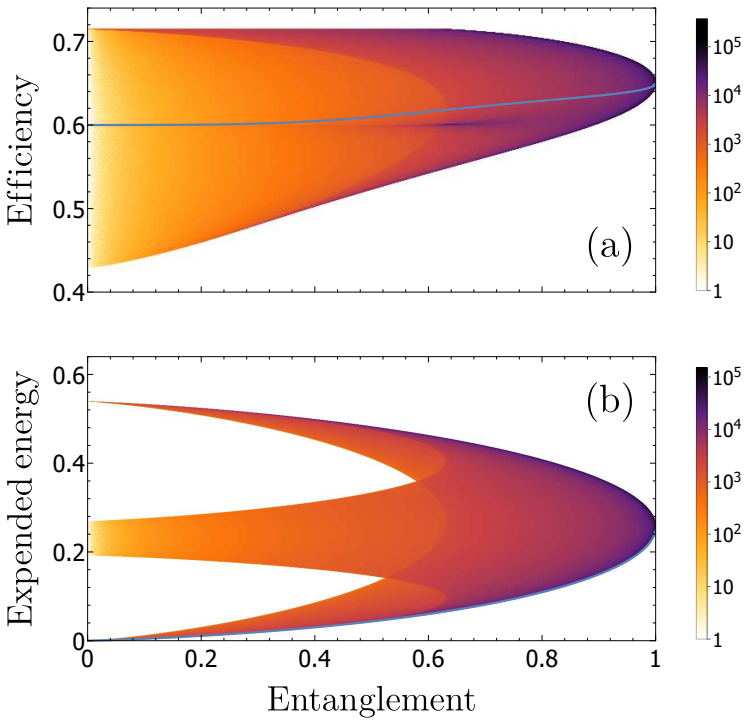

Figure 7.7: Same plots of Fig. 7.4 but with the thermalization protocol based on the transformation of H_0 through $\tilde{U}_A$. Here, the same states of Fig. 7.5 have been used. With respect to the unitary global approach of Fig. 7.6, the efficiency is generally higher. The MEESs result to be cheaper to generate than the vast majority of all the possible pure states that can be obtained. The striking difference in the distribution comes from the difference of the sample set of states.

entanglement values the most efficient approach to produce a certain MEES is the MSSG unitary approach on system B. For higher entanglement values, the best approach seems to be given by the modified simple one. The plots also make clear that the two simple approaches behave the same for MEESs, with the difference originating only from the fact that $V_S > V_M$. We also notice that the two MSSG approaches cross at a certain point. This is probably due to the fact the, towards higher entanglement values, the second excited level of both subsystems becomes more important. Therefore, the only positive term in the sum of Eq. (7.5.22), i.e., the last one becomes higher. As predicted analytically, the global unitary approach always performs worse than the MSSG ones.

7.7 Application of MEESs to quantum technologies

Our results on the entanglement-energy connections can be particularly relevant in protocols exploiting partially entangled qudits. Although maximally entangled states

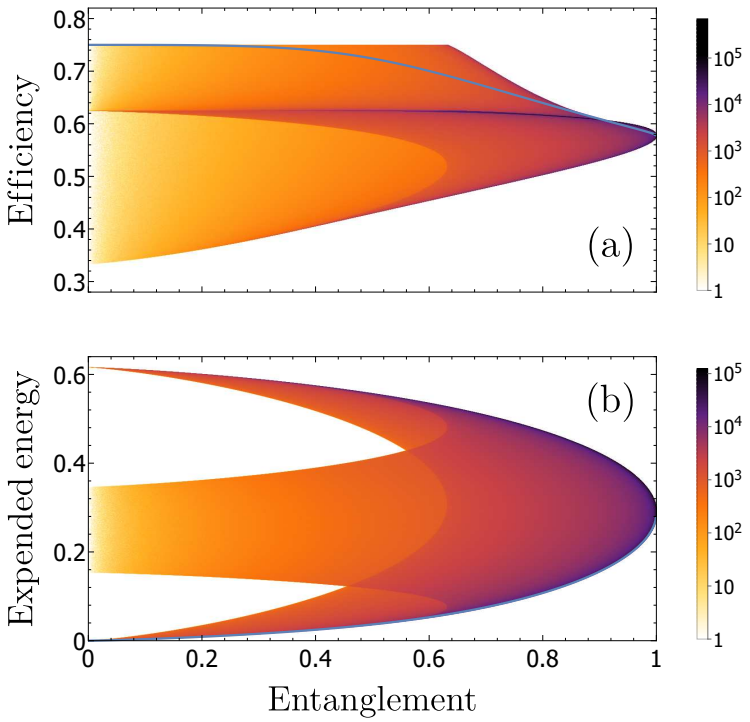

Figure 7.8: Same plots of Fig. 7.4 but with the thermalization protocol based on the transformation of H_0 through $\tilde{U}_B$. Here, the same states of Figs. 7.5 and 7.7 have been used. This is the only case in which MEESs practically attain the maximum efficiency, even if only for the low entanglement zone. Concerning the expended energy, the MEESs are cheaper to generate than the vast majority of all the possible pure states that can be generated.

are requested in many applications, non-maximally entangled states have been proven useful in quantum technologies, for example in processes involving two-mode squeezed states [150, 264], in quantum telecloning of qudits [265], and in probabilistic quantum teleportation [266]. In the last two cases, our results allow one to implement the procedure by exploiting less expensive entangled states, through the direct utilization of MEESs or of Theorem 7.1.1.

Our results also permit to identify bounds in the production of pure entangled states within the framework of TRT[55], which has recently drawn a lot of attention [86, 120]. Its goal is to study what states are reachable through thermal operations given an arbitrary starting state ρ and an environment at temperature T. Since the energy amount of reachable states from the state ρ is bounded, when TRT is equipped with our results, it lets us individuate which are the reachable pure states with the maximum allowed degree of entanglement. Indeed, allowing the use of catalysts [86], the state we search is one of

[55] See section 2.3.1.

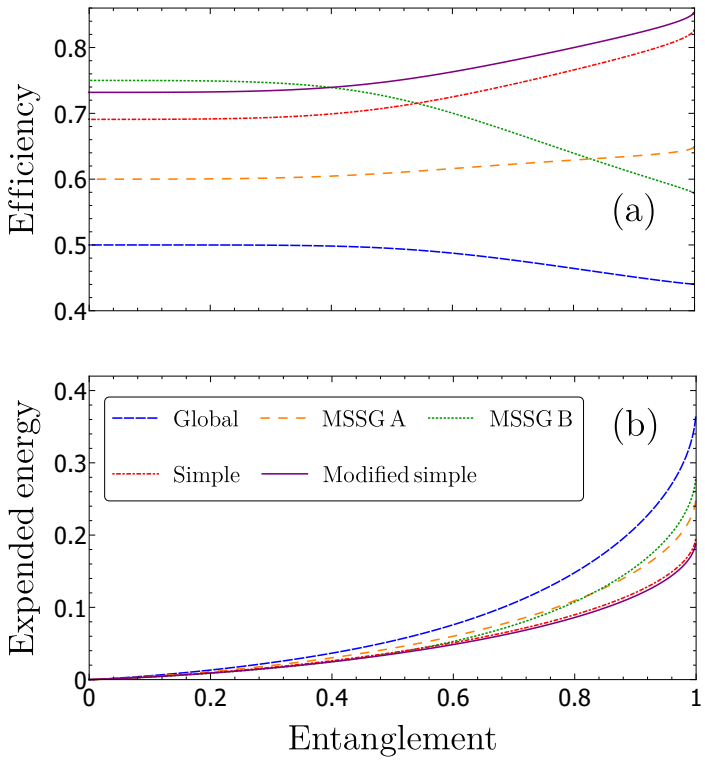

Figure 7.9: Comparison of the five approaches analyzed in section 7.6. For both plots, we report the normalized entropy of entanglement $\mathcal{E}$ on the X-axis. On the Y-axis, we report, respectively, the efficiency (a) and the normalized expended energy (b). As in Fig. 7.4, the entanglement and the expended energy are normalized, respectively, with respect to $\ln(3)$ and $2 \max \sigma(H_0)$. Depending on how much entanglement is required, the most efficient states to generate can be obtained through the MSSG approach based on $\tilde{U}_B$ or the modified simple approach. We also observe that, as predicted analytically, the modified simple approach always performs better than the non-modified one and that the unitary approach based on U_S is worse than the other two for any value of the entanglement.

our minimum energy states with energy equal to $\mathrm{Tr}\{\rho(H_A + H_B)\} - k_B T S(\rho)$.

In the following, we analyze more in detail some applications of MEESs to quantum technologies.

7.7.1 Increasing the energy efficiency of quantum protocols exploiting partial entanglement

Here, we show how Theorem 7.1.1 can be used to increase the energy efficiency of certain protocols.

In most quantum protocols exploiting partially entangled pure states, the quality of the protocols only depends on the Schmidt coefficients of the entangled states used, where the quality of the protocol is quantified by quantities such as the fidelity of the result obtained with respect to the desired one or the success probability of the protocol. For a fixed set of Schmidt coefficients, Theorem 7.1.1 provides states having the lowest local energy. Therefore, for a given protocol with some possible contraints, once the Schmidt coefficients maximizing the quality of the protocol are given, Theorem 7.1.1 naturally applies allowing one to allocate the least possible amount of energy on the two subsystems.

For example, in Ref. [266], Alice wants to teleport a qudit of dimension d to Bob using a partially entangled state which she shares with Bob. Their shared state is given by

$$|\psi\rangle = \sum_{i=0}^{d-1} \sqrt{\lambda_i}\, |a_i b_i\rangle\,, \tag{7.7.1}$$

where $0 \leq \sqrt{\lambda_{N_A-1}} \leq \cdots \leq \sqrt{\lambda_1} \leq \sqrt{\lambda_0} \leq 1$. The optimal mean fidelity of the quantum teleportation is given by [266]

$$\bar{f} = \frac{1}{d+1}\left[1 + \left(\sum_{i=0}^{d-1} \sqrt{\lambda_i}\right)^2\right]. \tag{7.7.2}$$

Among the states at fixed entropy of entanglement, maximizing the fidelity selects some sets of Schmidt coefficients. Theorem 7.1.1 provides the states with the lowest energy for each of these sets. In particular, if we call the Schmidt coefficients belonging to an optimal set, $\sqrt{\gamma_i}$, where $i < j \implies \gamma_i \geq \gamma_j$. Then, the state having the lowest local energy with these Schmidt coefficients is

$$|\psi_{\text{Opt}}\rangle = \sum_{i=0}^{d-1} \sqrt{\gamma_i}\, |A_i B_i\rangle\,. \tag{7.7.3}$$

More in general, Theorem 7.1.1 can greatly simplify maximization problems involving energy bounds since, for the states identified by the theorem, it allows to associate to every squared Schmidt coefficient λ_i the energy $E_i = A_i + B_i$. Indeed, using the same example as before, if, for instance, the energy of the shared state provided to Alice and Bob is bounded from above by E_c, the optimization problem reads

$$\begin{cases} \langle\psi|(H_A + H_B)|\psi\rangle \leq E_c, \\ \max_{|\psi\rangle}\, \bar{f}(|\psi\rangle), \end{cases} \tag{7.7.4}$$

while, using Theorem 7.1.1 it can be cast in the simplified form

$$\begin{cases} \sum_{i=0}^{d-1} \lambda_i E_i \leq E_c, \\ \max_{\vec{\lambda}}\, \bar{f}(\vec{\lambda}). \end{cases} \tag{7.7.5}$$

The search in Eq. (7.7.5) is much simpler since it is limited to the minimum energy states (for fixed $\vec{\lambda}$) selected by Theorem 7.1.1.

7.7.2 Producing more entanglement with less energy

In the LOCC asymptotic limit, n copies of a state $|\phi\rangle$ can be converted to m copies of a state $|\phi'\rangle$ if and only if $n\mathcal{E}(|\phi\rangle) \geq m\mathcal{E}(|\phi'\rangle)$, with $n, m \to \infty$, thus making the entropy of entanglement the quantifier of the resource entanglement [10][56]. Here, we show how producing partially entangled minimum energy states can increase the production of the resource entanglement with respect to the energy spent for generating it, in the LOCC asymptotic limit.

Suppose that we have at our disposal a great number of copies of systems A and B in their ground states with Hamiltonians, respectively, H_A and H_B. We want to increase the production of entanglement between systems A and B with respect to the energy we have to provide to them. For example, let us analyze the same system considered in several figures of this chapter, such as Figs. 7.1 and 7.3: systems A and B have Hamiltonians with spectra given by $\sigma(H_A) = \{0, 2, 4\}$ and $\sigma(H_B) = \{0, 1, 6, 9\}$ in arbitrary units and, initially, all the systems are in their ground state. To generate a maximally entangled state, we need to give to the bipartite system at least 13/3 of energy in arbitrary units. On the other hand, a minimum energy state with energy equal to one half of the latter (13/6) has an entanglement equal to roughly $\simeq 0.861$ times the maximal one. Therefore, creating two states of minimal energy with energy equal to 13/6 we provide the systems with the same amount of energy but generate about 72% more of the resource entanglement.

We can turn this into a maximization problem. When both H_A and H_B have degeneracies in their lowest eigenvalue, the problem is trivial since there are entangled states with ground state energy. Generating n MEESs with entanglement $\mathcal{E}$ costs $E_T = nE_g(\mathcal{E})$[57] of energy and the total amount of entanglement generated is

$$\mathcal{E}_T = n\mathcal{E} = E_T \frac{\mathcal{E}}{E_g(\mathcal{E})}. \tag{7.7.6}$$

Therefore, we want to maximize the ratio $\mathcal{E}/E_g$. Using Eq. (7.2.5) we find

$$\frac{\partial}{\partial \mathcal{E}} \left(\frac{\mathcal{E}}{E_g} \right) = \frac{1}{E_g} \left[1 - \frac{\mathcal{E}}{\beta_g E_g} \right] < 0, \ \forall \mathcal{E} > 0, \tag{7.7.7}$$

since $\mathcal{E} = \beta_g E_g + \ln[Z_g]$ and $Z_g(\mathcal{E}) > 1$[58]. Therefore, one can generate more entanglement with the same amount of disposable energy by producing many copies of minimum energy states with lower energy.

7.7.3 Two-mode squeezed states of two harmonic oscillators

Here, we show that two-mode squeezed states of two harmonic oscillators are MEESs. In section 7.1.2, we conjecture that our main result on the minimum energy states holds

[56] See also section 2.1.3.
[57] For simplicity, we set $A_0 = B_0 = 0$.
[58] See Eq. (7.1.9) and use $E_g = -\partial_{\beta_g} \ln Z_g$.

good even for discrete infinite systems. Then, if this conjecture is correct, two-mode squeezed states are minimum energy states for a given entanglement, as shown in the following.

Consider two harmonic oscillators with Hamiltonians $H_A = \hbar\omega_A a^\dagger a$ and $H_B = \hbar\omega_B b^\dagger b$, where $\omega_{A(B)}$ is their frequency and $a^\dagger(b^\dagger)$ and $a(b)$ are the usual creation and annihilation operators. In this case, the state of Eq. (7.1.13) takes the form (up to phase factors):

$$|\psi_g\rangle = \sqrt{1 - e^{-\beta_g \hbar\omega}} \sum_{n=0}^{\infty} e^{-\frac{\beta_g \hbar\omega}{2} n} |n_A n_B\rangle \,, \tag{7.7.8}$$

where $\omega = \omega_A + \omega_B$ and $|n_{A(B)}\rangle$ are number states in the Fock basis.

A two-mode squeezed state is obtained by applying the following unitary operator on a vacuum state [150, 267]:

$$U_{\text{sq}} = \exp\Big[r\left(e^{-i\phi} ab - e^{i\phi} a^\dagger b^\dagger\right)\Big], \quad r > 0,\ \phi \in [0, 2\pi[, \tag{7.7.9}$$

which, by naming $|\psi_{\text{sq}}\rangle = U_{\text{sq}}|0_A 0_B\rangle$, leads to

$$|\psi_{\text{sq}}\rangle = \frac{1}{\cosh(r)} \sum_{n=0}^{\infty} \Big[-e^{i\phi} \tanh(r)\Big]^n |n_A n_B\rangle \,. \tag{7.7.10}$$

We recall that this kind of states are also Gaussian states[59] and are often used in quantum optics laboratories for various tasks, usually exploiting their entanglement [150]. They can be generated, for instance, through four-wave mixing optical parametric oscillator [268].

One can easily check that[60]

$$|\psi_g\rangle = |\psi_{\text{sq}}\rangle \iff \beta_g \hbar\omega = -\ln\Big[\tanh^2(r)\Big] \,. \tag{7.7.11}$$

Then, if our conjecture holds good, every two-mode squeezed state is also a minimum energy state for a couple of harmonic oscillators. Therefore, these states, extensively exploited in quantum optics laboratories [150, 264, 267, 268], are the most energetically convenient states to generate in order to obtain a certain amount of entanglement.

7.8 Conclusions

In this chapter, we have found the minimum and maximum allowed local energy of an arbitrary finite bipartite system for a given amount of entanglement. We have also found the explicit form of a family of minimum and maximum energy states, which we called, respectively, minimum energy entangled states (MEESs) and maximum energy entangled states (MaxEESs). This analysis also holds for mixed states when using entanglement quantifiers with the convexity property, a requirement met by almost all entanglement quantifiers [92]. These extremal states have a formal connection with thermal states

[59] See section 2.4.1 for an introduction to the Gaussian formalism.

[60] Up to phase factors.

and are LOCC-connected, in the sense exposed in section 7.3.3. Furthermore, we have shown that MEESs naturally emerge as the ground state of some interacting many-body systems.

After having characterized MEESs, we have proposed several protocols to generate them. Some of these protocols are based on the direct use of unitary operators, while others exploit a zero-temperature thermalization for their realization. Moreover, we have numerically investigated the energy distribution of entangled pure states, finding, in all the studied configurations, that the probability of randomly generating states with a fixed entanglement close to the energy bounds is extremely low except for the two-qubit case and highly degenerate cases. This implies the advantage of using unitary operators that can specifically generate MEESs.

Regarding the proposed generation methods, on the one hand, we have provided three different unitary operators connecting the ground state of S to an arbitrary MEES. While the first operator, U_S, can be decomposed as the product of non-local operators, the others, $\tilde{U}_A$ and $\tilde{U}_B$, can be decomposed as the product of simple two-level local rotations and a local change of phase on a subsystem, and, subsequently, a generalized CNOT gate on the bipartite system. Therefore, the implementation of these unitary transformations in quantum circuits should be easier with respect to the case of U_S. On the other hand, we have identified five different interaction Hamiltonians that, added to the free ones, make it possible to generate MEESs through a zero-temperature thermalization process. Two of these processes are based on what we have called a simple and a modified simple approach, while the others are based on the unitary operators previously identified, U_S, $\tilde{U}_A$, and $\tilde{U}_B$.

We have then compared the efficiency of these zero-temperature generation processes as well as the expended energy to run them, both in general and in the case of a specific 3×4 system, complex enough to unveil the difference between the various protocols. In doing so, we have exploited the relevant fact that our protocols can also generate states different from the MEESs. Through a detailed comparison, we have identified, in the specific 3×4 system, which the best-performing protocols are. Depending on how much entanglement is required and the spectra of the systems, the better approaches are, in general, one between those based on $\tilde{U}_A$ and $\tilde{U}_B$, or the modified simple one. Even if the MEESs are not the states minimizing the expended energy to run the generation protocol, we have numerically found, in all systems we have simulated, that they are very close to the optimal states. Therefore, in general, MEESs are cheaper to generate than the vast majority of the other states. Concerning an experimental implementation of the corresponding interaction Hamiltonians, one can easily find the matrix for all five approaches and realize which is the easiest to implement.

MEESs can be important in quantum technologies since, fixed the degree of entanglement necessary for a certain application, they belong to the class of states whose unitary generation requires the lowest energy cost. Such an identification appears even more important also in the light of our numerical simulations, showing that the energies of the majority of the states with a fixed entanglement lie quite far from the energy bounds. Finally, we stress that Theorem 7.1.1 can bring by itself great practical advantages in

optimization problems depending exclusively on the Schmidt coefficients, given some energy constraints, as discussed in detail in section 7.7.1.

7.A Lowest energy state for a given set of Schmidt coefficients

Here, we prove Theorem 7.1.1, to this aim we will need four lemmas.

Lemma 7.A.1. *Consider two sets of real quantities* $\{p_i\}_0^{N-1}$ *and* $\{E_i\}_0^{N-1}$*, where* $0 \leq p_i \leq A\ \forall i$ *and* $\sum_{i=0}^{N-1} p_i = MA$*, with* $M \leq N,\ A \in \mathbb{R}^+$*. Then,*

$$\sum_{i=0}^{N-1} p_i E_i \geq \sum_{i=0}^{N-1} p_i^{\downarrow} E_i^{\uparrow} \geq A \sum_{i=0}^{M-1} E_i^{\uparrow}, \tag{7.A.1}$$

where $\left\{p_i^{\downarrow}\right\}_0^{N-1}$ *is the set* $\{p_i\}_0^{N-1}$ *with the elements put in decreasing order and* $\left\{E_i^{\uparrow}\right\}_0^{N-1}$ *is the set* $\{E_i\}_0^{N-1}$ *with the elements put in increasing order. Moreover, if the set* $\{E_i\}_0^{N-1}$ *has no repeated values and at least one* $p_i > 0$ *with* $i \geq M$*, then*

$$\sum_{i=0}^{N-1} p_i E_i > A \sum_{i=0}^{M-1} E_i^{\uparrow}. \tag{7.A.2}$$

Proof. In the first part of the proof we show that $\sum_{i=0}^{N-1} p_i E_i \geq \sum_{i=0}^{N-1} p_i^{\downarrow} E_i^{\uparrow}$. Without loss of generality, we can first put the p_i in decreasing order and continue to use E_i to indicated the elements of the permutated set. Then, if $E_n < E_m$, with $m < n$ we have

$$\sum_{i=0}^{N-1} p_i^{\downarrow} E_i \geq \sum_{i \neq n,m}^{N-1} p_i^{\downarrow} E_i + p_m^{\downarrow} E_n + p_n^{\downarrow} E_m. \tag{7.A.3}$$

The possibility of iterating this procedure concludes the first part of the proof.

For the second part of the proof, we consider the two sets already in the correct order (decreasing for the p_i and increasing for the E_i) and we avoid the arrows to lighten the notation. We consider the following iterative procedure. If $p_0 + p_{N-1} < A$, we write

$$\sum_{i=0}^{N-1} p_i E_i \geq \sum_{i=1}^{N-2} p_i E_i + (p_0 + p_{N-1}) E_0 = \sum_{i=0}^{N-2} q_i E_i, \tag{7.A.4}$$

and repeat the procedure with the new set $\{q_i\}_0^{N-2}$, where $q_i = p_i\ \forall\ 1 \leq i \geq N-2$ and $q_0 = p_0 + p_{N-1}$. Also, notice that the above inequality becomes strict if $E_{N-1} > E_0$ and $p_{N-1} > 0$. Otherwise, we have $p_0 + p_{N-1} = A + \tilde{p}_{N-1} \geq A$ and

$$\begin{aligned} \sum_{i=0}^{N-1} p_i E_i &= \sum_{i=1}^{N-2} p_i E_i + p_0 E_0 + (A - p_0) E_{N-1} + \tilde{p}_{N-1} E_{N-1} \\ &\geq \sum_{i=1}^{N-2} p_i E_i + A E_0 + \tilde{p}_{N-1} E_{N-1} = A E_0 + \sum_{i=1}^{N-1} \tilde{p}_i E_i, \end{aligned} \tag{7.A.5}$$

where, in the new set $\{\tilde{p}_i\}_1^{N-1}$, $\tilde{p}_i = p_i \ \forall\ 1 \leq i \leq N-2$ and we recall that $\tilde{p}_{N-1} = p_0 + p_{N-1} - A$. In this case, the next step has to be done on $\sum_{i=1}^{N-1} \tilde{p}_i E_i$.

The step represented by Eq. (7.A.4) conserves the sum of the p_i, i.e., $\sum_{i=0}^{N-1} p_i = \sum_{i=0}^{N-2} q_i$, while in Eq. (7.A.5), $\sum_{i=0}^{N-1} p_i = \sum_{i=1}^{N-1} \tilde{p}_i + A$. At each step of the procedure, we lose an element of the sum. Thus, at the end of the procedure, only the terms AE_i produced by the steps such as the one of Eq. (7.A.5) survive. The number of times this kind of step takes place is equal to M because of the hypothesis $\sum_{i=0}^{N-1} p_i = MA$ and, in the end, we will get $A\sum_{i=0}^{M-1} E_i$, which concludes the proof of the validity of Eq. (7.A.1). The particular case of no degeneracies in the set $\{E_i\}_0^{N-1}$ and at least one $p_i > 0$ with $i \geq M$ follows by considering that, in this case, at least one passage of Eq. (7.A.4) or of Eq. (7.A.5) with the strict inequality has to be performed. □

Lemma 7.A.2. *Consider an Hamiltonian of the form $H = \sum_{i=0}^{N-1} E_i |E_i\rangle\langle E_i|$, where $E_i \leq E_j$ for $i < j$ and a set of orthonormal vectors on the same Hilbert space $\{|a_i\rangle\}_{i=0}^{M-1}$. It holds that*

$$\sum_{i=0}^{M-1} \langle a_i|H|a_i\rangle \geq \sum_{i=0}^{M-1} E_i \quad \forall M \leq N. \tag{7.A.6}$$

Moreover, if the spectrum of the Hamiltonian is non degenerate, the equality sign is obtained if and only if we can write $|a_i\rangle = \sum_{n=0}^{M-1} \alpha_{i,n}|E_n\rangle\ \forall i$.

Proof. Let us start by considering that

$$\sum_{i=0}^{M-1} \langle a_i|H|a_i\rangle = \sum_{n=0}^{N-1} p_n E_n, \tag{7.A.7}$$

where $p_n = \sum_{i=0}^{M-1} |\langle E_n|a_i\rangle|^2 \leq 1$. Moreover, $\sum_{n=0}^{N-1} p_n = M$. Then, because of lemma 7.A.1

$$\sum_{i=0}^{N-1} p_n E_n \geq \sum_{n=0}^{M-1} E_n, \tag{7.A.8}$$

which concludes the first part of the proof. The second part follows by considering that if a ket $|a_i\rangle$ exists such that it cannot be obtained as a linear combination of the first M energy eigenvectors, then at least one $p_n > 0$ with $n \geq M$ exists. Then, because of lemma 7.A.1 the above inequality is strict. On the other hand, if the conditions on the kets $|a_i\rangle$ are valid, the equality sign of Eq. (7.A.8) is trivially obtained. □

Let us now consider a set of D real numbers $\{\Delta_i\}_0^{D-1}$ such that $\sum_{i=0}^{N-1} \Delta_i \geq 0, \quad \forall N \leq D$. The following lemmas (7.A.3 and 7.A.4) are valid.

Lemma 7.A.3. *Given a set of real non-negative numbers λ_i such that $\lambda_i \leq \lambda_j$ for $i > j$ then*

$$\sum_{i=0}^{N-1} \lambda_i \Delta_i \geq 0, \quad \forall N \leq D. \tag{7.A.9}$$

Proof. We show this by induction. Obviously, $\lambda_0\Delta_0 \geq 0$. Suppose that the lemma is true for $M < D$, that is

$$\sum_{i=0}^{N-1} \lambda_i\Delta_i \geq 0, \quad \forall N \leq M < D. \tag{7.A.10}$$

We have to analyze

$$\lambda_0\Delta_0 + \ldots \lambda_{M-1}\Delta_{M-1} + \lambda_M\Delta_M \geq 0. \tag{7.A.11}$$

If Δ_M is non-negative, the result is trivial. If Δ_M is negative we have

$$\lambda_0\Delta_0 + \cdots + \lambda_{M-1}\Delta_{M-1} + \lambda_M\Delta_M \geq \underbrace{\lambda_0\Delta_0 + \ldots}_{\text{True}} + \lambda_{M-1}(\Delta_{M-1} + \Delta_M). \tag{7.A.12}$$

If $(\Delta_{M-1} + \Delta_M) \geq 0$, Eq. (7.A.11) is satisfied. Otherwise, we go on and consider

$$\underbrace{\lambda_0\Delta_0 + \ldots}_{\text{True}} + \lambda_{M-2}(\Delta_{M-2} + \Delta_{M-1} + \Delta_M) \geq 0. \tag{7.A.13}$$

In the worst case we arrive at

$$\lambda_0 \left(\sum_{i=0}^{M} \Delta_i \right) \geq 0, \tag{7.A.14}$$

which is true by hypothesis. This concludes the proof. □

Lemma 7.A.4. *Given a set of real positive numbers λ_i such that $\lambda_i < \lambda_j$ for $i > j$, if there exists $i_0 = \min_i \{i : \Delta_i > 0\}$ then*

$$\sum_{i=0}^{N-1} \lambda_i\Delta_i > 0, \quad \forall \ (i_0 + 1) \leq N \leq D. \tag{7.A.15}$$

Proof. Of course, $\lambda_{i_0}\Delta_{i_0} > 0$. Then, we can repeat the reasoning of the proof of lemma 7.A.3, keeping into account that when one inequality such as that of Eq. (7.A.12) has to be considered, it will be a strict inequality. □

Now we are ready to prove theorem 7.1.1.

Proof. Let be $|\psi\rangle = \sum_{i=0}^{N_A-1} \sqrt{\lambda_i}|a_ib_i\rangle$ an arbitrary pure state with the given set of Schmidt coefficients. Let us calculate:

$$\langle\psi|H|\psi\rangle - \left\langle \psi_{\vec{\lambda}} \middle| H \middle| \psi_{\vec{\lambda}} \right\rangle = \sum_{i=0}^{N_A-1} \lambda_i\Delta_i, \tag{7.A.16}$$

where

$$\Delta_i = \langle a_ib_i|H|a_ib_i\rangle - \langle A_iB_i|H|A_iB_i\rangle = \langle a_i|H_A|a_i\rangle - A_i + \langle b_i|H_B|b_i\rangle - B_i. \tag{7.A.17}$$

Because of lemma 7.A.2,

$$\sum_{i=0}^{N-1} \Delta_i \geq 0, \ \ \forall \ N \leq N_A. \tag{7.A.18}$$

Then, because of lemma 7.A.3, $\sum_{i=0}^{N_A-1} \lambda_i \Delta_i \geq 0$ and the first part of the theorem is proven.

For the second part of the theorem, because of lemma 7.A.4, the energy of the arbitrary state $|\psi\rangle$ is equal to the energy of $|\psi_{\vec{\lambda}}\rangle$ if and only if $\Delta_i = 0$ for each i. Starting from Δ_0, the only way to make it zero is to set $|a(b)_0\rangle = |A(B)_0\rangle$, up to phase factors, because $A(B)_0$ is the lowest eigenvalue. Then, the only way to set $\Delta_1 = 0$ is to set $|a(b)_1\rangle = |A(B)_1\rangle$, up to phase factors, because this ket has to be orthogonal to $|a(b)_0\rangle$. The continuation of this reasoning leads to the conclusion of the proof. □

7.B Construction of the unitary operator in the general case

Theorem 7.B.1. *Be $\{|e_i\rangle\}_{i=0}^{N-1}$ a basis for an $N-$dimensional Hilbert space and be $|\psi_0\rangle = \sum_{i=0}^{N-1} e^{i\theta_i}\sqrt{\lambda_i}\,|e_i\rangle$ an arbitrary normalized state with $\lambda_0 > 0$, $\lambda_i \geq 0\ \forall i \geq 1$, and $\sum_i \lambda_i = 1$. The following states, together with $|\psi_0\rangle$, form another basis:*

$$|\psi_k\rangle = \left(\gamma_k\,|e_k\rangle - e^{i(\theta_0-\theta_k)}\sqrt{\lambda_0\lambda_k}\,|e_0\rangle - \sum_{i=k+1}^{N-1} e^{i(\theta_i-\theta_k)}\sqrt{\lambda_k\lambda_i}\,|e_i\rangle\right)/\sqrt{\gamma_k\gamma_{k-1}}, \quad (7.B.1)$$

where $1 \leq k \leq N-1$, $\gamma_k = 1 - \sum_{i=1}^{k}\lambda_i = \lambda_0 + \sum_{i=k+1}^{N-1}\lambda_i$, and $\gamma_0 = 1$.

Proof. First we prove that any two states of the set are orthogonal. We start by considering $n > k \geq 1$:

$$\langle\psi_n|\psi_k\rangle \propto e^{-i(\theta_k-\theta_n)}\sqrt{\lambda_k\lambda_n}\left(\lambda_0 - \gamma_n + \sum_{i=n+1}^{N-1}\lambda_i\right)$$
$$= e^{-i(\theta_k-\theta_n)}\sqrt{\lambda_k\lambda_n}\,(\lambda_0 - \gamma_n + \gamma_n - \lambda_0) = 0. \quad (7.B.2)$$

Indeed, the same holds for $1 \leq n < k$. In the same manner, it is easy to show that $\langle\psi_0|\psi_k\rangle = 0\ \forall k$. Lastly, we prove that the states are normalized:

$$\gamma_k\gamma_{k-1}\,\langle\psi_k|\psi_k\rangle = \gamma_k^2 + \lambda_k\left(\lambda_0 + \sum_{i=k+1}^{N-1}\lambda_i\right) = \gamma_k^2 + \lambda_k\gamma_k = \gamma_k\,(\gamma_k + \lambda_k) = \gamma_k\gamma_{k-1}. \quad (7.B.3)$$

□

We remark that when $\lambda_k = 0$, $|\psi_k\rangle = |e_k\rangle$.

Theorem 7.B.1 lets us write down a unitary operator connecting two arbitrary states. Suppose we want to obtain state $|\psi'\rangle$ from state $|\psi\rangle$. As first step, we define the operator

$$U(|\psi\rangle) = \sum_{i=0}^{N-1} |\psi_i\rangle\langle e_i|\,, \quad (7.B.4)$$

which maps the state $|e_0\rangle$ to $|\psi_0\rangle = |\psi\rangle$. If $\lambda_0 = 0$, the state $|\psi_{N-1}\rangle$[61] cannot be properly defined since, e.g., $\gamma_{N-1} = 0$. However, we can write the target state with respect to the basis $\{|\tilde{e}_i\rangle\}_{i=0}^{N-1}$ in which $|\tilde{e}_{i^*}\rangle = |e_0\rangle$ and $|\tilde{e}_0\rangle = |e_{i^*}\rangle$, where i^* is any index value such that $\lambda_{i^*} > 0$, while for $i \neq 0$, i^*, $|\tilde{e}_i\rangle = |e_i\rangle$. Accordingly, we write the states of Theorem 7.B.1 and the corresponding new $\tilde{U}(|\psi\rangle)$ with respect to this new basis. Then, before $\tilde{U}(|\psi\rangle)$, we apply another unitary operator, U_{SWAP}, which swaps the states $|e_0\rangle$ and $|e_{i^*}\rangle$. In this way, when $\lambda_0 = 0$, we can define $U(|\psi\rangle)$ as $U(|\psi\rangle) = \tilde{U}(|\psi\rangle)U_{\text{SWAP}}$, thus assuring the transition $|e_0\rangle \to |\psi\rangle$.

By applying the same reasoning to $|\psi'\rangle$, i.e., $|\psi'\rangle = U(|\psi'\rangle)\,|e_0\rangle$, with the proper modification if for the state $|\psi'\rangle$, $\lambda_0 = 0$, one gets

$$|\psi'\rangle = U(|\psi'\rangle)U^\dagger(|\psi\rangle)\,|\psi\rangle\,. \tag{7.B.5}$$

The transition from $|e_0\rangle$ to $|\psi\rangle$ can be obtained in another way, i.e., by exploiting the composition of elementary two-dimensional rotations. We can write

$$U_R\left(|\psi\rangle\right) \equiv \prod_{i=1}^{N} U_i\left(|\psi\rangle\right), \tag{7.B.6}$$

where, for $1 \leq i < N$[62],

$$U_i = \sqrt{\frac{\gamma_i}{\gamma_{i-1}}}\left(|e_0\rangle\langle e_0| + |e_i\rangle\langle e_i|\right) + \sum_{j\neq 0,i} |e_j\rangle\langle e_j| + \sqrt{\frac{\lambda_i}{\gamma_{i-1}}}\left(e^{i\theta_i}\,|e_i\rangle\langle e_0| - e^{-i\theta_i}\,|e_0\rangle\langle e_i|\right), \tag{7.B.7}$$

while, for $i = N$,

$$U_N = e^{i\theta_0}\,|e_0\rangle\langle e_0| + \sum_{j=1}^{N-1} |e_i\rangle\langle e_i|\,. \tag{7.B.8}$$

To compute the action of U_R we first compute the action of its constituents ($1 \leq i < N$) for $k = 0$ and $k > 0$:

$$\begin{aligned} U_i\,|e_0\rangle &= \sqrt{\frac{\gamma_i}{\gamma_{i-1}}}\,|e_0\rangle + e^{i\theta_i}\sqrt{\frac{\lambda_i}{\gamma_{i-1}}}\,|e_i\rangle\,, \\ U_i\,|e_k\rangle &= \begin{cases} \sqrt{\frac{\gamma_k}{\gamma_{k-1}}}\,|e_k\rangle - e^{-i\theta_k}\sqrt{\frac{\lambda_k}{\gamma_{k-1}}}\,|e_0\rangle\,, & i = k, \\ |e_k\rangle\,, & i \neq k. \end{cases} \end{aligned} \tag{7.B.9}$$

Let us start by studying the action of U_R on the state $|e_0\rangle$. By applying the first $n-1$ matrices U_i[63], the amplitude of $|e_0\rangle$ goes to $\sqrt{\gamma_{n-1}}$ while that of $|e_n\rangle$ remains zero. Then, the application of the n-th U_i matrix makes the amplitude of $|e_0\rangle$ go to $\sqrt{\gamma_n}$ and that of $|e_n\rangle$ from zero to

$$\sqrt{\gamma_{n-1}}e^{i\theta_n}\sqrt{\frac{\lambda_n}{\gamma_{n-1}}} = e^{i\theta_n}\sqrt{\lambda_n}, \tag{7.B.10}$$

[61] And others if there exist other null λ_i in addition to λ_0.
[62] Hereafter we drop the argument $|\psi\rangle$ to lighten the notation.
[63] That is, with i going from 1 to $n-1$ in Eq. (7.B.6).

which is the final amplitude of $|e_n\rangle$ in the state $|\psi\rangle$, and will remain unvaried by the action of the subsequent unitaries U_i with $i > n$. The application of all unitaries but U_N brings the amplitude of $|e_0\rangle$ to $\sqrt{\gamma_{N-1}} = \sqrt{\lambda_0}$. Therefore, since U_N correctly changes the phase of $|e_0\rangle$, it follows that $U_R |e_0\rangle = |\psi\rangle$.

We can also calculate $U_R |e_k\rangle$. First, we notice that

$$U_R |e_k\rangle = \prod_{i=k}^{N} U_i |e_k\rangle , \tag{7.B.11}$$

since the application of the first $k-1$ matrices make no effect. Then,

$$\begin{aligned} \prod_{i=k}^{N-1} U_i |e_k\rangle &= \prod_{i=k+1}^{N-1} U_i \left(\sqrt{\frac{\gamma_k}{\gamma_{k-1}}} |e_k\rangle - e^{-i\theta_k} \sqrt{\frac{\lambda_k}{\gamma_{k-1}}} |e_0\rangle \right) , \\ &= \sqrt{\frac{\gamma_k}{\gamma_{k-1}}} |e_k\rangle - e^{-i\theta_k} \sqrt{\frac{\lambda_k}{\gamma_{k-1}}} \prod_{i=k+1}^{N-1} U_i |e_0\rangle . \end{aligned} \tag{7.B.12}$$

This last term can be computed too:

$$\begin{aligned} \prod_{i=k+1}^{N-1} U_i |e_0\rangle &= \prod_{i=k+2}^{N-1} U_i \left(\sqrt{\frac{\gamma_{k+1}}{\gamma_k}} |e_0\rangle + e^{i\theta_{k+1}} \sqrt{\frac{\lambda_{k+1}}{\gamma_k}} |e_{k+1}\rangle \right) , \\ &= \sqrt{\frac{\gamma_{N-1}}{\gamma_k}} |e_0\rangle + \sum_{i=k+1}^{N-1} e^{i\theta_i} \sqrt{\frac{\lambda_i}{\gamma_k}} |e_i\rangle . \end{aligned} \tag{7.B.13}$$

Eventually, we get[64]

$$U_R |e_k\rangle = \sqrt{\frac{\gamma_k}{\gamma_{k-1}}} |e_k\rangle - e^{i(\theta_0-\theta_k)} \sqrt{\frac{\lambda_0\lambda_k}{\gamma_k\gamma_{k-1}}} |e_0\rangle - \sum_{i=k+1}^{N-1} e^{i(\theta_i-\theta_k)} \sqrt{\frac{\lambda_k\lambda_i}{\gamma_k\gamma_{k-1}}} |e_i\rangle , \tag{7.B.14}$$

which is equal to Eq. (7.B.1). Therefore, we have just shown how the matrix $U(|\psi\rangle)$ is explicitly decomposable as a product of elementary two-dimensional rotations, i.e., $U(|\psi\rangle) = U_R(|\psi\rangle)$.

7.C Minimization of the expended energy in the modified simple thermalization protocol

Here, we show how to find the states minimizing E_{exp} for a fixed entanglement $\mathcal{E}$ in the modified simple approach of section 7.5.1 using the interaction Hamiltonian of Eq. (7.5.9). Since this Hamiltonian can only generate states belonging to the subspace generated by

[64] Also using $\gamma_{N-1} = \lambda_0$.

the kets $|E_i\rangle$, any target state has the form of Eq. (7.4.1). Therefore, we can rewrite the formula of E_{exp}[65] as follows:

$$E_{\text{exp}} = \sum_{i=1}^{N_A-1} \lambda_i E_i + V_M \left(1 - \lambda_0\right) = \sum_{i=1}^{N_A-1} \lambda_i \left(E_i + V_M\right). \tag{7.C.1}$$

The minimization problem can be now easily solved by considering the coefficients λ_i as the coefficients of a thermal state with respect to a fictitious Hamiltonian with eigenvalues $\tilde{E}_i = E_i + V_M$ and $\tilde{E}_0 = 0$[66]. By doing so we get

$$\tilde{\lambda}_i = \frac{e^{-\beta_c \tilde{E}_i}}{\sum_{j=0}^{N_A-1} e^{-\beta_c \tilde{E}_j}}, \tag{7.C.2}$$

where β_c is obtained by requiring that

$$-\sum_{i=0}^{N_A-1} \tilde{\lambda}_i \ln \tilde{\lambda}_i = \mathcal{E}. \tag{7.C.3}$$

7.D Construction of the interaction matrix obtained through a unitary transformation

In the zero-temperature limit, dissipation can be used to generate pure states. If a system is described by a Hamiltonian H_0 with a non-degenerate lowest eigenvalue, dissipation due to the interaction with a zero-temperature bath will generally lead to the ground state of the system [12]. Let us call $\{e_i\}_{i=0}^{N-1}$ an eigenbasis for H_0. For any desired state $|\psi\rangle$ (for simplicity, we only consider states with $\lambda_0 > 0$), by using a proper unitary operator $U(|\psi\rangle)$ defined as in Eq. (7.B.4), it is possible to write an Hermitian operator $H'(|\psi\rangle) = U(|\psi\rangle)H_0U^\dagger(|\psi\rangle)$ such that $|\psi\rangle$ is the ground state of H':

$$H'(|\psi\rangle) = U(|\psi\rangle)H_0U^\dagger(|\psi\rangle) = \sum_{i=0}^{N-1} e_i \left|\psi_i\right\rangle\!\left\langle\psi_i\right|, \tag{7.D.1}$$

where e_i runs over all the eigenvalues of H_0, i.e., with respect to the notation of the main text of this chapter, e_i is a shorthand for all combinations of $A_j + B_k$, for all A_j and B_k, and with $e_0 = E_0 = A_0 + B_0$. Writing $H' = H_0 + H_I$[67], we obtain

$$H_I = \sum_{i=0}^{N-1} e_i \Big(\left|\psi_i\right\rangle\!\left\langle\psi_i\right| - \left|e_i\right\rangle\!\left\langle e_i\right| \Big). \tag{7.D.2}$$

[65] See Eq. (7.5.11), where we set $E_0 = 0$ for simplicity of notation.
[66] See section 7.1.2.
[67] We drop the explicit dependence on $|\psi\rangle$ to lighten the notation.

We can explicitly find the coefficients of the Hamiltonian H_I by calculating $U(|\psi\rangle)_{ik} = \langle e_i|U(|\psi\rangle)|e_k\rangle = \langle e_i|\psi_k\rangle$[68]. For $k \geq 1$, using Eq. (7.B.1), we get:

$$\langle e_i|\psi_k\rangle = \begin{cases} -e^{i(\theta_0-\theta_k)}\sqrt{\frac{\lambda_0\lambda_k}{\gamma_k\gamma_{k-1}}}, & i=0, \\ 0, & 0<i<k, \\ \sqrt{\frac{\gamma_k}{\gamma_{k-1}}}, & i=k, \\ -e^{i(\theta_i-\theta_k)}\sqrt{\frac{\lambda_i\lambda_k}{\gamma_k\gamma_{k-1}}}, & i>k. \end{cases} \tag{7.D.3}$$

Let us start from the diagonal elements. For $j=0$ we get

$$\langle e_0|H_I|e_0\rangle = e_0(\lambda_0-1) + \lambda_0 \sum_{i=1}^{N-1} \frac{\lambda_i e_i}{\gamma_i\gamma_{i-1}}, \tag{7.D.4}$$

while for $j>0$ we have

$$\langle e_j|H_I|e_j\rangle = \lambda_j \left(e_0 - \frac{e_j}{\gamma_{j-1}} + \sum_{k=1}^{j-1} \frac{\lambda_k e_k}{\gamma_k\gamma_{k-1}} \right). \tag{7.D.5}$$

Since H_I is an Hermitian matrix, it suffices to continue the calculations by analyzing the $j>i\geq 0$ case. For $j>i=0$ we get

$$\langle e_0|H_I|e_j\rangle = e^{i(\theta_0-\theta_j)}\sqrt{\lambda_0\lambda_j} \left(e_0 - \frac{e_j}{\gamma_{j-1}} + \sum_{k=1}^{j-1} \frac{\lambda_k e_k}{\gamma_k\gamma_{k-1}} \right), \tag{7.D.6}$$

while for $j>i>0$ we have

$$\langle e_i|H_I|e_j\rangle = \sum_{k=0}^{N-1} e_k \langle e_i|\psi_k\rangle\langle\psi_k|e_j\rangle = e^{i(\theta_i-\theta_j)}\sqrt{\lambda_i\lambda_j} \left(e_0 - \frac{e_i}{\gamma_{i-1}} + \sum_{k=1}^{i-1} \frac{\lambda_k e_k}{\gamma_k\gamma_{k-1}} \right). \tag{7.D.7}$$

By focusing on the case in which the target states are like those of Eq. (7.4.1), we get Eq. (7.5.15).

7.E Efficiency and expended energy for the global unitary approach

In this Appendix, we obtain the general formulas for the efficiency and expended energy of the global unitary approach by using their definition of Eq. (7.5.1).

By using Eqs. (7.D.1), (7.D.2), and (7.D.3) in Eq. (7.5.1), we get

$$\eta = \frac{e_0(\lambda_0-1) + \sum_{i=1}^{N-1}\lambda_i e_i}{2e_0(\lambda_0-1) + \sum_{i=1}^{N-1}\lambda_i e_i\left[1+\lambda_0/\left(\gamma_i\gamma_{i-1}\right)\right]}. \tag{7.E.1}$$

[68] Compare with Eq. (7.B.4).

If we set $e_0 = 0$, which can always be done by adding a constant term to H_0, we get

$$\eta = \frac{\sum_{i=1}^{N-1} \lambda_i e_i}{\sum_{i=1}^{N-1} \lambda_i e_i \left[1 + \lambda_0 / \left(\gamma_i \gamma_{i-1}\right)\right]}, \tag{7.E.2}$$

which makes clear that $\eta < 1$, as it should be. When considering target states like those of Eq. (7.4.1), the efficiency of Eq. (7.E.2) and the denominator therein appearing become, respectively, the efficiency and the energy expense reported in Eq. (7.5.16).

Now, we prove that E^S_{exp} [see Eq. (7.5.1)] cannot be higher than $2(e_{N-1} - e_0)$ in the global unitary approach:

$$\begin{aligned} E^S_{\text{exp}} &= \langle e_0|H_I|e_0\rangle - \langle\psi|H_I|\psi\rangle \\ &= \langle e_0|(H_I + H_0 - H_0)|e_0\rangle - \langle\psi|(H_I + H_0 - H_0)|\psi\rangle \\ &= \langle e_0|UH_0U^\dagger|e_0\rangle - e_0 - \langle\psi|UH_0U^\dagger|\psi\rangle + \langle\psi|H_0|\psi\rangle \\ &= \langle e_0|\Big(UH_0U^\dagger + U^\dagger H_0 U\Big)|e_0\rangle - 2e_0 \leq 2e_{N-1} - 2e_0, \end{aligned} \tag{7.E.3}$$

where the last inequality comes from the invariance of the spectrum for unitary transformations.

7.F Efficiency and expended energy in the MSSG unitary approaches

Here, we want to calculate the quantities of Eq. (7.5.1) in the case of the states obtainable within the MSSG unitary approaches, i.e., states $|\phi\rangle$ of the form of Eq. (7.4.1). In these approaches, a state $|\phi\rangle$ is obtained by applying U_A or U_B to $|E_0\rangle$ and then the corresponding generalized CNOT gate[69] is applied to the resulting state on system S. Let us focus on the U_A case, where

$$H_I = U_{G_A} U_A H_0 U_A^\dagger U_{G_A}^\dagger - H_0. \tag{7.F.1}$$

First, we notice that $U_{G_A}|A_0B_i\rangle = U_{G_A}^\dagger|A_0B_i\rangle = |A_0B_i\rangle$. Therefore, using also Eqs. (7.4.8) and (7.D.3) applied to the calculation of $\left\langle A_i \middle| \psi_k^A \right\rangle$, we obtain

$$\langle E_0|H_I|E_0\rangle = \langle A_0|U_A H_A U_A^\dagger|A_0\rangle + B_0 - E_0 = A_0\left(\lambda_0 - 1\right) + \lambda_0 \sum_{i=1}^{N_A-1} \frac{\lambda_i A_i}{\gamma_i \gamma_{i-1}}. \tag{7.F.2}$$

Then, we calculate

$$\langle\phi|H_I|\phi\rangle = E_0\left(1 - \lambda_0\right) - \sum_{i=1}^{N_A-1} \lambda_i E_i. \tag{7.F.3}$$

[69] See Eqs. (7.4.13) and (7.4.14).

Eventually, the expended energy in this case is equal to

$$E^A_{\text{exp}} = \sum_{i=1}^{N_A-1} \left[\lambda_i \left(E_i + \frac{\lambda_0 A_i}{\gamma_i \gamma_{i-1}}\right)\right] - (A_0 + E_0)(1-\lambda_0)\,. \tag{7.F.4}$$

Now, we show that the expended energy within the global approach is higher that in the MSSG unitary approaches when they generate the same state $|\phi\rangle$. The expended energy in the global approach can be written as[70]

$$E^S_{\text{exp}} = \sum_{i=1}^{N_A-1} \lambda_i E_i \left[1 + \frac{\lambda_0}{\gamma_i \gamma_{i-1}}\right] - 2E_0(1-\lambda_0)\,, \tag{7.F.5}$$

and the difference between E^S_{exp} and E^A_{exp} is equal to

$$E^S_{\text{exp}} - E^A_{\text{exp}} = \lambda_0 \sum_{i=1}^{N_A-1} \frac{\lambda_i B_i}{\gamma_i \gamma_{i-1}} - B_0(1-\lambda_0)\,. \tag{7.F.6}$$

Since we can set $B_0 = 0$ without changing the above quantity, we conclude that the MSSG version of the protocol always performs better than the global one. The derivation of E^B_{exp} is similar since, analogously to the previous case, $U_{G_B}|A_iB_0\rangle = U^\dagger_{G_B}|A_iB_0\rangle = |A_iB_0\rangle$, and leads to the same expression of Eq. (7.F.4) with the quantities A_i and B_i swapped between them.

To complete the analysis we also write the difference regarding the expended energy in the two MSSG approaches:

$$E^B_{\text{exp}} - E^A_{\text{exp}} = \lambda_0 \sum_{i=1}^{N_A-1} \frac{\lambda_i (B_i - A_i)}{\gamma_i \gamma_{i-1}} - (B_0 - A_0)(1-\lambda_0)\,. \tag{7.F.7}$$

In this case, which approach is better depends both on the target state and the spectra of H_A and H_B.

7.G Explicit calculations for two qubits

In this Appendix, we explicitly calculate the three unitary transformations proposed in section 7.4 and the interaction Hamiltonians proposed in section 7.5 for the archetypical example of a bipartite system composed of two qubits, having as free Hamiltonians

$$H_A = \frac{\hbar\omega_A}{2}\sigma_z^A, \qquad H_B = \frac{\hbar\omega_B}{2}\sigma_z^B, \tag{7.G.1}$$

where σ_z^X is the z-Pauli matrix of qubit X ($X = A, B$). As basis for H_0 we use $\{|00\rangle, |01\rangle, |10\rangle, |11\rangle\}$, where, for each qubit, $\sigma_z^X|1\rangle = |1\rangle$ and $\sigma_z^X|0\rangle = -|0\rangle$. Let

[70] Compare with Eq. (7.E.1) applied to a state $|\phi\rangle$.

us define $\omega = (\omega_A + \omega_B)/2$, then the MEES for a two qubit system, as reported in section 7.1.4, and considering arbitrary phases, is given by

$$|\psi_g\rangle = e^{i\theta_0}\sqrt{\lambda}\,|00\rangle + e^{i\theta_1}\sqrt{1-\lambda}\,|11\rangle\,, \quad \text{where} \quad \lambda = \frac{1}{1+e^{-2\beta\hbar\omega}}. \tag{7.G.2}$$

Starting from Eqs. (7.4.3), (7.4.8), (7.4.13), and (7.4.14)[71], straightforward calculations for U_S, $\tilde{U}_A = U_{G_A}U_A$, and $\tilde{U}_B = U_{G_B}U_B$ give

$$U_S = \begin{pmatrix} e^{i\theta_0}\sqrt{\lambda} & 0 & 0 & -e^{i\Delta\theta}\sqrt{1-\lambda} \\ 0 & 1 & 0 & 0 \\ 0 & 0 & 1 & 0 \\ e^{i\theta_1}\sqrt{1-\lambda} & 0 & 0 & \sqrt{\lambda} \end{pmatrix}, \tag{7.G.3}$$

$$\tilde{U}_A = \begin{pmatrix} e^{i\theta_0}\sqrt{\lambda} & 0 & -e^{i\Delta\theta}\sqrt{1-\lambda} & 0 \\ 0 & e^{i\theta_0}\sqrt{\lambda} & 0 & -e^{i\Delta\theta}\sqrt{1-\lambda} \\ 0 & e^{i\theta_1}\sqrt{1-\lambda} & 0 & \sqrt{\lambda} \\ e^{i\theta_1}\sqrt{1-\lambda} & 0 & \sqrt{\lambda} & 0 \end{pmatrix}, \tag{7.G.4}$$

and

$$\tilde{U}_B = \begin{pmatrix} e^{i\theta_0}\sqrt{\lambda} & -e^{i\Delta\theta}\sqrt{1-\lambda} & 0 & 0 \\ 0 & 0 & e^{i\theta_1}\sqrt{1-\lambda} & \sqrt{\lambda} \\ 0 & 0 & e^{i\theta_0}\sqrt{\lambda} & -e^{i\Delta\theta}\sqrt{1-\lambda} \\ e^{i\theta_1}\sqrt{1-\lambda} & \sqrt{\lambda} & 0 & 0 \end{pmatrix}, \tag{7.G.5}$$

where $\Delta\theta = \theta_0 - \theta_1$. We can see, explicitly, that the three unitary operators proposed in section 7.4 are different.

Regarding the thermalization approach, we can immediately write down the interaction Hamiltonian obtained through the simple approach:

$$H_I^{\text{si}} = \begin{pmatrix} \hbar\omega - V_S\lambda & 0 & 0 & -e^{i\Delta\theta}V_S\sqrt{\lambda(1-\lambda)} \\ 0 & \hbar\delta_A & 0 & 0 \\ 0 & 0 & \hbar\delta_B & 0 \\ -e^{-i\Delta\theta}V_S\sqrt{\lambda(1-\lambda)} & 0 & 0 & -V_S(1-\lambda) - \hbar\omega \end{pmatrix}, \tag{7.G.6}$$

where $\delta_A = (\omega_A - \omega_B)/2$ and $\delta_B = (\omega_B - \omega_A)/2$. For comparison, the modified simple approach leads to

$$\tilde{H}_I^{\text{si}} = \begin{pmatrix} \hbar\omega - V_M\lambda & 0 & 0 & -e^{i\Delta\theta}V_M\sqrt{\lambda(1-\lambda)} \\ 0 & 0 & 0 & 0 \\ 0 & 0 & 0 & 0 \\ -e^{-i\Delta\theta}V_M\sqrt{\lambda(1-\lambda)} & 0 & 0 & -V_M(1-\lambda) - \hbar\omega \end{pmatrix}, \tag{7.G.7}$$

which lacks the diagonal terms $\hbar\delta_A$ et $\hbar\delta_B$.

[71] Notice that U_B is defined analogously to what done in Eq. (7.4.8).

Turning to the zero-temperature approach based on the global unitary transformation, the use of U_S leads to

$$H_I^S = 2\hbar\omega \begin{pmatrix} 1-\lambda & 0 & 0 & -e^{i\Delta\theta}\sqrt{\lambda(1-\lambda)} \\ 0 & 0 & 0 & 0 \\ 0 & 0 & 0 & 0 \\ -e^{-i\Delta\theta}\sqrt{\lambda(1-\lambda)} & 0 & 0 & \lambda-1 \end{pmatrix}. \tag{7.G.8}$$

Even if this Hamiltonian is similar to that of Eq. (7.G.7), it is not the same one. This was predictable since the modified simple approach changes the spectrum of H_0 while all unitary ones do not. Moreover, it does not exist a number c such that $\tilde{H}_I^{\text{si}} = cH_I^S$ so that the two Hamiltonians cannot describe the same physics even with a rescaling of the energy.

Moving to the MSSG thermalization approaches, the use of $\tilde{U}_A$ leads, for $H_I^A/(\hbar\omega_A)$, to

$$\begin{pmatrix} 1-\lambda & 0 & 0 & -e^{i\Delta\theta}\sqrt{\lambda(1-\lambda)} \\ 0 & 1-\lambda & -e^{i\Delta\theta}\sqrt{\lambda(1-\lambda)} & 0 \\ 0 & -e^{-i\Delta\theta}\sqrt{\lambda(1-\lambda)} & \lambda-1+\frac{\omega_B}{\omega_A} & 0 \\ -e^{-i\Delta\theta}\sqrt{\lambda(1-\lambda)} & 0 & 0 & \lambda-1-\frac{\omega_B}{\omega_A} \end{pmatrix}, \tag{7.G.9}$$

while the use of $\tilde{U}_B$ for $H_I^B/(\hbar\omega_B)$ to

$$\begin{pmatrix} 1-\lambda & 0 & 0 & -e^{i\Delta\theta}\sqrt{\lambda(1-\lambda)} \\ 0 & \lambda-1+\frac{\omega_A}{\omega_B} & -e^{-i\Delta\theta}\sqrt{\lambda(1-\lambda)} & 0 \\ 0 & -e^{i\Delta\theta}\sqrt{\lambda(1-\lambda)} & 1-\lambda & 0 \\ -e^{-i\Delta\theta}\sqrt{\lambda(1-\lambda)} & 0 & 0 & \lambda-1-\frac{\omega_A}{\omega_B} \end{pmatrix}. \tag{7.G.10}$$

Since all of these interaction Hamiltonians are different[72], we can conclude that the five methods give rise to physically different interactions.

At the beginning of section 7.5, the following interaction Hamiltonian was proposed to make $|\psi_g\rangle$ the ground state

$$H_I^{\text{emp}} = \frac{\hbar g}{2}\left(\sigma_x^A\sigma_x^B - \sigma_y^A\sigma_y^B\right), \tag{7.G.11}$$

where σ_i^X are Pauli operators on system X with $i = x, y$. The matrix structure of this operator is

$$H_I^{\text{emp}} = \hbar g \begin{pmatrix} 0 & 0 & 0 & 1 \\ 0 & 0 & 0 & 0 \\ 0 & 0 & 0 & 0 \\ 1 & 0 & 0 & 0 \end{pmatrix}, \tag{7.G.12}$$

which lacks the diagonal terms present in all the general approaches we provided. Therefore, the methods that we presented in this chapter cannot be used to obtain this empirical Hamiltonian.

[72] Even considering rescaling.

Chapter 8

Conclusions and perspectives

In this Thesis, we have dealt with different setups in which dissipation or quantum correlations (or both) play an important role. The content of this Thesis can be summarized as follows. After providing the necessary background and context (chapter 2), we have concentrated on thermodynamic setups in the first part of the thesis (chapters 3 and 4). In particular, in chapters 3, we have studied a work extraction protocol onto a bipartite system exploiting a single bath using a work quantifier from thermodynamic resource theory (TRT), which has turned out to be connected with the internal correlations of the system, and two-stroke thermal cycles based on non-resonant exchange Hamiltonians, where we have taken into account the role of the waiting times, i.e., of the required relaxation times plus other times inherent to the specific machine at hand. In the second part (chapters 5 and 6), we have focused on the open dynamics of two different systems: a driven harmonic oscillator in a possibly non-Markovian collisional environment and the Dicke model with two-photon coupling in the bad-cavity limit. For the former, which is still in the *work in progress* phase, we have been able to derive a nonadiabatic Markovian master equation in the continuous limit of the collision model while, for the non-Markovian case, we have made its computation easier by exploiting the Markovian embedding technique. For the latter, we have found, for the first time, an effective master equation describing the collective dynamics of the qubits in a quite general setup, and we have shown how the new features of this dynamics can bring advantages with respect to the correspondent one-photon dynamics, for example, by strengthening the collective quantum effects called superradiance and subradiance. Finally, in the last part of the thesis (chapter 7), we have connected the entanglement and the energy of non-interacting arbitrary bipartite systems, also identifying what we have called the minimum energy entangles states (MEESs), i.e., the states having the minimum amount of energy for a given amount of entanglement, and showing methods to generate them. These states turn out to be connected to other, apparently unrelated, physics fields, and we show how they can be used to improve the energetic efficiency of different quantum information protocols.

Let us now discuss our results more in detail and focus on future research that can stem from them. In chapter 3, we have analyzed the work extraction from a resource system

R to a bipartite storage system S, based on the thermalization of the latter. We have first described this without referring to a specific implementation, argued that it should be easily implementable because of its simplicity, and used TRT results to quantify the extracted work W and the efficiency η. We have then applied this protocol to two models: a simple two-qubit system and a system described by the Rabi Hamiltonian. In both cases, entropic terms turned out to play an important role when the temperature (times the Boltzmann constant) is comparable with the subsystems energies. Moreover, we have shown that a great part of the extracted work is stored in the bipartite system internal correlations. Notably, the extracted work is comparable with the systems frequencies, and, in the Rabi model case, the efficiency is always higher than one half. Finally, as a proof of principle, we have shown how the energy extracted after one cycle of the thermalization protocol (single-shot extraction protocol) can be transferred to an external work storage system through a transfer process, which makes the complete protocol iterable. Thus, we have pointed out that simple processes like thermalization and the switching on/off of interactions between quantum systems can be exploited as a potential resource for thermal machines. We believe it would be interesting to generalize our study of the Rabi model to the case of N qubits interacting with a harmonic oscillator. This will allow one to study if the correlations built among the qubits allow for a greater work extraction. Finally, further studies could suggest how to improve our transfer protocol and pave the way to proposals in specific physical scenarios.

In chapter 4, we have examined two different two-stroke quantum thermal machines. In both, two collections of identical systems with evenly spaced non-variable energy levels can be put in contact, respectively, with a cold and a hot thermal bath. Because of the evenly spaced energy levels, we can characterize each system through a single frequency. In the first version, a system of a collection interacts with a system of the other one, and then they thermalize. In the second one, we have added a mediator system that interacts alternately with one or more systems of each collection. Assuming that the interaction Hamiltonian conserves the number of excitations during the interaction, we have shown that the efficiency depends only on the frequencies of the two collections in both versions of the cycle. We have then analyzed the problem of power maximization in the cycle without the mediator, focusing on the high impact of the waiting time on the optimal collision time and the optimal frequencies. When maximizing over the frequencies, we have shown that it is possible to exceed the Curzon-Ahlborn efficiency when using qubits while it is not possible with harmonic oscillators. Next, we have added the mediator, and we have shown that its addition can bring performance advantages when the waiting time of the corresponding cycle without the mediator is of the same order of the collision time. In most other cases, the cycle without mediator performs better. However, there could be experimental platforms where it is easier to implement the cycle with the mediator. Finally, we have compared the first version of our cycle with two examples of Otto cycles enhanced by shortcuts to adiabaticity. The comparison has shown that one does not need high coupling ($g \gg \omega_c, \omega_h$)[1] to obtain a power output comparable to that of the

[1]Here, g is the coupling strength during the collision between the systems of the two collections while ω_c and ω_h are, respectively, the frequencies of the cold and hot collections.

Otto cycle with shortcuts to adiabaticity at maximum power. Future research directions include the possibility of multiple mediators with or without time-dependent frequencies.

In chapter 5, we have dealt with a driven harmonic oscillator in contact with a collisional environment which can be studied both in the Markovian and non-Markovian cases. To investigate this setup, we employed the Gaussian state formalism, assuming all the first moments equal to zero. In the Markovian case, we have managed to derive a nonadiabatic master equation in the continuous limit of the collision model by using two different techniques leading to similar results. In the non-Markovian case, we have made use of the Markovian embedding technique to compute the dynamics of the open quantum system, which we have then studied for the non-driven harmonic oscillator case. Moreover, we have used a quantifier of non-Markovianity developed specifically for harmonic oscillators in Gaussian states and showed that it presents peaks of non-Markovianity in correspondence of the usual non-Markovian oscillations of the excitation number of the open system. This quantifier should let us to distinguish between fluctuations due to non-Markovianity and those due to the driving when studying the driven harmonic in the non-Markovian case. Although the results of this work are still partial, we deem they are encouraging since they seem to well reflect other results found in literature for non-collision models and include the appearance of a nonadiabatic time-dependent term in the master equation we have derived in the Markovian case.

Chapter 6 deals with the two-photon Dicke model in the bad-cavity limit. In particular, we have studied the case of a damped harmonic oscillator interacting with N qubits via a two-photon coupling in the bad-cavity limit in the presence of finite temperature baths, a coherent pumping on the harmonic oscillator, and an incoherent pumping on the qubits, comparing it to the one-photon coupling case. We have succeeded in applying a recent adiabatic elimination technique in the two-photon model to derive a reduced master equation governing the collective evolution of the qubits. This presents two fundamental differences compared to the dipolar case: an enhancement of the spontaneous-like emission rate, including a thermal contribution and a quadratic term in the coherent driving, and an increased temperature of the effective bath experienced by the qubits. This novel phenomenology makes it possible to accelerate the generation of non-diagonal steady states and to observe a drastic change of the temperature-dependent behavior of quantum collective phenomena, leading to a stronger resilience of these phenomena to high temperatures. We finally remark that the models here investigated can be feasibly implemented with both atomic and solid-state existing quantum technologies (see section 2.4.2). In particular, we have provided an example of a possible implementation with superconducting circuits of the two-photon coupling Hamiltonian (see Appendix 6.A). Different research lines can be seen as natural extensions of this work. First of all, finding the approximate dynamics of the harmonic oscillator in the presence of the qubits can help us describe the harmonic oscillator output in experiments. Secondly, a direct generalization of our results would consist of deriving the qubits effective dynamics when they are not resonant with the harmonic oscillator. Lastly, the limit of a large number of qubits could be explored to see if there are significant differences compared to the dipolar Dicke model in the same limit.

Finally, chapter 7 is entirely dedicated to the connection between energy and entanglement, with a focus on the MEESs. There, we have found the minimum and maximum permitted energy of an arbitrary finite and non-interacting bipartite system for a given quantity of entanglement, and we have called the states saturating the lower bounds MEESs. Next, we have proposed several protocols to generate MEESs. Three of these protocols are based on the direct use of unitary operators, while five others exploit a zero-temperature thermalization for their realization. The usefulness of generating MEESs through unitary operations is first confirmed by a numerical investigation about the energy distribution of entangled pure states. We have found that, in all the studied configurations, MEESs are extremely rare except for the two-qubit case and bipartite systems with a highly degenerate spectrum. Notably, two of the unitary protocols can be decomposed as the product of simple two-level local rotations and of a local change of phase on a subsystem and, subsequently, a generalized CNOT gate on the bipartite system. Therefore, these implementation of these two unitary transformations in quantum circuits should be easier compared to another unitary transformation that we have identified, based on a global approach. On the other hand, for the five different zero-temperature thermalization based protocols, we have compared their performances when applied to MEESs and generic target states, showing that MEESs practically represent the best target states in terms of the energy cost for their generation. MEESs can be important in quantum technologies since, fixed the degree of entanglement necessary for a certain application, they allow one to convert in entanglement the least amount of energy. They appear even more important in the light of our numerical simulations, showing that the energy required for the energy-entanglement conversion is higher for the majority of states. A natural but difficult extension of this research consists of finding the MEESs for the general case of interacting bipartite systems.

To conclude, we believe that the results presented in this Thesis shed light on various aspects of how dissipative processes can be treated and exploited, and on the interplay between quantum correlations and other physical parameters in both isolated and open quantum systems. In different parts of the Thesis we have made connections among the various topics investigated in the Thesis. However, further interlacing among them can be sought off, for example by searching for generation of MEESs through structured collisional environments or by trying to obtain MEESs as the output of a thermal cycle. Collision models could be also used to obtain another point of view on the two-photon Dicke model, by re-visiting the same model of chapter 6 with the substitution of the phenomenological approach with a collisional one.

Bibliography

[1] A. Einstein, B. Podolsky, and N. Rosen. "Can Quantum-Mechanical Description of Physical Reality Be Considered Complete?" In: *Phys. Rev.* 47 (1935), pp. 777–780.

[2] J. P. Dowling and G. J. Milburn. "Quantum technology: the second quantum revolution". In: *Philos. Trans. Royal Soc. A* 361 (2003), pp. 1655–1674.

[3] C. H. Bennett, G. Brassard, C. Crépeau, R. Jozsa, A. Peres, and W. K. Wootters. "Teleporting an unknown quantum state via dual classical and Einstein-Podolsky-Rosen channels". In: *Phys. Rev. Lett.* 70 (1993), pp. 1895–1899.

[4] D. Bouwmeester, J.-W. Pan, K. Mattle, M. Eibl, H. Weinfurter, and A. Zeilinger. "Experimental quantum teleportation". In: *Nature* 390 (1997), pp. 575–579.

[5] A. Furusawa, J. L. Sørensen, S. L. Braunstein, C. A. Fuchs, H. J. Kimble, and E. S. Polzik. "Unconditional quantum teleportation". In: *Science* 282 (1998), pp. 706–709.

[6] A. K. Ekert. "Quantum cryptography based on Bell's theorem". In: *Phys. Rev. Lett.* 67 (1991), pp. 661–663.

[7] C. H. Bennett. "Quantum cryptography using any two nonorthogonal states". In: *Phys. Rev. Lett.* 68 (1992), pp. 3121–3124.

[8] N. Gisin, G. Ribordy, W. Tittel, and H. Zbinden. "Quantum cryptography". In: *Rev. Mod. Phys.* 74 (2002), pp. 145–195.

[9] L.-M. Duan, M. D. Lukin, J. I. Cirac, and P. Zoller. "Long-distance quantum communication with atomic ensembles and linear optics". In: *Nature* 414 (2001), pp. 413–418.

[10] M. A. Nielsen and I. L. Chuang. *Quantum Computation and Quantum Information: 10th Anniversary Edition*. Cambridge University Press, 2010.

[11] M. Hotta, J. Matsumoto, and G. Yusa. "Quantum energy teleportation without a limit of distance". In: *Phys. Rev. A* 89 (2014), p. 012311.

[12] H.-P. Breuer and F. Petruccione. *The Theory of Open quantum systems*. Oxford University Press, New York, 2007.

[13] B. Bellomo, R. Lo Franco, and G. Compagno. "Non-Markovian Effects on the Dynamics of Entanglement". In: *Phys. Rev. Lett.* 99 (2007), p. 160502.

[14] D. Chruściński and S. Pascazio. "A brief history of the GKLS equation". In: *Open Syst. Inf. Dyn.* 24 (2017), p. 1740001.

[15] V. Gorini, A. Kossakowski, and E. C. G. Sudarshan. "Completely positive dynamical semigroups of N-level systems". In: *J. Math. Phys.* 17 (1976), pp. 821–825.

[16] G. Lindblad. "On the generators of quantum dynamical semigroups". In: *Commun. Math. Phys.* 48 (1976), pp. 119–130.

[17] C. H. Bennett, F. Bessette, G. Brassard, L. Salvail, and J. Smolin. "Experimental quantum cryptography". In: *J. Cryptol.* 5 (1992), pp. 3–28.

[18] J. Preskill. "Quantum Computing in the NISQ era and beyond". In: *Quantum* 2 (2018), p. 79.

[19] F. Arute, K. Arya, R. Babbush, D. Bacon, J. C. Bardin, R. Barends, R. Biswas, S. Boixo, F. G. Brandao, D. A. Buell, et al. "Quantum supremacy using a programmable superconducting processor". In: *Nature* 574 (2019), pp. 505–510.

[20] F. Binder, L. Correa, C. Gogolin, J. Anders, and G. Adesso. *Thermodynamics in the Quantum Regime*. Springer International Publishing, 2018.

[21] P. Kirton, M. M. Roses, J. Keeling, and E. G. Dalla Torre. "Introduction to the Dicke Model: From Equilibrium to Nonequilibrium, and *Vice Versa*". In: *Adv. Quantum Technol.* 2 (2019), p. 1800043.

[22] S. Haroche and J.-M. Raimond. *Exploring The Quantum: Atoms, Cavities, and Photons*. Oxford University Press, 2006.

[23] M. B. Plenio, S. F. Huelga, A. Beige, and P. L. Knight. "Cavity-loss-induced generation of entangled atoms". In: *Phys. Rev. A* 59 (1999), pp. 2468–2475.

[24] D. Braun. "Creation of Entanglement by Interaction with a Common Heat Bath". In: *Phys. Rev. Lett.* 89 (2002), p. 277901.

[25] F. Benatti, R. Floreanini, and M. Piani. "Environment Induced Entanglement in Markovian Dissipative Dynamics". In: *Phys. Rev. Lett.* 91 (2003), p. 070402.

[26] F Benatti and R Floreanini. "Entangling oscillators through environment noise". In: *Journal of Physics A: Mathematical and General* 39 (2006), pp. 2689–2699.

[27] B. Bellomo, R. Lo Franco, S. Maniscalco, and G. Compagno. "Entanglement trapping in structured environments". In: *Phys. Rev. A* 78 (2008), p. 060302(R).

[28] A. Sarlette, J. M. Raimond, M. Brune, and P. Rouchon. "Stabilization of Nonclassical States of the Radiation Field in a Cavity by Reservoir Engineering". In: *Phys. Rev. Lett.* 107 (2011), p. 010402.

[29] H. Krauter, C. A. Muschik, K. Jensen, W. Wasilewski, J. M. Petersen, J. I. Cirac, and E. S. Polzik. "Entanglement Generated by Dissipation and Steady State Entanglement of Two Macroscopic Objects". In: *Phys. Rev. Lett.* 107 (2011), p. 080503.

[30] B. Bellomo and M. Antezza. "Steady entanglement out of thermal equilibrium". In: *Europhys. Lett.* 104 (2013), p. 10006.

[31] B. Bellomo and M. Antezza. "Nonequilibrium dissipation-driven steady many-body entanglement". In: *Phys. Rev. A* 91 (2015), p. 042124.

[32] R. Azouit, F. Chittaro, A. Sarlette, and P. Rouchon. "Towards generic adiabatic elimination for bipartite open quantum systems". In: *Quantum Sci. Technol.* 2 (2017), p. 044011.

[33] R. Azouit. "Adiabatic elimination for open quantum systems". Doctoral dissertation. PSL Research University, 2017.

[34] R. Horodecki, P. Horodecki, M. Horodecki, and K. Horodecki. "Quantum entanglement". In: *Rev. Mod. Phys.* 81 (2009), pp. 865–942.

[35] H. Ollivier and W. H. Zurek. "Quantum Discord: A Measure of the Quantumness of Correlations". In: *Phys. Rev. Lett.* 88 (2001), p. 017901.

[36] L Henderson and V Vedral. "Classical, quantum and total correlations". In: *J. Phys. A: Math. Theor.* 34 (2001), pp. 6899–6905.

[37] J. S. Bell. "On the Einstein Podolsky Rosen paradox". In: *Phys. Phys. Fiz.* 1 (1964), pp. 195–200.

[38] J. F. Clauser, M. A. Horne, A. Shimony, and R. A. Holt. "Proposed Experiment to Test Local Hidden-Variable Theories". In: *Phys. Rev. Lett.* 23 (1969), pp. 880–884.

[39] S. J. Freedman and J. F. Clauser. "Experimental Test of Local Hidden-Variable Theories". In: *Phys. Rev. Lett.* 28 (1972), pp. 938–941.

[40] A. Aspect, J. Dalibard, and G. Roger. "Experimental Test of Bell's Inequalities Using Time-Varying Analyzers". In: *Phys. Rev. Lett.* 49 (1982), pp. 1804–1807.

[41] B. Hensen *et al.* "Loophole-free Bell inequality violation using electron spins separated by 1.3 kilometres". In: *Nature* 526 (2015), pp. 682–686.

[42] L. D. Landau and E. Lifshitz. *Quantum Mechanics: Non-Relativistic Theory.* Elsevier, 1981.

[43] V. B. Braginsky and F. Y. Khalili. *Quantum Measurement.* Cambridge University Press, 1992.

[44] H. Nakazato, T. Takazawa, and K. Yuasa. "Purification through Zeno-Like Measurements". In: *Phys. Rev. Lett.* 90 (2003), p. 060401.

[45] B. Militello and A. Messina. "Distilling angular momentum nonclassical states in trapped ions". In: *Phys. Rev. A* 70 (2004), p. 033408.

[46] B. Militello, K. Yuasa, H. Nakazato, and A. Messina. "Influence of dissipation on the extraction of quantum states via repeated measurements". In: *Phys. Rev. A* 76 (2007), p. 042110.

[47] B. Bellomo, G. Compagno, H. Nakazato, and K. Yuasa. "Extraction of a squeezed state in a field mode via repeated measurements on an auxiliary quantum particle". In: *Phys. Rev. A* 80 (2009), p. 052113.

[48] B. Bellomo, G. Compagno, H. Nakazato, and K. Yuasa. "Distillation by repeated measurements: Continuous spectrum case". In: *Phys. Rev. A* 82 (2010), 060101(R).

[49] H. Bechmann-Pasquinucci and A. Peres. "Quantum Cryptography with 3-State Systems". In: *Phys. Rev. Lett.* 85 (2000), pp. 3313–3316.

[50] S. S. Bullock, D. P. O'Leary, and G. K. Brennen. "Asymptotically Optimal Quantum Circuits for d-Level Systems". In: *Phys. Rev. Lett.* 94 (2005), p. 230502.

[51] G. Vallone, V. D'Ambrosio, A. Sponselli, S. Slussarenko, L. Marrucci, F. Sciarrino, and P. Villoresi. "Free-Space Quantum Key Distribution by Rotation-Invariant Twisted Photons". In: *Phys. Rev. Lett.* 113 (2014), p. 060503.

[52] X.-Y. Yan, N.-R. Zhou, L.-H. Gong, Y.-Q. Wang, and X.-J. Wen. "High-dimensional quantum key distribution based on qudits transmission with quantum Fourier transform". In: *Quantum Inf. Process.* 18 (2019), p. 271.

[53] E. O. Kiktenko, A. S. Nikolaeva, P. Xu, G. V. Shlyapnikov, and A. K. Fedorov. "Scalable quantum computing with qudits on a graph". In: *Phys. Rev. A* 101 (2020), p. 022304.

[54] B. P. Lanyon, M. Barbieri, M. P. Almeida, T. Jennewein, T. C. Ralph, K. J. Resch, G. J. Pryde, J. L. O'Brien, A. Gilchrist, and A. G. White. "Simplifying quantum logic using higher-dimensional Hilbert spaces". In: *Nat. Phys.* 5 (2009), p. 134.

[55] L. Neves, G. Lima, J. G. Aguirre Gómez, C. H. Monken, C. Saavedra, and S. Pádua. "Generation of Entangled States of Qudits using Twin Photons". In: *Phys. Rev. Lett.* 94 (2005), p. 100501.

[56] M. Kues *et al.* "On-chip generation of high-dimensional entangled quantum states and their coherent control". In: *Nature* 546 (2017), p. 622.

[57] C. Godfrin, A. Ferhat, R. Ballou, S. Klyatskaya, M. Ruben, W. Wernsdorfer, and F. Balestro. "Operating Quantum States in Single Magnetic Molecules: Implementation of Grover's Quantum Algorithm". In: *Phys. Rev. Lett.* 119 (2017), p. 187702.

[58] M. S. Blok, V. V. Ramasesh, T. Schuster, K. O'Brien, J. M. Kreikebaum, D. Dahlen, A. Morvan, B. Yoshida, N. Y. Yao, and I. Siddiqi. "Quantum Information Scrambling in a Superconducting Qutrit Processor". In: *arXiv:2003.03307* (2020).

[59] M. Kues, C. Reimer, P. Roztocki, L. R. Cortés, S. Sciara, B. Wetzel, Y. Zhang, A. Cino, S. T. Chu, B. E. Little, et al. "On-chip generation of high-dimensional entangled quantum states and their coherent control". In: *Nature* 546 (2017), p. 622.

[60] C. Reimer, S. Sciara, P. Roztocki, M. Islam, L. R. Cortés, Y. Zhang, B. Fischer, S. Loranger, R. Kashyap, A. Cino, et al. "High-dimensional one-way quantum processing implemented on d-level cluster states". In: *Nat. Phys.* 15 (2019), pp. 148–153.

[61] P. Imany, J. A. Jaramillo-Villegas, M. S. Alshaykh, J. M. Lukens, O. D. Odele, A. J. Moore, D. E. Leaird, M. Qi, and A. M. Weiner. "High-dimensional optical quantum logic in large operational spaces". In: *npj Quantum Inf.* 5 (2019), p. 59.

[62] C. Wilmott. "On swapping the states of two qudits". In: *Int. J. Quantum Inf.* 09 (2011), pp. 1511–1517.

[63] X. Gao, M. Krenn, J. Kysela, and A. Zeilinger. "Arbitrary d-dimensional Pauli X gates of a flying qudit". In: *Phys. Rev. A* 99 (2019), p. 023825.

[64] T.-A. Isdrailă, C. Kusko, and R. Ionicioiu. "Cyclic permutations for qudits in d dimensions". In: *Sci. Rep.* 9 (2019), p. 6337.

[65] P. J. Low, B. M. White, A. A. Cox, M. L. Day, and C. Senko. "Practical trapped-ion protocols for universal qudit-based quantum computing". In: *Phys. Rev. Research* 2 (2020), p. 033128.

[66] M.-H. Yung and S. Bose. "Perfect state transfer, effective gates, and entanglement generation in engineered bosonic and fermionic networks". In: *Phys. Rev. A* 71 (2005), p. 032310.

[67] J. Fulconis, O. Alibart, J. L. O'Brien, W. J. Wadsworth, and J. G. Rarity. "Nonclassical Interference and Entanglement Generation Using a Photonic Crystal Fiber Pair Photon Source". In: *Phys. Rev. Lett.* 99 (2007), p. 120501.

[68] Y. Lin, J. P. Gaebler, F. Reiter, T. R. Tan, R. Bowler, A. S. Sørensen, D. Leibfried, and D. J. Wineland. "Dissipative production of a maximally entangled steady state of two quantum bits". In: *Nature* 504 (2013), pp. 415–418.

[69] B. Bellomo, R. Lo Franco, and G. Compagno. "N identical particles and one particle to entangle them all". In: *Phys. Rev. A* 96 (2017), p. 022319.

[70] X.-Y. Luo, Y.-Q. Zou, L.-N. Wu, Q. Liu, M.-F. Han, M. K. Tey, and L. You. "Deterministic entanglement generation from driving through quantum phase transitions". In: *Science* 355 (2017), pp. 620–623.

[71] B. Çakmak, S. Campbell, B. Vacchini, Ö. E. Müstecaplıoğlu, and M. Paternostro. "Robust multipartite entanglement generation via a collision model". In: *Phys. Rev. A* 99 (2019), p. 012319.

[72] A. Z. Goldberg and D. F. V. James. "Entanglement generation via diffraction". In: *Phys. Rev. A* 100 (2019), p. 042332.

[73] A. Castellini, B. Bellomo, G. Compagno, and R. Lo Franco. "Activating remote entanglement in a quantum network by local counting of identical particles". In: *Phys. Rev. A* 99 (2019), p. 062322.

[74] D. J. Egger, M. Ganzhorn, G. Salis, A. Fuhrer, P. Müller, P. Kl. Barkoutsos, N. Moll, I. Tavernelli, and S. Filipp. "Entanglement Generation in Superconducting Qubits Using Holonomic Operations". In: *Phys. Rev. Applied* 11 (2019), p. 014017.

[75] O. Katz, R. Shaham, E. S. Polzik, and O. Firstenberg. "Long-Lived Entanglement Generation of Nuclear Spins Using Coherent Light". In: *Phys. Rev. Lett.* 124 (2020), p. 043602.

[76] Y. Xi, T. Zhang, Z.-J. Zheng, X. Li-Jost, and S.-M. Fei. "Converting quantum coherence to genuine multipartite entanglement and nonlocality". In: *Phys. Rev. A* 100 (2019), p. 022310.

[77] K. Korzekwa, C. T. Chubb, and M. Tomamichel. "Avoiding Irreversibility: Engineering Resonant Conversions of Quantum Resources". In: *Phys. Rev. Lett.* 122 (2019), p. 110403.

[78] F. Bakhshinezhad, F. Clivaz, G. Vitagliano, P. Erker, A. Rezakhani, M. Huber, and N. Friis. "Thermodynamically optimal creation of correlations". In: *J. Phys. A: Math. Theor.* 52 (2019), p. 465303.

[79] N. Piccione, B. Militello, A. Napoli, and B. Bellomo. "Energy bounds for entangled states". In: *Phys. Rev. Research* 2 (2020), 022057(R).

[80] J. Ikonen, J. Salmilehto, and M. Möttönen. "Energy-efficient quantum computing". In: *npj Quantum Inf.* 3 (2017), p. 17.

[81] F. Galve and E. Lutz. "Energy cost and optimal entanglement production in harmonic chains". In: *Phys. Rev. A* 79 (2009), p. 032327.

[82] C. Bény, C. T. Chubb, T. Farrelly, and T. J. Osborne. "Energy cost of entanglement extraction in complex quantum systems". In: *Nat. Commun.* 9 (2018), p. 3792.

[83] L. Hackl and R. H. Jonsson. "Minimal energy cost of entanglement extraction". In: *Quantum* 3 (2019), p. 165.

[84] G. Chiribella and Y. Yang. "Optimal quantum operations at zero energy cost". In: *Phys. Rev. A* 96 (2017), p. 022327.

[85] E. Chitambar and G. Gour. "Quantum resource theories". In: *Rev. Mod. Phys.* 91 (2019), p. 025001.

[86] M. Lostaglio. "The resource theory of quantum thermodynamics". Doctoral dissertation. Imperial College London, 2016.

[87] M. A. Nielsen. "Conditions for a Class of Entanglement Transformations". In: *Phys. Rev. Lett.* 83 (1999), pp. 436–439.

[88] G. Vidal. "Entanglement of Pure States for a Single Copy". In: *Phys. Rev. Lett.* 83 (1999), pp. 1046–1049.

[89] F. D. Cunden, P. Facchi, G. Florio, and G. Gramegna. "Volume of the set of LOCC-convertible quantum states". In: *J. Phys. A: Math. Theor.* 53 (2020), p. 175303.

[90] C. H. Bennett, H. J. Bernstein, S. Popescu, and B. Schumacher. "Concentrating partial entanglement by local operations". In: *Phys. Rev. A* 53 (1996), pp. 2046–2052.

[91] G. Vidal. "Entanglement monotones". In: *J. Mod. Opt.* 47 (2000), pp. 355–376.

[92] M. B. Plenio and S. Virmani. "An Introduction to Entanglement Measures". In: *Quantum Inf. Comput.* 7 (2007), pp. 1–51.

[93] H.-P. Breuer, E.-M. Laine, J. Piilo, and B. Vacchini. "Colloquium: Non-Markovian dynamics in open quantum systems". In: *Rev. Mod. Phys.* 88 (2016), p. 021002.

[94] H.-P. Breuer, E.-M. Laine, and J. Piilo. "Measure for the Degree of Non-Markovian Behavior of Quantum Processes in Open Systems". In: *Phys. Rev. Lett.* 103 (2009), p. 210401.

[95] P. Siegle, I. Goychuk, P. Talkner, and P. Hänggi. "Markovian embedding of non-Markovian superdiffusion". In: *Phys. Rev. E* 81 (2010), p. 011136.

[96] D. Tamascelli, A. Smirne, S. F. Huelga, and M. B. Plenio. "Nonperturbative Treatment of non-Markovian Dynamics of Open Quantum Systems". In: *Phys. Rev. Lett.* 120 (2018), p. 030402.

[97] F. Mascherpa, A. Smirne, A. D. Somoza, P. Fernández-Acebal, S. Donadi, D. Tamascelli, S. F. Huelga, and M. B. Plenio. "Optimized auxiliary oscillators for the simulation of general open quantum systems". In: *Phys. Rev. A* 101 (2020), p. 052108.

[98] A. A. Budini. "Embedding non-Markovian quantum collisional models into bipartite Markovian dynamics". In: *Phys. Rev. A* 88 (2013), p. 032115.

[99] S. Campbell, F. Ciccarello, G. M. Palma, and B. Vacchini. "System-environment correlations and Markovian embedding of quantum non-Markovian dynamics". In: *Phys. Rev. A* 98 (2018), p. 012142.

[100] R. Vasile, S. Maniscalco, M. G. A. Paris, H.-P. Breuer, and J. Piilo. "Quantifying non-Markovianity of continuous-variable Gaussian dynamical maps". In: *Phys. Rev. A* 84 (2011), p. 052118.

[101] G. Torre, W. Roga, and F. Illuminati. "Non-Markovianity of Gaussian Channels". In: *Phys. Rev. Lett.* 115 (2015), p. 070401.

[102] J. Jin and C. shui Yu. "Non-Markovianity in the collision model with environmental block". In: *New J. Phys.* 20 (2018), p. 053026.

[103] Q. Zhang, Z.-X. Man, and Y.-J. Xia. "Non-Markovianity in the presence of multiple thermal environments via collision model". In: *Phys. Lett. A* 383 (2019), pp. 2456 –2461.

[104] M. Scala, B. Militello, A. Messina, J. Piilo, and S. Maniscalco. "Microscopic derivation of the Jaynes-Cummings model with cavity losses". In: *Phys. Rev. A* 75 (2007), p. 013811.

[105] G. L. Giorgi, A. Saharyan, S. Guérin, D. Sugny, and B. Bellomo. "Microscopic and phenomenological models of driven systems in structured reservoirs". In: *Phys. Rev. A* 101 (2020), p. 012122.

[106] R. Bonifacio, P. Schwendimann, and F. Haake. "Quantum Statistical Theory of Superradiance. I". In: *Phys. Rev. A* 4 (1971), pp. 302–313.

[107] R. Bonifacio, P. Schwendimann, and F. Haake. "Quantum Statistical Theory of Superradiance. II". In: *Phys. Rev. A* 4 (1971), pp. 854–864.

[108] S. Popescu, A. J. Short, and A. Winter. "Entanglement and the foundations of statistical mechanics". In: *Nat. Phys.* 2 (2006), p. 754758.

[109] J. Gemmer, A. Otte, and G. Mahler. "Quantum Approach to a Derivation of the Second Law of Thermodynamics". In: *Phys. Rev. Lett.* 86 (2001), pp. 1927–1930.

[110] J. Gemmer, M. Michel, and G. Mahler. *Quantum Thermodynamics*. Springer-Verlag Berlin Heidelberg, 2009.

[111] S. Vinjanampathy and J. Anders. "Quantum thermodynamics". In: *Contemp. Phys.* 57 (2016), pp. 545–579.

[112] J. Roßnagel, S. T. Dawkins, K. N. Tolazzi, O. Abah, E. Lutz, F. Schmidt-Kaler, and K. Singer. "A single-atom heat engine". In: *Science* 352 (2016), pp. 325–329.

[113] H. T. Quan, Y.-x. Liu, C. P. Sun, and F. Nori. "Quantum thermodynamic cycles and quantum heat engines". In: *Phys. Rev. E* 76 (2007), p. 031105.

[114] H. T. Quan, Y. D. Wang, Y. X. Liu, C. P. Sun, and F. Nori. "Maxwell's demon assisted thermodynamic cycle in superconducting quantum circuits". In: *Phys. Rev. Lett.* 97 (2006), p. 180402.

[115] S. W. Kim, T. Sagawa, S. De Liberato, and M. Ueda. "Quantum Szilard Engine". In: *Phys. Rev. Lett.* 106 (2011), p. 070401.

[116] T. E. Humphrey, R. Newbury, R. P. Taylor, and H. Linke. "Reversible Quantum Brownian Heat Engines for Electrons". In: *Phys. Rev. Lett.* 89 (2002), p. 116801.

[117] B. Leggio, B. Bellomo, and M. Antezza. "Quantum thermal machines with single nonequilibrium environments". In: *Phys. Rev. A* 91 (2015), p. 012117.

[118] M. James and X. André. "Perspective on quantum thermodynamics". In: *New J. Phys.* 18 (2016), p. 11002.

[119] A. Hewgill, A. Ferraro, and G. De Chiara. "Quantum correlations and thermodynamic performances of two-qubit engines with local and common baths". In: *Phys. Rev. A* 98 (2018), p. 042102.

[120] M. Horodecki and J. Oppenheim. "Fundamental limitations for quantum and nanoscale thermodynamics". In: *Nat. Commun.* 4 (2013), p. 2059.

[121] P. Skrzypczyk, A. J. Short, and S. Popescu. "Work extraction and thermodynamics for individual quantum systems". In: *Nat. Commun.* 5 (2014), pp. 1–8.

[122] M. Lostaglio, Á. M. Alhambra, and C. Perry. "Elementary Thermal Operations". In: *Quantum* 2 (2018), p. 52.

[123] C. Perry, P. Ćwikliński, J. Anders, M. Horodecki, and J. Oppenheim. "A Sufficient Set of Experimentally Implementable Thermal Operations for Small Systems". In: *Phys. Rev. X* 8 (2018), p. 041049.

[124] M. T. Mitchison. "Quantum thermal absorption machines: refrigerators, engines and clocks". In: *Contemp. Phys.* 60 (2019), pp. 164–187.

[125] S. Deffner and S. Campbell. *Quantum Thermodynamics: An introduction to the thermodynamics of quantum information*. Morgan & Claypool Publishers, 2019.

[126] F. L. Curzon and B. Ahlborn. "Efficiency of a Carnot engine at maximum power output". In: *Am. J. Phys.* 43 (1975), pp. 22–24.

[127] C. Van den Broeck. "Thermodynamic Efficiency at Maximum Power". In: *Phys. Rev. Lett.* 95 (2005), p. 190602.

[128] M. Esposito, K. Lindenberg, and C. Van den Broeck. "Universality of Efficiency at Maximum Power". In: *Phys. Rev. Lett.* 102 (2009), p. 130602.

[129] M. Esposito, R. Kawai, K. Lindenberg, and C. Van den Broeck. "Efficiency at Maximum Power of Low-Dissipation Carnot Engines". In: *Phys. Rev. Lett.* 105 (2010), p. 150603.

[130] J. Wang, Z. Ye, Y. Lai, W. Li, and J. He. "Efficiency at maximum power of a quantum heat engine based on two coupled oscillators". In: *Phys. Rev. E* 91 (2015), p. 062134.

[131] N. Shiraishi, K. Saito, and H. Tasaki. "Universal Trade-Off Relation between Power and Efficiency for Heat Engines". In: *Phys. Rev. Lett.* 117 (2016), p. 190601.

[132] N. Shiraishi and H. Tajima. "Efficiency versus speed in quantum heat engines: Rigorous constraint from Lieb-Robinson bound". In: *Phys. Rev. E* 96 (2017), p. 022138.

[133] A. E. Allahverdyan, K. Hovhannisyan, and G. Mahler. "Optimal refrigerator". In: *Phys. Rev. E* 81 (2010), p. 051129.

[134] M. Campisi, J. Pekola, and R. Fazio. "Nonequilibrium fluctuations in quantum heat engines: theory, example, and possible solid state experiments". In: *New J. Phys.* 17 (2015), p. 035012.

[135] F. G. S. L. Brandao, M. Horodecki, N. H. Y. Ng, J. Oppenheim, and S. Wehner. "The second laws of quantum thermodynamics". In: *Proc. Natl. Acad. Sci.* 112 (2015), 3275 LP –3279.

[136] M. Lostaglio, D. Jennings, and T. Rudolph. "Description of quantum coherence in thermodynamic processes requires constraints beyond free energy". In: *Nat. Commun.* 6 (2015).

[137] R. Gallego, J. Eisert, and H. Wilming. "Thermodynamic work from operational principles". In: *New J. Phys.* 18 (2016), p. 103017.

[138] H. Wilming, R. Gallego, and J. Eisert. "Axiomatic Characterization of the Quantum Relative Entropy and Free Energy". In: *Entropy* 19 (2017), p. 241.

[139] M. Campisi, P. Hänggi, and P. Talkner. "Colloquium: Quantum fluctuation relations: Foundations and applications". In: *Rev. Mod. Phys.* 83 (2011), pp. 771–791.

[140] M. Perarnau-Llobet, E. Bäumer, K. V. Hovhannisyan, M. Huber, and A. Acin. "No-Go Theorem for the Characterization of Work Fluctuations in Coherent Quantum Systems". In: *Phys. Rev. Lett.* 118 (2017), p. 070601.

[141] H. E. D. Scovil and E. O. Schulz-DuBois. "Three-Level Masers as Heat Engines". In: *Phys. Rev. Lett.* 2 (1959), pp. 262–263.

[142] O. Abah and E. Lutz. "Energy efficient quantum machines". In: *Europhys. Lett.* 118 (2017), p. 40005.

[143] B. Çakmak and O. E. Müstecaplğlu. "Spin quantum heat engines with shortcuts to adiabaticity". In: *Phys. Rev. E* 99 (2019), p. 032108.

[144] O. Abah, M. Paternostro, and E. Lutz. "Shortcut-to-adiabaticity quantum Otto refrigerator". In: *Phys. Rev. Research* 2 (2020), p. 023120.

[145] S. Campbell and S. Deffner. "Trade-Off Between Speed and Cost in Shortcuts to Adiabaticity". In: *Phys. Rev. Lett.* 118 (2017), p. 100601.

[146] Y.-X. Du, Z.-T. Liang, Y.-C. Li, X.-X. Yue, Q.-X. Lv, W. Huang, X. Chen, H. Yan, and S.-L. Zhu. "Experimental realization of stimulated Raman shortcut-to-adiabatic passage with cold atoms". In: *Nat. Comm.* 7 (2016), pp. 1–7.

[147] B. B. Zhou, A. Baksic, H. Ribeiro, C. G. Yale, F. J. Heremans, P. C. Jerger, A. Auer, G. Burkard, A. A. Clerk, and D. D. Awschalom. "Accelerated quantum control using superadiabatic dynamics in a solid-state lambda system". In: *Nat. Phys.* 13 (2017), pp. 330–334.

[148] A. Serafini. *Quantum Continuous Variables: A Primer of Theoretical Methods*. CRC Press, 2017.

[149] S. D. Bartlett, B. C. Sanders, S. L. Braunstein, and K. Nemoto. "Efficient Classical Simulation of Continuous Variable Quantum Information Processes". In: *Phys. Rev. Lett.* 88 (2002), p. 097904.

[150] G. Adesso, S. Ragy, and A. R. Lee. "Continuous Variable Quantum Information: Gaussian States and Beyond". In: *Open Syst. Inf. Dyn.* 21 (2014), p. 1440001.

[151] B. Reid. "Cold Atoms & Heat Engines: Effective Control of Quantum Motional States of Matter". Doctoral dissertation. Queen's University Belfast, 2018.

[152] D. Braak. "Integrability of the Rabi Model". In: *Phys. Rev. Lett.* 107 (2011), p. 100401.

[153] Q. Xie, H. Zhong, M. T. Batchelor, and C. Lee. "The quantum Rabi model: solution and dynamics". In: *J. Phys. A: Math. Theor.* 50 (2017), p. 113001.

[154] F. Yoshihara, T. Fuse, S. Ashhab, K. Kakuyanagi, S. Saito, and K. Semba. "Superconducting qubit-oscillator circuit beyond the ultrastrong-coupling regime". In: *Nat. Phys.* 13 (2017), pp. 44–47.

[155] F. Beaudoin, J. M. Gambetta, and A. Blais. "Dissipation and ultrastrong coupling in circuit QED". In: *Phys. Rev. A* 84 (2011), p. 043832.

[156] Y. Wang and J. Y. Haw. "Bridging the gap between the Jaynes–Cummings and Rabi models using an intermediate rotating wave approximation". In: *Phys. Lett. A* 379 (2015), pp. 779 –786.

[157] J. Casanova, G. Romero, I. Lizuain, J. J. García-Ripoll, and E. Solano. "Deep Strong Coupling Regime of the Jaynes-Cummings Model". In: *Phys. Rev. Lett.* 105 (2010), p. 263603.

[158] N. K. Langford, R. Sagastizabal, M. Kounalakis, C. Dickel, A. Bruno, F. Luthi, D. J. Thoen, A. Endo, and L. Dicarlo. "Experimentally simulating the dynamics of quantum light and matter at deep-strong coupling". In: *Nat. Commun.* 8 (2017).

[159] C. Maissen, G. Scalari, F. Valmorra, M. Beck, J. Faist, S. Cibella, R. Leoni, C. Reichl, C. Charpentier, and W. Wegscheider. "Ultrastrong coupling in the near field of complementary split-ring resonators". In: *Phys. Rev. B* 90 (2014), p. 205309.

[160] E. K. Irish. "Generalized Rotating-Wave Approximation for Arbitrarily Large Coupling". In: *Phys. Rev. Lett.* 99 (2007), p. 173601.

[161] Q.-H. Chen, C. Wang, S. He, T. Liu, and K.-L. Wang. "Exact solvability of the quantum Rabi model using Bogoliubov operators". In: *Phys. Rev. A* 86 (2012), p. 023822.

[162] F. Beaudoin, J. M. Gambetta, and A. Blais. "Dissipation and ultrastrong coupling in circuit QED". In: *Phys. Rev. A* 84 (2011), p. 043832.

[163] M. G. Benedict. *Super-radiance: Multiatomic Coherent Emission*. CRC Press, 1996.

[164] M. Gross and S. Haroche. "Superradiance: An essay on the theory of collective spontaneous emission". In: *Phys. Rep.* 93 (1982), p. 301.

[165] D. Meiser, J. Ye, D. R. Carlson, and M. J. Holland. "Prospects for a Millihertz-Linewidth Laser". In: *Phys. Rev. Lett.* 102 (2009), p. 163601.

[166] D. Meiser and M. J. Holland. "Steady-state superradiance with alkaline-earth-metal atoms". In: *Phys. Rev. A* 81 (2010), p. 033847.

[167] D. Meiser and M. J. Holland. "Intensity fluctuations in steady-state superradiance". In: *Phys. Rev. A* 81 (2010), p. 063827.

[168] A Auffèves, D Gerace, S Portolan, A Drezet, and M. F. Santos. "Few emitters in a cavity: from cooperative emission to individualization". In: *New J. Phys.* 13 (2011), p. 093020.

[169] N. Shammah, N. Lambert, F. Nori, and S. De Liberato. "Superradiance with local phase-breaking effects". In: *Phys. Rev. A* 96 (2017), p. 023863.

[170] P. Kirton and J. Keeling. "Superradiant and lasing states in driven-dissipative Dicke models". In: *New J. Phys.* 20 (2018), p. 015009.

[171] N. Shammah, S. Ahmed, N. Lambert, S. De Liberato, and F. Nori. "Open quantum systems with local and collective incoherent processes: Efficient numerical simulations using permutational invariance". In: *Phys. Rev. A* 98 (2018), p. 063815.

[172] F. Damanet, A. J. Daley, and J. Keeling. "Atom-only descriptions of the driven-dissipative Dicke model". In: *Phys. Rev. A* 99 (2019), p. 033845.

[173] I. D. Leroux, M. H. Schleier-Smith, and V. Vuletić. "Implementation of Cavity Squeezing of a Collective Atomic Spin". In: *Phys. Rev. Lett.* 104 (2010), p. 073602.

[174] G. Tóth and I. Apellaniz. "Quantum metrology from a quantum information science perspective". In: *J. Phys. A: Math. Theor.* 47 (2014), p. 424006.

[175] F. Jahnke, C. Gies, M. Aßmann, M. Bayer, H. Leymann, A. Foerster, J. Wiersig, C. Schneider, M. Kamp, and S. Höfling. "Giant photon bunching, superradiant pulse emission and excitation trapping in quantum-dot nanolasers". In: *Nat. Commun.* 7 (2016), p. 11540.

[176] A. Asenjo-Garcia, M. Moreno-Cardoner, A. Albrecht, H. J. Kimble, and D. E. Chang. "Exponential Improvement in Photon Storage Fidelities Using Subradiance and "Selective Radiance" in Atomic Arrays". In: *Phys. Rev. X* 7 (2017), p. 031024.

[177] F. J. Garcia-Vidal and J. Feist. "Long-distance operator for energy transfer". In: *Science* 357 (2017), pp. 1357–1358.

[178] A. Goban, C.-L. Hung, J. D. Hood, S.-P. Yu, J. A. Muniz, O. Painter, and H. J. Kimble. "Superradiance for Atoms Trapped along a Photonic Crystal Waveguide". In: *Phys. Rev. Lett.* 115 (2015), p. 063601.

[179] R. G. DeVoe and R. G. Brewer. "Observation of Superradiant and Subradiant Spontaneous Emission of Two Trapped Ions". In: *Phys. Rev. Lett.* 76 (1996), pp. 2049–2052.

[180] S. D. Jenkins, J. Ruostekoski, N. Papasimakis, S. Savo, and N. I. Zheludev. "Many-Body Subradiant Excitations in Metamaterial Arrays: Experiment and Theory". In: *Phys. Rev. Lett.* 119 (2017), p. 053901.

[181] V. N. Pustovit and T. V. Shahbazyan. "Cooperative emission of light by an ensemble of dipoles near a metal nanoparticle: The plasmonic Dicke effect". In: *Phys. Rev. Lett.* 102 (2009), p. 077401.

[182] A. Angerer et al. "Superradiant emission from colour centres in diamond". In: *Nat. Phys.* 14 (2018), p. 1168.

[183] M. Scheibner, T. Schmidt, L. Worschech, A. Forchel, G. Bacher, T. Passow, and D. Hommel. "Superradiance of quantum dots". In: *Nat. Phys.* 3 (2007), p. 106.

[184] J. A. Mlynek, A. A. Abdumalikov, C. Eichler, and A. Wallraff. "Observation of Dicke superradiance for two artificial atoms in a cavity with high decay rate". In: *Nat. Commun.* 5 (2014), p. 5186.

[185] S. Felicetti, D. Z. Rossatto, E. Rico, E. Solano, and P. Forn-Díaz. "Two-photon quantum Rabi model with superconducting circuits". In: *Phys. Rev. A* 97 (2018), p. 013851.

[186] S. Felicetti, M.-J. Hwang, and A. Le Boité. "Ultrastrong-coupling regime of nondipolar light-matter interactions". In: *Phys. Rev. A* 98 (2018), p. 053859.

[187] S. Felicetti, J. S. Pedernales, I. L. Egusquiza, G. Romero, L. Lamata, D. Braak, and E. Solano. "Spectral collapse via two-phonon interactions in trapped ions". In: *Phys. Rev. A* 92 (2015), p. 033817.

[188] X.-H. Cheng, I. Arrazola, J. S. Pedernales, L. Lamata, X. Chen, and E. Solano. "Nonlinear quantum Rabi model in trapped ions". In: *Phys. Rev. A* 97 (2018), p. 023624.

[189] R. Puebla, J. Casanova, O. Houhou, E. Solano, and M. Paternostro. "Quantum simulation of multiphoton and nonlinear dissipative spin-boson models". In: *Phys. Rev. A* 99 (2019), p. 032303.

[190] P. Schneeweiss, A. Dareau, and C. Sayrin. "Cold-atom-based implementation of the quantum Rabi model". In: *Phys. Rev. A* 98 (2018), 021801(R).

[191] A. Dareau, Y. Meng, P. Schneeweiss, and A. Rauschenbeutel. "Observation of Ultrastrong Spin-Motion Coupling for Cold Atoms in Optical Microtraps". In: *Phys. Rev. Lett.* 121 (2018), p. 253603.

[192] J. Goetz, F. Deppe, K. G. Fedorov, P. Eder, M. Fischer, S. Pogorzalek, E. Xie, A. Marx, and R. Gross. "Parity-Engineered Light-Matter Interaction". In: *Phys. Rev. Lett.* 121 (2018), p. 060503.

[193] D. Lv, S. An, Z. Liu, J.-N. Zhang, J. S. Pedernales, L. Lamata, E. Solano, and K. Kim. "Quantum Simulation of the Quantum Rabi Model in a Trapped Ion". In: *Phys. Rev. X* 8 (2018), p. 021027.

[194] F. Minganti, N. Bartolo, J. Lolli, W. Casteels, and C. Ciuti. "Exact results for Schrödinger cats in driven-dissipative systems and their feedback control". In: *Sci. Rep.* 6 (2016), p. 26987.

[195] M. Malekakhlagh and A. W. Rodriguez. "Quantum Rabi Model with Two-Photon Relaxation". In: *Phys. Rev. Lett.* 122 (2019), p. 043601.

[196] Z. Leghtas et al. "Confining the state of light to a quantum manifold by engineered two-photon loss". In: *Science* 347 (2015), pp. 853–857.

[197] I. Travěnec. "Solvability of the two-photon Rabi Hamiltonian". In: *Phys. Rev. A* 85 (2012), p. 043805.

[198] L. Duan, Y.-F. Xie, D. Braak, and Q.-H. Chen. "Two-photon Rabi model: analytic solutions and spectral collapse". In: *J. Phys. A: Math. Theor.* 49 (2016), p. 464002.

[199] A. J. Maciejewski and T. Stachowiak. "A novel approach to the spectral problem in the two photon Rabi model". In: *J. Phys. A: Math. Theor.* 50 (2017), p. 244003.

[200] Y.-F. Xie, L. Duan, and Q.-H. Chen. "Generalized quantum Rabi model with both one- and two-photon terms: A concise analytical study". In: *Phys. Rev. A* 99 (2019), p. 013809.

[201] L. Cong, X.-M. Sun, M. Liu, Z.-J. Ying, and H.-G. Luo. "Polaron picture of the two-photon quantum Rabi model". In: *Phys. Rev. A* 99 (2019), p. 013815.

[202] R. J. A. Rico, F. H. Maldonado-Villamizar, and B. M. Rodriguez-Lara. "Spectral collapse in the two-photon quantum Rabi model". In: *Phys. Rev. A* 101 (2020), p. 063825.

[203] F. Zou, X.-Y. Zhang, X.-W. Xu, J.-F. Huang, and J.-Q. Liao. "Multiphoton blockade in the two-photon Jaynes-Cummings model". In: *Phys. Rev. A* 102 (2020), p. 053710.

[204] L. Garbe, I. L. Egusquiza, E. Solano, C. Ciuti, T. Coudreau, P. Milman, and S. Felicetti. "Superradiant phase transition in the ultrastrong-coupling regime of the two-photon Dicke model". In: *Phys. Rev. A* 95 (2017), p. 053854.

[205] X.-Y. Chen and Y.-Y. Zhang. "Finite-size scaling analysis in the two-photon Dicke model". In: *Phys. Rev. A* 97 (2018), p. 053821.

[206] S. Cui, F. Hébert, B. Grémaud, V. G. Rousseau, W. Guo, and G. G. Batrouni. "Two-photon Rabi-Hubbard and Jaynes-Cummings-Hubbard models: Photon-pair superradiance, Mott insulator, and normal phases". In: *Phys. Rev. A* 100 (2019), p. 033608.

[207] L. Garbe, P. Wade, F. Minganti, N. Shammah, S. Felicetti, and F. Nori. "Dissipation-induced bistability in the two-photon Dicke model". In: *Sci. Rep.* 10 (2020), p. 13408.

[208] S. Cui, B. Grémaud, W. Guo, and G. G. Batrouni. "Nonlinear two-photon Rabi-Hubbard model: Superradiance, photon, and photon-pair Bose-Einstein condensates". In: *Phys. Rev. A* 102 (2020), p. 033334.

[209] C. J. Villas-Boas and D. Z. Rossatto. "Multiphoton Jaynes-Cummings Model: Arbitrary Rotations in Fock Space and Quantum Filters". In: *Phys. Rev. Lett.* 122 (2019), p. 123604.

[210] J. Casanova, R. Puebla, H. Moya-Cessa, and M. B. Plenio. "Connecting nth order generalised quantum Rabi models: Emergence of nonlinear spin-boson coupling via spin rotations". In: *Npj Quantum Inf.* 4 (2018), p. 47.

[211] C. A. González-Gutiérrez and J. M. Torres. "Atomic Bell measurement via two-photon interactions". In: *Phys. Rev. A* 99 (2019), p. 023854.

[212] T. Kadowaki and H. Nishimori. "Quantum annealing in the transverse Ising model". In: *Phys. Rev. E* 58 (1998), pp. 5355–5363.

[213] C. M. Dawson and M. A. Nielsen. "Frustration, interaction strength, and ground-state entanglement in complex quantum systems". In: *Phys. Rev. A* 69 (2004), p. 052316.

[214] G. L. Deçordi and A. Vidiella-Barranco. "Two coupled qubits interacting with a thermal bath: A comparative study of different models". In: *Opt. Commun.* 387 (2017), pp. 366–376.

[215] K. Maruyama, F. Nori, and V. Vedral. "Colloquium: The physics of Maxwell's demon and information". In: *Rev. Mod. Phys.* 81 (2009), pp. 1–23.

[216] J. Johansson, P. Nation, and F. Nori. "QuTiP: An open-source Python framework for the dynamics of open quantum systems". In: *Comp. Phys. Comm.* 183 (2012), pp. 1760 –1772.

[217] J. Johansson, P. Nation, and F. Nori. "QuTiP 2: A Python framework for the dynamics of open quantum systems". In: *Comp. Phys. Comm.* 184 (2013), pp. 1234 –1240.

[218] M. Esposito, K. Lindenberg, and C. V. den Broeck. "Entropy production as correlation between system and reservoir". In: *New J. Phys.* 12 (2010), p. 013013.

[219] R. Uzdin, A. Levy, and R. Kosloff. "Quantum Heat Machines Equivalence, Work Extraction beyond Markovianity, and Strong Coupling via Heat Exchangers". In: *Entropy* 18 (2016), p. 124.

[220] R. Dann, A. Tobalina, and R. Kosloff. "Shortcut to Equilibration of an Open Quantum System". In: *Phys. Rev. Lett.* 122 (2019), p. 250402.

[221] R. Dann, A. Tobalina, and R. Kosloff. "Fast route to equilibration". In: *Phys. Rev. A* 101 (2020), p. 052102.

[222] R. Dann and R. Kosloff. "Quantum signatures in the quantum Carnot cycle". In: *New J. Phys.* 22 (2020), p. 013055.

[223] N. Pancotti, M. Scandi, M. T. Mitchison, and M. Perarnau-Llobet. "Speed-Ups to Isothermality: Enhanced Quantum Thermal Machines through Control of the System-Bath Coupling". In: *Phys. Rev. X* 10 (2020), p. 031015.

[224] P. Menczel, T. Pyhäranta, C. Flindt, and K. Brandner. "Two-stroke optimization scheme for mesoscopic refrigerators". In: *Phys. Rev. B* 99 (2019), p. 224306.

[225] O. A. D. Molitor and G. T. Landi. "Stroboscopic two-stroke quantum heat engines". In: *Phys. Rev. A* 102 (2020), p. 042217.

[226] A. Hewgill, A. Ferraro, and G. De Chiara. "Quantum correlations and thermodynamic performances of two-qubit engines with local and common baths". In: *Phys. Rev. A* 98 (2018), p. 042102.

[227] A. Manatuly, W. Niedenzu, R. Román-Ancheyta, B. Çakmak, Ö. E. Müstecaplıoğlu, and G. Kurizki. "Collectively enhanced thermalization via multiqubit collisions". In: *Phys. Rev. E* 99 (2019), p. 042145.

[228] D. Heineken, K. Beyer, K. Luoma, and W. T. Strunz. "Quantum memory enhanced dissipative entanglement creation in non-equilibrium steady states". In: *arXiv:2008.04359* (2020).

[229] B. Reid, S. Pigeon, M. Antezza, and G. D. Chiara. "A self-contained quantum harmonic engine". In: *Europhys. Lett.* 120 (2017), p. 60006.

[230] G. D. Chiara, G. Landi, A. Hewgill, B. Reid, A. Ferraro, A. J. Roncaglia, and M. Antezza. "Reconciliation of quantum local master equations with thermodynamics". In: *New J. Phys.* 20 (2018), p. 113024.

[231] C. de Tomás, A. C. Hernández, and J. M. M. Roco. "Optimal low symmetric dissipation Carnot engines and refrigerators". In: *Phys. Rev. E* 85 (2012), p. 010104.

[232] E. Geva and R. Kosloff. "On the classical limit of quantum thermodynamics in finite time". In: *J. Chem. Phys.* 97 (1992), pp. 4398–4412.

[233] M. O. Scully. "Quantum Afterburner: Improving the Efficiency of an Ideal Heat Engine". In: *Phys. Rev. Lett.* 88 (2002), p. 050602.

[234] R. Kosloff and Y. Rezek. "The Quantum Harmonic Otto Cycle". In: *Entropy* 19 (2017), p. 136.

[235] Y. Zheng, S. Campbell, G. De Chiara, and D. Poletti. "Cost of counterdiabatic driving and work output". In: *Phys. Rev. A* 94 (2016), p. 042132.

[236] E. Torrontegui, I. Lizuain, S. González-Resines, A. Tobalina, A. Ruschhaupt, R. Kosloff, and J. G. Muga. "Energy consumption for shortcuts to adiabaticity". In: *Phys. Rev. A* 96 (2017), p. 022133.

[237] O. Abah, R. Puebla, A. Kiely, G. D. Chiara, M. Paternostro, and S. Campbell. "Energetic cost of quantum control protocols". In: *New J. Phys.* 21 (2019), p. 103048.

[238] G. De Chiara and M. Antezza. "Quantum machines powered by correlated baths". In: *Phys. Rev. Research* 2 (2020), p. 033315.

[239] D. Grimmer, E. Brown, A. Kempf, R. B. Mann, and E. Martín-Martínez. "Gaussian ancillary bombardment". In: *Phys. Rev. A* 97 (2018), p. 052120.

[240] L. E. Estes, T. H. Keil, and L. M. Narducci. "Quantum-Mechanical Description of Two Coupled Harmonic Oscillators". In: *Phys. Rev.* 175 (1968), pp. 286–299.

[241] D. Grimmer, D. Layden, R. B. Mann, and E. Martín-Martínez. "Open dynamics under rapid repeated interaction". In: *Phys. Rev. A* 94 (2016), p. 032126.

[242] D. Grimmer. "Interpolated Collision Model Formalism". Doctoral dissertation. UWSpace, 2020.

[243] S. Felicetti, M.-J. Hwang, and A. Le Boité. "Ultrastrong-coupling regime of nondipolar light-matter interactions". In: *Phys. Rev. A* 98 (2018), p. 053859.

[244] Á. Rivas, A. D. K. Plato, S. F. Huelga, and M. B. Plenio. "Markovian master equations: a critical study". In: *New J. Phys.* 12 (2010), p. 113032.

[245] G. L. Giorgi, A. Saharyan, S. Guérin, D. Sugny, and B. Bellomo. "Microscopic and phenomenological models of driven systems in structured reservoirs". In: *Phys. Rev. A* 101 (2020), p. 012122.

[246] A. Streltsov, G. Adesso, and M. B. Plenio. "*Colloquium*: Quantum coherence as a resource". In: *Rev. Mod. Phys.* 89 (2017), p. 041003.

[247] Z. Wang, W. Wu, G. Cui, and J. Wang. "Coherence enhanced quantum metrology in a nonequilibrium optical molecule". In: *New J. Phys.* 20 (2018), p. 033034.

[248] A Smirne, A Lemmer, M. B. Plenio, and S. F. Huelga. "Improving the precision of frequency estimation via long-time coherences". In: *Quantum Sci. Technol.* 4 (2019), p. 025004.

[249] A. Blais, A. L. Grimsmo, S. Girvin, and A. Wallraff. "Circuit Quantum Electrodynamics". In: *arXiv:2005.12667* (2020).

[250] T. P. Orlando, J. E. Mooij, L. Tian, C. H. van der Wal, L. S. Levitov, S. Lloyd, and J. J. Mazo. "Superconducting persistent-current qubit". In: *Phys. Rev. B* 60 (1999), pp. 15398–15413.

[251] C. H. van der Wal, A. C. J. ter Haar, F. K. Wilhelm, R. N. Schouten, C. J. P. M. Harmans, T. P. Orlando, S. Lloyd, and J. E. Mooij. "Quantum Superposition of Macroscopic Persistent-Current States". In: *Science* 290 (2000), pp. 773–777.

[252] M. Tinkham. *Introduction to Superconductivity.* Dover Publications, New York, 2004.

[253] L. D. Landau and E. M. Lifshitz. *Mechanics,* Vol. 1 of *Course of Theoretical Physics,* 3rd ed. Butterworth-Heinemann, 1976.

[254] S. Popescu, A. J. Short, and A. Winter. "Entanglement and the foundations of statistical mechanics". In: *Nat. Phys.* 2 (2006), pp. 754–758.

[255] F. G. Brandão and M. B. Plenio. "Entanglement theory and the second law of thermodynamics". In: *Nat. Phys.* 4 (2008), pp. 873–877.

[256] H. Li and F. D. M. Haldane. "Entanglement spectrum as a generalization of entanglement entropy: Identification of topological order in non-Abelian fractional quantum hall effect states". In: *Phys. Rev. Lett.* 101 (2008), p. 010504.

[257] I. Peschel and V. Eisler. "Reduced density matrices and entanglement entropy in free lattice models". In: *J. Phys. A: Math. Theor.* 42 (2009), p. 504003.

[258] I. Peschel and M. C. Chung. "On the relation between entanglement and subsystem Hamiltonians". In: *Europhys. Lett.* 96 (2011), p. 50006.

[259] N. Laflorencie. "Quantum entanglement in condensed matter systems". In: *Phys. Rep.* 646 (2016), pp. 1–59.

[260] M Dalmonte, B Vermersch, and P Zoller. "Quantum simulation and spectroscopy of entanglement Hamiltonians". In: *Nat. Phys.* 14 (2018), pp. 827–831.

[261] J. A. Miszczak. "Generating and using truly random quantum states in Mathematica". In: *Comput. Phys. Commun.* 183 (2012), pp. 118–124.

[262] D. N. Page. "Average entropy of a subsystem". In: *Phys. Rev. Lett.* 71 (1993), pp. 1291–1294.

[263] S. K. Foong and S. Kanno. "Proof of Page's conjecture on the average entropy of a subsystem". In: *Phys. Rev. Lett.* 72 (1994), pp. 1148–1151.

[264] N. Takei et al. "Experimental demonstration of quantum teleportation of a squeezed state". In: *Phys. Rev. A* 72 (2005), p. 042304.

[265] G. Araneda, N. Cisternas, and A. Delgado. "Telecloning of qudits via partially entangled states". In: *Quantum Inf. Process.* 15 (2016), pp. 3443–3458.

[266] K. Banaszek. "Optimal quantum teleportation with an arbitrary pure state". In: *Phys. Rev. A* 62 (2000), p. 024301.

[267] B. L. Schumaker and C. M. Caves. "New formalism for two-photon quantum optics. II. Mathematical foundation and compact notation". In: *Phys. Rev. A* 31 (1985), pp. 3093–3111.

[268] A. Dutt, K. Luke, S. Manipatruni, A. L. Gaeta, P. Nussenzveig, and M. Lipson. "On-Chip Optical Squeezing". In: *Phys. Rev. Appl.* 3 (2015), p. 044005.

Titre : Dissipation-assisted processes and quantum correlations

Mots clés : Quantum thermodynamics, Work, Collision models,
Two-photon interaction, Adiabatic elimination, Entanglement.

Dissipative dynamics of open quantum systems and quantum correlations are topics of great actual interest. The former because of its necessity when describing realistic systems and the latter because quantum correlations enable, in general, genuine quantum protocols.
This thesis aims to study physical processes relying on dissipation, also focusing on quantum correlations and their role in these processes, and on how to use dissipation to generate quantum correlations. We first introduce the reader to the various topics treated within the thesis which are connected to various research fields such as open quantum systems, quantum thermodynamics, quantum optics, and quantum information. Then, each chapter deals with a different subject.
The first part of the thesis consists of two studies in the context of quantum thermodynamics. The first study concerns a protocol of work extraction exploiting a single thermal bath. The work, defined within thermodynamic resource theory, is extracted from a resource and stored into a bipartite system by turning on and off its internal interaction. Then, we apply this protocol to two relevant physical systems: two interacting qubits and the Rabi model. In both cases, we obtain a work extraction comparable with the bare energies of the systems. In the second study, we investigate quantum thermal machines based on two-stroke thermodynamic cycles using two baths at different temperatures. The working fluid is composed of systems with evenly spaced energy levels, and all the considered interactions are of the exchange type. We maximize the power of two different cycles, also focusing on the role of the machines waiting time.
In the second part of this thesis, strongly connected to open quantum systems, we first study the Markovian and non-Markovian dynamics of a driven quantum harmonic oscillator within the collision model. While this is still a "work in progress" research project, we already have promising results such as the appearance of a non-adiabatic time-dependent term in the continuous limit of the Markovian dynamics. Then, we study the two-photon Dicke model in the bad-cavity limit, considering a quite general setup comprising finite temperature baths and coherent and incoherent drivings. We manage to derive an effective master equation for the qubits dynamics and compare it to the one-photon case. In the two-photon model, we point out an enhancement of the qubits spontaneous-like emission rate and an increment of the effective temperature perceived by the qubits. These differences lead to a faster generation of steady states with coherence and a richer dependence of the collective effects on temperature.
In the last part of the thesis, we explore the connection between energy and entanglement in an arbitrary finite non-interacting bipartite system, also finding the minimum energy entangled states (MEESs), i.e., the states having the minimum energy amount for a given degree of entanglement. We also study how these states can be generated both through unitary and dissipative processes, finding for the latter that the MEESs are practically the cheapest ones to produce. Moreover, the MEESs can be connected among them through local operations and classical communication and seem to have remarkable connections to quantum thermodynamics and many-body physics. Finally, we analyze how to use our results to lower the energetic cost of different quantum information protocols.

Titre : Processus assistés par dissipation et corrélations quantiques

Mots clés : Thermodynamique quantique, Travail, Modèles collisionnels ,
Interaction à deux-photons, Élimination adiabatique, Intrication quantique.

La dynamique dissipative des systèmes quantiques ouverts et les corrélations quantiques sont des sujets de grand intérêt actuel. Le premier en raison de sa nécessité pour décrire des systèmes réalistes et le second parce que les corrélations quantiques permettent de réaliser, en général, des protocoles véritablement quantiques.
Cette thèse vise à étudier des processus physiques reposant sur la dissipation, en se concentrant également sur les corrélations quantiques et leur rôle dans ces processus, et sur la façon d'utiliser la dissipation pour générer des corrélations quantiques. Tout d'abord, nous présentons au lecteur les différents sujets abordés dans la thèse qui sont liés à divers domaines de recherche tels que les systèmes quantiques ouverts, la thermodynamique quantique, l'optique quantique et l'information quantique. Ensuite, chaque chapitre traite d'un sujet différent.
Une première partie de la thèse inclut deux études dans le domaine de la thermodynamique quantique. Une première étude concerne un protocole d'extraction de travail exploitant un seul bain thermique. Le travail, défini dans la théorie des ressources thermodynamiques, est extrait d'une ressource et stocké dans un système bipartite en activant et en désactivant son interaction interne. Ensuite, nous appliquons ce protocole à deux systèmes physiques pertinents : deux qubits en interaction et le modèle de Rabi. Dans les deux cas, nous obtenons une extraction de travail comparable aux énergies nues des systèmes. Dans une seconde étude, nous analysons des machines thermiques quantiques basées sur des cycles thermodynamiques à deux temps utilisant deux bains à des températures différentes. Le fluide de travail est composé de systèmes avec des niveaux d'énergie régulièrement espacés et toutes les interactions considérées sont de type d'échange. Nous maximisons la puissance de deux cycles différents, en nous concentrant également sur le rôle du temps d'attente des machines.
Dans une seconde partie de cette thèse, fortement liée aux systèmes quantiques ouverts, nous étudions d'abord la dynamique Markovienne et non-Markovienne d'un oscillateur harmonique quantique guidé au sein du modèle collisionnel. Même si ce projet de recherche est "en cours", nous avons déjà des résultats prometteurs tels que l'apparition d'un terme non adiabatique dans la limite continue de la dynamique Markovienne. Ensuite, nous étudions le modèle de Dicke à deux photons dans la limite de mauvaise cavité, en considérant un modèle assez général comprenant des bains de température finis et des pilotages cohérents et incohérents. Nous parvenons à dériver une équation maîtresse efficace pour la dynamique des qubits et à la comparer au cas à un photon. Dans le modèle à deux photons, nous observons une augmentation du taux d'émission de type spontané des qubits et une augmentation de la température effective perçue par les qubits. Ces différences conduisent à une génération plus rapide d'états stationnaires avec cohérence et à une dépendance plus riche des effets collectifs sur la température.
Dans la dernière partie de la thèse, nous explorons la connexion entre l'énergie et l'intrication quantique dans un système bipartite fini arbitraire sans interaction, trouvant également les états intriqués d'énergie minimale (MEESs), c'est-à-dire les états ayant la quantité d'énergie minimale pour un degré donné d'intrication quantique. Nous étudions également comment ces états peuvent être générés à la fois par des processus unitaires et dissipatifs, trouvant, pour ces derniers, que les MEESs sont pratiquement les plus économiques à produire. De plus, les MEESs peuvent être connectés entre eux au moyen d'opérations locales et de communication classique et semblent avoir des connexions remarquables avec la thermodynamique quantique et la physique à plusieurs corps. Enfin, nous analysons comment utiliser nos résultats pour réduire le coût énergétique de différents protocoles d'information quantique.